INTERACTIONS WITHIN THE TRIPARTITE DRUG-EFFLUX PUMPS OF GRAM-NEGATIVE BACTERIA

by

ROBERT LUKE MARSHALL

A thesis submitted to the University of Birmingham for the degree of DOCTOR OF PHILOSOPHY

School of Biosciences

College of Life and Environmental Sciences

University of Birmingham

September 2017

Abstract

Antibiotic resistance, particularly amongst Gram-negative bacteria, has emerged as a major global health concern. Working synergistically with the permeability barrier created by the cell envelope, multidrug efflux pumps contribute significantly to the intrinsic resistance of Gram-negative bacteria to clinically relevant drugs. The majority of bacterial multidrug efflux pumps are multi-component assemblies, within which the interaction interfaces may represent potential inhibitor binding sites. The *Escherichia coli* AcrA-TolC interactions and the functional roles of sub-domains of these proteins have been assessed using computationally directed mutants with a combination of *in vivo* and *in vitro* approaches.

Results reported here indicate that regions both at the tip of and halfway up the TolC coiled-coil domain are involved in determining the compatibility of AcrA with TolC. On the other side of the interaction, both the tip region and the helices of the AcrA hairpin are essential for normal function. The hairpin tip is required to maintain the permeability barrier, while the helices are necessary for a stable AcrA-TolC interaction.

Based on these results, I present a dynamic model of tripartite complex assembly, in which initial bundling of AcrA and TolC coiled-coil domains opens the TolC channel. Transition to a tip-to-tip interaction drives channel closing and is required for complex disassembly in an energy-dependent manner. This model provides rationale for future development of complex-specific peptidomimetic efflux inhibitors that could prolong the usability of clinical antimicrobials through combinatorial therapy.

Acknowledgements

The first thanks go to my supervisors, Vass and Klaus, for allowing me to work under their supervision and offering the chance to obtain my PhD and to EPSRC for funding my studentship, without which I would not have been able to study towards my PhD. I would also like to thank both Martin Picard for hosting me in his laboratory during a visit during which I learnt techniques that look likely to have huge potential, and thanks to FEMS for funding this visit.

For providing general intellectual challenge and ideas for experiments, and for challenging my interpretations of results, thanks to both Jess Blair and Mark Webber. Along with Jess and Mark, I am also very appreciative of everyone in both labs T101 and T102 for welcoming and accommodating me in their lab spaces. For asking lots of questions about the wider project, thanks also to Michelle Buckner and Xuan Wang-Kan.

The general support of my family helped my determination to complete these studies. My parents in particular have given me strength of mind to never give up. Last but certainly not least, my wife, Sophie – you gave me the confidence to get myself into a position where I could get a studentship and have supported me throughout the whole process before and during my studentship. I really could not have done this without your support.

Table of contents

List of figures

List of tables

CHAPTER 1: INTRODUCTION

Disclaimer: Parts of this Introduction, and figures therein, may appear in this or a revised form in either the textbook ***Bacterial Resistance to Antibiotics: From Molecules to Man*** *(edited by B. Bonev, N.Brown and D. Turner) or in the review article Symmons et al., 2015.*

This project investigates how the TolC outer membrane channel protein interacts with its partner proteins to produce an effective efflux pump that is known to have physiological, pharmaceutical, and biotechnological significance. Through understanding the assembly structure, it is likely to be possible to develop drugs to prevent efflux action and therefore decrease antimicrobial resistance, and to develop new biotechnological systems to improve yields of certain products. In 2012, two of the top ten causes of death globally can be directly attributed to bacterial infection, according to World Health Organisation (WHO) statistics (World Health Organisation, 2014), and in a further four of the remaining eight causes, bacterial infections are likely to be a major contributing factor to the death. This project will focus on the assembly of a multidrug efflux complex, AcrAB-TolC, given its importance in societal and clinical context with increasing prevalence of drug resistant infections.

1.1 Outer membranes exist to protect the cell by decreasing permeability

It is easy to think only about how bacteria respond to changes that we as humans impose upon them, be they in a clinical or laboratory setting, and to forget that most interactions involving bacteria occur without any intentional manipulation on our part. The natural environments in which bacteria are found drove their evolution, and forced them to develop an intrinsic resistance to toxic substances. Perhaps the most notable structure hypothesised to have developed as a result of antibiotic-mediated selection pressure is the outer membrane (Gupta, 2011), a defining feature of Gram-negative bacteria. This hypothesis postulates that development of an outer membrane structure occurred primarily to form an additional permeability barrier

against the influx of toxic substances, including antibiotics, and thus enabled survival of early didermic bacteria in hostile environments – particularly following the evolution of antibiotic-producing bacteria.

Several outer membrane structures have been found in nature, as analysed by Sutcliffe (2010). These structures can consist of combinations of fatty acids (including mycolic acids, phospholipids, polyacylglycerol and other fatty acids; Bansal-Mutalik & Nikaido, 2014), lipopolysaccharide (which is discussed below) and sugars, or be proteinaceous (Huber *et al.*, 1986; Olabarria *et al.*, 1996) . Regardless of composition, each of these structures protect the cell from environmental factors. Components of the inter-membrane space – the periplasm of Gram-negative bacteria – are also protected by the outer membrane permeability barrier. Given that some essential processes such as cell wall synthesis take place outside the cytoplasmic membrane, protection of such components is vital to survival in hostile environments.

Perhaps the most widely-known outer membrane is that of the Gram-negative bacteria. This membrane is an asymmetric bilayer (Kamio & Nikaido, 1976), of which the inner leaflet consists of glycerophospholipids, enriched in phosphatidylethanolamine and saturated fatty acids compared with the inner membrane. The outer leaflet, formed of lipopolysaccharide (LPS), provides the main permeability barrier of this membrane. LPS varies by both species and strain, affecting a range of biological processes and membrane fluidity (Rottem & Leive, 1977). Variation is seen throughout the LPS molecule (Wilkinson, 1996; Delcour, 2009), but characteristic variations include those within the length of the O-antigen (which extends outside the cell) and the acylation of Lipid A. Representative structures of both LPS and the outer membrane are shown in Figure 1:1.

Lipid A consists of a disaccharide of hexosamines. Each of the hexosamines is acylated by amide and ester bonds at their 2- and 3- positions, respectively, providing

the minimum of tetra-acylation seen naturally. A maximum of eight acyl chains have been observed in natural LPS – ester bonds can be made between the 3-hydroxy position of one fatty acid and the carboxylic acid of another, forming an acyloxyacyl moiety that can be attached to the dihexosamine at each of the four positions. The fatty acids found in LPS are often, though not always, saturated, and thus pack closer together for a greater combined hydrophobicity. This is one of the main factors contributing to the decreased fluidity and permeability of the outer membrane compared to the inner membrane. The acyl chains, which interact at a hydrophobic interface with the fatty acids of the inner leaflet glycerophospholipids in the middle of the outer membrane, to form the bilayer required of a membrane, are usually between ten and sixteen carbon atoms long, but chains as long as 22 carbon atoms have been reported in LPS (Heine *et al.*, 2003). The hexosamines of Lipid A are phosphorylated, increasing hydrophilicity of the backbone region at the external face of the membrane, providing negative charge and decreasing permeability to hydrophobic substances that would otherwise cross the hydrophobic fatty-acid portion of the membrane.

The core oligosaccharide of LPS is attached to the free 6-hydroxy position of the hexosamine. The core region consists of a series of 1-5` linked other sugars, which vary by species – in enteric bacteria, this is usually a series of three heptose sugars followed by up to six other sugars. Strains with shorter core regions are more susceptible to lipophilic drugs (Delcour, 2009), thus the LPS core region has a role in preventing access of drugs to the cellular target. Variability of this core region, in terms of length, composition and branching, is great, and will not be discussed further.

On the outside of the cell is the O-antigen, which can vary from lacking entirely (in “rough-type” cells) to as many as 50 subunits each consisting of up to eight sugar

units (Caroff & Karibian, 2003). The number of different sugars, modifications and interlinking compounds (such as organic acids) that can make up each subunit, combined with the possible variations in number of sugars per subunit, provides huge scope for variation in O-antigen structure between different serotypes. This variation determines the immunogenicity of the outer membrane, but is not generally regarded as significant in decreasing permeability of the membrane to drugs, despite evidence that permeation of the outer membrane by macrolides is dependent upon the length of the O-antigen (Tsujimoto *et al.*, 1999).

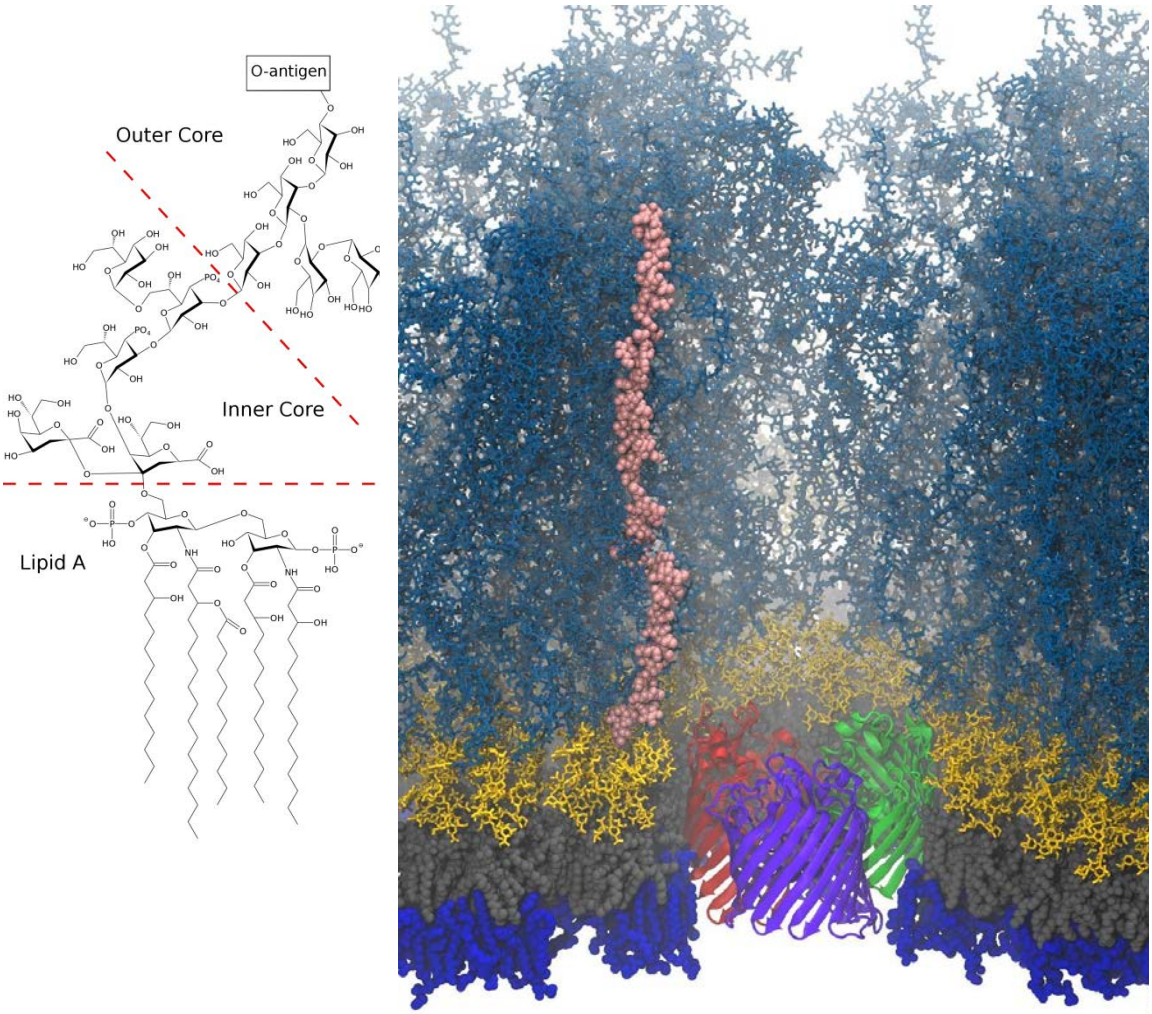

Figure 1:1 – Structure of the Gram-negative outer membrane.
Representative chemical structure of an LPS molecule (left), excluding detail of the O-antigen, and a full atomic model of a section of outer membrane from *Salmonella* Typhimurium (right; courtesy of J.C.Gumbart). Many modifications are possible to the LPS molecule, including additional acylation, acylation with different chain lengths, incorporation of extra or alternative sugar subunits, and further phosphorylation. The full atomic model shows a single O-antigen chain (pink) and the acyl chains (grey) in space-fill, while the core (yellow) and all other LPS molecules are shown in line format only. A trimer of OmpD is shown in ribbon format with each monomer in a different colour. Clearing of O-antigen above the porin can be seen. The true density of packing of LPS molecules is greater than visualised here, due to the use of lines rather than space-fill.

1.2 Transmembrane substance translocation

The permeability barrier provided by LPS prevents toxic substances and nutrients from easily crossing the outer membrane. Gram-negative bacteria have outer membrane porins to allow uptake of nutrients. Porins are proteins which form a β-barrel through the outer membrane, introducing a water-filled pore through the otherwise highly hydrophobic membrane (Cowan *et al.*, 1992). Between the strands that form the barrel are loops of various sizes, some incorporating short helices. These loops act as a filter, allowing some selectivity of solute transport. Some of the porins are therefore cation- or anion-specific, others are sugar-specific, while others do not show solute specificity and are regarded as general porins. General porins tend to have a wider accessible opening than specific porins, and can be a route of entry for many drugs (Danilchanka *et al.*, 2015). Increased expression of porins can lead to increased sensitivity of a strain to antibiotics (Krishnamoorthy *et al.*, 2016). Conversely, loss or down-regulation of porins is associated with drug resistance. The low expression levels of open general porins in *Pseudomonas spp.* and *Acinetobacter spp.* is attributable for their increased drug tolerance compared to *E. coli* (Delcour, 2009). Size, number and specificity of the porins contribute greatly in determining how resistant or susceptible a cell will be to antibiotics, but changes in the porin profile are relatively slow in the context of responding to an environmental change. For a quicker response, porins can be closed by ligand binding under certain conditions, and cannot be thought of as constitutively open holes in the membrane. Not all drugs can fit through these porins, due to either their size or charge. Macrolides, for example, are thought to access the cell by permeating the lipid bilayer itself rather than utilising a protein as route of entry (Tsujimoto *et al.*, 1999; Delcour, 2009). Vancomycin is a large drug which cannot pass through the porins or the outer membrane bilayer, ironically gaining entry to the Gram-negative bacterium

through a drug efflux channel protein, which is gated at the periplasmic end, occluded except for during efflux events.

Channel proteins have also evolved to form essential parts of multidrug efflux pumps, which actively remove toxic substances from within the cell. The combination of an influx barrier with efflux pumps improves the survival of Gram negative bacteria in the presence of toxic substances, including antibiotics, quite considerably (Piddock, 2006; Nikaido, 2009); over-expression of or even a point mutation (such as G288D in AcrB, which causes resistance to fluoroquinolones) in these efflux pumps can cause clinically significant multidrug resistance and change the drug susceptibility profile of the strain (Webber *et al.*, 2005; Tavio *et al.*, 2014; Blair *et al.*, 2015; Kinana *et al.*, 2016).

1.3 Removal of substances from cell interior

Transmembrane pump proteins are present and common throughout all kingdoms of life, and can be responsible for either active uptake of such substances as nutrients and vitamins, or for active efflux of unwanted (toxic) substances (Saier *et al.*, 2014). Bacterial drug efflux pumps, which are grouped into six families based primarily upon common architectures (Piddock, 2006; Hassan *et al.*, 2015), can increase tolerance to a wide variety of substances. To pump against the chemical concentration gradient, these pumps all require an energy source – one of the families, the ATP-binding cassette (ABC) family uses ATP hydrolysis (Kobayashi *et al.*, 2001; Lu & Zgurskaya, 2012), while the remaining five families utilise an electrochemical gradient across the cytoplasmic membrane (Thanassi *et al.*, 1997; Law *et al.*, 2008; Hassan *et al.*, 2013; Ogawa *et al.*, 2015; Dastvan *et al.*, 2016; Gayen *et al.*, 2016). This thesis will consider only assembly of the resistance-nodulation-cell division (RND) family of transporters, though members of other families that utilise the same outer membrane channel protein will be also be used for comparison.

Transmembrane pump proteins are present and common throughout all kingdoms of life, and can be responsible for either active uptake of things such as nutrients and vitamins, or for active efflux of unwanted (toxic) substances (Saier *et al.*, 2014). Of particular interest in the context of multidrug resistance are the drug efflux pumps, which are grouped into six families, based primarily upon common architectures. Models of the common architecture are shown in Figure 1:2.

1.3.1 ABC transporters

Of these families, one uses substrate hydrolysis to provide translocation energy directly – the proteins utilise ATP, and are thus nominated **A**TP-**b**inding **c**assette (ABC) transporters. Multidrug efflux ABC transporters like MacB (macrolide efflux pump) are dimeric, with each monomer consisting of a four-helix transmembrane domain, a cytoplasmic nucleotide binding domain and a mixed α/β periplasmic domain. The periplasmic domain interacts with partner proteins, while the nucleotide binding domain binds and hydrolyses nucleotides (primarily ATP). The transmembrane helices are predicted to bind the substrate and undergo a conformational change both upon binding of the substrate and upon hydrolysis of ATP. Such conformational changes move the substrate across the inner membrane within the binding cleft formed by the helices. The mechanism of ABC multidrug transporters is predicted based upon that of ABC transporters with other roles.

1.3.2 MFS transporters

All of the other five families utilise ion gradients for symport or antiport, or transport only one substrate by assisted diffusion. The largest family of transporters is the **m**ajor **f**acilitator **s**uperfamily (MFS), which contains examples of all three of these transport types, indicating that although a single superfamily has common architecture and a common mechanism for the transport action, the directionality of and energy source for the transport event may vary. The common mechanism in MFS

transporters is the use of a rocker-switch type movement of a single binding site, which alternates to which side of the membrane the binding pocket is open (Law *et al.*, 2008). Crystal structures are available for members of this superfamily of transporters, which show the proteins to be formed almost entirely of a bundle of transmembrane helices, with virtually no periplasmic or cytoplasmic domains except for any protrusion of the transmembrane helices and their interconnecting loops. Most proteins in this family contain either 12 or 14 transmembrane helices; these helices account for 240 out of 394 residues in the EmrD multidrug efflux pump from *E. coli*, though these pumps are usually slightly larger, up to 600 amino acids long. The EmrD crystal structure indicates a dimeric structure (Yin *et al.*, 2006), although this may be a crystallographic artefact. Within each MFS protein monomer is a narrow pore, which has been identified as the route through which the substrate translocates. This pore is open to only one side of the protein at a time, for binding or release of the substrate. The rocker-switch motion rearranges the helices around the active site, temporarily occluding the protein lumen during the translocation process, until the pore re-opens at the other side of the protein. In the case of antiport-driven pumps, this process will then reverse with the binding of the antiporting substrate.

1.3.3 SMR transporters

The smallest proteins currently identified as multidrug transporters are the so-called **s**mall **m**ultidrug **r**esistance (SMR) family of proteins, which fall under the category of drug/metabolite transporter superfamily. SMR proteins have greater limitations to their range of substrates than the other families of transporters, as they have only been found to transport lipophilic compounds, including quaternary ammonium compounds and cationic dyes (Bay *et al.*, 2008). While they have a limited substrate range, single proteins within this family are capable of transporting several structurally distinct substrates, and are therefore legitimately classified as multidrug transporters. All members of this family for which the transport type is known

function by drug/proton antiport. SMR transporters are encoded both chromosomally and on mobile genetic elements (plasmids and integrons). Similarly to MFS transporters, SMR proteins contain virtually no cytoplasmic or periplasmic regions. The functional oligomeric state of SMR proteins is unclear, as the multimerisation state determined experimentally is dependent upon the conditions used in the investigation (Bay *et al.*, 2010). There have been several mechanisms of pump activity proposed over the years, but more recent studies are converging towards a similar rocker-switch type mechanism as in MFS transporters, but in SMR transporters both the binding pocket and pore form between dimers (Dastvan *et al.*, 2016; Gayen *et al.*, 2016).

1.3.4 MATE transporters

Multidrug **a**nd **t**oxic compound **e**xtrusion (MATE) efflux pumps consist of three sub-types: cluster 2 proteins are eukaryotic, clusters 1 and 3 include bacterial and archaeal proteins whereby cluster 1 proteins (of the NorM-type) follow the same phylogenetic patterns as the organisms from which they originate while cluster 3 proteins (of the DinF-type) follow no such pattern. MATE transporters utilise electrochemical potential, antiporting protons, Na^+, or K^+. One example protein (KetM from *Klebsiella pneumoniae*) has been found to be energised by any one of protons, Na^+, K^+ or Li^+, and to pump several structurally-related compounds (Ogawa *et al.*, 2015). Proteins within the MATE family have been shown to pump a variety of substrates of unrelated structure (Kuroda & Tsuchiya, 2009). Though they are therefore recognised as multidrug transporters, MATE proteins seemingly contribute little to the overall intrinsic resistance of bacteria to toxic compounds. Crystal structures of MATE transporters from different organisms are available, showing different binding states (He *et al.*, 2010; Lu *et al.*, 2013a; Lu *et al.*, 2013b; Lu, 2016). These show the protein to form 12 transmembrane helices, which undergo major conformational changes upon substrate binding. Uniquely among antiporters, MATE

proteins have been shown bound to both substrate and cation simultaneously, although the binding of the cation causes such a significant conformational change as to force release of the substrate and enable continuation of the cycle. MATE proteins of the NorM family have also shown for the first time that Na^+ - π bonding can occur in membrane proteins, thus indicating that selectivity for Na^+ as an energy source is dependent on the presence of an aromatic residue at the cation-binding position. The drug and cation binding sites in the NorM family of MATE transporters are separated by a helix – the two moieties interact neither with each other nor with the same binding pocket of the protein. The DinF family functions by a very different mechanism: competition between protonation and substrate binding causes release of the separate moieties, from the same binding site (Lu, 2016). The NorM-type and DinF-type sub-families of MATE transporters are therefore clearly distinct, despite the structural similarity.

1.3.5 PACE transporters

The most recently discovered family of multidrug efflux pumps is the **p**roteobacterial **a**ntimicrobial **c**ompound **e**fflux (PACE) family. The nomenclature here may require re-defining, as this family of pumps is not limited to the proteobacteria, nor do all proteobacteria encode any (Hassan *et al.*, 2015b). The natural substrates for this family of proteins have not yet been determined, as they have only so far been found to pump synthetic biocides (Hassan *et al.*, 2015a). The only factor apparently common to the identified substrates is the presence of at least one aromatic ring. At the time of writing, no structural or mechanistic information is available for this family of pumps.

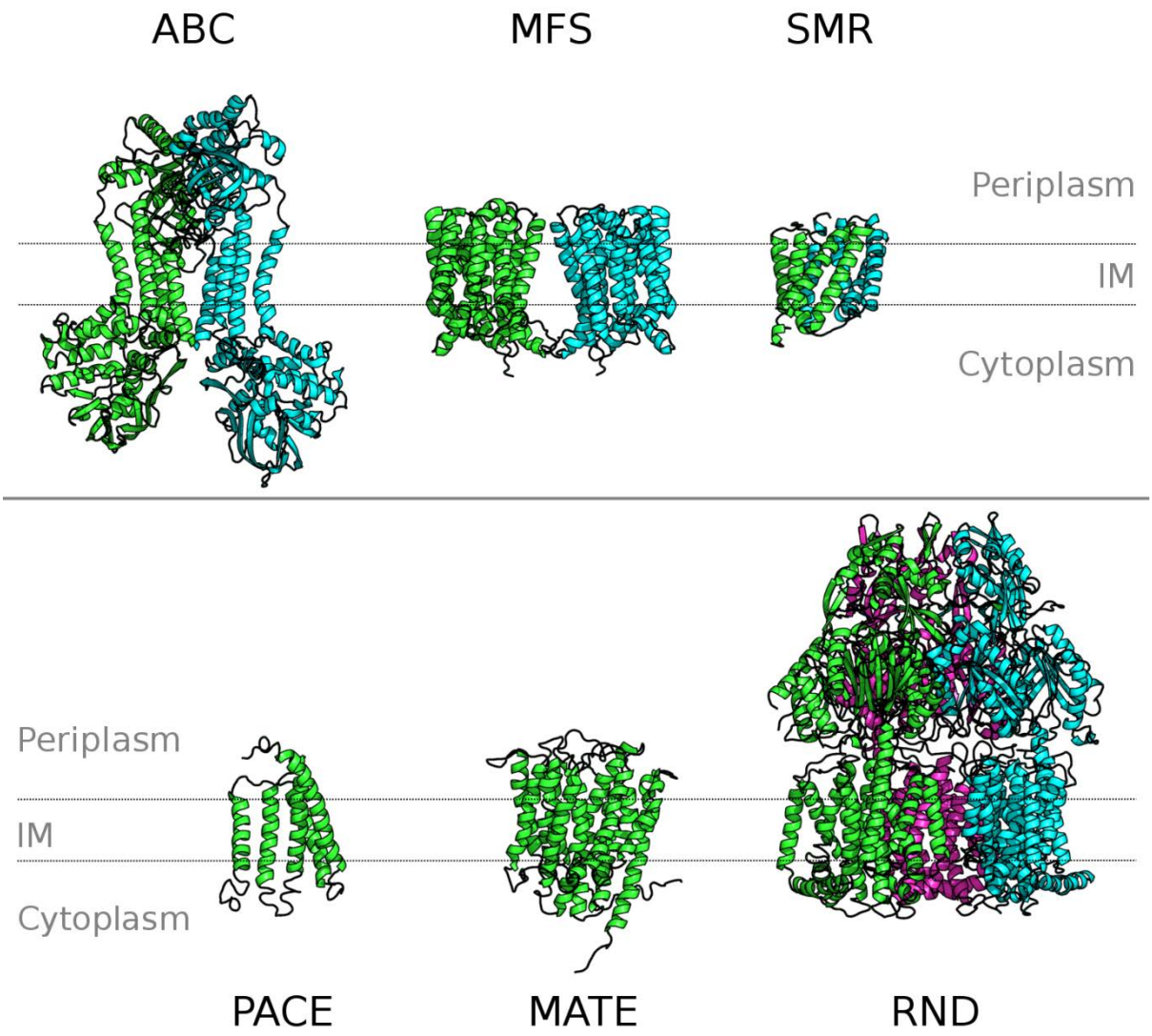

Figure 1:2 - Models or crystal structures of an example from each class of MDR transporter.

Each is displayed to the same scale to give a representation of the relative sizes of each transporter class. The inner membrane (IM) has been drawn at a position of best fit for each protein. Monomers within a protein are coloured separately. As stoichiometry is not known for PACE or MATE transporters, they are here represented as monomers. ABC: a homology model of MacB from *E. coli*. MFS: EmrD crystal structure, 2GFP. SMR: EmrE crystal structure, 3B61. PACE: homology model for AceI protein from *Acinetobacter baumannii*, generated by I-TASSER (Yang *et al.*, 2015). MATE: NorM crystal structure, 4HUL. RND: AcrB crystal structure 1IWG.

1.3.6 RND transporters

Of the pumps present in Gram negative bacteria, RND multidrug transporters show the greatest contribution to multidrug resistance (Sulavik *et al.*, 2001). The extent of this is such that in wild-type cells, they can mask efflux activities of some other pumps and study of these other pumps might require their overexpression , or use of a strain in which major RND pumps have been disrupted (Tikhonova *et al.*, 2007). Such observations may raise issues regarding the classification of pumps contributing so little to natural efflux – are these pumps really drug efflux pumps? There are two main ideas regarding this: the first is that they are not naturally drug efflux pumps, but they normally do something different and fulfil a drug efflux role in a facultative manner (Lu & Zgurskaya, 2013), which is apparent only in artificial laboratory conditions. The other is that most minor efflux pumps contribute to multidrug resistance via the activity of a major RND efflux pump, with multiple transporters moving substances from the cytoplasm to the periplasm, from where the RND transporter collects them for removal to the extracellular space (Tal & Schuldiner, 2009).

Efflux pumps are capable of increasing a cell's tolerance to a substance by decreasing the intracellular concentration of that substance. Such activity is necessary not only for chemicals with an origin outside the cell, but also for toxic waste substances produced by the cell (Blanco *et al.*, 2016). Unlike mechanisms of modifying or degrading antibiotics, efflux activity does not detoxify the environment; it only detoxifies the cell. The drug therefore remains in the environment and, as the pump acts against the concentration gradient, the drug is constantly diffusing into the cell. The permeability barrier of the OM therefore acts synergistically with efflux pumps to restrict intracellular drug accumulation (Nikaido, 1994).

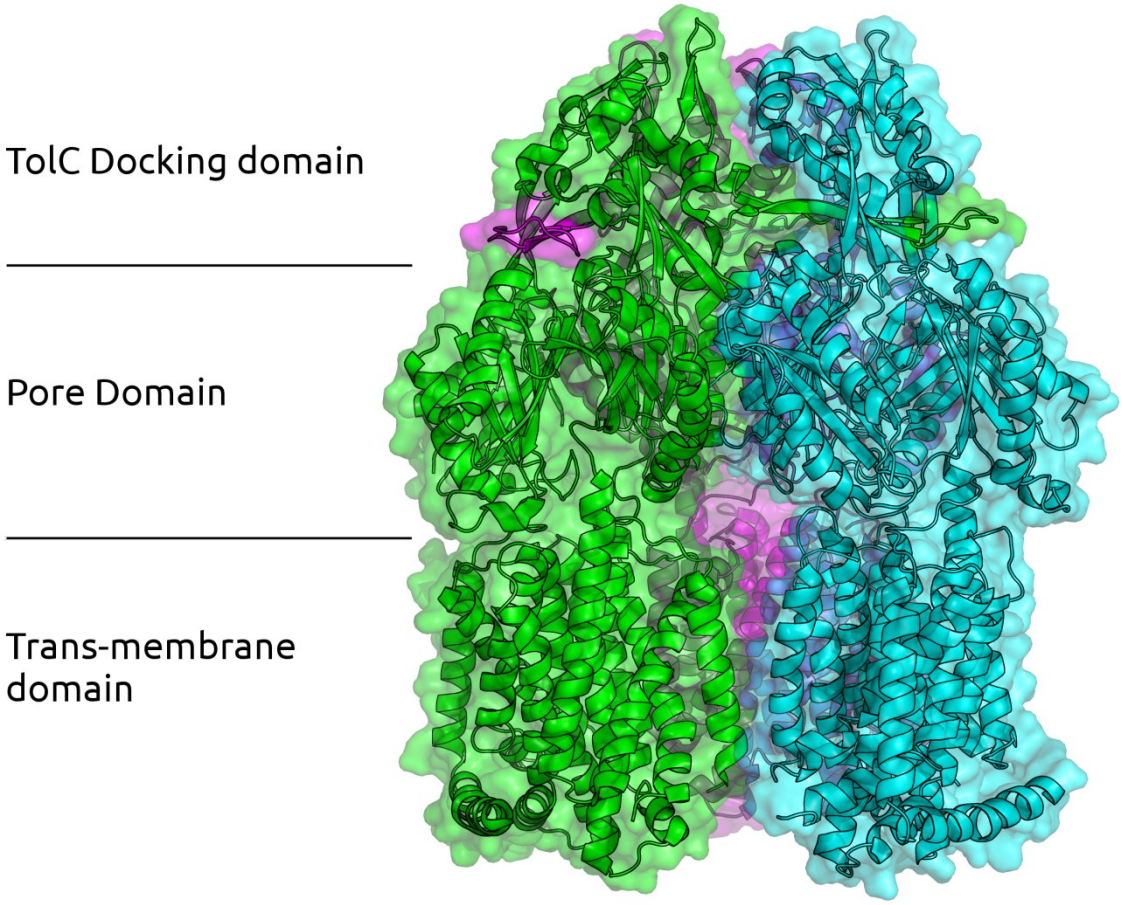

Figure 1:3 - Crystal structure of RND transporter AcrB.
The crystal structure of AcrB (1IWG) is shown in both ribbon and transparent format with each protomer in a unique colour. The inner membrane is not drawn, though the twelve helices of the trans-membrane domain of each protomer span the membrane.

Given the significant contribution of RND transporters to MDR, these pumps have been extensively studied, and the mechanisms of translocation are reasonably well understood (Seeger *et al.*, 2008; Eicher *et al.*, 2012; Eicher *et al.*, 2014; Zuo *et al.*, 2015; Oswald *et al.*, 2016; Schuster *et al.*, 2016). Crystal structures of the prototypical RND drug transporter from *E. coli*, AcrB, show the homotrimeric protein to go through a cycle of conformations, with each protomer in a different conformation and binding state (Seeger *et al.*, 2006). By cycling through conformations, the pump undergoes a peristaltic action, to effectively squeeze the substrate through multiple binding pockets towards an external pore (Seeger *et al.*, 2008). These conformational

changes are driven by proton motive force; a network of charged and polar residues in the transmembrane region of the protein relay the proton and trigger the conformational changes. The charge network is very well conserved in homologues of AcrB – in particular, two aspartic acid residues in the transmembrane helices (D407 and D408 of AcrB) essential for AcrB activity appear to be absolutely conserved in all RND multidrug efflux pumps from alpha-, beta-, gamma-, delta-, and epsilon-proteobacteria. A major requirement for efflux activity of a substance is that it must be capable of occupying the binding pockets only with low affinity – anything with high affinity will bind to the protein instead of passing through it, resulting in an inhibitive effect, as is the case with phenylalanine-arginine-β-naphthylamide (PAβN) and the pyranopyridines (Vargiu *et al.*, 2014). Otherwise, the RND multidrug transporters are relatively non-selective, capable of exporting a multitude of compounds (Pos, 2009), with a wide range of physical characteristics – the only selectivity requirements seem to be that the compound must be lipophilic and capable of physically fitting through the different binding pockets, tunnels, and outer membrane channel.

RND pump proteins can fulfil multiple functions. These can include export of multiple and unrelated toxic substances, transport of outer membrane lipid components (Varela *et al.*, 2012; Yang *et al.*, 2014), or export of quorum sensing molecules (Aendekerk *et al.*, 2005). The role in transport of outer membrane lipids in the Corynebacterineae is an example of how an RND pump can contribute to multidrug resistance without directly extruding the drugs (Yang *et al.*, 2014). Examples of substrates, inhibitors and a non-substrate of the MDR RND transporters of interest to this project are shown in Figure 1:4, including examples of linear and cyclic, large and small toxic compounds. Given the variety of substrates, it is perhaps not surprising that single substitution mutations mapping to the binding pockets can

affect how effectively the pump will transport any given substance (Blair *et al.*, 2015), and can have significant impact on clinical outcome.

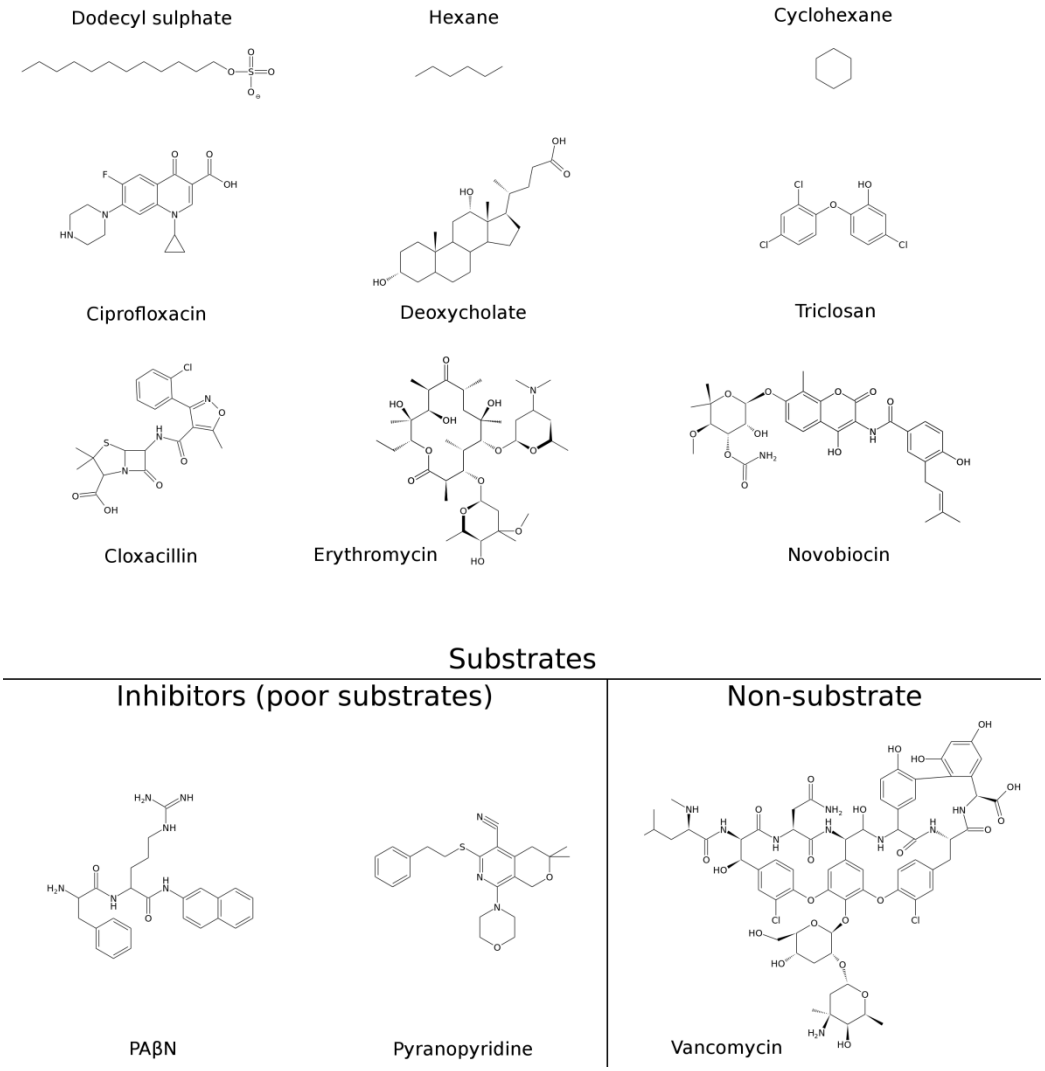

Figure 1:4 - Substrates, inhibitors, and a non-substrate of common RND multi-drug transporters.

Great variation in size, shape and hydrophobicity can be seen between different substrates. PAβN and pyranopyridines are competitive inhibitors of the pumps, although PAβN is also a poor substrate. Vancomycin is not an efflux substrate, but utilises open complexes required for RND efflux pump activity to gain entry to the cell.

1.4 Moving a substrate beyond the cell envelope

All of the inner membrane transport proteins have a transmembrane domain to facilitate substrate transport across the inner membrane. However, they do not span the entire Gram-negative cell envelope on their own, and would therefore not remove the drug past the main permeability barrier of the outer membrane. For many toxic substances, their removal from the cytoplasm would be sufficient to prevent their action, as any drug which acts at the level of DNA, RNA, protein synthesis or on any other cytoplasmic function would be removed from its location of activity. It does however seem to be an inefficient mechanism of drug removal, as the energy is being used to overcome only a lesser permeability barrier, and the drug will likely re-enter the cytoplasm relatively quickly.

In Gram-negative bacteria, the ABC, RND and some major facilitator superfamily (MFS) multidrug transporters form part of tripartite complexes capable of spanning the entire cell envelope, and thus transport their substrates to the external environment. Tripartite assemblies consist of the inner membrane transporter protein, an outer membrane channel protein, and a membrane fusion protein (MFP; may elsewhere be called periplasmic adaptor protein) which links the pump and channel proteins to ensure a continuous conduit from the inner membrane to the extracellular environment. Some complexes may have an additional small protein that is non-essential for efflux activity. These small proteins are currently poorly understood, but affect the efflux profile of the pump (Hobbs *et al.*, 2012). Analysis of the genetic context of *acrZ* suggests that the small protein may naturally form part of a different complex, as the gene forms part of the *modABC* gene cluster, which encodes a molybdate ABC-transporter complex. For drug efflux to be detectable *in vivo*, all of the transporter, MFP and channel protein must be expressed, and there must be an energy source. Such activity can be derived through several approaches, including assays to determine minimum inhibitory concentration (MIC), fluorescent

substrate accumulation rate and removal of fluorescent substrate from pre-loaded cells (Blair & Piddock, 2016).

1.5 Tripartite complexes

1.5.1 Outer membrane channels

As stated above, tripartite complexes consist of the transporter, an outer membrane channel protein, and a membrane fusion protein – Figure 1:8 shows the components in an exploded format after each component has been introduced. The channel protein is perhaps the most straightforward of the three proteins, as it essentially must form a conduit that is wide enough to allow passage of the pumped antibiotics. Members of this family form homotrimers. The prototypical member of this family of proteins, TolC from *E. coli*, is the main focus of this thesis.

The first reports of the *tolC* gene identified gene loci in which mutation or disruption caused tolerance to colicin in a conditional manner (temperature-dependent), hence the name (Nagel de Zwaig & Luria, 1969). At this same time, it was also observed that these mutants were more susceptible to deoxycholate (Nagel de Zwaig & Luria, 1967). It was therefore proposed that the *tolC* gene must in some way be required for normal cell envelope structure. It was later found that *tolC* mutants are deficient in expression of one of the major outer membrane proteins (OMPs), OmpF (Morona & Reeves, 1982) - an observation that seems to have been largely overlooked since the finding that TolC is itself an OMP (Morona *et al.*, 1983). As an OMP, TolC not surprisingly contains a signal sequence that is cleaved as the protein matures (Hackett *et al.*, 1983).

Following the observation that TolC is an OMP, its requirement in the secretion of haemolysin was shown (Wandersman & Delepelaire, 1990), demonstrating for the first time that it is part of secretion pump assemblies - although this was not directly concluded by the authors, who only stated that TolC may allow interaction of the

other pump components with the outer membrane (OM). Conductivity experiments showed that TolC is a channel protein (Benz *et al.*, 1993), providing further evidence for its direct role as part of a pump assembly. TolC was then shown to also be required for activity of AcrAB and does not affect expression of AcrA (Fralick, 1996), again suggesting a role for TolC as the export channel component of a pump complex. This finding also explained the early observations that strains in which *tolC* is disrupted are more susceptible to deoxycholate, as *acrB* mutants display the same phenotype (Ma *et al.*, 1995; Lacroix *et al.*, 1996).

As with most outer membrane proteins, these channels contain a β-barrel domain, which spans the outer membrane and acts as an exit pore (Koronakis *et al.*, 2000). Each protomer within the homotrimer contributes four β-strands to a 12-stranded barrel. While the β-barrel is sufficient for insertion into the outer membrane, one OMC (OprM) from *Pseudomonas aeruginosa* is known to be lipidated at its N-terminal cysteine residue, and the crystal structure suggests that this lipid moiety inserts to the outer, not the inner, membrane (Monlezun *et al.*, 2015). Despite forming a β-barrel for insertion into the outer membrane, TolC expressed without a signal sequence folds and forms trimers in the cytoplasm, with the β-barrel not inserted to a membrane (Masi *et al.*, 2009). In TolC, the internal pore diameter is approximately 20 Å at the membrane; this extends at an almost continuous diameter (fluctuating to as wide as 26 Å, but retaining a minimum diameter of 20 Å) approximately 60 Å into the periplasm, at which point it begins to narrow to a diameter of less than 4 Å, closing the channel at the periplasmic end. The overall length of the channel is approximately 140 Å, of which 40 Å consists of the outer membrane β-barrel, and the remaining 100 Å is an α-helical barrel-type assembly extending into the periplasm from the outer membrane. The structure of TolC is shown in Figure 1:5. The occlusion at the periplasmic end prevents the channel from simply acting as a large porin, and

occurs due to the twisting of α-helical coiled coils, of which the lower portion of the periplasmic domain is formed (Figure 1:6).

At the very tip of the coiled coils, there is a network of charged and polar residues, which interact to form a "gate" that must be opened before any efflux activity is possible (Andersen *et al.*, 2002a; Andersen *et al.*, 2002b). Mutational analysis shows that disruption of this network results in a channel which is constitutively open (Bavro *et al.*, 2008; Pei *et al.*, 2011). A second "gate" is present a few helical turns up the inside of the coiled coils, which can consist of either a pair of rings of aspartate residues, or one acidic and one hydrophobic ring (Andersen *et al.*, 2002c; Vediyappan *et al.*, 2006). Opening of the wild-type channel requires its interaction with a MFP – though some channel proteins form part of several efflux complexes within a single species: in *Salmonella enterica*, at least seven transporter/MFP pairs utilise one channel protein, TolC (Horiyama *et al.*, 2010).

These proteins also contain a mixed α-helical/β-stranded "equatorial domain" that forms a ring around the simple tube approximately halfway along the periplasmic portion. While parts of the equatorial domain are essential for TolC function (Yamanaka *et al.*, 2001; Yamanaka *et al.*, 2002; Yamanaka *et al.*, 2004; Yamanaka *et al.*, 2007), exactly what the domain does or why it is present remain unclear. This domain is formed from both the N- and C-termini, plus a 34 amino acid sequence in the middle of the mature protein. A structural repeat is visible in TolC, leading to the suggestion that a gene duplication event took place (Koronakis *et al.*, 2000), in which the second "copy" would start within the equatorial domain. The extent to which the sequence is also repeated within the structural repeat is assessed in Chapter 3.2, including figures showing the sequence and structural repeats.

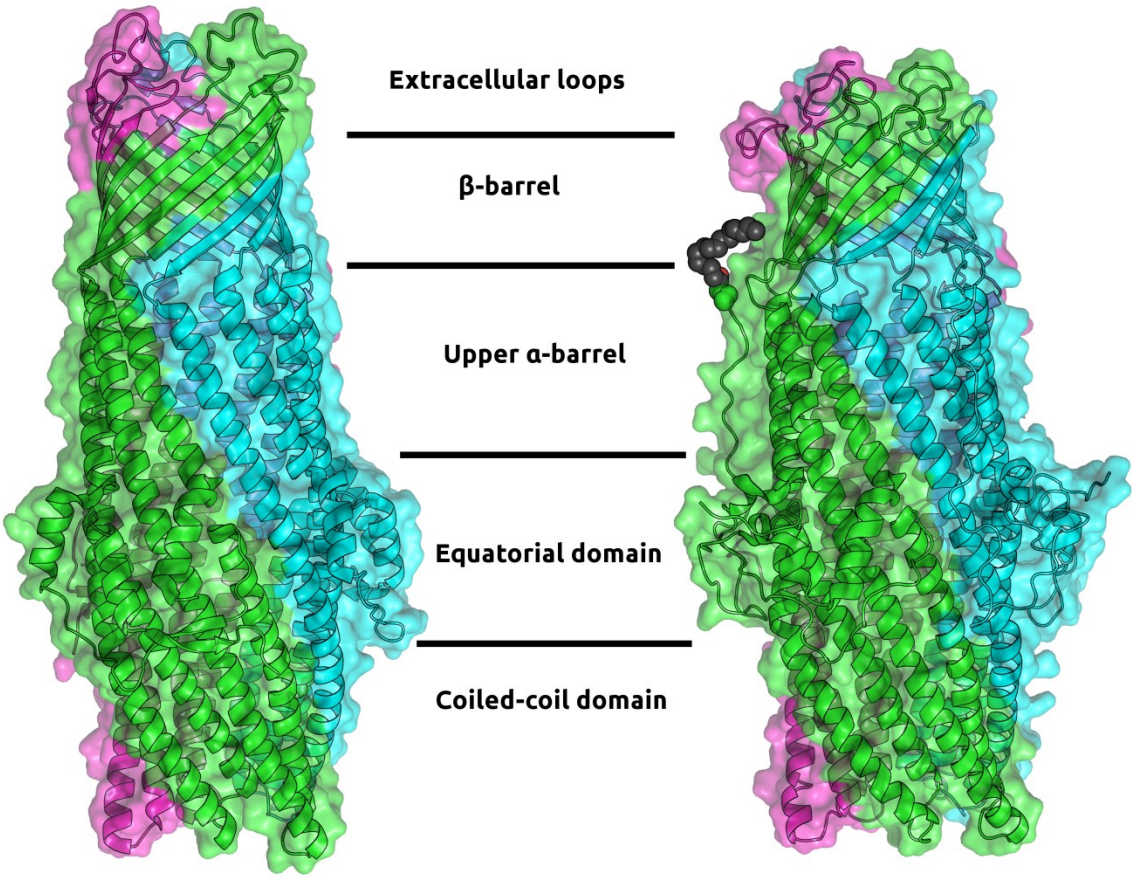

Figure 1:5 - Structure of outer membrane channel proteins.
Crystal structures of TolC (left; 1EK9) and OprM (right; 4Y1K) are shown in both ribbon and transparent surface representation with each protomer in a unique colour. The N-terminal cysteine residue and palmitoyl group of a single protomer of OprM are shown in spacefill, with the palmitoyl group in grey.

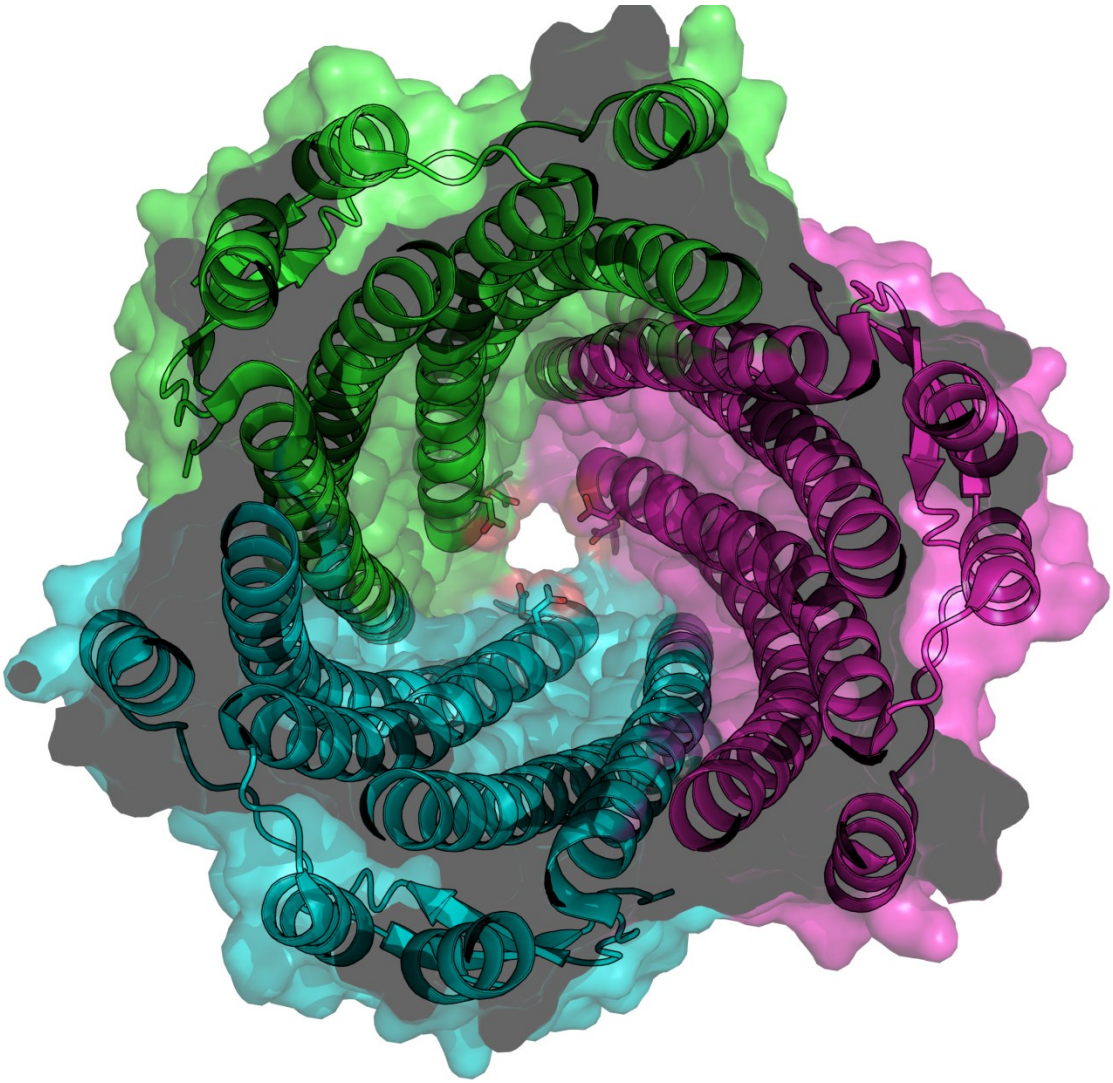

Figure 1:6 - The TolC channel is occluded at the periplasmic tip.
Viewed from a section through the equatorial region towards the periplasmic tip of TolC, the protein becomes occluded towards the periplasmic end, with clear constriction visible from the surface which, when properly ion-coordinated, is too narrow even to allow passage of water. The two aspartate rings (D371 and D374) are shown in stick form at the periplasmic end of the TolC lumen.

1.5.2 Membrane fusion proteins

Membrane fusion proteins consist of several domains, as they must interact specifically with both their cognate transporter and channel proteins. Of particular interest to this thesis is AcrA, the cognate MFP of the main MDR efflux pump AcrB. The presence and size of certain domains within MFPs are determined by the type of transporter with which they function (Symmons *et al.*, 2015). Separating the domains are flexible regions that appear to act like hinges (Mikolosko *et al.*, 2006); such flexibility must be considered during any docking modelling.

Most MFPs have a hairpin (helix-turn-helix) structure to contact the channel protein – for ease of nomenclature, the loop of the helix-turn-helix, and one complete helical turn each side of it, is referred to as the hairpin tip. The length of the hairpin, determined in helical turns, is dependent mainly upon how large a periplasmic domain the transporter possesses (Symmons *et al.*, 2015). It thus follows that MFPs that function with RND transporters, which have large periplasmic domains, require relatively short hairpins, while those that function with an MFS transporter require much longer hairpins as they must bridge a substantial gap between the transporter and channel proteins. Somewhat illogically, at eight helical turns (approximately 58 Å), the hairpin of AcrA is longer than that of MexA (Akama *et al.*, 2004; Higgins *et al.*, 2004a; Mikolosko *et al.*, 2006), its homologue from *Pseudomonas aeruginosa*, even though *P. aeruginosa* has a wider periplasmic space than *E. coli* (Matias *et al.*, 2003). One example of an MFP lacking the hairpin domain entirely, instead having a loop, has been found from the spirochete, *Borrelia burgdorferi* (Greene *et al.*, 2013). Although homology modelling suggests that the cognate channel protein, BesC, lacks some of the interactions that maintain its normal closed state (Bunikis *et al.*,

2008), the implications of the lack of a hairpin domain, such as in BesA-BesC and possibly BesB-BesC interactions, have not been studied.

All MFPs characterised to date contain both lipoyl and β-barrel domains. Both of these domains consist entirely of β-strands and connecting loops, and are required for normal function. Each of these domains can be cross-linked to the transporter protein, suggesting that one of the roles of these domains is to interact with the transporter component of the complex (Symmons *et al.*, 2009). More direct evidence for this role within the β-barrel domain has been seen from adaptive mutagenesis, whereby a non-cognate transporter was utilised with the MFP and mutations tested for gain-of-function to determine which positions are required to determine specificity between two proteins (Krishnamoorthy *et al.*, 2008).

MFPs associated with transporters that have large periplasmic domains usually have a membrane-proximal domain. Via lipidation of an N-terminal cysteine residue (C25 in AcrA), this domain tethers the MFP to the inner membrane (Zgurskaya & Nikaido, 1999). This same cysteine residue is also essential for normal signal sequence cleavage on AcrA (Kawabe *et al.*, 2000). In MFPs associated with transporters lacking a large periplasmic domain, the lipidated membrane-proximal domain is not present; these proteins instead have a transmembrane helix for anchorage (Hinchliffe *et al.*, 2014). As with the lipoyl and β-barrel domains, membrane-proximal domains interact with the transporter proteins (Elkins & Nikaido, 2003; Ge *et al.*, 2009). On the available crystal structure of AcrA (2F1M), the membrane-proximal domain is missing as it had been proteolytically removed prior to crystallisation. Without the membrane-proximal domain, the total length of the AcrA protein is approximately 105 Å (Mikolosko *et al.*, 2006), meaning it is capable of spanning around half of the total periplasmic distance of 180-235 Å (Matias *et al.*, 2003).

The roles of the MFP appear to be complex. At the simplest level, these proteins interact with the other components of tripartite complexes to stabilise an IMT-OMC assembly (Tikhonova & Zgurskaya, 2004), although stabilisation can only be true in RND-type systems, where the IMT contains large periplasmic domains, otherwise the MFP bridges a gap between the transporter and channel proteins. *In vitro* studies have shown that the MFP is required for activation of the transporter protein, but only when a substrate is also present (Verchère *et al.*, 2012). This activation of the transporter is independent of the outer membrane channel protein, as the activity can be seen *in vitro* even in the absence of a channel protein. In heavy metal RND-type efflux systems, it has been shown that the substrate is passed from the MFP to the transporter (Bagai *et al.*, 2008; De Angelis *et al.*, 2010; Mealman *et al.*, 2012), and an investigation of pump inhibitors suggest that this is also a possibility for some substrates of multidrug efflux complexes (Abdali *et al.*, 2017). Constriction of the channel protein is relieved by the MFP, opening the channel ready for an efflux event (Janganan *et al.*, 2011). Such opening of the channel protein is independent of either a substrate or the transporter protein, as shown by determination of susceptibility to vancomycin (a drug which is too large to efficiently traverse the outer membrane unless a wide channel such as TolC is available) for combinations of complex components and mutants thereof (Janganan *et al.*, 2013).

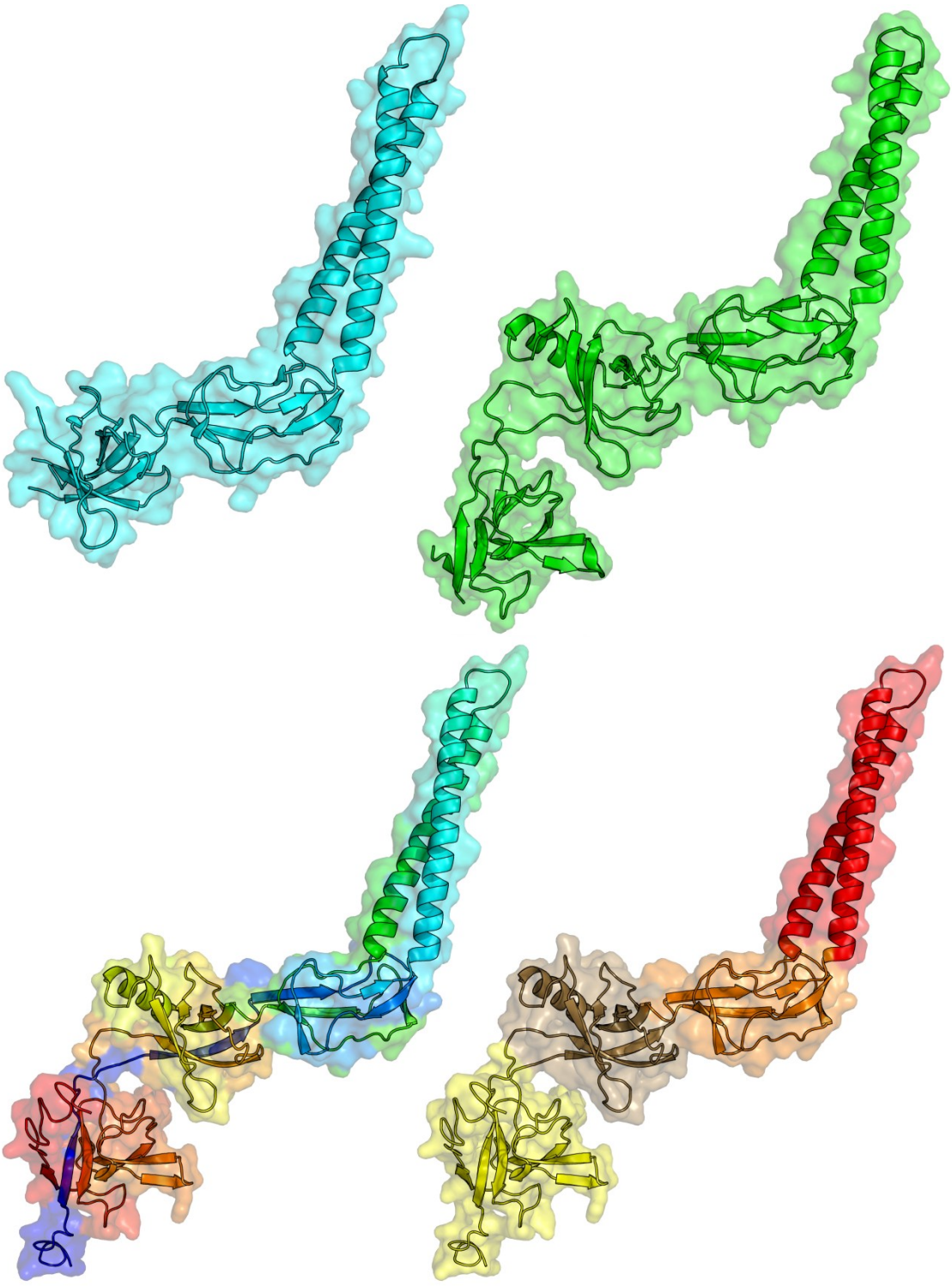

Figure 1:7 - Structure of MFPs.

Top: The crystal structures of AcrA (2F1M, left) and the re-refined structure of MexA complete with the membrane-proximal domain (2V4D, right). Bottom: a homology model of the complete AcrA structure showing the protein coloured by sequence (left) and domains (right). The domains are uniquely coloured: yellow – membrane-proximal domain, brown – β-barrel, orange – lipoyl , red – hairpin.

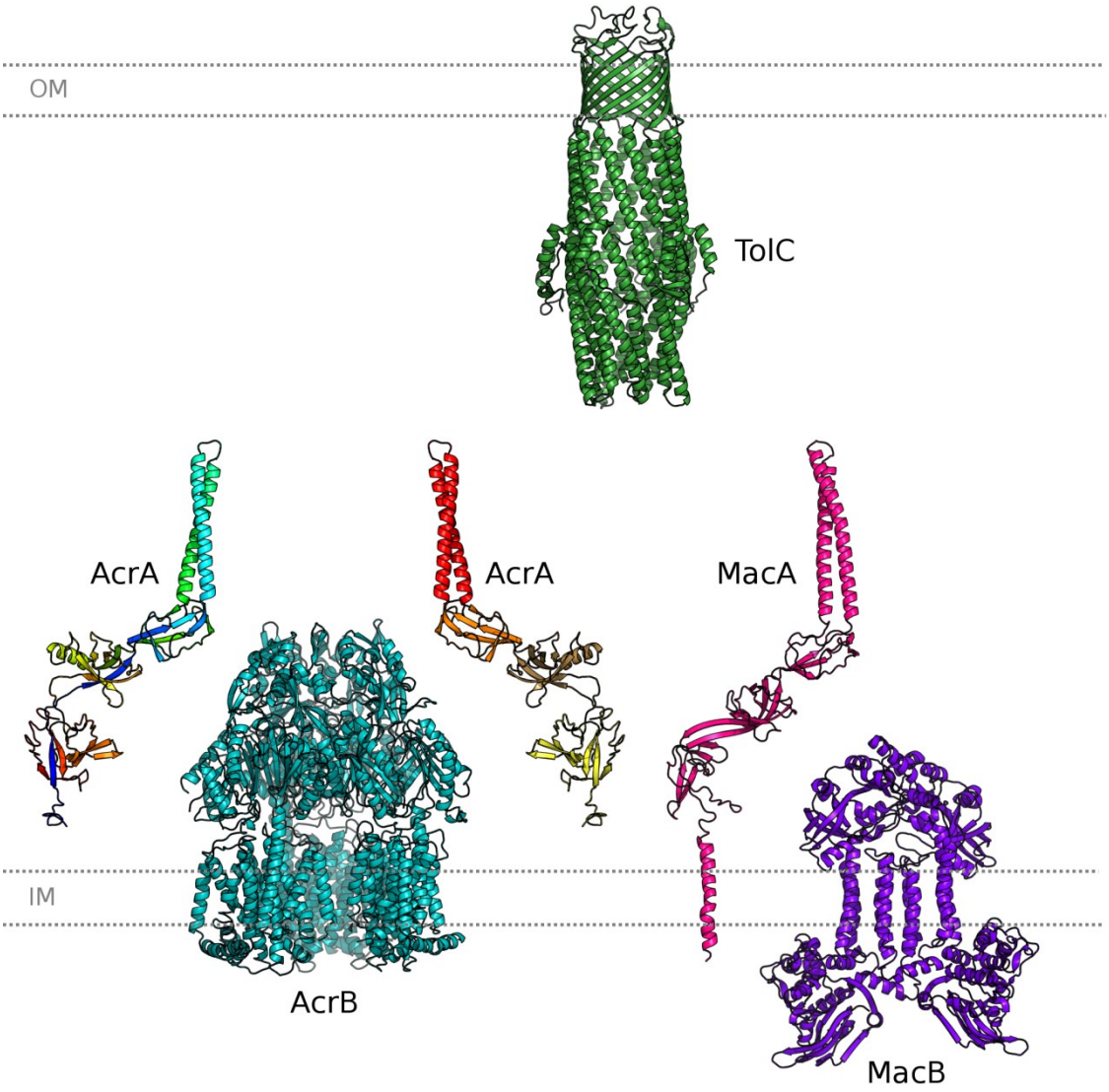

Figure 1:8 - Exploded view of tripartite complexes.
Distances are not shown to scale, and the distances between proteins should not therefore be taken as representative of a model of interaction. Two transporters which function in association with TolC are shown: the RND transporter AcrB (1IWG) and ABC transporter MacB (manually generated homology model), as the physiologically relevant trimer and dimer, respectively. The OMC protein TolC (1EK9) is shown in the closed state of its physiological trimer. The MFPs MacA (3FPP) and AcrA (full-length homology model based on 2F1M) are shown as monomers. The N-terminal lipidation of AcrA is not shown in either monomer, while the two monomers shown are coloured as in Figure 1:7.

1.5.3 Models of complete assembly

There are two general and opposing models of how the complete tripartite complex assembles (Figure 1:1010). Both of these do of course place the transporter protein within the inner membrane and the channel protein with its β-barrel in the outer membrane. In the classical model of interaction, the first to be proposed, there is a bundling of helices between the MFP and channel proteins, which allows for direct interaction between the channel and large transporter proteins such as RND transporters (Symmons *et al.*, 2009). One contributing factor for this model being the first proposed was that the top of the AcrB "TolC-docking domain" contains two β-hairpins per protomer (Figure 1:9), from which the interconnecting loops form a putative docking site that matches the diameter of the periplasmic tip of TolC (Koronakis *et al.*, 2000; Murakami *et al.*, 2002).

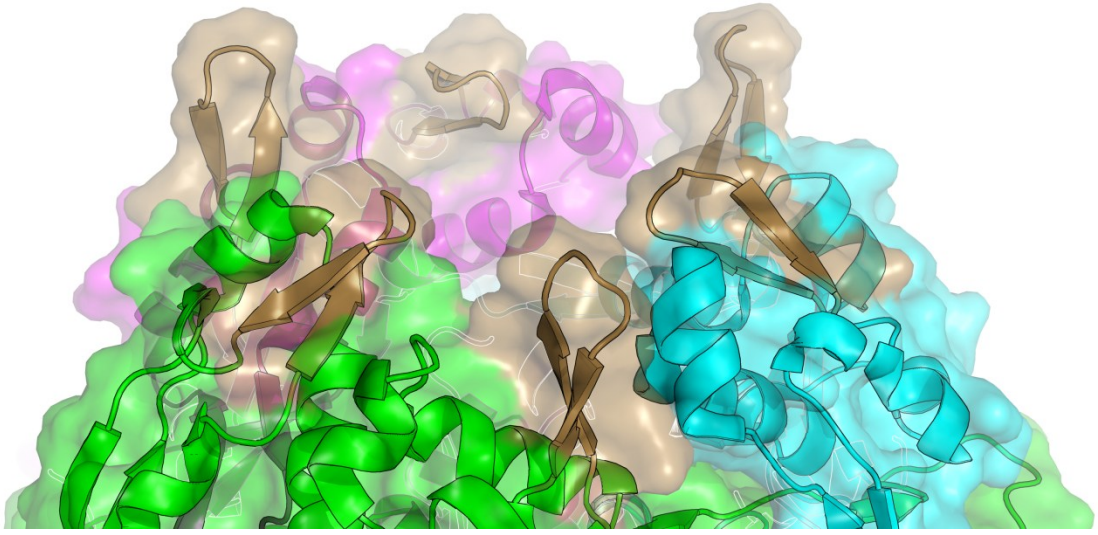

Figure 1:9 - Putative TolC-interactive loops of AcrB.
Each protomer of AcrB is shown in a unique colour, while the β-hairpins on all protomers are shown in brown. The diameter of the pore formed by the loops of these β-hairpins approximately matches that of the periplasmic tip of the static helices of TolC.

The later model, which was first proposed based upon crystal packing in structural studies (Yum *et al.*, 2009), suggests interaction between the MFP and channel only at the tips of their respective coiled coil structures. This spaces the transporter and channel proteins apart by at least the length of the MFP hairpin (Xu *et al.*, 2010). Henceforth, these models of assembly will be referred to as the "bundling" and "tip-to-tip" models, respectively. Research groups supporting either model argue that the other cannot be correct in light of available evidence for their preferred model (evidence for each model is presented in Sections 1.5.5 and 1.5.6 below). However, there is no logical reason why both cannot be correct but at different stages of the complex assembly/efflux event/complex disassembly process.

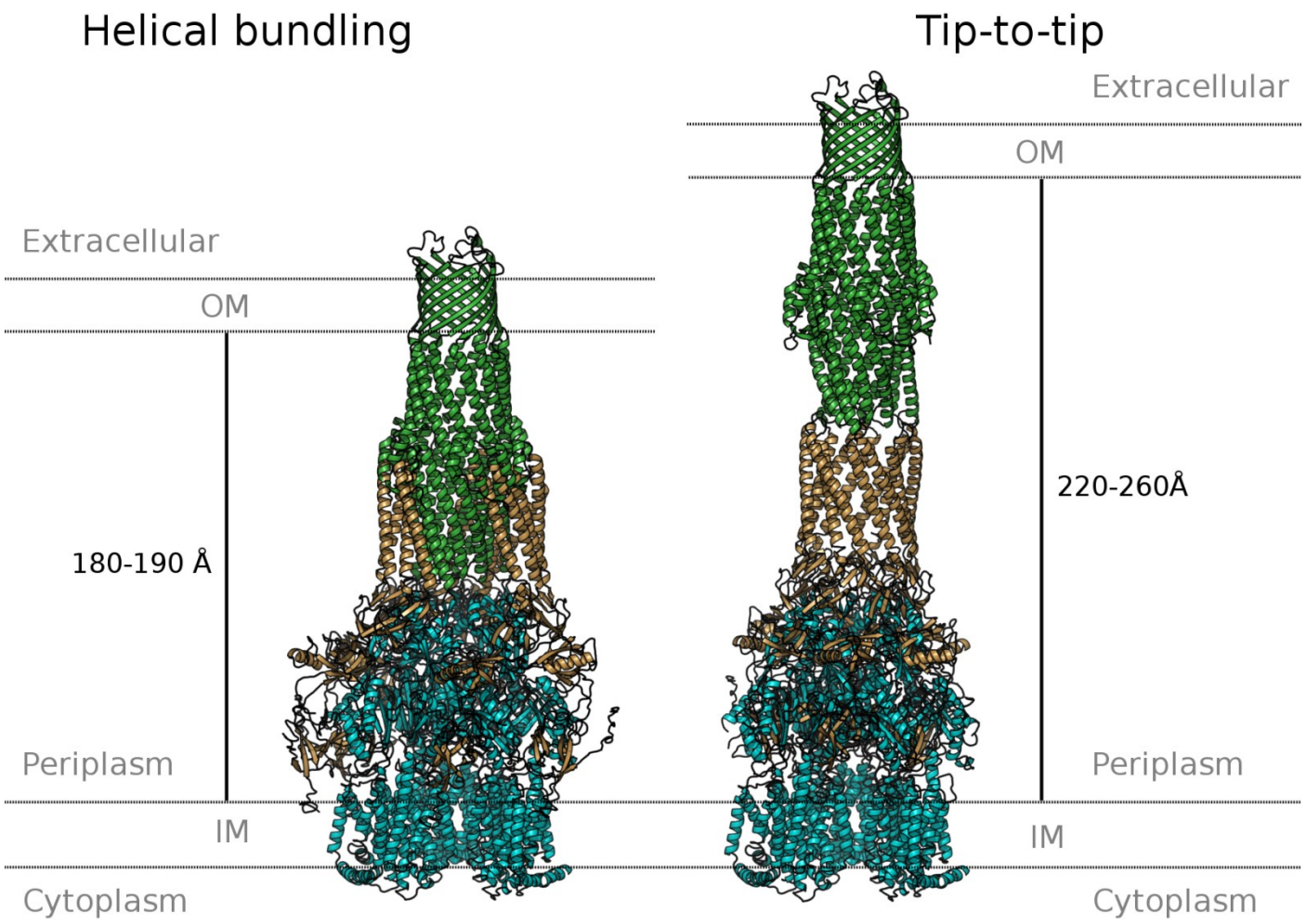

Figure 1:10 - The two models of tripartite assembly.

Representative depictions of the helical bundling and tip-to-tip models of assembly for the AcrA(brown)-AcrB(blue)-TolC (green) efflux complex. The inter-membrane distance is indicated for each model.

1.5.4 Stoichiometry of complex assembly

The stoichiometry of the complex is yet to be definitively determined, though the general consensus is that 3:6:3 transporter:MFP:channel is most likely in either model. Such consensus derives from multiple lines of evidence. Crystallographic studies show that MFPs often form dimers and some can form hexamers under crystallographic conditions (Akama *et al.*, 2004; Mikolosko *et al.*, 2006; Yum *et al.*, 2009). Genetic and functional analysis utilising AcrA-AcrA fusions shows that a forced dimer is functional (Xu *et al.*, 2011a). Surface plasmon resonance studies show AcrA dimerisation to occur spontaneously upon lipidation, and that this increases affinity for AcrB (Tikhonova *et al.*, 2011). A natural complex which requires two unique MFPs has been identified (Weeks *et al.*, 2015). Electron microscopy images attempting to show the fully assembled complex directly show a 3:6:3 stoichiometry (Du *et al.*, 2014; Kim *et al.*, 2015; Daury *et al.*, 2016).

Despite this, it has also been shown that the AcrAB-TolC complex in *E. coli* is capable of functioning with 3:3:3 stoichiometry, as AcrA-AcrB fusions remain functional without any other copy of *acrA* (Hayashi *et al.*, 2016).

1.5.5 Evidence supporting the tip-to-tip model

A functional hexameric tube-like assembly of the MFP was first proposed upon solving of the MacA crystal structure (Yum *et al.*, 2009). While this structure indicated that MacA has the same general modular configuration of other MFPs, the crystal packing generated a hexameric tube. As this tube, formed from the hairpin domains, was approximately the same diameter as the α-barrel of TolC, the authors hypothesised that the α-barrels of the oligomeric MacA and TolC assemblies may sit one atop the other to form a continuous channel.

Following the structure being solved, a new conserved motif was identified at the tip region of the MFP hairpin – the RLS motif – which was proposed to be common and

essential (Xu *et al.*, 2010).When mapped to the crystal structure of AcrA (2F1M), the proposed RLS motif (RxxxLxxxxxxS, in which "x" is any amino acid) is shown to be located at the tip of the AcrA hairpin, with the arginine located on the N-terminal side of the loop turn, one helical turn down from the top of the hairpin, and facing away from the other helix. The leucine and serine positions are located at the ends of the loop turn, being the first and last amino acids not to form part of the helical structures. This RLS motif has been studied in various MFPs, with most of the mutations mapping to this motif published to date abolishing function and binding of MFP to OMF, summarised in Table 1:1.

Table 1:1 - Published mutations of the RLS motif.

Protein	Mutation	Capable of binding	Capable of functioning	Reference
MacA	R131A	No	No	(Xu *et al.*, 2010)
	L135D	No	No	
	S142D	No	No	
	S142A	Not tested	Yes	(Xu *et al.*, 2011b)
AcrA	L132C	Not tested	No	(Xu *et al.*, 2011a)
	R128D	Not tested	No	(Kim *et al.*, 2010)
	L132D	Not tested	No	
	S139D	Not tested	No	
MdsA	R135D	No	Yes	(Song *et al.*, 2014)
	L139D	No	Yes	
	S146D	No	Yes	

Chimaeric constructs of *Actinobacillus actinomycetemcomitans* (Aa) MacA on which the tip region was replaced by the tip regions of the TolC α-barrel have been analysed for structural formation with wild-type *E. coli* MacA by electron microscopy , and showed dumbbell-shaped structures with a central bulge (Xu *et al.*, 2011b).

Similar studies, replacing the hairpin tip of *E. coli* MacA with that of MexA or AcrA and the hairpin tip of Aa MacA with the tip regions of the OprM or TolC α-barrel showed the same bulged dumbbell-shaped structures (Xu *et al.*, 2011a; Xu *et al.*, 2012). In all of these studies the bulges in the structures were modelled as an intermeshing of the tip regions of the two proteins, with the TolC aperture fully opened. Furthermore, positions that may interact were identified from the MexA-OprM docking model, with the authors proposing that R119, L123 and S130 of the MexA RLS motif interact with the OprM backbone carbonyl group, V201/V408, and S138 of OprM, respectively, and that additionally, MexA L122 makes hydrophobic contacts with OprM V199/T406 (Xu *et al.*, 2012).

The latest evidence supporting either model comes from electron microscopy images of complete complexes and the 3D reconstruction based thereupon. These should generate an image of the most stable configuration of the complex, which can therefore be interpreted as being the structure of the complete complex. However, in practice it is far more difficult to get such direct analysis of these complexes. To date, only one study using wild-type proteins has been published to show the entire complex assembly (Daury *et al.*, 2016). Others have made use of highly engineered proteins that are likely to alter the complex assembly (Du *et al.*, 2014; Kim *et al.*, 2015). It must also be remembered that all structural studies require isolation of the proteins, therefore the proteins are analysed in an unnatural environment, which may also affect the binding of the component proteins. Finally, these studies identify only a single state – the complex in its most stable configuration under the artificial conditions to which it is subjected – while the complex must be dynamic in the cell as it assembles and disassembles. Though the electron micrographs may therefore look convincing and conclusive, questions remain. All of these studies have identified a tip-to-tip type interaction, indicating that this model is almost certainly accurate during some stage of the efflux cycle.

1.5.6 Evidence supporting the bundling model

Studies utilising more traditional biochemical and mutagenesis approaches conflict with the results from electron microscopy. Both cross-linking experiments and isothermal titration calorimetry show that the transporter and channel proteins are in close proximity and interact directly, which is entirely incompatible with the tip-to-tip model (Touzé *et al.*, 2004; Tamura *et al.*, 2005; Tikhonova *et al.*, 2011). Mutation to the β-hairpins on AcrB decreases efflux activity, while suppressor mutations appear to stabilise the entire complex or facilitate TolC opening (Weeks *et al.*, 2014). From isothermal titration calorimetry, it is seen that transporter-channel binding is enhanced at mildly acidic pH, but hindered by drug binding, suggesting that the two proteins might not be in direct contact during the actual efflux event. Other cross-linking experiments have shown that positions along the entire length of the MFP hairpin can be cross-linked to the channel, and that positions high up the channel protein, as high as the equatorial domain, can be cross-linked to the MFP (Lobedanz *et al.*, 2007).

Mutagenesis studies both with cognate partners and generating gain-of-function mutants to function with non-cognate partners, show that positions along the entire MFP hairpin and throughout both the coiled-coil and equatorial domains of channel proteins are required for functionality (Yamanaka *et al.*, 2004; Bokma *et al.*, 2006; Vediyappan *et al.*, 2006; Lee *et al.*, 2012). Again, these results are incompatible with the tip-to-tip model. Such evidence for the bundling model might indicate that *in vivo*, the conditions are more favourable for this model than for the tip-to-tip model, while the conditions used *in vitro* are usually less favourable. They also suggest that stretching and contracting of the assembly might occur during efflux, to switch between the two models.

1.5.7 Specificity of interactions

Individual channel proteins are capable of functioning with a variety of transporter-MFP pairs. As these interactions are selective and not random, this poses conflicting considerations at the interaction interface – the interface on different MFPs that share a channel must be very similar, while interfaces on MFPs that are not capable of functioning with those same channels must be quite different. For example, AcrA and MacA from *E. coli* both function with TolC (Fralick, 1996; Kobayashi *et al.*, 2001), but do not function with OprM from *P. aeruginosa* (Stegmeier *et al.*, 2006), while MexA from *P. aeruginosa* functions with OprM but not TolC (Bokma *et al.*, 2006). It would therefore be expected that the interfaces presented by AcrA and MacA would be very similar while that presented by MexA would be quite different. In *Pseudomonas aeruginosa*, the requirement for specificity is exaggerated by the presence of multiple channel proteins and RND systems (Yoshihara *et al.*, 2002), which are only partially cross-reactive despite their structural similarity (Maseda *et al.*, 2000; Phan *et al.*, 2015; Yonehara *et al.*, 2016).

Trying to fit these factors into the two models suggests that the bundling model is more likely than the tip-to-tip, given the relative sizes of their interfaces. Early evidence in support of the tip-to-tip model identified the RLS motif, which was hypothesised to be conserved in all MFPs as it represents the MFP-side of the interface. Opponents to the tip-to-tip model point out that such a conserved interface would break the rule regarding specificity of the interaction, as all MFPs with that interface should function with all of the channels that normally function with any MFP that contains it (Symmons *et al.*, 2015). Later developments showed that this proposed motif is neither always present, nor always located at the tip of the MFP hairpin, even when comparing MFPs which pair with a common channel (Kim *et al.*, 2016).

To further complicate the issue, it is necessary to separate the concepts of interaction and functionality. A combination of proteins that does not show activity in an assay may still form a complex, even if it is non-functional, as several studies have shown (Bokma *et al.*, 2006; Stegmeier *et al.*, 2006; Vediyappan *et al.*, 2006). The proteins can therefore form a complex, but may be missing a crucial interaction required to enable efflux activity. As such, any study investigating the interaction interface must consider both the structural and functional aspects, in addition to how any potential interface would fit into the rules about functioning very specifically with a small variety of partners.

1.5.8 Energy requirements within the complex

To transport a substance against its concentration gradient, as is the case during antibiotic efflux, energy is required by the pump protein. As mentioned earlier, this energy is provided either by ATP hydrolysis, the proton motive force or another electrochemical gradient, dependent upon the pump type. The requirements for assembly of an MFP and channel protein was first shown in a type 1 secretion system, in which the substrate was required for assembly but ATPase activity was not (Thanabalu *et al.*, 1998). If the same were true in multidrug transporters, then the transporter and MFP would be expected to assemble as an inner membrane complex, which would then engage the channel protein upon binding of the substrate, regardless of whether or not an energy source was present.

In RND complexes, each component is capable of interacting with each of the others, even in the absence of either the third component or any substrate (Tikhonova *et al.*, 2011). While assembly of the full complex appears to be independent of the availability of an energy source, the *in vitro* affinity between MFP and channel protein is higher at mildly acidic pH, suggesting that the presence of the energy source will

likely stabilise the complex (Tikhonova *et al.*, 2009). However, this effect is observed in the absence of the transporter protein or a substrate, so it is clearly not the case that transport activity stabilises the assembly. Therefore, the actual interactions between MFP and channel protein are stabilised by the decreased pH. Whether this is purely a pH-dependent effect on the protein interfaces or if it is related to the availability of an energy source remains to be seen – equivalent experiments investigating ABC systems may be required for this. The presence of ATP, and thus the presence of the energy source, stabilises the interaction between the MacB ABC transporter and its cognate MFP, MacA, suggesting that energy availability may increase complex stability (Lu & Zgurskaya, 2012).

While some papers refer to MFPs transducing energy from the transporter to the channel protein to induce opening of the channel, it is well-documented that opening of the channel requires no such transduction of conformational information (Tikhonova & Zgurskaya, 2004; Janganan *et al.*, 2013). Both TolC from *E. coli* and MtrE from *Neisseria gonorrhoeae* have been shown to open in the absence of a functional cognate transporter protein, indicating that transporter activity and channel opening are not linked. However, the same studies also show that an MFP must be present to induce channel opening, in an energy-independent manner. The channel must not be dilated prior to complex formation, as the channel in an open state is unable to efficiently bind either the MFP or transporter protein (Tikhonova & Zgurskaya, 2004). Consistent with this, the complete complex is unable to form from a channel-MFP pre-assembly – presumably because the MFP-bound channel is open (Tikhonova *et al.*, 2011), further supporting the notion that energy is not required for either complex assembly or channel opening.

Use of an MtrE mutant which is hypersensitive to vancomycin when its cognate MFP (MtrC) is also present, shows that energy is required for dissociation of the complex

(Janganan *et al.*, 2013). Cells expressing this MtrE mutant, MtrC, and the RND transporter MtrD are mildly sensitive to vancomycin, while those expressing an inactivated mutant of MtrD, in which the proton relay network is disrupted, are resistant. This is explained by the transporter plugging the end of the channel to prevent vancomycin influx – the inactive mutant always plugs the channel because the lack of energy transduction prevents complex dissociation. These experiments are explained visually in Figure 1:11.

The energy requirement for dissociation of the complex has been shown directly by pull-down assays with wild-type and proton-relay-deficient RND transporters using an *in vitro* system. The OMF could only be pulled-down with the wild-type transporter in the absence of a proton gradient, while it always pulled-down with the inactive transporter, regardless of the proton gradient (Enguéné *et al.*, 2015). Although the use of an outer membrane channel protein allows extrusion of the drug entirely out of the cell, the channel protein is not essential for transporter activity, as seen *in vitro* (Verchère *et al.*, 2012). Each of the transporter, MFP, proton gradient and a substrate must be present, however, for maximum activity to be observed (Verchère *et al.*, 2014).

Within RND multidrug efflux systems, energy is therefore required for substrate translocation and for complex dissociation. Energy is **not** required for complex assembly or channel opening, and the channel protein does not contribute to utilisation of the energy source by the RND transporter.

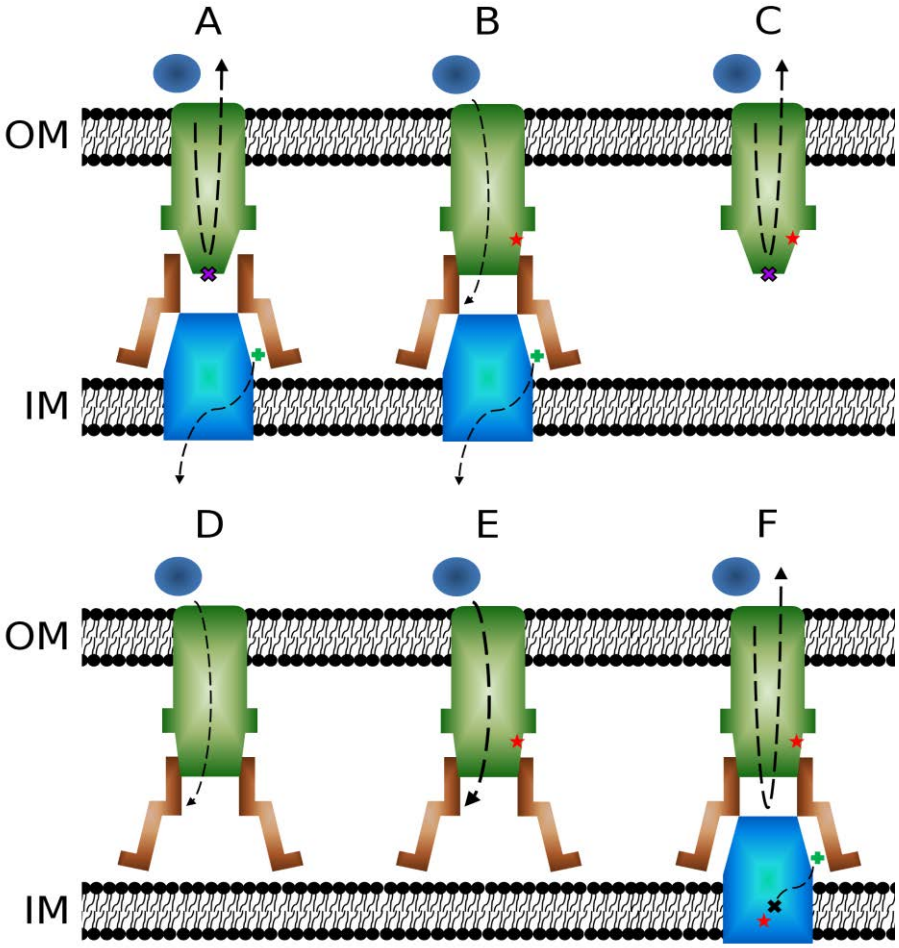

Figure 1:11 - Energy is required for disassembly but not opening of the OMC. This figure summarises the conclusions made by Janganan *et al.* (2013). Light blue - MtrD RND-pump; brown – MtrC MFP; green – MtrE outer membrane channel protein; dark blue – the large efflux-restricted drug vancomycin; green plus symbol – protons; red star – approximate position of mutation; crosses – transport is blocked. The wild-type MtrCDE complex (A) does not allow penetration of vancomycin. Introduction of the E434K mutation in MtrE to the entire complex (B) causes a low increase in susceptibility to vancomycin, although the mutation does not cause the channel to become constitutively open (C). MtrCE only (D), lacking the pump component, shows low-level susceptibility, indicating that the pump component is not required for channel opening. MtrC-MtrE(E434K) causes much higher susceptibility to vancomycin (E), suggesting that the mutation prevents channel closing. An inactive mutant of MtrD blocks the periplasmic end of the channel to prevent vancomycin entry to the cell (F) even when the channel cannot close – combined with the information from panels B and E, this indicates that energy is required for disassembly of the complex and normal closure of the channel protein.

1.6 Efflux pump inhibitors

Efforts to identify inhibitors of efflux pump activity have yielded mixed results. While compounds have been identified which achieve this function, not all are inhibitors of the pumps, their effect instead coming by removal of the energy source. An inhibitor commonly used in research studies, CCCP (Carbonyl cyanide m-chlorophenyl hydrazone) is a protonophore and thus causes inhibition by chelating the protons that would otherwise generate proton motive force - while this is an effective inhibitor for *in vitro* studies, it is not a specific inhibitor of efflux pumps and cannot be considered for combinatorial therapy in clinical practice (Coldham *et al.*, 2010). There are, however, some substances that have been shown to competitively and non-competitively bind to RND transporters, such as another inhibitor commonly used in research studies, phenylalanine-arginine-β-naphthylamide (PAβN). PAβN has been shown to competitively inhibit RND transporters such as AcrB (Vargiu *et al.*, 2014), but given that it is a substrate of AcrB, it is only effective at relatively high concentrations. Some researchers also question whether or not the apparent decrease in efflux activity caused by PAβN is purely due to its pump inhibition, as it appears that PAβN may permeabilise the outer membrane (Lamers *et al.*, 2013), thus increasing influx. As most studies indirectly measure the net movement of molecules, without separation of influx or efflux, the increased rate of influx would appear the same as a decrease in efflux activity in these experiments.

A new series of efflux pump inhibitors (the MBX series of pyranopyridine derivatives) has been identified which do not show any bactericidal or membrane permeabilising activity (Sjuts *et al.*, 2016). The first of these compounds to be confirmed as a pump inhibitor has been co-crystallised with AcrB, identifying the exact binding position and the residues involved in the interaction. From the crystal structure, it was clear that a water-filled cavity between the inhibitor and AcrB binding pocket had formed. This information was used to develop new inhibitor compounds with improved

binding capacity, to fill the cavity - representing the first time that an efflux inhibitor has been successfully designed based upon information derived from a crystal structure of the pump in complex with an inhibitor. This series of inhibitors binds a hydrophobic pocket adjacent to the distal binding pocket, and locks the conformational state of the protein, thereby preventing the peristaltic action of the pump. This would seemingly require only a relatively minor mutation to arise in order for the inhibitor to be rendered ineffective, and therefore poses a threat to the potential clinical use of efflux pump inhibitors. It also remains to be seen whether or not mutations in or over-expression of alternative efflux pumps may occur to ultimately mask the effect of the inhibitor in a clinical setting, as the inhibitor may be revealed as highly selective for only certain transporters.

Apart from inhibiting the translocation activity of the transporter component, addition of large radius multi-valent cations from the extracellular side has been shown to decrease the conductivity of TolC (Andersen *et al.*, 2002c). Added cations form ion bridges with the aspartate ring located just inside the lumen at the periplasmic end of the protein. This has been shown both from conductance experiments comparing wild-type protein with mutants lacking the aspartate rings, and by resolving the structure of TolC crystals soaked with hexamine cobalt (Higgins *et al.*, 2004b).

1.7 Inhibiting complex assembly

As an alternative to inhibiting the pump activity directly, it may be possible to instead target assembly of the complex, at the level of the protein-protein interactions. While there are several theoretical interfaces (transporter-MFP, transporter-channel, MFP-channel, MFP-MFP), finding exactly what these interfaces are remains a challenge. The efflux system is clearly a dynamic one – as discussed earlier, the

complex assembles and disassembles while the channel opens and closes and the transporter undergoes conformational changes to pump the substrate. Meanwhile, all of the approaches available, except for computational molecular dynamics simulations (Vargiu *et al.*, 2014; Sjuts *et al.*, 2016), are incapable of being interpreted in a time-resolved manner. While molecular dynamics are providing insights into each of the individual components of the systems, they become limited at the complexity of the entire assembly, as the number of possible outcomes increases with system complexity and a consensus therefore becomes less likely.

Each of the theoretical interfaces may be targeted, but do any of them present a good candidate for inhibition? Perhaps the simplest interface to predict is that of the MFP homodimerisation face. From all available structural data, and from mapping of mutations in the MFP that compensate for inactivating mutations in channel proteins, the lipoyl domain of the MFP almost certainly contains at least some of the dimerisation interface. In the tip-to-tip model of interaction, the hairpin domain also forms a dimerisation interface – in the bundling model, this same interface would instead interact with the channel. The largest and most complex of the potential interfaces is that between the transporter and MFP; the implication being that this is not a promising therapeutic target, as it would be most prone to mutation. The smallest of the possible interfaces lies between the transporter and channel, but the existence of such an interface is disputed, in spite of the body of evidence in support of a direct interaction between these two proteins. In a transporter-channel interface, the face on the channel would be the same as that in the tip-to-tip model interface between channel and MFP – suggesting that this could be a promising candidate for interruption, as it may affect multiple interfaces and stages of the pumping cycle, thus being most resilient to mutation.

Regardless of the interaction that is disrupted, questions regarding what type of inhibitor to use, and how to administer it, will remain. The obvious candidates as inhibitors would be small peptides that specifically bind with high affinity to the target, out-competing the native cognate binding partner as a competitive inhibitor. Administration of such an inhibitor would not be trivial – the whole reason for targeting a tripartite efflux pump is that it removes toxic substances to the outside of a permeability barrier; that permeability barrier will also prevent access of the inhibitor to its site of action. It is widely accepted that only very short peptide chains, no more than six amino acids long, can be taken up by Gram-negative cells. Biotinylation of peptides has proven to enable peptides up to 31 amino acids in length to enter the Gram-negative cell, making use of the biotin uptake system, though this has not yet been shown to localise the peptide to the periplasm (Walker & Altman, 2005).

1.8 Project context: multidrug resistance

Antibiotic resistance is a growing global concern, and has been labelled by WHO as one of the three greatest threats to global health (Piddock, 2012). In 2014, antibiotic resistance was also made a Research Council UK strategic funding priority area, due to the potential threat posed to human health. Antibiotic resistance was described even before the introduction of antibiotics as therapeutic agents - indeed Fleming himself identified that some bacteria were unaffected by penicillin, in the very same paper as he first described the antibiotic (Fleming, 1929). Since therapeutic use of antibiotics began, emergence of resistant clinical isolates has always closely followed introduction of the drug (see Figure 1 in Clatworthy *et al.* (2007) for a diagrammatic representation of this). This emergence of resistance causes us to require new classes of antibiotic, but is also partly responsible for the lack of recent progress in

bringing new classes of antibiotic to market (Coates *et al.*, 2011; Piddock, 2012). Despite the difficulties in bringing new and effective classes of antibiotic to market, new antibacterial molecules are being developed, even of novel classes (O'Daniel *et al.*, 2014), and it remains to be seen whether or not these will be introduced for therapeutic use. A system has been developed (the isolation chip, or iChip) to grow previously unculturable soil-borne bacteria (Nichols *et al.*, 2010), recently leading to the identification of a new antibiotic to which the minimum inhibitory concentration (MIC) of *Staphylococcus aureus* did not increase over 25 days of serial passaging at sub-inhibitory concentrations (Ling *et al.*, 2015). The iChip approach to growing previously unidentified bacterial species from soil may provide the means required to identify further new antibiotics, as more soil samples are tested with the system.

Classical resistance mechanisms that were identified relatively early in the use of antibiotics relied upon inactivation or degradation of the drug by enzymatic action (Abraham & Chain, 1940; Kirby, 1944). Enzymatic action upon a drug affects only that drug or a family of chemically similar compounds. While this may cause a delay in successful treatment of an infection, treatment with a different class of antibiotic can usually circumvent the issue. Due to the inactivation of the drug, this enzymatic action has a detoxifying effect upon the environment local to the producer of the enzyme, thus allowing otherwise sensitive bacteria to survive in the same environment (Finkelshtein *et al.*, 2015).

Many antimicrobials are produced naturally, or are synthetic derivatives of a natural product. Those produced in nature must not kill the producing organism, and so the producer must have an anti-suicide system in place to resist the antibiotic. Clearly, if the organism that produced an antibiotic protected itself by enzymatically inactivating that antibiotic, then production of the antibiotic would have been a wasteful process, and resistance is therefore better achieved by alternative means.

Given that antibiotics generally bind a particular target and inhibit a particular process, having a "target" variant that enables the same process but to which the antibiotic cannot bind, is a useful way by which resistance can be achieved. Species of *Pseudomonas*, for example, which are common antibiotic-producers (Fuller *et al.*, 1971; Demain, 2009; Darabpour *et al.*, 2010), are known to utilise this method (Yanagisawa & Kawakami, 2003). This mechanism of resistance provides very high intrinsic levels of resistance to a particular substance or class of substances. Being a novel gene, this type of resistance can spread by gene transfer, particularly when these resistance genes are encoded on a plasmid or other mobile genetic element.

Accumulation of genes that provide resistance to specific antibiotics can lead to multi-drug resistance (MDR), though as this is a cumulative process, it is slow (Nikaido, 2009). MDR can otherwise arise from prevention of the increase of intracellular drug concentrations, which can be a result of either decreased membrane permeability or increased drug efflux (Nikaido, 1994). These changes can arise within a strain by a single mutation, for example by mutation in a non-coding gene regulatory region which increases efflux pump expression or decreases porin expression (Ohneck *et al.*, 2011; Fournier *et al.*, 2013), and can therefore spontaneously increase resistance to a variety of drugs.

All of the above may indicate that multidrug efflux pumps are a severe threat to humans. However, they may also prove to have uses beneficial for industrial processes. In a world moving away from fossil fuel use, biofuels are likely to become increasingly important. Engineering of AcrB has been shown to increase tolerance to short-chain alcohols which could be used as biofuels (Fisher *et al.*, 2014).

1.9 Challenges in preventing multidrug resistance

Put simply, we have become dependent upon antibiotics to support our population growth, and bacteria have become dependent upon their resistance mechanisms to survive our use of antibiotics. It is a variation of the Red Queen model of evolution, in which a species must continue to evolve purely to survive the evolution of its ecological neighbours, except that in this case, the "evolution" of human use of antibiotics is technological rather than genetic. The situation now appears to be one of the bacteria winning this arms race, as their natural evolution of resistance has outpaced our ability to find new and effective drugs (Fox, 1996). The non-specific nature of antibiotics also does not aid our cause. Our bodies naturally consist of more bacterial cells than human cells, of many different species and performing a variety of commensal tasks; antibacterial agents used to treat a bacterial infection do not only affect the pathogen in question, but most of the other bacteria present too, whether they are causing harm at the time or not. Our bodies also naturally produce antibacterial substances, such as bile salts, that encourage development of antibiotic resistance. There is evidence that dietary changes may also cause temporary increases in expression of multidrug efflux pumps (Fadli *et al.*, 2014); if a mutation leads to a strain becoming pre-adapted, this may give the strain an advantage over others that must instead respond to the change. This causes directionality to the evolution of the entire microbiota (towards antibiotic resistant), and also provides clearances and new bacterially-naïve niches to open for colonisation by bacteria that were not previously a part of the microbiota, increasing the threat for subsequent infection.

Multidrug efflux pumps are a major contributor to multidrug resistance, but some have other, possibly more ancient, functions that were discovered more recently than was their contribution to drug resistance (Poole, 2008). These functions may have once been, and possibly still are, the primary function of the pumps. Roles in

quorum sensing (Minagawa *et al.*, 2012), biofilm formation (Baugh *et al.*, 2012; Baugh *et al.*, 2014), acid survival (Deininger *et al.*, 2011), iron scavenging (Bleuel *et al.*, 2005; Tatsumi & Wachi, 2008), and host colonisation (Lin *et al.*, 2003), all mean that these multidrug efflux pumps may be essential outside the laboratory environment – despite knockout strains being perfectly viable in the laboratory. It is clear that efflux pumps are required for survival in the hostile environment of the host, and it appears that over-expression of the pumps, or mutation to alter their range of substrates, does not have the detrimental effect that would be required to prevent the spread of the multidrug resistance thus conferred. The spread of multidrug resistance is therefore difficult to prevent because the fitness cost to the bacteria of being multidrug resistant is insufficient for the absence of antibiotic challenge to select for the susceptible strains. In the case of single drug resistances encoded on mobile genetic elements, the maintenance of the additional genetic material and expression of the genes causes a great enough fitness cost that over time, the resistant population is outcompeted, in the absence of antibiotic challenge, by the susceptible population. The population dynamics are therefore different between single drug resistance and multidrug resistance, with multidrug resistance being the more difficult to stop.

1.10 Gaps and conflicts within the literature, to be addressed

Crystal structures are available for representative proteins of each component within the tripartite multidrug efflux pumps. Docking of these into EM-generated structures of the complete assembly indicates a different method of interaction compared to that suggested by other biochemical and mutagenic approaches. Both of these models have been shown only in a static format. If neither model of interaction can

be categorically disproved using the approaches that support the other model, can the two models be reconciled in a dynamic system?

The available structures give little information as to the role of various regions of the MFP and OMC proteins. For example, the structures indicate that the OMC contains an equatorial domain around the outside of the channel, which has been shown to be essential for function, but what this domain does is unclear. Likewise, the MFP contains a hairpin structure which, when the cognate transporter has only a small periplasmic domain, makes sense to bridge the gap between the transporter and the channel, but why is this retained in RND-associated MFPs?

As stated above, the tripartite models available to date are static. The system is known to associate and dissociate dynamically. If functional roles of the sub-domain regions of the MFP and OMC, and the interaction interfaces, can be determined, a dynamic model of interaction needs to be developed.

1.11 Aims and objectives

The overall aim of this project is to develop a mechanistic understanding of the assembly of multidrug efflux complexes in Gram negative bacteria, particularly the assembly and disassembly at the MFP-OMC interface. This can be split into smaller aims:

1. Identify the interfaces presented by partner proteins for functional interaction.
2. Assign a role for positions within each interface with respect to the binding-extrusion-disassembly process.
3. Derive a dynamic model of complex assembly and disassembly.

To progress towards these aims, this project has the following objectives:

1. Make strains of *E. coli* suitable for analysing TolC and AcrA function *in vivo*, namely being a suitable knockout strain with a suitable expression plasmid.
2. Generate a library of mutations in both *tolC* and *acrA* that might impact the interface between the TolC and AcrA proteins.
3. Identify which mutations likely have an effect on efflux pump function by screening the mutations using *in vivo* functional assays.
4. Confirm that the effects observed are due to functional effects and not due to low protein production or protein instability.
5. Confirm that the effects observed are due to a difference in efflux activity and not due to other effects on general cellular function, using purified protein for *in vitro* assays.
6. Identify whether pump deficiencies are due to loss of interaction, or whether a non-function complex forms, using *in vitro* assays.

CHAPTER 2: MATERIALS AND METHODS

2.1 Bacterial strains used in this study

E. coli strains BW25113 (Datsenko & Wanner, 2000), the BL21-derivative C43(DE3) (Miroux & Walker, 1996), and the Keio collection strains (Baba *et al.*, 2006) JW5503 (here referred to as BW *tolC::aph*), JW0451 (BW *acrB::aph*) and JW0452 (BW *acrA::aph*) were provided by Dr Faye Morris in the laboratory of Professor Ian Henderson at University of Birmingham. Strains C43*acrA::aph* and C43*acrB::aph* were made by P1 transduction from the relevant Keio collection strains. Strain C43 *tolC::aph* was made by homologous recombination with PCR products. Strains BWΔ*tolC,* BWΔ*acrA*, C43Δ*acrA*, C43Δ*acrB* and C43Δ*tolC* were made by curing of the *aph* cassette using pCP20, as described at the end of Section 2.7.1.

Table 2:1 – List of strains used in this study, and their genotypes

Strain	Genotype	Description	Source
MG1655	F^-, $lambda^-$, rph-1	A "wild-type" *E. coli* laboratory strain	(Blattner *et al.*, 1997)
BW25113	F^-, DE(araD-araB)567, lacZ4787(del)::rrnB-3, LAM^-, rph-1, DE(rhaD-rhaB)568, hsdR514	A "wild-type" *E. coli* laboratory reference strain, the parental strain for the Keio library	(Datsenko & Wanner, 2000)
BW *acrA*::*aph*	As BW25113, additionally *acrA*	BW25113 with the *acrA* gene replaced by a kanamycin resistance marker	(Baba *et al.*, 2006)
BW *acrB*::*aph*	As BW25113,	BW25113 with the *acrB*	(Baba *et al.*, 2006)

	additionally *acrB*	gene replaced by a kanamycin resistance marker	
BW *tolC*::*aph*	As BW25113, additionally *tolC*	BW25113 with the *tolC* gene replaced by a kanamycin resistance marker	(Baba *et al.*, 2006)
BWΔtolC	As BW *tolC::aph*, with *aph* gene replaced by Frt-recognition scar	BW *tolC::aph* with *aph* kanamycin marker removed by pCP20	This study
BWΔacrA	As BW *acrA::aph*, with *aph* gene replaced by Frt-recognition scar	BW *acrA::aph* with *aph* kanamycin marker removed by pCP20	This study
BL21-C43 (DE3) (also referred to as C43)	ompT, hsdSB (rB-mB-), gal dcm (DE3), (with other unpublished differences to BL21 strain)	A laboratory strain of *E. coli* capable of expressing membrane proteins at higher levels than other strains, due to deficiency in the OmpT protease. Contains DE3 - the T7 phage RNA polymerase under control of the Lac repressor. Differs from other strains developed for high expression by	Miroux & Walker, 1996

		unpublished mutations.	
C43 *acrA*::*aph*	As C43, additionally *acrA::aph*	C43 with the *acrA* gene replaced by a kanamycin resistance marker	This study
C43 *acrB*::*aph*	As C43, additionally *acrB::aph*	C43 with the *acrB* gene replaced by a kanamycin resistance marker	This study
C43 *tolC*::*aph*	As C43, additionally *tolC::aph*	C43 with the *tolC* gene replaced by a kanamycin resistance marker	This study
C43 Δ*acrA*	As C43 *acrA::aph*, with *aph* gene replaced by FRT-recognition scar sequence	C43 *acrA::aph* with *aph* kanamycin marker removed by pCP20	This study
C43 Δ*acrB*	As C43 *acrB::aph*, with *aph* gene replaced by FRT-recognition scar sequence	C43 *acrB::aph* with *aph* kanamycin marker removed by pCP20	This study
C43 Δ*tolC*	As C43 *tolC::aph*, with *aph* gene replaced by FRT-recognition scar sequence	C43 *tolC::aph* with *aph* kanamycin marker removed by pCP20	This study

2.2 Plasmids used in this study

The plasmids pET26b and pKD46 were gifted by Dr Douglas Browning of University of Birmingham, and pCP20 was gifted by Dr Faye Morris. The vector pASK-IBA13plus was purchased from IBA-Lifesciences, and was converted to the vector of choice for the *in vivo* work in this study, pASK-RM, as described below. Plasmids pEX-K4-acrA(Δhelices) and pEX-K4-acrA(Δhairpin) were purchased from Eurogentec under the gene synthesis service.

Plasmid pASK-RM was generated from pASK-IBA13plus by three rounds of site-directed mutagenesis-type manipulation, as described in Section 2.5.7 (figures indicating the changes made are also in Section2.5.7 – Figures 3:1 to 3:4). The first round used the pASK-NdeI-F and pASK-NdeI-R primers, the second round used pASK-altNde-F and pASK-altNde-R primers, and the final round pASK-STOP-F and pASK-STOP-R primers. Incorporation of the required changes was tested by NdeI (New England Biolabs) digest, NdeI/XhoI (New England Biolabs) double digest or by sequencing using either the pASK-seq-F or pASK-seq-R primers. Digest reactions were set up according to manufacturer's instructions, and the digest incubations were 1 h at 37°C. Digests were resolved on 1% agarose stained with SYBRsafe (Invitrogen), against Hyperladder I (rebranded as 1 KB DNA ladder; Bioline), and visualised on a GelDoc system (Syngene).

The plasmids pASK-*acrAB* and pASK-*tolC* were generated by restriction cloning (Sections 2.5.4and 2.5.5) of PCR products generated using the MG1655 chromosomal DNA as template (Sections 2.5.2 and 2.5.3) using primer pairs acrA-WT-F and acrB-WT-R or tolC-WT-F and tolC-WT-R. Mutant genes of *tolC* or *acrA* in the pASK-RM plasmid were generated by site-directed mutagenesis as described in Section 2.5.7 to generate pASK-*tolC* and pASK-*acrAB* variants, except for pASK-*acrA(Δhelices)* and

pASK-*acrA(Δhairpin)*, which were generated by restriction cloning from pEX-K4-*acrA(Δhelices)* and pEX-K4-*acrA(Δhairpin)*.

Wild-type and mutant variants of *tolC* were cloned from pASK-RM to pET26b by restriction cloning directly from pASK-{gene} to generate pET26-*tolC* variants. Wild-type and mutant variants of *acrA* were cloned by PCR amplification from the pASK-{gene} plasmid using the acrA-WT-F and acrA-WT-R primer pair, and the PCR product ligated into the pET26b vector at the NdeI and XhoI sites to generate pET26-*acrA* variants. The pET26-*acrB* plasmid was generated via restriction cloning of PCR products generated by two rounds of PCR, first using the SL1344 strain as a template with the Salm-pWKS-F and Salm-pWKS-R primer pair, then using the resulting PCR product as template with the salm-acrB-F and salm-acrB-R primer pair – the product from this second PCR was used for restriction cloning into the pET26b vector.

2.3 PCR primers

Primers used in this study were obtained from Alta Bioscience (Abingdon Health, Birmingham, UK), Eurogentec (Liège, Belgium) or Thermo Fisher Scientific (Invitrogen or Life Technologies Limited, Paisley, UK). All primers were supplied de-salted by SePOP and stored as 100 mM in Tris-EDTA (TE) buffer at -20°C. For standard PCR reactions and mutagenesis, the primers were diluted to 10 mM with sterile distilled water (sdH_2O; Gibco, Life Technologies) by ten-fold dilution, and this working stock was further diluted three-fold to 3.2 mM with dH_2O for sequencing reactions. Each of the diluted stocks was stored at 4°C. Annealing temperatures for each primer pair were calculated using the IDTDNA OligoAnalyzer 3.1 (http://eu.idtdna.com/analyzer/applications/oligoanalyzer/), with parameters for primer, dNTP and divalent cation concentrations corrected for the relevant PCR systems. For a list of primer names and sequences used in this study, see Appendix 2.

2.4 Bacterial growth conditions

Growth media were usually prepared from powders supplied by Oxoid, according to manufacturer's instructions; when pre-mixed powders were not used, LB-broth (LBB) was prepared by dissolving 10 g tryptone, 5 g yeast extract and 5 g NaCl in 1 l of deionised water. For strains containing resistance markers, ampicillin or kanamycin were added to final concentrations of 100 $\mu l.ml^{-1}$ or 50 $\mu g.ml^{-1}$, respectively either to the cooled molten agar before pouring plates or to the broth before inoculation. For routine propagation of bacteria, cells were grown at 37°C overnight (12-16 h) on LB-agar. When liquid cultures were required, cells were picked from colonies on agar plates into Universal bottles containing 5 ml LBB and incubated at 37°C overnight (12-16 h) with shaking at 180 rpm to provide aeration.

2.5 Genetic manipulations

2.5.1 Plasmid extraction

For sequencing, plasmids were extracted using a Thermo Fisher GeneJET plasmid miniprep kit (product number K0503) as per manufacturer's instructions, with elution from the column in 30 µl sdH_2O. For routine laboratory use, isopropanol precipitation was used as described below.

From overnight cultures, 3 ml culture was harvested by centrifugation at 21000 x *g* for 5 min at room temperature, and resuspended in 250 µl GTE (50mM glucose, 25 mM Tris from pH8.0 stock, 10 mM EDTA). Cells were lysed by addition of 250 µl lysis buffer (1% SDS, 0.2 M NaOH), with gentle agitation by inversion of the tube, and incubated at room temperature for 5 minutes. Cell debris was precipitated by addition of 350 µl neutralisation buffer (3 M potassium, 5 M acetate), with gentle agitation by inversion of the tube and incubated on ice for 10 min before removal of the precipitate by centrifugation at 21000 x *g* at 4°C for 10 minutes. The supernatant was added to 600 µl isopropanol cooled to -20°C, mixed by inversion, and incubated

at -20°C for 30 minutes. The precipitated DNA was pelleted by centrifugation at 21000 x *g* at 4°C for10 min, then the pellet washed with 200 µl 70% ethanol followed by 200 µl 100% ethanol. The ethanol was aspirated and any residual ethanol evaporated by incubating the open tubes at 65°C for 5 min, before the pellet was resuspended in 50 µl TE (10 mM Tris from pH8.0 stock, 0.1 mM EDTA).

2.5.2 Chromosomal DNA extraction

To extract chromosomal DNA, the same isopropanol precipitation approach was used as for plasmid extraction (Section 2.5.1), except that following addition of lysis buffer, the mixture was vortexed intensively for 1 min to shear the chromosome.

2.5.3 PCR reactions

Either the Q5 DNA-polymerase or MyTaq RedMix systems were used for PCR reactions, depending upon their purpose. For screening purposes, MyTaq RedMix was used, using 25 µl of the pre-mix, 1 µl of template, 2.5 µl of each primer from 10 mM stocks, and 19 µl sdH_2O. For normal PCR reactions, template refers to the plasmid prep, while for "colony" PCR, a 1 ml culture was incubated under appropriate growth conditions for 2 h, cells harvested by centrifugation at 20000 x *g* for 5 min at room temperature, and the cells resuspended in 50 µl sterile water before boiling at 99°C for 30 min to form the template solution. For purposes where sequence fidelity is essential, such as cloning, Q5 polymerase was used. The Q5 reaction mix consisted of 0.5 µl Q5 polymerase, 10 µl Q5 buffer, 10 µl Q5 GC enhancer, 1 µl template, 2.5 µl of each primer from 10 mM stocks and 23 µl Gibco sterile distilled water. The reaction cycles are set out in Table 2:2.

Table 2:2 - PCR reaction cycle conditions

		Q5	MyTaq
1x	Initial denaturing	98°C, 5 min	95°C, 5 min
30 cycles	Denaturing	98°C, 30 s	95°C, 20 s
	Annealing	20 s, primer-specific	15 s, primer-specific
	Extension	72°C, 1 min per kb	68°C, 30 s per kb
1x	Final extension	72°C, 2 min + 1 min/kb	68°C, 2 min + 30 s/kb

2.5.4 Restriction digest conditions

Restriction enzymes were purchased from New England Biolabs. Digests were set up using 0.5 µl of each restriction enzyme required, plus 5 µl of the 10x CutSmart buffer, 5 µl PCR product or 20 µl plasmid miniprep to be digested, and made up to 50 µl with Gibco sterile distilled water. To vectors being cut to receive an insert, 1 µl calf intestinal phosphatase was also added. The reaction was incubated at 37°C for 12-16 hours. Following restriction digest, if the change in fragment size would be too small to detect by agarose gel electrophoresis, DNA was purified by PCR clean-up kit (Qiagen). Where possible, digested fragments were analysed by agarose gel electrophoresis and extracted from the gel using a gel extraction kit (Qiagen).

2.5.5 Ligation conditions

To ligate DNA fragments, 1 µl T4 DNA ligase (NEB), 4 µl 5x T4 DNA ligase buffer, 5 µl digested vector and 10 µl digested insert were mixed and incubated on a thermocycler at 16°C for 1 h, 14°C for 1 h, 12°C for 2 h, 10°C for 2 h, 8°C for 30 min, 6°C for 30 min and 4°C on hold until removed from the thermocycler (8-10 h). Ligations were used directly in transformations, without clean-up.

2.5.6 DNA sequencing

DNA samples for sequencing were prepared as described in Section 2.5.1, using a spin kit. Primers were diluted to 3.2 mM in Gibco sterile distilled water, and 1 µl of the diluted primer added to 2 µl purified DNA and 7 µl Gibco sterile distilled water. The mixture was sequenced by the Functional Genomics facility at University of Birmingham.

2.5.7 Site-directed mutagenesis

Mutations were incorporated by site-directed mutagenesis with QuikChange Lightning (Agilent Technologies) according to the manufacturer's instructions (revision D). Mutagenesis primers were designed through the Agilent Technologies web-based QuikChange Primer Design tool, optimised for the Lightning system. Plasmid preparations from BW25113 (WT) or MG1655 (WT) were used as templates for the mutagenesis PCR. Following mutagenic PCR, the template was digested by DpnI enzyme supplied with the mutagenesis kit as per the manufacturer's instructions with the exception of the incubation time being increased to 30 min. The mutagenesis product was used to transform BW25113 according to the TSS transformation approach (as described in Section 2.6.1); if no colonies were formed, the approach was repeated but the transformation was into XL-10 Gold cells, using a heat-shock approach as per supplier's instructions.

For mutagenesis that failed using the complementary primer (QuikChange) approach, a blunt-end ligation approach was used instead. New primers were ordered with the mutation at the 5'- end of one primer or, for larger mutations, the mutation split over the 5'- ends of both primers in the pair. These primers were diluted to 10 mM in sdH_2O and phosphorylated with T4 polynucleotide kinase (NEB) by mixing 5 µl each primer in the pair, 5 µl T4 polynucleotide kinase buffer, 4.5 µl 11 mM ATP, 0.5 µl T4 polynucleotide kinase enzyme and 30 µl sdH_2O, and incubated at 37°C for 2 hours.

The phosphorylated primers were used in a Q5 PCR reaction to amplify the entire plasmid. The PCR product was purified using a PCR clean-up kit as per manufacturer's instructions, and subsequently used in a self-ligation reaction (as described in Section 2.5.5, but sdH_2O replaced the insert). The ligation mixture was used directly in transformation of BW25113 cells using the TSS approach as described in Section 2.6.1.

Transformant colonies were picked into overnight cultures in selective LBB and incubated at 37°C (180 rpm) 12-16 h, plasmids extracted as described in Section 2.5.1 and sequenced as described in Section 2.5.6.

2.6 Preparation and transformation of competent cells

2.6.1 Chemically competent cells

Cells were made chemically competent using the single-step transformation and storage solution (TSS) approach, as published (Chung *et al.*, 1989). Namely, cells were picked from a colony into 5 ml LBB and incubated at 37°C for 12-20 h with shaking at 180 rpm. The overnight culture was diluted 1 in 1000 into 100 ml fresh LBB and incubated at 37°C with shaking at 180 rpm until OD_{600} was between 0.3 and 0.6, with OD readings beginning after 2 h incubation. The culture at OD_{600} 0.3-0.6 was incubated on ice for 30 min before the cells were harvested by centrifugation of a total of 80 ml culture at 4000 x*g* at 4°C for 10 minutes. Cell pellets were resuspended in 8 ml total ice-cold TSS (LBB supplemented with 10% (w/v) PEG-4400, 5% (v/v) DMSO and 25 mM Mg^{2+} ions (provided by addition of solution containing 1.25 M $MgSO_4$ and 1.25 M $MgCl_2$)). Resuspended cells were aliquoted to 100 µl in cold microcentrifuge tubes and stored at -80°C until use.

Cells made chemically competent in TSS were transformed by addition of DNA, the volume of which was dependent upon the source of the DNA, and incubated on ice for 30 minutes. Recovery solution, termed TSR (for TSS-recovery) consisting of LBB supplemented with 20 mM glucose was added (900 µl) and the recovering cells incubated at 37°C, unless otherwise specified, for 1 hour. Following recovery, cells were harvested by centrifugation at 20000 x*g* for 5 min at room temperature, the supernatant decanted and the cells resuspended in the residual supernatant, all of which was subsequently spread onto selective LB-agar medium (supplemented with 100 µg.ml^{-1}ampicillin, 50 µg.ml^{-1} kanamycin or 50 µg.ml^{-1} chloramphenicol). Transformants were selected after overnight incubation at 37°C on selective medium.

2.6.2 Electrocompetent cells

Note: any incubation at 37°C was changed to 30°C for any strains harbouring the pCP20 or pKD46 plasmids.

Cells were picked from a colony into 5 ml LBB and incubated at 37°C for 12-20 h with shaking at 180 rpm. The overnight culture was diluted 1 in 1000 into 1 l fresh LBB and incubated at 37°C with shaking at 180 rpm until OD_{600} was between 0.3 and 0.4, with OD readings beginning after 2 h incubation. Once OD_{600} was between 0.3 and 0.4, the culture was transferred to ice and incubated on ice for 30 min before harvesting the cells by centrifugation at 4000 x*g* at 4°C for 20 minutes. The cell pellets were resuspended in a total of 200 ml ice-cold sterile water (Ultrapure water from an Elga water purifier was filter sterilised by passing through a membrane with pore size of 0.22 µm – larger volumes in Stericup units (Corning); smaller volumes by Millex syringe filter (Merck Millipore)) and harvested again by centrifugation at 4000 x*g* at 4°C for 20 minutes. The cell pellets were resuspended in a total of 100 ml ice-cold sterile water and harvested by centrifugation at 4000 x*g* at 4°C for 20 minutes. Cells

were resuspended in a total of 40 ml ice-cold 10% glycerol, harvested once more by centrifugation at 4000 x*g* at 4°C for 20 minutes and resuspended in a total of 1 ml ice-cold 10% glycerol. Cells were then aliquoted to 100 µl in cold microcentrifuge tubes and stored at -80°C until use.

Electro-competent cells were transformed by addition of 1-5 µl DNA added to the cells on ice, mixed gently by movement of the pipette tip within the cell suspension. The mixture was incubated on ice for 5 min before being transferred to an ice-cold electroporation cuvette with 1 mm electrode gap. The cells were then immediately subjected to a 1600 V electrical pulse, and 900 µl LBB added. The resulting solution was transferred to a microcentrifuge tube and incubated at 37°C for 1 h to recover. Following recovery, cells were harvested by centrifugation at 20000 x*g* for 5 min at room temperature, the supernatant decanted and the cells resuspended in the residual supernatant, all of which was subsequently spread onto selective LB-agar medium. Transformants were selected after overnight incubation at 37°C on selective medium.

2.7 Chromosomal gene deletion

2.7.1 P1 phage transduction

Deletions of the *acrA* or *acrB* genes were made in the chromosome of *E. coli* strain C43(DE3) by P1 phage transduction, using the Keio collection knockout strains JW0452 and JW0451 as donors (Baba *et al.*, 2006). The donor strain was grown as 1 ml culture in Lennox broth supplemented with $CaCl_2$ to a final concentration of 2 mM, at 37°C (180 rpm) for 12-16 h in a Universal bottle. From this culture, 500 µl was removed and the culture replenished with the same volume of Lennox broth supplemented with $CaCl_2$ to a final concentration of 2 mM, and the new culture incubated at 37°C (180 rpm) for 5 h. After 5 h incubation, 100 µl each of the culture

and of diluted P1 phage stock were added to soft agar overlay consisting of 1 ml Lennox agar and 2 ml Lennox broth at 45°C. The overlay with P1 phage and the donor bacterial strain was vortex-mixed before being poured over a Lennox agar plate supplemented with glucose to a final concentration of 0.2% and $CaCl_2$ to a final concentration of 2 mM, and incubated at 37°C for 12-16 h. From plates displaying a plaque following this overnight incubation, the soft agar was harvested with 2 ml Lennox broth, and homogenised in 1 ml chloroform on ice in a pre-chilled glass homogeniser before being transferred to a 15 ml centrifuge tube and spun at 4000 x*g* (4°C) for 15 min in a benchtop centrifuge. The supernatant, including the chloroform, was collected in Universal bottles and stored at 4°C as P1-{gene} stock.

A culture of the recipient strain (1 ml in Lennox broth supplemented with $CaCl_2$ to a final concentration of 2 mM) incubated for 12-16 h at 37°C (180 rpm) was transferred from a Universal bottle to conical flask containing 20 ml of the same medium and incubated at 37°C (180 rpm) for 5 h. The cells were then harvested by spinning 5 ml aliquots in 15 ml centrifuge tubes at 4000 x*g* for 3 min and the pellet resuspended in 500 µl Lennox broth supplemented with $CaCl_2$ to a final concentration of 2 mM. To these cells, 100 µl of the P1-{gene} stock and dilutions thereof (ten-fold in Lennox broth, to a final 1 in 100 by a second (serial) dilution) was added, and the cells plus phage incubated at 45°C for 20 min in a waterbath. The bacterial cells were then washed of phage by harvesting the cells by spinning at 4000 x*g* for 3 min and washed by resuspending in 4 ml phosphate buffered saline solution (PBS), repeated to a total of 3 washes. When washed three times, the cells were harvested again, resuspended in 2 ml Lennox broth, and incubated at 37°C for 1 h for cell recovery. The recovered cells were harvested by centrifugation at 4000 x*g* for 3 min and resuspended in 200 µl PBS, all of which was spread onto plates of LB-agar supplemented with 50 $\mu g.ml^{-1}$ kanamycin. The plates were incubated at 37°C overnight (12-16 h) to select for transductant cells.

Colonies from transduction were screened by colony PCR using the seq-{gene}-upst and seq-{gene}-dnst primers with Q5 DNA Polymerase PCR, using an amplification step of 3 min to ensure adequate time for extension of the entire gene. The PCR products were resolved on 1% agarose gels stained with SYBRsafe and visualised on a GelDoc system (Syngene), against HyperLadder I. PCR products of the expected size were purified from the remainder of the PCR product using a PCR clean-up kit (Qiagen), and the PCR product sequenced (Functional Genomics Facility, University of Birmingham) using each of the up- and down-stream primers for the respective gene.

Colonies for which sequencing had shown the *aph* (Kan^R) replacement of the target gene were made competent using the TSS method, and transformed with pCP20 using a modified TSS approach in which the recovery step was increased to 80 min at room temperature (18-26°C) and the overnight incubation temperature was 30°C. Transformants were selected for on ampicillin. Colonies resistant to ampicillin were inoculated to non-selective LB-agar plates and incubated overnight (16-20 h) at 43°C. From this plate, colonies were picked with a pipette tip containing 1 ml LBB and expelled into microcentrifuge tubes, spun for 5 min at 15000 x *g* and the cell pellet resuspended in 10 µl LBB, of which 3 µl was spotted onto each of LB-agar, Kan and Amp plates, and incubated overnight (16-20 h) at 37°C, 37°C and 30°C respectively. Clones susceptible to kanamycin were retained with the chromosomal marker having been removed, and clones susceptible to both kanamycin and ampicillin were retained as having additionally been cured of the pCP20 plasmid. When pCP20 was retained in all colonies, the process was repeated with a colony from the latest LB-agar plate being inoculated to fresh LB-agar and incubated at 43°C overnight.

2.7.2 Homologous recombination of PCR products

The strain C43Δ*acrB tolC::aph* was made essentially from a shortcut approach to the commonly used approach developed by Datsenko and Wanner (Datsenko & Wanner,

2000). Chromosomal DNA from BW*tolC::aph* was isolated as described in Section 2.5.2, and the *tolC::aph* cassette amplified by PCR as described as in Section 2.5.3 using Q5 and the tolC-upst-seq-f and tolC-dnst-seq-R primer pair, which anneal 430-406 bp upstream of the *tolC* start site and 462-481 bp downstream of the *tolC* stop site, respectively. The PCR product was analysed by agarose gel electrophoresis and purified from the gel.

Electrocompetent C43Δ*acrB* (DE3) cells were transformed with the recombination helper plasmid pKD46. Transformants were made electro-competent as described in Section 2.6.2, with the addition of 10 mM arabinose and 100 $mg.ml^{-1}$ ampicillin to the 1 l culture. Electro-competent C43Δ*acrB* (DE3) pKD46 cells were transformed with 5 µl of the above PCR product, with overnight outgrowth at 42°C on LB-Kan agar plates to cure the cells of the pKD46 plasmid and select for *tolC::aph* recombinant cells. Candidates were screened by PCR using the tolC-upst-seq-F and tolC-dnst-seq-R primer pair to check for the *tolC::aph* mutation.

C43Δ*acrB tolC::aph* (DE3) strains were cured of the *aph* marker by use of pCP20, as described in Section 2.7.1 above, but using an electro-competent approach rather than TSS.

2.8 Minimum inhibitory concentration (MIC) assays

All MIC assays were designed to comply with standards set out by the British Society of Antimicrobial Chemotherapy (BSAC), in accordance with the guidelines updated in 2006 and made available online as the latest version in 2012 (Andrews, 2012).

2.8.1 Liquid broth MIC

Cells were picked from colonies into 5 ml selective LBB (supplemented with appropriate antibiotic to select for the plasmid) and incubated overnight (16-20 h) at 37°C with shaking at 180 rpm. Subject antibiotics were diluted in Iso-sensitest broth (Oxoid) to a concentration quadruple the expected MIC of the wild-type control

strain, based on previous data from literature sources and within the laboratory group, and anhydrotetracycline added to appropriate concentration. To all wells in columns 2-12, 50 µl Iso-sensitest broth containing anhydrotetracycline at appropriate concentrations was added. To all wells in columns 1 and 2, 50 µl antibiotic in Iso-sensitest broth was added. The antibiotic was diluted through columns 2-11 by serial dilution, transferring 50 µl from one column to the next and mixing by pipette. Following serial dilution, 50 µl of solution was removed from all wells in column 11, making the total volume 50 µl in all wells on the plate. Antibiotic was not diluted into column 12, which instead contained only Iso-sensitest broth to act as a positive growth control.

Overnight cultures were diluted by two-step dilution to 1 in 2000 in sterile water. Of the diluted cultures, 50 µl was added to each well in a row on the 96-well plate (one row per strain). As a negative control, row H was not inoculated. The 96-well plate was covered with a corresponding lid, and then incubated at 37°C overnight (12-16 h) with no shaking. Following overnight incubation, the OD_{600} was measured on a Fluostar plate reader.

2.8.2 Agar dilution MIC

Cells were picked from colonies into 5 ml selective LBB (supplemented with appropriate antibiotic to select for the plasmid) and incubated overnight (16-20 h) at 37°C with shaking at 180 rpm. Subject antibiotics were diluted to 10000, 1000, 100 and 10 $mg.ml^{-1}$ in appropriate solvent. Into labelled sterile plastic universal bottles, antibiotic solution was added at volumes appropriate for the final concentration of the antibiotic in the agar plates, before addition of agar. Iso-sensitest agar (Oxoid) was melted and allowed to cool to 50°C before addition of anhydrotetracycline to appropriate concentration. Agar supplemented with anhydrotetracycline was dispensed by Perifill to aliquot 20 ml into the universal bottles containing subject

antibiotic. Immediately upon dispensing of agar, the universal was swirled to mix the antibiotic and agar, and the agar poured to appropriately labelled petri dish.

Overnight cultures were diluted 1 in 100 in sterile water and transferred to a multi-point inoculator template tray. The plates were inoculated by multi-point inoculator and incubated at 37°C overnight (12-16 h). Levels of growth were recorded for each strain on each plate to determine the minimum antibiotic concentration at which the strain was inhibited, based upon visual perception of the colony density.

2.8.3 Chequerboard assays

Cells were picked from colonies into 5 ml selective LBB (supplemented with appropriate antibiotic to select for the plasmid) and incubated overnight (16-20 h) at 37°C with shaking at 180 rpm. Fusidic acid was diluted to 2048 $\mu g.ml^{-1}$ and, separately, anhydrotetracycline to 512 $ng.ml^{-1}$ in Iso-sensitest broth.

To columns 2-12 of a 96-well plate, 50 µl Iso-sensitest broth (with no supplements) was added. From the above fusidic acid stock, 50 µl was added to every well in the first two columns of the 96-well plate, and the second column used as the starting point for step-wise dilution through columns 3-11, transferring 50 µl from one column to the next, with mixing by pipette at each step. From column 11, 50 µl was then removed and discarded. From the above anhydrotetracycline stock, 50 µl was added to every well in the first row. Anhydrotetracycline was diluted by step-wise transfer of 50 µl from the first row through each subsequent row, to the seventh row, and 50 µl removed from the seventh row. The final concentrations in each column and row are shown in Figure 2:1.

	1	2	3	4	5	6	7	8	9	10	11	12
A	512F/ 128	256F/ 128	128F/ 128	64F/ 128	32F/ 128	16F/ 128	8F/ 128	4F/ 128	2F/ 128	1F/ 128	05F/ 128	0F/ 128
B	512F/ 64	256F/ 64	128F/ 64	64F/ 64	32F/ 64	16F/ 64	8F/ 64	4F/ 64	2F/ 64	1F/ 64	0.5F/ 64	0F/ 64
C	512F/ 32	256F/ 32	128F/ 32	64F/ 32	32F/ 32	16F/ 32	8F/ 32	4F/ 32	2F/ 32	1F/ 32	0.5F/ 32	0F/ 32
D	512F/ 16	256F/ 16	128F/ 16	64F/ 16	32F/ 16	16F/ 16	8F/ 16	4F/ 16	2F/ 16	1F/ 16	0.5F/ 16	0F/ 16
E	512F/ 8	256F/ 8	128F/ 8	64F/ 8	32F/ 8	16F/ 8	8F/ 8	4F/ 8	2F/ 8	1F/ 8	0.5F/ 8	0F/ 8
F	512F/ 4	256F/ 4	128F/ 4	64F/ 4	32F/ 4	16F/ 4	8F/ 4	4F/ 4	2F/ 4	1F/ 4	0.5F/ 4	0F/ 4
G	512F/ 2	256F/ 2	128F/ 2	64F/ 2	32F/ 2	16F/ 2	8F/ 2	4F/ 2	2F/ 2	1F/ 2	0.5F/ 2	0F/ 2
H	512F/ 0	256F/ 0	128F/ 0	64F/ 0	32F/ 0	16F/ 0	8F/ 0	4F/ 0	2F/ 0	1F/ 0	0.5F/ 0	0F/ 0

Figure 2:1 - Layout of chequerboard assays

Each row (A-H) contains a different concentration of anhydrotetracycline, while each column (1-12) contains a different concentration of fusidic acid. The values indicate [fusidic acid] in $\mu g.ml^{-1}$ (labelled with F) / [anhydrotetracycline] in $ng.ml^{-1}$.

Following overnight growth, cultures were diluted 1 in 2000 in Iso-sensitest broth, by 1 in 100 dilution followed by 1 in 20 dilution. To each well on the 96-well plate, 50 µl of this cell suspension was added. A corresponding 96-well plate lid was put over the plate, and the plate was then incubated at 37°C for 24 h without agitation. Following incubation, the plate was read on a Fluostar plate reader and OD_{600} values recorded.

2.9 Growth kinetics

To 100 ml Iso-sensitest broth, anhydrotetracycline was added to a final concentration of 2 $ng.ml^{-1}$ and the test antibiotic to the final concentration as required. The mixture was then filter sterilised in a Stericup and stored at 4°C for a maximum of two days until use.

Single colonies were inoculated into 2 ml LBB supplemented with 100 $\mu g.ml^{-1}$ ampicillin and 2 $ng.ml^{-1}$ anhydrotetracycline, in Universal bottles and incubated at 37°C with shaking at 200 rpm for 8 hours. Cells were harvested from 100 µl of these cultures by centrifugation (20000 x *g* for 5 min at room temperature), the supernatant removed by aspiration, and the cells resuspended in 1 ml Iso-sensitest broth supplemented with 2 $ng.ml^{-1}$ anhydrotetracycline. Cells were kept on ice to prevent growth in the fresh medium whilst handling. To every well on a 96-well plate, 190 µl Iso-sensitest broth supplemented with anhydrotetracycline (final concentration of 2 $ng.ml^{-1}$) was added. From the cell suspensions, 10 µl was added to wells on the 96-well plate, and the positions recorded – the layout was such that the complete set of strains to be analysed were present thrice – in wells A1-C8, C9-F4 and F5-H12 – allowing two wells in each set to not be inoculated, as negative controls. This plate formed a template, from which the assay plates could be quickly inoculated by use of a multi-channel pipette.

Assay plates were set up from the pre-prepared broth stocks with test antibiotic and anhydrotetracycline already added. Three assay plates were set up in parallel. To every well in each of the three groups of wells (A1-C8, C9-F4 and F5-H12), 200 µl stock broth was added; broth containing different antibiotics was added to each of the groups, for example broth containing vancomycin to all wells in A1-C8, broth containing deoxycholic acid to all wells in C9-F4 and broth containing fusidic acid to all wells in F5-H12. Assay plates were inoculated by transfer of 2 µl from wells in the template plate to the same positions on the assay plate. Each plate was sealed with a Breathe-Easy membrane (Diversified Biotech), and placed in a Fluostar plate reader – one plate each into the three readers.

Each of the Fluostar plate readers was set up with the same programme. Machines were pre-warmed to 37°C whilst plates were being prepared. The plates were incubated at 37°C throughout the assay, with orbital shaking at 200 rpm between read cycles. The OD_{600} was measured every 3 min for 8 h using 10 flashes per well per read.

2.10 Dye efflux assays

Efflux assays using Nile Red as the substrate were modified from previously published methods (Bohnert *et al.*, 2010; Iyer *et al.*, 2015). Cells were picked from colonies into5 ml LBB supplemented with 100 µg.ml^{-1} ampicillin, in Universal bottles and incubated at 37°C with shaking at 200 rpm for 12-16 hours. From the overnight culture, 5 µl was used to inoculate 5 ml fresh LBB supplemented with 100 µg.ml^{-1} ampicillin and 2 ng.ml^{-1} anhydrotetracycline, and subsequently incubated at 37°C with shaking at 180 rpm for 2 h to allow cultures to reach late exponential phase. Cells were harvested from 1 ml of this culture by centrifugation at 21000 x *g* for 5 min at room temperature, while the OD_{600} was measured from a further 1 ml of culture. Cell

pellets were resuspended in phosphate buffered saline (PBS, prepared from tablets) in a volume equal to the OD_{600} of that culture (example: if the culture OD_{600} was 0.625, then 625 µl PBS was used), to equalise cell density of each sample. Of the resuspended cells, 150 µl were added to a clean microfuge tube, to which 1.7 µl 10 mM CCCP and 16 µl 50 µM Nile Red were subsequently added. The cells were incubated at room temperature for 1 h in this solution. Free Nile Red and CCCP were removed by harvesting of the cells (21000 x *g* for 5 min at room temperature), aspiration of the supernatant that contains the free Nile Red and CCCP, and subsequent resuspension of the cell pellet in 150 µl fresh PBS.

To each well on a black-sided tissue-culture treated 96-well plate (4titude), 150 µl PBS was added. Pre-loaded cells (25 µl) were added to the wells and the plate transferred to a Fluostar plate reader, pre-heated to 37°C. The OD_{600} was measured as a single step, before changing to fluorescence mode. The fluorescence in each well was measured with excitation at 550 nm and emission at 640 nm with 27 s between readings in plate mode or 2 s between readings in well mode. This was measured for 5 readings before injection of 25 µl 70 mM glucose by the automated injector on the Fluostar. Readings were continued for 25 readings post-injection.

2.11 Flow cytometry

Cells were picked from colonies into 5 ml LBB supplemented with 100 $\mu g.ml^{-1}$ ampicillin and incubated at 37°C for 12-16 h with shaking at 180 rpm. From the overnight culture, 50 µl was used to inoculate 5 ml fresh LBB supplemented with 100 $\mu g.ml^{-1}$ ampicillin and 2 $ng.ml^{-1}$ anhydrotetracycline (except where specified). This culture was grown for 3 h to get cells in late exponential or early stationary phase, at which point 1 ml was used to measure OD_{600} and 200 µl of the culture was harvested by centrifugation at 21000 x *g* for 5 min at room temperature and the cell pellet

resuspended in 200 µl 1x HEPES-buffered saline (Alfa-Aesar). For cultures that had OD_{600} greater than 0.7, 10 µl of the cell suspension and 90 µl HEPES-buffered saline were added to 500 µl HEPES-buffered saline, while for cultures with OD_{600} less than 0.7, 100 µl of the cell suspension was added. To this, 5 µl ethidium bromide stock solution (10 mM) and 10 µl Syto 84 (Thermo Fisher Scientific) solution (0.5 mM) were added, to form the cell suspensions used for flow cytometry. The cell suspension for use in flow cytometry was vortexed briefly (less than 3 s), incubated for a minimum of 5 min at room temperature. Immediately prior to loading to the Attune flow cytometer, samples were vortexed briefly again.

2.12 Isolation of membranes and protein purification

2.12.1 Cell growth and lysis

For high level expression of membrane proteins, genes were cloned to the pET26b vector and the relevant C43 (DE3) knockout strains were transformed with the resultant plasmids. Cells were picked from colonies to 5 ml LBB supplemented with 50 $\mu g.ml^{-1}$ kanamycin, and incubated at 37°C with shaking at 200 rpm for 16-20 hours. The overnight culture was used to inoculate 1 l of 2YT broth supplemented with 50 $\mu g.ml^{-1}$ kanamycin and pre-warmed to 37°C, in 2.5 l conical flasks. This culture was then incubated at 37°C with shaking at 120 rpm for 2 h, from which point 1 ml samples were taken at appropriate time intervals to monitor growth. When the culture reached OD_{600} 0.3 to 0.5, IPTG was added to a final concentration of 10 µM to induce protein expression. Incubation continued for a further 20 h post-induction at 20°C and shaking at 120 rpm. Cells were harvested by centrifugation at 6000 x *g* for 30 min at 4°C, resuspended in 30 ml Tris/ NaCl resuspension buffer (20 mM Tris pH8.0, 200 mM NaCl) and frozen at -80°C for at least 3 hours before lysis. Frozen cell suspensions were thawed with manual agitation at room temperature, and

transferred to incubate on ice when almost thoroughly thawed. Once thawed, cells were disrupted on a One Shot cell disruptor (CellD SARL, Roquemaure, France) at 30000 PSI with at least three passes of each suspension on the machine, until it appeared from the consistency of the material that lysis was complete.

2.12.2 Membrane isolation

Cell debris was removed from the suspension of lysed cells by centrifugation at 10000 x *g* for 30 min at 4°C. The membrane fraction was harvested by ultracentrifugation of the supernatant at 120,000 x *g* for 1 h at 4°C. Membranes were transferred from the ultracentrifuge tube to a glass homogeniser using a sterile 2 ml plastic inoculation loop. The membranes were then resuspended in 2 ml Tris/glycerol solution (20 mM Tris pH6.8, 10% glycerol) by homogenisation on ice.

2.12.3 Membrane protein purification

To the 2 ml homogenised membranes isolated in Section 2.12.2, stock solutions were added to make the volume up to 10 ml and convert the solution composition to that of the membrane solubilisation buffer in Table 2:3. To solubilise the membrane proteins, the homogenised membranes were incubated in this solution for 12-16 h at 4°C on a carousel rotating at 10 rpm and set at approximately 45° from vertical. Any remaining insoluble parts were removed by centrifugation at 120,000 x *g* for 1 hour at 4°C and only the supernatant retained.

Table 2:3 - Buffers used in membrane protein purification.

	Solubilisation	Equilibration	Wash	Elution
Tris(pH8.0)	20 mM	20 mM	20 mM	20 mM
NaCl	500 mM	0	0	0
Glycerol	10%	10%	10%	10%
Detergent	1%	0.01%	0.01%	0.01%
Imidazole	10 mM	0	25 mM	300 mM

To a gravity flow column, 2 ml of Ni-NTA saturated ethanol was added. The resin was washed with 10 ml ethanol (100%) and twice with 20 ml of Ultrapure water, before equilibration by two washes with 20 ml of the equilibration buffer in Table 2:3. Once the level of buffer had dropped to the top of the resin, the solubilised membrane was added. To ensure maximum binding, the flow-through of the solubilised membrane was re-applied to the resin and allowed to flow through a second time. The protein-bound resin was washed twice with 10 ml resin wash solution in Table 2:3 and the proteins eluted in 10 ml resin elution buffer in Table 2:3.Purified proteins were concentrated by spinning at 4000 x *g* for 5 min through Amicon-15 concentrator cartridges (Merck Millipore; 30 kDa variant for AcrA, 100 kDa variant for AcrB or TolC), desalted by passing through a PD-10 desalting column and eluting in 3.5 ml resin elution buffer in Table 2:3, followed by concentrating as before. Protein concentration was estimated by Nanodrop measurement, and the purified proteins stored at -20°C until use.

2.13 SDS-PAGE, Coomassie staining and Western blots

Polyacrylamide gels were cast manually using the recipes in Table 2:4. Protein or membrane samples were prepared for gel resolution by addition of a loading buffer to a final 1x concentration (10% glycerol, 50 mM Tris (pH6.8), 2% SDS, 0.01% bromophenol blue and 1% β-mercaptoethanol, modified slightly from that described by Laemmli, 1970). To avoid aggregation of proteins, samples were not boiled. Prepared samples were loaded to the wells of the gels and resolved with SDS running buffer (0.3% w/v Tris, 1.4% w/v glycine, 0.1% w/v SDS) with 40 V applied whilst the proteins moved through the stacking gel and 100 V applied for the resolution. Gels were run until the dye in the loading buffer was observed to be at the bottom edge of the gel.

Table 2:4 - Recipes for SDS-polyacrylamide gels.

	Resolving gel	Stacking gel
Water	3.9 ml	2.7 ml
Tris	2.5 ml (1.5 M, pH 8.0)	500 µl (1.0 M, pH 6.8)
Protogel (National Diagnostics)	3.3 ml	670 µl
10% SDS	100 µl	40 µl
10% APS	100 µl	40 µl
TEMED	5 µl	4 µl

Gels not being subjected to a Western blot were stained with Coomassie blue. Gels were rinsed briefly with Ultrapure water, then incubated in staining solution (0.1% w/v Coomassie Blue G-250, 40% methanol, 10% acetic acid), such the entire gel was submerged, at room temperature with gentle agitation on a 2D rocking plate for 12-16 hours. The stain solution was removed, and the gel rinsed with tap water to remove any residual solution. To destain the gel, it was incubated in destain solution (20% methanol, 5% acetic acid) with gently agitation on a 2D rocking plate at room temperature. The destain solution was replaced after 15, 30, 45, 60 and 120 minutes, and every 60 minutes thereafter until the background staining of the gel was sufficiently removed.

For Western blotting of the proteins of the gel-resolved proteins, a semi-dry approach was used on the iBlot transfer system. Using the sandwich prepared as per manufacturer's instructions, with filter paper and membranes having been soaked in water, the proteins were transferred to nitrocellulose (TolC) or PVDF (AcrA) membranes, using 8 min transfer time. For all subsequent incubations and washes, the solution was gently agitated on a 2D rocker plate, unless stated otherwise. Membranes with the proteins bound were then blocked in a tris-buffered saline buffer with 10% (v/v) Tween-20 (TBS-T) and 5% (w/v) skimmed milk, by incubation for

2 h at room temperature. Membranes were washed 3 times for 5 min per wash in TBS-T, before incubation in 25 ml blocking buffer (TBS-T with 5% milk) with 1 µl α-AcrA or 1 µl α-TolC rabbit-raised polyclonal antibody solution (gifted to the laboratory of Laura Piddock by Helen Zgurskaya) added. Membranes were incubated with the antibodies at 4°C for 12-16 h with agitation on a 2D plate rocker, then incubated for 30 min at room temperature. The antibody/blocking solution was removed, and the membrane rinsed with Ultrapure water before washing thrice for 15 min per wash in TBS-T buffer. Goat-raised anti-rabbit alkaline phosphatase conjugated secondary antibody was used for detection. From the supplier's antibody solution, 0.5 µl was added to 50 ml blocking buffer, and the membrane was incubated in this solution for 1 h at room temperature. The membrane was then washed three times for 10 min per wash in TBS-T, followed by a wash for 5 min in TBS lacking Tween20. To develop the blot, 2 ml BCIP/NBT solution (Thermo Fisher Scientific) was run over the membrane, ensuring equal coverage, constantly moving it across the membrane by pipetting until coloured bands had sufficiently developed.

2.14 Glycerol gradients

Solutions of glycerol were prepared at 2% increments, at minimum concentration 10% and maximum concentration 28%. Into 3.5 ml ultracentrifuge tube inserts (Beckman Coulter), 300 µl of the glycerol solutions were added in order of concentration, with highest concentration first, and with freezing at -80°C between each addition to form layers of different glycerol concentration. Once all of the layers had been formed, the tube was allowed to thaw.

Proteins were mixed with biotinylated amphipol (BA-Pol) at a 5:1 BA-Pol:protein ratio, by weight, in Ultrapure water. Combinations of AcrA, AcrB and TolC were mixed, adding 40 µg of any AcrA variant, 50 µg of any TolC variant and 120 µg of

AcrB. The mixtures were then loaded onto the top of the glycerol gradient, taking care not to disturb the layers. Ultrapure water was added to balance the tubes for ultracentrifugation. The protein-loaded gradients were spun at 100000 x *g* at 4°C for 12 h on a benchtop ultracentrifuge. The gradient was fractionated by transfer of the top 100 µl to a unique well on a 96-well plate, until the entire gradient had been transferred. Each fraction was then treated as a protein sample for resolution by SDS-PAGE as in Section 2.13.

2.15 Computational analyses

JANUS is a programme designed to determine positions in a protein sequence that make up part of the active site of an enzyme (Addington *et al.*, 2013). While TolC is not an enzyme, and therefore does not have an active site as such, JANUS was used with the idea that the interface with MFPs might be considered as the functionally important part of the protein. The programme calculates importance from a series of sequence alignments, each of which must be similar proteins that have a different substrate and each of which must be based upon a structural alignment. The conservation at each position for each alignment is used to determine whether or not a position is important for that family of proteins – if a position is variable in proteins that perform the same function with the same substrate, then that position is highly unlikely to be important for the function of the protein, although this is calculated based on similarity, not identity. Next, the positions are compared between alignments – if a position shows conservation in both sets of sequences, then it is not responsible for determining specificity, regardless of whether or not it is important for function. The positions that are conserved only within the respective alignments, but not when comparing the two sets of alignments, are potentially important for determining specificity, and the scores for these positions are therefore calculated based upon an algorithm taking into account differences in size, charge and hydrophobicity between the two alignments.

All full-length sequences available in the UniProt database matching {gene: tolC AND organism: coli}, {(gene: tolC OR oprM) AND organism: Pseudomonas}, {gene: tolC AND organism: Vibrio} and {(gene: tolC OR mtrE) AND organism: Neisseria} were aligned using Clustal Omega. This alignment was then separated into four smaller alignments, one for each of *E. coli*, *Pseudomonas spp.*, *Vibrio spp.* and *Neisseria spp.*, keeping the same alignment positions as generated by Clustal Omega. The *E. coli* alignment was used as input file 1, with each of the other files used individually as input file 2. The output files were analysed to determine likely importance of positions only at or below the equatorial domain, as positions closer to the outer membrane are unlikely to be involved in an interaction with the cognate MFP. Positions at which the side chain faces into the lumen were also disregarded from this analysis, as they are also unlikely to contact the MFP.

Results from JANUS were used in conjunction with Consurf (Ashkenazy *et al.*, 2010), an online server which automatically generates sequence alignments based on a single pdb code as the input, scores the conservation at each position, and maps the categorised conservation score to the input pdb file. Partial sequences and duplicate entries were excluded from the alignment using the manual selection feature. Positions that show limited variability were taken to be those with potential to determine specificity of interaction with the MFP. Those that have a very low conservation score (hypervariable positions) were assumed to be unimportant, while those that showed maximum conservation are likely to be required for structural reasons and so were not selected for use in this study.

To assess co-evolution of positions between MFPs and OMCs, a selection of MFP sequences were aligned and, separately, their cognate OMC sequences were aligned. The hairpin sequences were extracted from the MFP alignment, and the coiled-coil domains extracted from the OMC alignment. These extracts were combined, such

that the MFP hairpin and its cognate OMC formed a single sequence in a new multiple sequence alignment. This new chimaeric alignment was used as the input for CAPS (Fares & McNally, 2006), which assesses co-evolution of positions within a multiple sequence alignment.

CHAPTER 3: RESULTS – GENETIC MANIPULATIONS AND COMPUTATIONAL ANALYSES

3.1 Making a compatible derivative of pASK-IBA13(plus)

To generate a plasmid from which genes of interest could be expressed in a titratable fashion, with no tag, and from which the gene could easily be transferred to the pET26 vector for high expression of His-tagged protein, the pASK-IBA13plus vector was modified. First, the NdeI restriction site within the coding sequence of the tetracycline repressor protein was removed by silent mutation by site-directed mutagenesis using the pASK-altNde-F and pASK-altNde-R primer pair. To screen for loss of this NdeI restriction site, purified plasmid was digested in a double digest with XhoI and NdeI, whereby successful mutagenesis would cause a single band to seen on an agarose gel following this digest, as in Figure 3:1, as the DNA would cut only at the XhoI site.

The resultant plasmid, designated pASK-IBA-/NdeI was subjected to a second round of mutagenesis using the pASK-NdeI-F and pASK-NdeI-R primer pair, to introduce a new NdeI restriction site at the transcriptional start site under control of the tetracycline promoter (Figure 3:2). To screen for gain of this restriction site, purified plasmid was digested with NdeI only, to see linearisation of the plasmid on an agarose gel, as a result of NdeI activity at the new restriction site; plasmids that were not mutagenised failed to cut, resulting in multiple bands corresponding to varying extents of supercoiling of circular DNA. The single bands were extracted from the agarose gel and digested with XhoI (Figure 3:3), to confirm that the NdeI activity seen was indeed at the new restriction site, and not as a result of failure to remove the original site in pASK-IBA13plus. From this XhoI digest, the multiple cloning site (MCS) alone would be excised and thus no observable change seen in fragment size if the NdeI site was in the new position - if the NdeI site had been the original, then the XhoI digest would result in fragments of 2.1 and 1.1 Kb in size. This plasmid was designated pASK-altNdeI as it has an alternative NdeI site to the original vector.

To allow expression of proteins resembling the wild type as far as possible, the tail sequence between the XhoI and three-frame STOP positions must be curtailed. A new STOP codon was therefore introduced adjacent to the XhoI site, on the 3'- side of the restriction site on the coding strand. This was done by a third round of mutagenesis, using the pASK-STOP-F and pASK-STOP-R primer pair. The final plasmid here could only be confirmed by sequencing (trace shown in Figure 3:4). The purified plasmid was therefore sequenced by Functional Genomics Facility at University of Birmingham, using the pASK-seq-F primer, and the plasmid sequence shown to be as designed. The final plasmid was designated pASK-RM. The STOP site is in-frame with the coding sequence provided that the gene of interest is amplified such that the CTC of the XhoI site on the PCR primer is in-frame to encode leucine.

This new plasmid, pASK-RM, is a new derivative of the commercially available vector pASK-IBA13(plus), with added benefits, including a new NdeI site at the transcriptional start site, placing the START site 9 bases downstream of the Shine-Dalgarno sequence. This allows very simple design of PCR primers for amplification of genes of interest, as the NdeI site can be incorporated into the primers at the START position. There is also a new STOP site adjacent and downstream of the XhoI site, allowing only a two amino acid (LE) “scar” tail sequence to be added to proteins expressed from a gene cloned into the NdeI and XhoI sites, allowing for a near-natural protein sequence to be expressed. This in turn allows for easy transfer of genes of interest by NdeI/XhoI restriction cloning between this vector, suitable for *in vivo* studies, and the pET26b vector which encodes a hexa-histidine tag adjacent to and downstream of the XhoI site, for protein overexpression and purification. Genes were cloned into pASK-RM and pET26b as described in the methods.

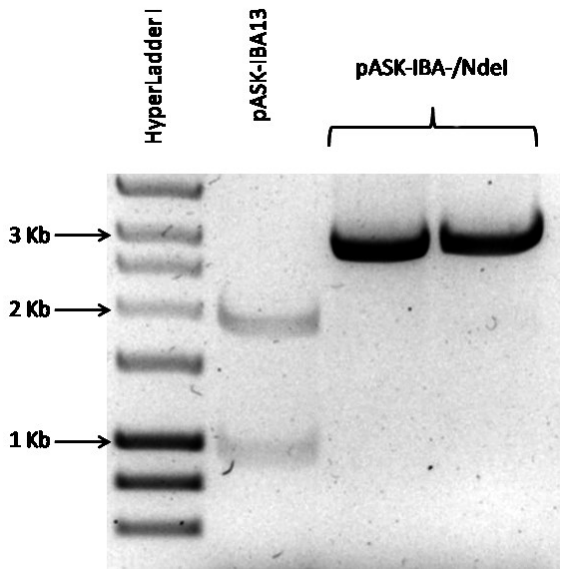

Figure 3:1 - Restriction digest after removal of NdeI site from pASK-IBA13(plus). Gel resolution image of XhoI/NdeI double digests of two candidate plasmids resulting from site-directed mutagenesis of pASK-IBA13 to remove the NdeI restriction site (product designated pASK-IBA-/NdeI), and of the pASK-IBA13 vector used as the template for mutagenesis. Silent mutation resulted in loss of the NdeI restriction site at position 2438 of the plasmid map. Double digestion therefore acts as a single digest, only cutting at the XhoI restriction site at position 271, and gives a single band of the linearised full vector length (approximately 3 Kb). The pASK-IBA13 lane indicates the restriction profile when both restriction sites are present on the vector.

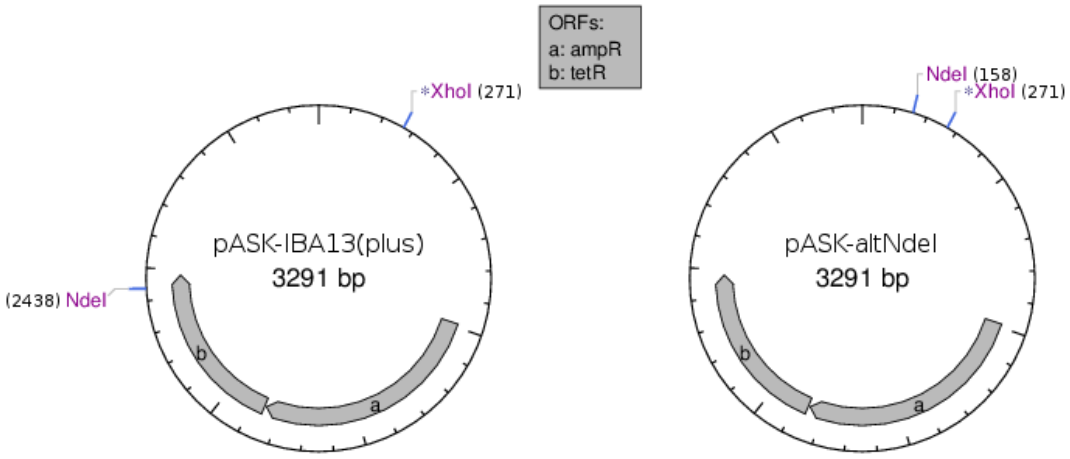

Figure 3:2 - Restriction map of NdeI and XhoI sites in pASK-IBA13(plus) and its new derivative.

A restriction map of the NdeI and XhoI sites from the original commercial vector pASK-IBA13(plus) and the modified vector pASK-altNdeI. The original NdeI site was located within the gene encoding the tetracycline repressor (labelled b on the diagrams), and a silent mutation was therefore made. Images generated using the NEBcutter online tool (http://nc2.neb.com/NEBcutter2/) and edited using GNU image manipulation program (GIMP).

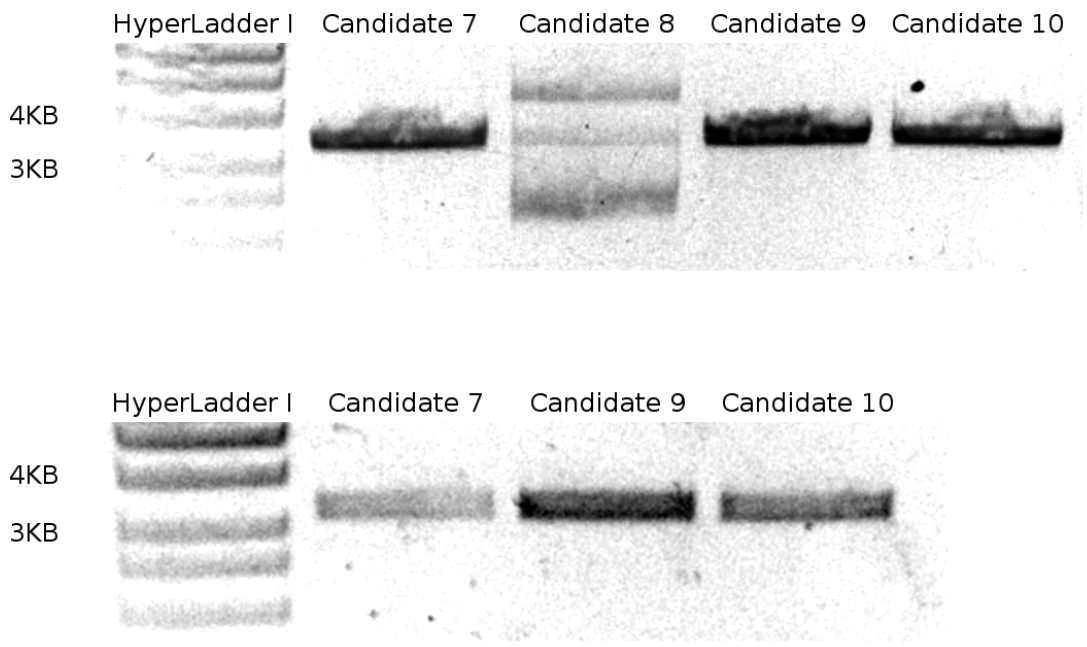

Figure 3:3 - Restriction digests of second pASK-IBA13(plus) derivative.
Top: NdeI digest on candidate plasmids resulting from a site-directed mutagenesis approach to insert a new NdeI restriction site covering the start site within the multiple cloning region of pASK-IBA-/NdeI. Successful incorporation of the change introduces a unique restriction site, causing linearisation of the plasmid upon NdeI digestion.
Bottom: XhoI digest on the gel-extracted NdeI digest of pASK-altNdeI candidates 7, 9 and 10, to test that the linearisation seen is from the new NdeI site and not from retention of the original site present in pASK-IBA13. Were the original NdeI site present, bands would be visible at approximately 2 Kb and 1 Kb.

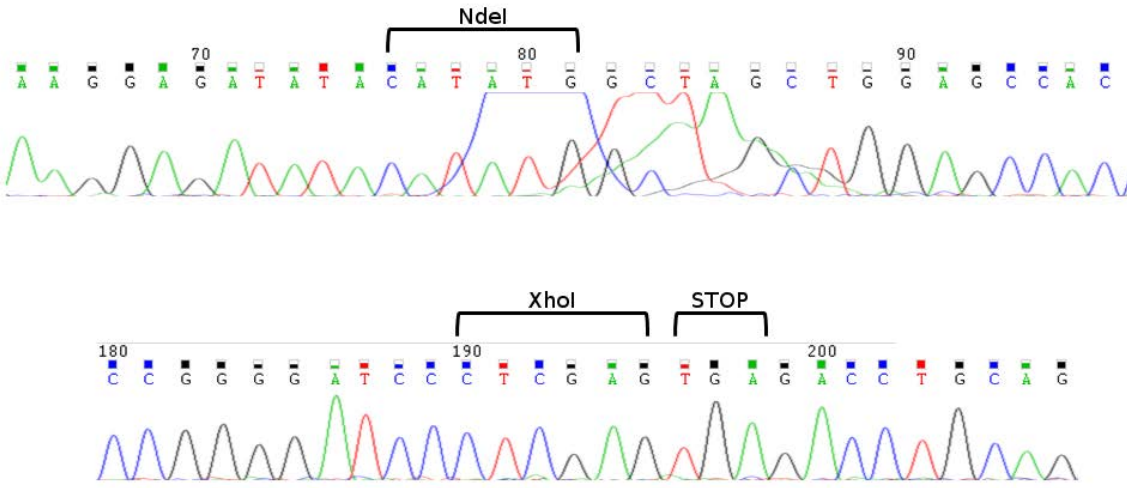

Figure 3:4 - Sequencing trace of final pASK-RM vector.
Sequencing trace as shown in Chromas from sequencing of the final pASK-RM plasmid using the pASK-seq-F primer, displaying the sequence at both the 5`- (upper trace) and 3`- (lower trace) ends of the MCS of the plasmid. Indicated by brackets are the restriction sites for NdeI (CATATG) and XhoI (CTCGAG), as well as the newly-introduced STOP codon (TGA) adjacent to and downstream of the XhoI site. On the upper trace, the Chromas software has detected the true sequence through the "BigDye Blob" that appears on all traces around positions 80-90.

3.2 The structural repeat of TolC

The structure of the TolC protein shows a clear structural repeat within each protomer (shown in Figure 3:5). Each repeat begins with a helix contributing to the equatorial domain, followed by a helix forming the “upward” part of the upper α-helical barrel, then two anti-parallel β-strand with an interconnecting loop, followed by a long helix stretching from the β-barrel to the periplasmic end of the protein, in turn leading into a turn and another helix which completes the α-barrel structure, and ending with a component of the equatorial domain.

To show the structural repeat and enable analysis of the sequence alignment of the two half-proteins, the C-terminal half was taken as beginning at the equivalent helix

(H5) as starts the N-terminal (H1) of the 1EK9 TolC protein structure. The entire sequence from H5 to the C-terminal end of the protein was extracted to a new object in PyMol, and aligned to the remaining N-terminal half of the protein. An overlay and sequence alignment (based upon the structural alignment) of the two half-protomers is shown in Figure 3:5. This structural repeat causes the formation of two non-identical grooves for potential MFP binding, one intra-protomer and the other inter-protomer. Given that it is generally accepted that six AcrA proteins bind each TolC trimer, it is logical that each groove might bind one copy of AcrA. Therefore, it is also logical that, if all six copies of the MFP are identical, the residues on TolC that are required for binding will be the same in each groove, and led to the hypothesis that essential residues will be conserved in the internal duplication. Therefore, the conserved positions were mapped onto the 1EK9 TolC structure (Figure 3:6) for use when considering what positions were suitable candidates for mutation in this study.

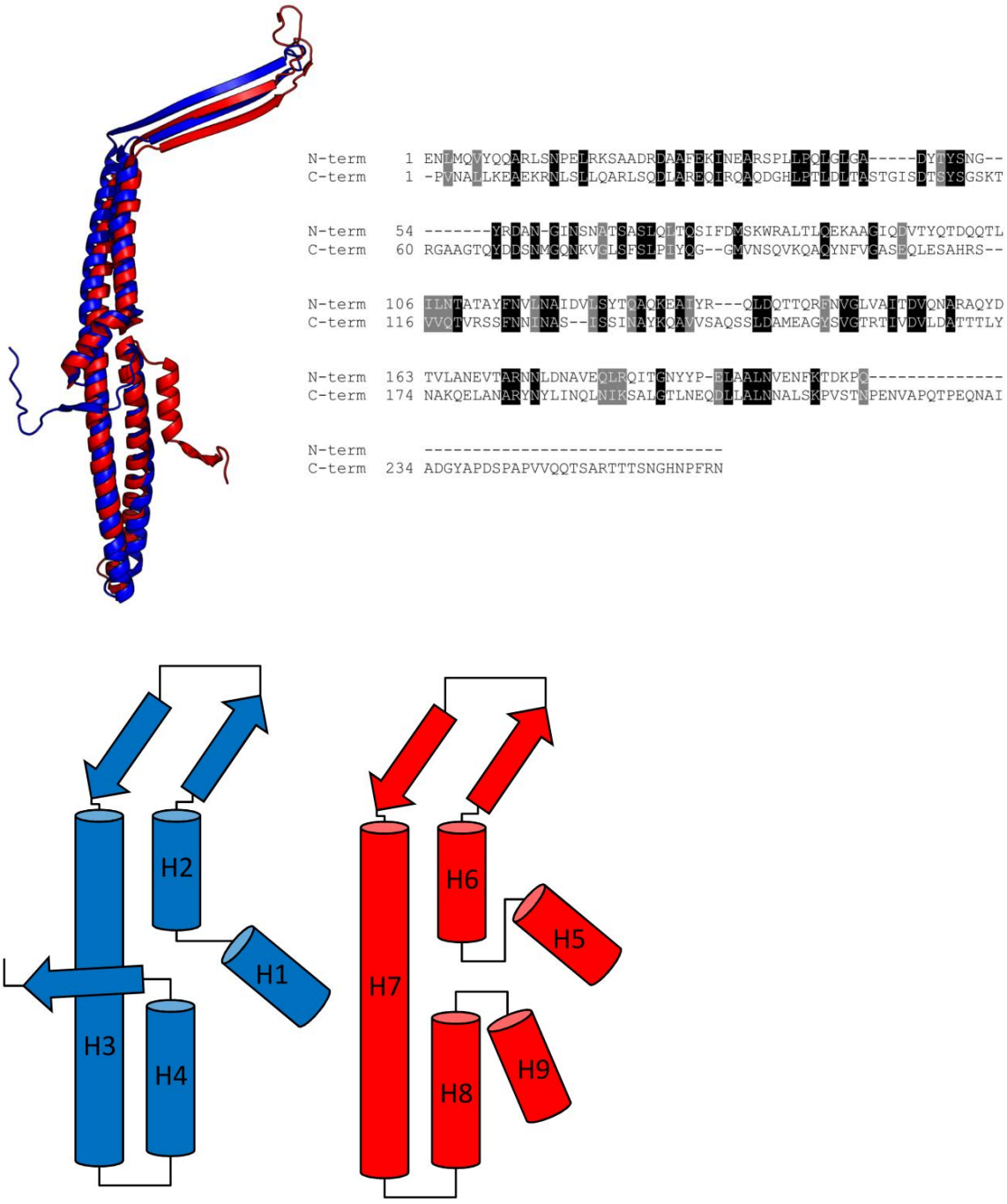

Figure 3:5 - The structural repeat within TolC.

When split into the N- (blue) and C-terminal (red) halves as described in the text body, the TolC monomer shows a structural repeat (left), which is also clear from the topology alone (bottom). Sequence alignment of the two halves of the protein (right) shows only limited similarity between the two halves.

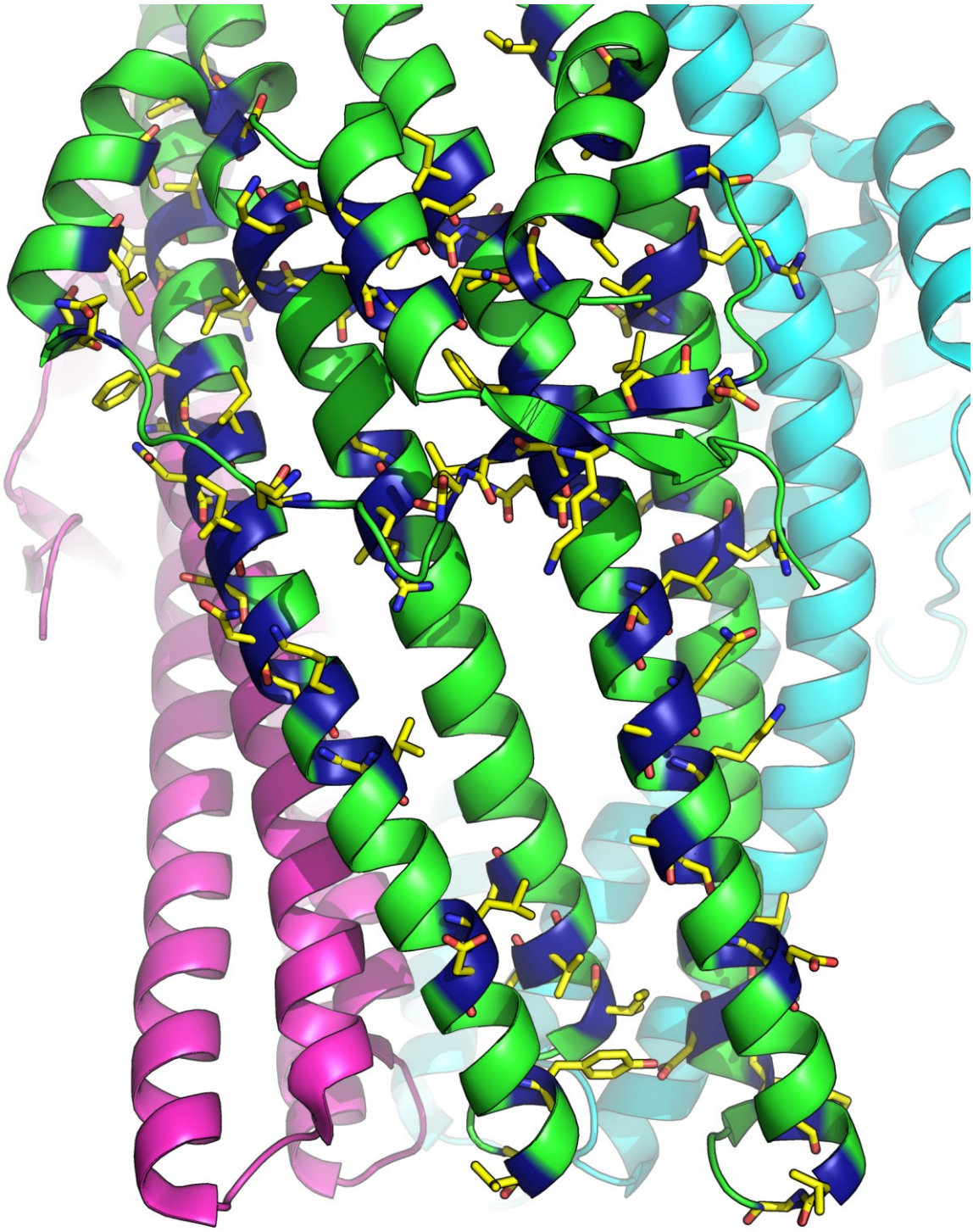

Figure 3:6 - Mapping of positions conserved in the TolC structural repeat.
Mapping of positions that are conserved (yellow) in both the N- and C-terminal halves of TolC. Each TolC protomer is shown in a unique colour (green, magenta or cyan), to differentiate the inter- and intra-protomer grooves. Only the equatorial domain and the portion of the α-barrel more distal to the outer membrane are shown.

3.3 *tolC* mutations used in this study

D121N - This mutation has previously been shown to adapt TolC to function with MexAB (Bokma *et al.,* 2006), but the reason behind this adaptation, and any effect of this mutation on the AcrAB-TolC complex have not been shown . Position 121 is close to the equatorial domain, and may interact with R390, an interaction which, if broken by AcrA, would weaken the inter-helical interactions that hold TolC in its closed conformation. The objectives of this mutation are therefore to determine firstly if the gain-of-function with MexAB is caused by constitutive opening of the TolC channel, and secondly if the mutation has an unreported detrimental effect on AcrAB-TolC function.

Q129L – Although this residue faces into the TolC lumen, it appears to interact with N381 on H8, which, upon initial stages of relaxation of the coiled coils, would be pulled towards the surface between H3 and H8. This would form a more hydrophilic environment at this position of the intra-protomer groove than what is presented in the closed structure. By mutation to leucine, the possible requirement for the conversion from a hydrophobic region to hydrophilic at this region will no longer be achieved upon realignment of the helices, and this may cause the interaction with AcrA to be less efficient. JANUS gives a high importance score (combined score of 397 when compared to MtrE, VceC and OprM) for this position, suggesting that it is likely to be involved in determining selection of the MFP.

N145L – Mutation to cysteine at this position cross-links quite poorly to AcrB, compared to mutation of other positions in the same turn between H3/H4 of TolC (Tamura *et al.*, 2005). The poor cross-linking upon mutation of this position may be indicative that it is involved in the interaction with AcrB, and that the mutation causes sufficient loss of interaction that the proteins are no longer in close proximity often enough or long enough for efficient cross-linking to occur. The distances

between the three N145 positions within the TolC trimer also match well with the distances between the Q255 and D256 on the AcrB trimer, and superimposing the TolC tip to the β-hairpins of AcrB suggest that these positions may well interact, although this would rotate TolC by 60° about an axis perpendicular to the membrane compared to the previously proposed AcrB-TolC interaction (Bavro *et al.*, 2008). This mutation is therefore hypothesised to disrupt the AcrB-TolC interaction, by removal of the hydrogen bonds between the two proteins.

R158D – Mutation of this position to cysteine has been shown to be unable to cross-link to AcrA even when the long cross-linking agent LC-SPDP (with a 15.7 Å linker arm) is used (Lobedanz *et al.*, 2007). Other positions in the same region of the protein do enable cross-linking when mutated to cysteine, which may indicate that this particular mutation prevents the TolC-AcrA interaction from being stable enough for cross-linking to take place. This position may also be involved in hydrogen bonding with Q346 and S350, as part of the inter-protomer interaction, disruption of which by binding of AcrA could facilitate outward movement of helices, dilating the channel. Even if not involved in channel dilation, this region of the external face of TolC contains a particularly high local concentration of hydrophilic residues, and switching of charge on one of these could disrupt binding of a partner protein. This mutation is therefore expected to cause loss of efflux activity and possibly to also increase channel dilation.

V198D – The reported gain of function with MexAB has not been entirely investigated - the reason for this gain of function, and any possible impact upon functionality with AcrAB are unknown (Bokma *et al.*, 2006). Located on the equatorial domain loop between the two structural repeats of TolC, this position would be a less obvious candidate for mutation were it not for the reported gain-of-function with MexAB. However, the positions around this in the structure are D121,

Y125, K383 and R390. This hydrophobic residue may therefore be required for interaction with a hydrophobic residue on the tip of the AcrA hairpin, possibly moving away from this otherwise very hydrophilic environment. Such a movement would be possible, being on a loop around the outside of the α-barrel of TolC, and such movement would possibly cause other residues on the loop to pull the helices with the loop; this is where the sharpest change of angle of the coiled-coils is located, and this movement could therefore induce maximum channel opening. By introducing an acidic residue at this position, it may cause the channel to become unable to open efficiently upon interaction with AcrA, and may also prevent AcrA from accessing its most interpenetrating position.

N332L – This residue is located on H7, at the equatorial domain. It forms part of a network of hydrophilic residues, including N173, D176, N177, E180 and R328, at an inter-protomer interface at the position where the α-barrel begins to twist to generate the closed conformation. Disruption of the interactions in this area by AcrA binding could therefore lead to channel opening. In other proteins, the equivalent position is alanine in MtrE and OprM, but asparagine in VceC. Given that VceAB is capable of functioning with TolC (Vediyappan *et al.*, 2006), but neither MtrC nor MexA are capable of functioning with TolC without mutational adaptation, this position could be one of the determinants for MFP selection. There is also conservation of this residue in the N- and C-terminal pseudo-copies of the protein, supporting the notion that this position is essential for interaction with partner proteins. This mutation is hypothesised to decrease the stability of AcrA binding, and therefore to decrease efflux activity, although it could instead lead to a separation of the helices at this area and thereby cause instability of the TolC protein.

N342A – Based on computational results, this position is hypervariable in OMCs from different species, but is well conserved within a species. Furthermore, the equivalent

position in the first half of the protein is glutamine, indicating good similarity even though there is not conservation at the identity level between the two halves of the protein. This indicates that the position could be essential for the interaction with partner proteins. The JANUS score at this position is a mid-range score ,as the combined score to each of the other proteins used in the comparison is 193 (ranked 233 out of 428), suggesting that there may be limited requirement for mutation at this position to switch binding partners. In the equivalent position in the other proteins analysed by JANUS, MtrE (aspartate) and VceC (arginine) have opposite charges to each other, while OprM contains glutamine. AcrA and OprM are known to interact in a non-functional manner, thus suggesting that this position may be required for the interaction but not for the functionality of the two proteins. This mutation is therefore predicted to abolish AcrA-TolC interaction and therefore prevent normal function of the efflux assemblies.

Y344F – Y344 appears to interact with T120 and N167, forming an inter-protomer interaction. However, in the 1EK9 crystal structure, the side chain is twisted around the helix, in such a way that movement of the helix during opening of the channel will force this interaction to break. Results from Consurf indicate that this position is quite well conserved (group 9; Figure 3:7), in a region which is otherwise largely poorly conserved but not hypervariable (groups 5 and 6). JANUS gives a mid-level score to this position (88 to MtrE and 97 to OprM), indicating that although possibly important in selection of the partner protein, it is not likely to be as important as other residues. The position is conserved in VceC (also tyrosine) but not in either MtrE or OprM (leucine and glutamine, respectively), and so may be involved in selection of the MFP once the channel has partially opened. Mutation of this position to phenylalanine will prevent any possible hydrogen bonds from forming, but the change is sufficiently conservative that it is unlikely to cause major disruption to the folding and trimerisation of TolC.

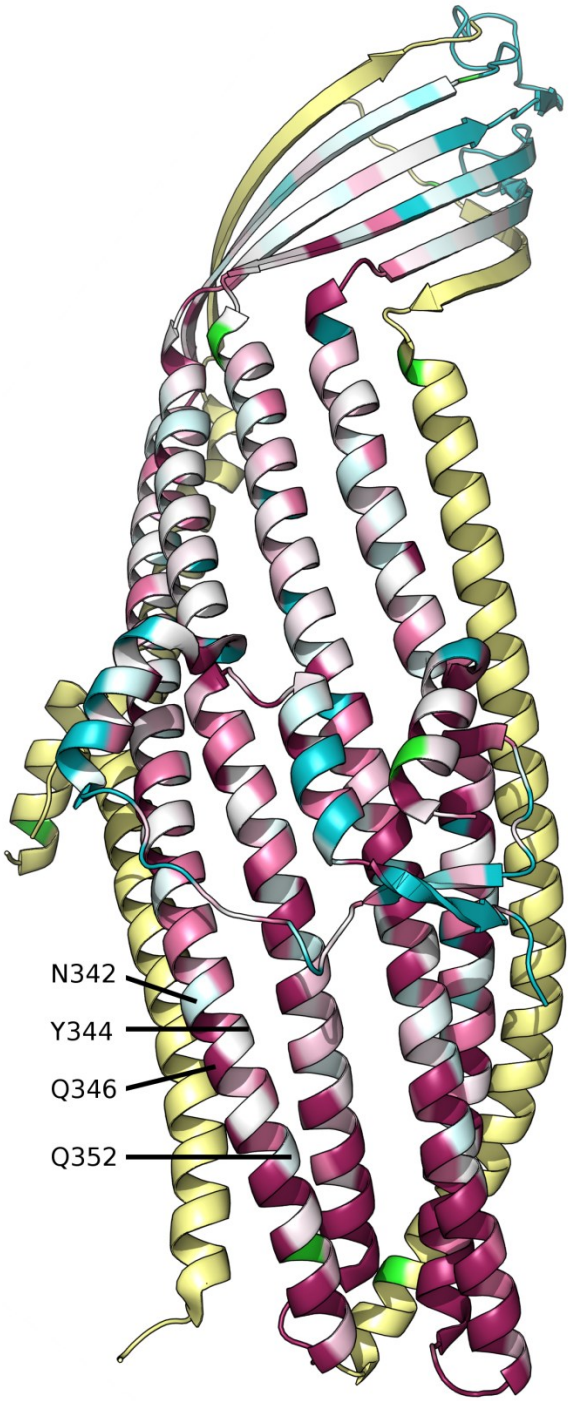

Figure 3:7 - Consurf output of conservation in OMC sequences.
Using the 1EK9 structure as the query, the Consurf results are mapped directly onto the same structure, to a single protomer. In pale yellow are adjacent helices of the other protomers. Each position is coloured on a scale from blue through white to purple, with blue being hypervariable, white being semi-variable and purple being most conserved. Positions in green are those lacking sufficient data in the alignment to calculate a conservation score. The labelled positions were chosen for mutation in part because of the Consurf results.

Q346L – Mutation of the equivalent position in MtrE (K397) has previously been shown to increase sensitivity to tetracycline, but not other antibiotics. The score from Consurf (group 9) indicates that this position is well conserved across many channel proteins, and manual analysis of multiple sequence alignments indicates that this is indeed the case, except for in OprJ, which is only known to function with MexCD, although MexCD-OprM is also functional when OprM is overexpressed. Glutamine at this position is conserved in VceC but not in MtrE or OprM (lysine and aspartic acid, respectively); the charged residues of MtrE and OprM, which are not capable of complementing TolC (or vice versa), suggests that this position may be partially responsible for the selective functionality, but not binding, of MFPs with TolC. The JANUS scores reflect this, giving a high score for the comparison with MtrE (192) and a medium score (78) for comparison with OprM. Analysis of the TolC structure indicates that this position interacts with R158 and D162, both of which are also highly conserved, in an inter-protomer interaction. Binding of the MFP may therefore disrupt this interaction, or, given the local structure and the twist-to-open mechanism of TolC, cause re-arrangement of the helices in order to maintain these inter-protomer interactions. Mutation to leucine will eliminate side-chain hydrogen bonding at this position, and is expected to switch MFP-OMC specificity, losing functionality with AcrA.

S350F – Conflicting information has been published regarding this mutation, by a single research group. Thorough analysis of the mutant is needed to determine what effect the mutation actually has. This position is part of an inter-protomer hydrogen- and ionic-bonding network, and introduction of a bulky side chain such as phenylalanine could logically push the protomers apart, although it may simply cause the aromatic ring to block the interprotomer groove and prevent binding of the MFP.

Therefore, this mutation should cause loss of function either due to the loss of interaction with its partner proteins or due to a dramatic increase in drug influx through an open TolC channel. It is also necessary to clarify the literature and determine to what extent this mutation causes degradation or otherwise decreased proteins levels. Intriguingly, serine is conserved at this position in OpmH and OprJ, while an alanine residue is conserved at the equivalent positions in MdsC, OprM, OprN and MtrE. MdsA can function with either TolC or MdsC, while AcrA is only capable of functioning with TolC. Similarly, MexC functions with either OprJ or OprM, and MexJ functions with either OprM or OpmH dependent upon the substrate, while MexA is only capable of functioning with OprM. Together, this may indicate that the hydroxyl group may be required for full functionality with a subset of partners, while other partners can function irrespective of whether the hydroxyl group is present.

Q352A/E – Despite being only 17 Å from the tip of TolC, mutation of this position to cysteine does not facilitate cross-linking to AcrA even when using a 15.7 Å linker arm (Lobedanz *et al.*, 2007), although mutation of S124 facilitated cross-linking with a shorter linker arm. This may indicate that Q352 is essential for the binding of AcrA to TolC, and mutation prevents this interaction from being sufficiently stable to facilitate cross-linking. Consurf indicates that this position is quite variable between proteins, although manual analysis of sequence alignments shows that when glutamine is not conserved at this position, a charged residue is present - this could indicate some charge-specific interaction takes place in certain OMC-MFP pairs. Based upon the possible charge-specific interactions, JANUS scores this position highly (a combined score of 384), indicating that it may be required in selection of partner proteins. This position will be assessed by two mutations - the first, to alanine, will prevent any hydrogen bonding at this position between AcrA and TolC, while the second, to glutamic acid, will determine whether or not the introduction of

a charge at this position has any effect on the interaction without changing any other parameters such as side-chain length.

Y362F/R367S (YFRS) – This double mutation is known to disrupt the hydrogen- and ionic-bonding network at the periplasmic tip of TolC, but to cause less dilation of the channel than does the YFRE mutation. The YFRE mutation has been shown to not only be more dilated than the wild-type protein, but also to be more susceptible to novobiocin (an efflux substrate) and to have lower binding affinity to both AcrA and AcrB. It is not known whether the YFRS mutation affects efflux activity or binding of partner proteins. The mutation is therefore included in this study to determine whether the partial opening of the channel, or the specific mutations, are responsible for the loss of activity and decreased partner protein binding propensity.

D371V – TolC has two aspartate rings at the periplasmic end of its lumen, which act as ion-selective gates (Andersen *et al.*, 2002c). This position has previously been mutated to alanine as part of a double mutation, along with D374A, which causes a loss of cation coordination, and subsequently causes greater permeability of the channel. Upon complete channel dilation, the outward movement of the H7/H8 helical pair may bring D371 into contact with R143, to stabilise the open state. Mutation to introduce a hydrophobic residue at this position may therefore either cause channel dilation due to disruption of the cation co-ordinated aspartate rings and possible conflict between the mutated position and its neighbours (potentially decrease trimer stability), or cause the channel to become unable to open as the hydrophobic ring cannot be opened by the same interactions as can the negatively charged ring.

D374V – As with the D371V mutant, above, this position forms an aspartate ring that acts as an ion-selective gate (Andersen *et al.*, 2002c). Being a helical turn higher in the TolC lumen, this position is unlikely to form new interactions at the periplasmic tip

that would stabilise the open state. However, it is possible that the change from an acidic residue to a hydrophobic residue low in the TolC lumen may impact the movement of efflux substrates, and possibly influx of substances, through the channel. Similarly to the D371V mutation, the D374V mutation may cause instability of the TolC trimer, cause channel dilation due to electrostatic incompatibility of other residues in the local environment, or cause the channel to become unable to open due to a different disruption mechanism being required to open the hydrophobic gate compared to an acidic gate. The structure of VceC, which has the equivalent of D371/V374 (Federici *et al.*, 2005), is stable and appears closed, indicating that trimer instability should not be an issue.

K383D/E – The K383D mutation has previously been reported to cause increased sensitivity to novobiocin, but not to vancomycin, suggesting that the increase in novobiocin sensitivity is not caused by a substantial increase of influx through the TolC channel (Bavro *et al.*, 2008). Charge reversal of the equivalent position in MtrE (E434) causes increased vancomycin sensitivity only in the presence of the MFP, indicating that the mutation itself does not cause constitutive opening of the channel. The mutation to aspartate is therefore included for more detailed analysis than previously reported, and to assess the impact of MFP binding *in vitro*, while the mutation to glutamate is included to determine whether the effect is caused only by the charge reversal or if the length of the side chain is also a factor.

R390E(/N392T) – In both TolC and at the equivalent position in MtrE, mutation of this position to glutamate has been shown to increase vancomycin susceptibility (Bavro *et al.*, 2008). This is possibly due to a rearrangement of the H7/H8 helical pair towards the loop of the equatorial domain, caused by loss of the positive charge repulsion between R390 and K201. Random mutagenesis of TolC has shown that the R390C mutation causes hypersensitivity to all tested drugs (efflux substrates and

vancomycin), suggesting that the apparent loss of function is probably at least in part due to increased influx of the efflux substrates through TolC, although decreased efflux activity may also contribute. The R390E mutation was therefore included to study in greater detail the effect of this mutation, particularly in a possible interaction with AcrA. During mutagenesis, the R390E/N392T double mutant was found to have spontaneously arisen on the transformation plate following mutagenesis. This double mutant was included to test whether it had arisen as a suppressor mutation.

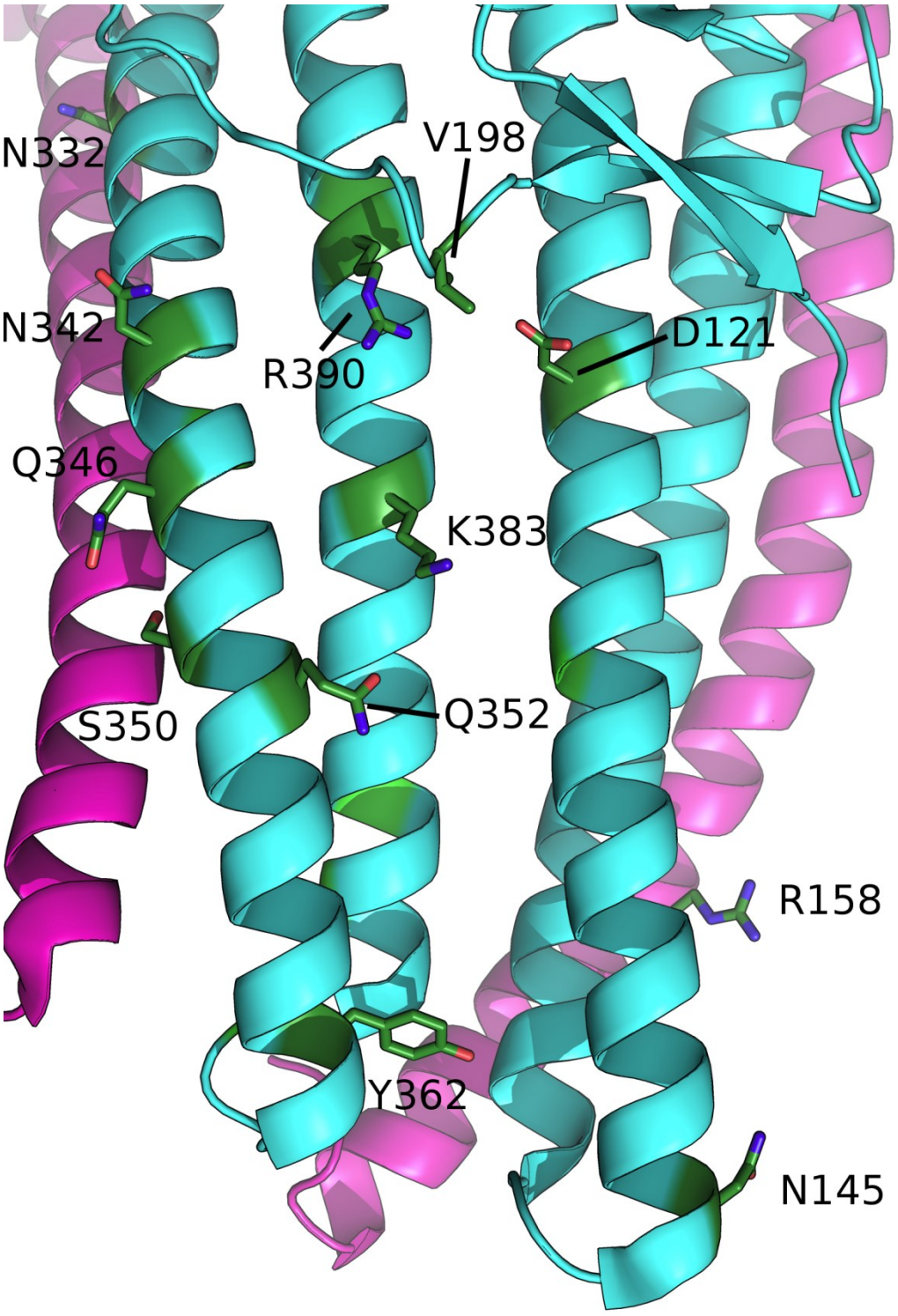

Figure 3:8 - Map of TolC mutants used, outside of the channel.
Positions mutated for use in this study (green) are mapped onto the 1EK9 TolC structure, to the protomer shown in blue. The view is from the periplasmic side of the channel. Shown in magenta are adjacent helices of the other two protomers.

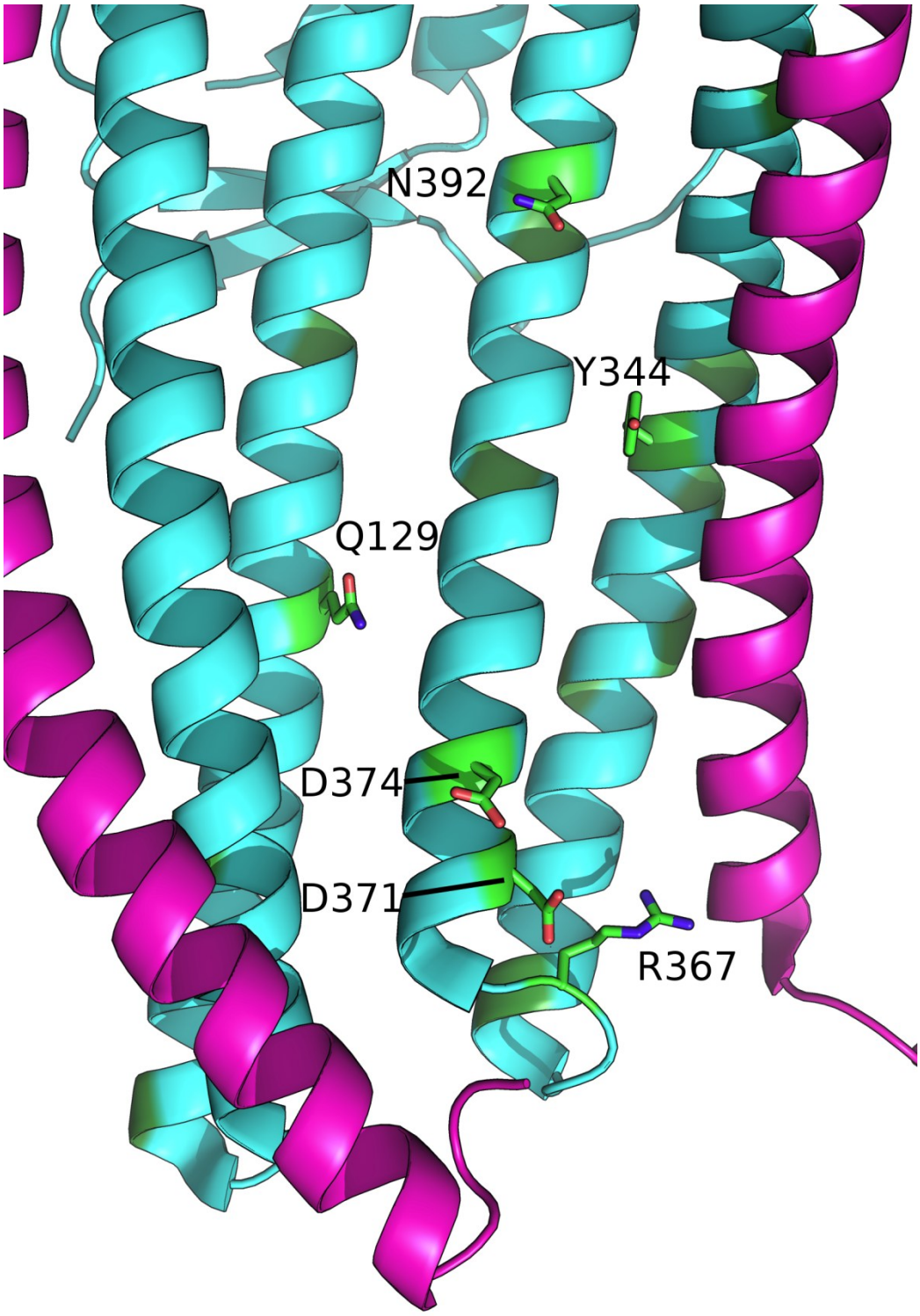

Figure 3:9 - Map of TolC mutants used, inside the channel.

Positions mutated for use in this study (green) are mapped onto the 1EK9 TolC structure, to the protomer shown in blue. The view is from inside the channel lumen. Shown in magenta are adjacent helices of the other two protomers. 1: R367. 2: D371. 3: D374. 4: Q129. 5: Y344. 6: N392

3.4 CAPS analysis

Sequences for MFPs and their cognate OMCs were prepared as described in the methods and used as the input for the CAPS programme. CAPS assesses differences at each position within a multiple sequence alignment, and calculates the Pearson correlation coefficient of the changes at every pair of positions. The output from the program only indicates pairs of positions that it indicates as co-evolving; any positions that are not indicated to co-evolve are not shown in the output file. Only pairs of positions that are ranked as likely to co-evolve in which one of the pair is a position in the MFP and the other a partner in the OMC are of interest from this programme. Positions that were shown as co-evolving only with another position from the same protein were disregarded for this study. The positions that CAPS determined as co-evolving on both the MFP and OMC within the chimaeric multiple sequence alignment are shown in Table 3:1 and mapped to the relevant structures in Figure 3:10. Given that the positions appear unlikely to co-evolve due to evolutionary pressure driven by the positions interacting, the positions were viewed in the sequence alignment (Figure 3:11). From the high conservation at each of these positions, it appears unlikely that they are co-evolved, and more likely that they are simply conserved between the input sequences.

Table 3:1 - CAPS output for co-evolution analysis of AcrA and TolC residues
The raw output from CAPS provides alignment positions, which have been manually replaced by extraction from the alignment. Positional numbers correspond to the annotation in the 2F1M and 1EK9 structures.

Position 1	Position 2	Correlation
AcrA-E88	TolC-Y362	0.845047
AcrA-E88	TolC-T406	0.864794
AcrA-D97	TolC-Y113	0.850882
AcrA-D97	TolC-N220	0.862368
AcrA-D97	TolC-T326	0.824756
AcrA-D97	TolC-D356	0.836107
AcrA-D97	TolC-Y362	0.914149
AcrA-D97	TolC-T406	0.914355
AcrA-S178	TolC-T326	0.834062
AcrA-S178	TolC-Y362	0.867773

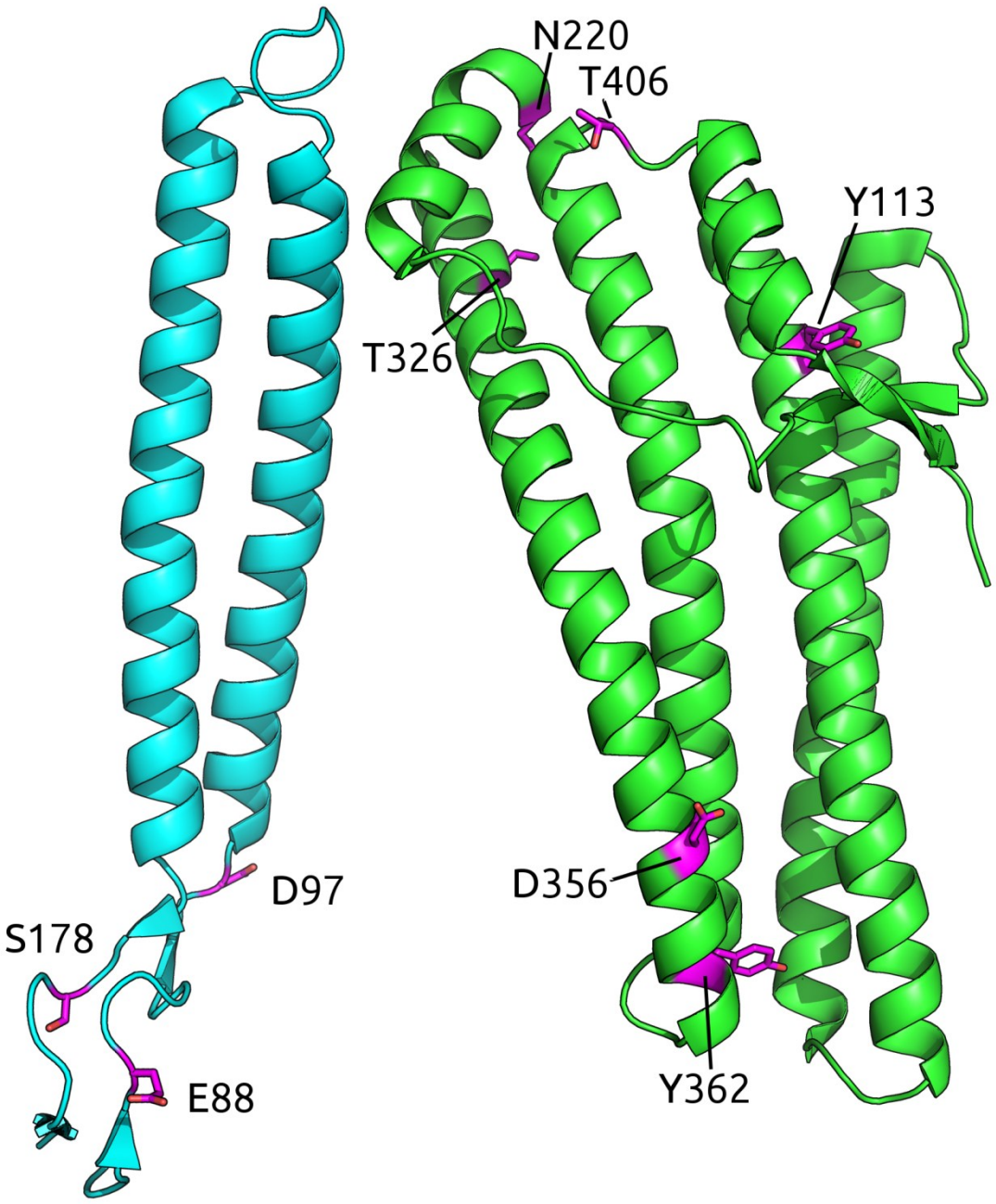

Figure 3:10 - Map of positions on AcrA and TolC that "co-evolve"
Positions identified by CAPS as co-evolving are highlighted in magenta on the structures of AcrA (cyan) and TolC (green). Each structure is shown as trimmed to remove positions not included in the alignment used as CAPS input.

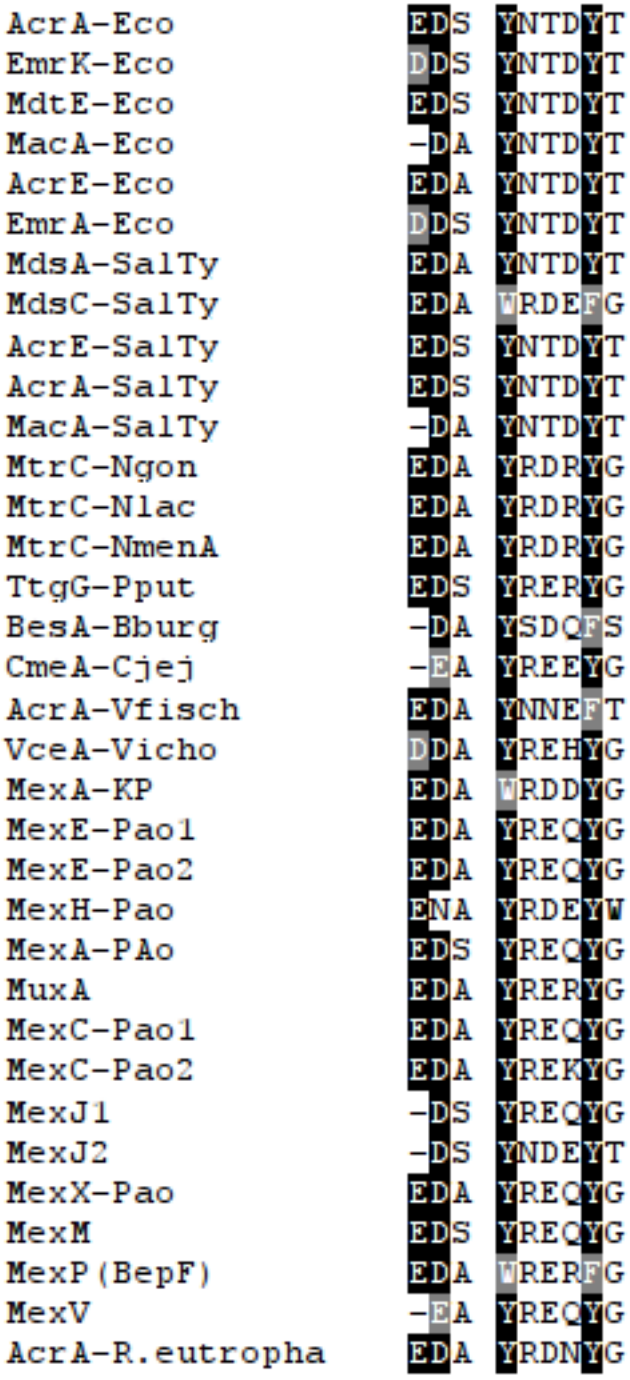

Figure 3:11 - Sequence alignment of positions identified by CAPS as co-evolving.

The CAPS input file was edited to remove all positions not identified as co-evolving. Positions left of the space are in MFPs, those to the right are in OMCs. From left to right, (AcrA-)E88, D97, S178, (TolC-) Y113, N220, T326, D356, Y362, T406. Those MFPs that have multiple cognate partners are shown with each partner in a new line.

3.5 *acrA* mutations used in this study

Using information mainly from published literature, mutations were designed in *acrA*, as detailed in Table 3:2, which details the actual mutations made for each named mutation and the logic behind all *acrA* mutations made. A sequence alignment of the three major hairpin mutants, with the wild-type sequence, is shown in Figure 3:12. The mutation sites and the major alterations to the hairpin are shown on the AcrA structure in Figure 3:13.

Table 3:2 - *acrA* mutations in this study.

Nomination	Mutation (2F1M numbering)	Logic
GS-tip	Δ131-141::"GSGGSG"	Replacement of the hairpin tip with a flexible linker sequence, leaving the helices as wild-type but removing sequence specificity at the tip.
Δhelices	Δ102-126/Δ143-170	Removal of the helical part of the hairpin, leaving the tip region intact.
Δhairpin	Δ101-175::BesA loop	Removal of the entire hairpin, replacing it with the loop sequence from the hairpin-less BesA.
S139G	S139G	Replacement of the serine from the published "RLS" motif with a non-reactive and flexible residue.
TVYF	T104V/Y105F	Putative manual docking models suggest that T104 may interact with TolC-R143, while in an alternative orientation, Y105 may interact with TolC-R367. Replacement by amino acids of similar structure but lacking hydroxyl groups to prevent hydrogen bonding.

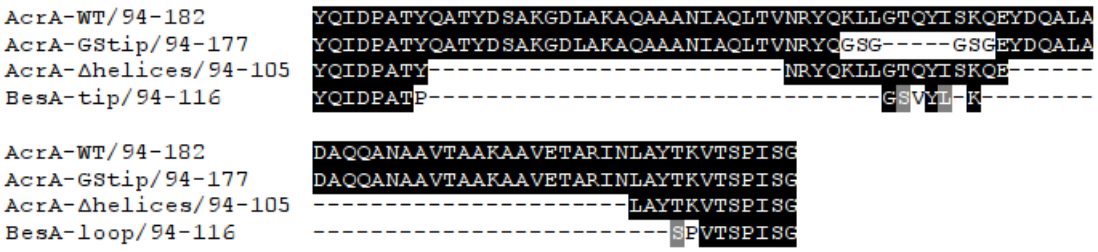

Figure 3:12 - Sequence alignment of hairpin mutants used in this study.

Only the hairpin sequences and the five positions either side of it are shown in this alignment. The alignment indicates the sequence differences between each of the mutations used in this study, compared to the wild-type sequence. The GS-tip mutant is identical to the wild-type sequence except at the hairpin tip region. The Δhelices mutation retains the sequence at the hairpin tip region, but the coding sequences for the helices of the hairpin have been removed. The BesA-loop sequence is as used for the Δhairpin mutant, in which the entire hairpin structure was replaced by the flexible loop from the BesA MFP from *Borrelia burgdorferi*.

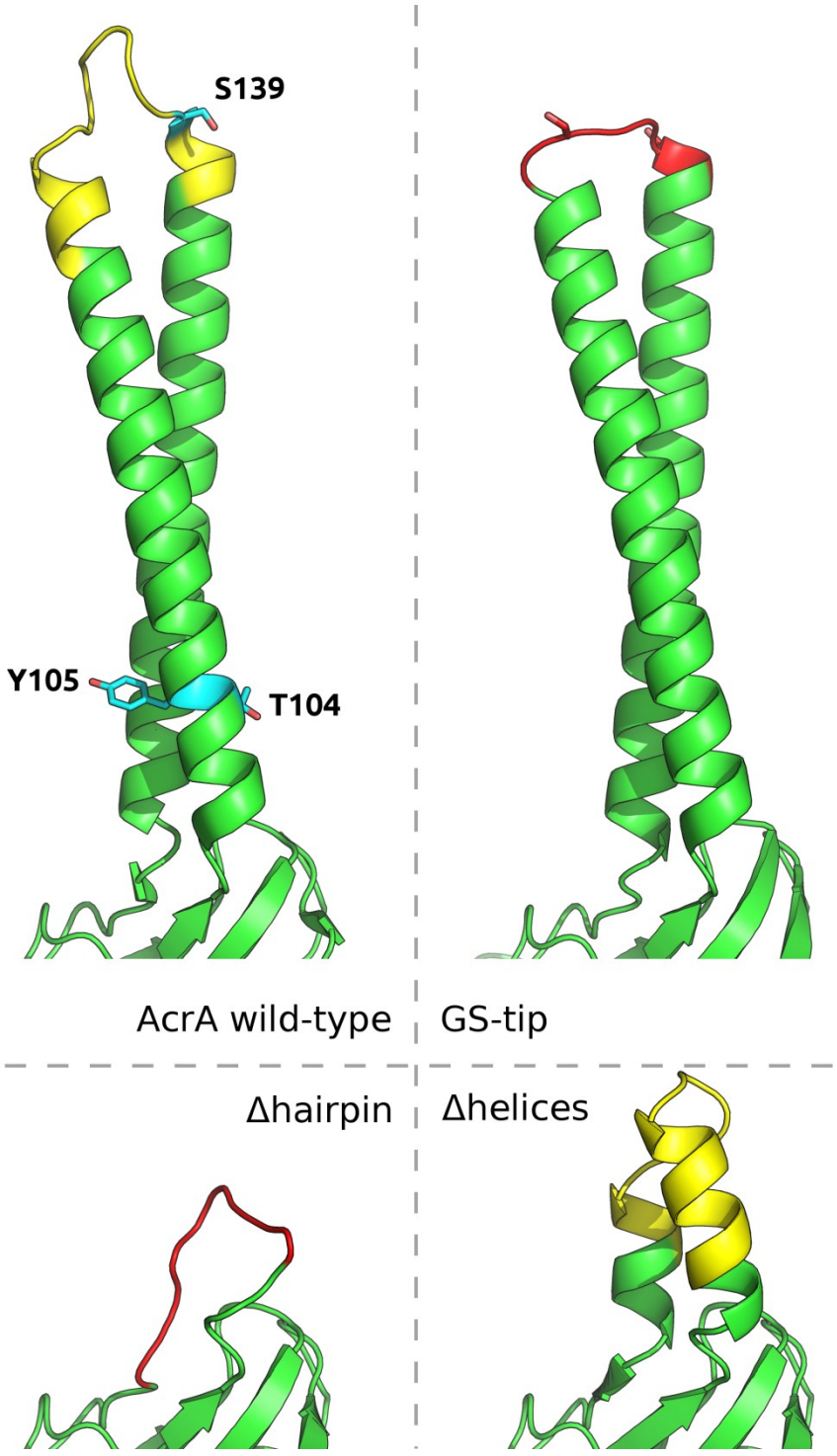

Figure 3:13 - Predicted structures of hairpin mutants and positions of point mutants on AcrA.

Indicated in blue on the wild-type sequence are the positions mutated in point mutants. In red are the GS-tip mutated sequence, with serine sidechains shown, and the BesA-loop of the Δhairpin variant. In yellow is the wild-type AcrA tip sequence that has been brought closer to the lipoyl domain by deletion of the hairpin helices (Δhelices)

3.6 The published MtrE structure is an unnatural protein

In an attempt to enable testing of cross-reactivity of proteins from non-cognate systems, efforts were made to clone *mtrE* from a pET21-mtrE plasmid received from the laboratory of Dr Adrian Walmsley. Upon failing to generate a PCR product, the received plasmid was sequenced to check that the primers used were suitable. The 3`- end of the gene in the plasmid had several mismatches to the cloning primer, including towards the 3`-end of the primer, meaning that the primer would fail to primer for elongation. To ensure the differences in sequence were silent, the received plasmid was sequenced using both the forward and reverse pET sequencing primers and the resulting DNA sequences translated using the translate tool on the expasy.org website. When analysing the translated sequences, it was noticed that the sequence for MtrE as presented in the 4MT0 crystal structure, which was stated as being the wild-type sequence (Lei *et al.*, 2014),was split between reading frames when sequenced from either end (Figure 3:14 and Figure 3:15).

To determine whether the sequence used to generate the MtrE structure was indeed the wild-type, the sequence used (FA136) was aligned to MtrE sequences from other species of *Neisseria* and to the translation of that from the FA19 wild-type reference strain (Abrams *et al.*, 2015). The sequence alignment showed that the FA136 sequence was a clear anomaly among these sequences (Figure 3:16), with the mismatch being the same as the part of the sequence that was highlighted in the translations. As this had initially been found from the translated sequences in each frame, the DNA sequences were aligned to find any frame-shift mutations (Figure 3:17). The DNA sequence alignment indicated that the FA136 sequence contains a single base insertion (T) and a single base deletion (G).

According to the authors of the 4MT0 MtrE structure, this protein is constitutively dilated, which is inconsistent with other information available about the MtrE protein

(Janganan *et al.*, 2013). The structure was resolved from protein expressed from a synthesised gene, in which the alternative sequence had been specified. The sequence from the plasmid received for use in this thesis corresponded to FA19 except for towards the end of the discernible sequence trace. In these regions of sequence traces, the confidence in the trace decreases, with an increased rate of mis-called bases, insertions and deletions, as the signal intensity decreases towards the same as the background. The authors of the 4MT0 structure were informed of these details, and *mtrE* in FA136 was re-sequenced. From the new sequences, it appears that the forward and reverse sequences had previously been misaligned due to the issue of low signal intensity. This has led to the MtrE protein being re-crystallised, and the new structure better matches those of OMCs from other species.

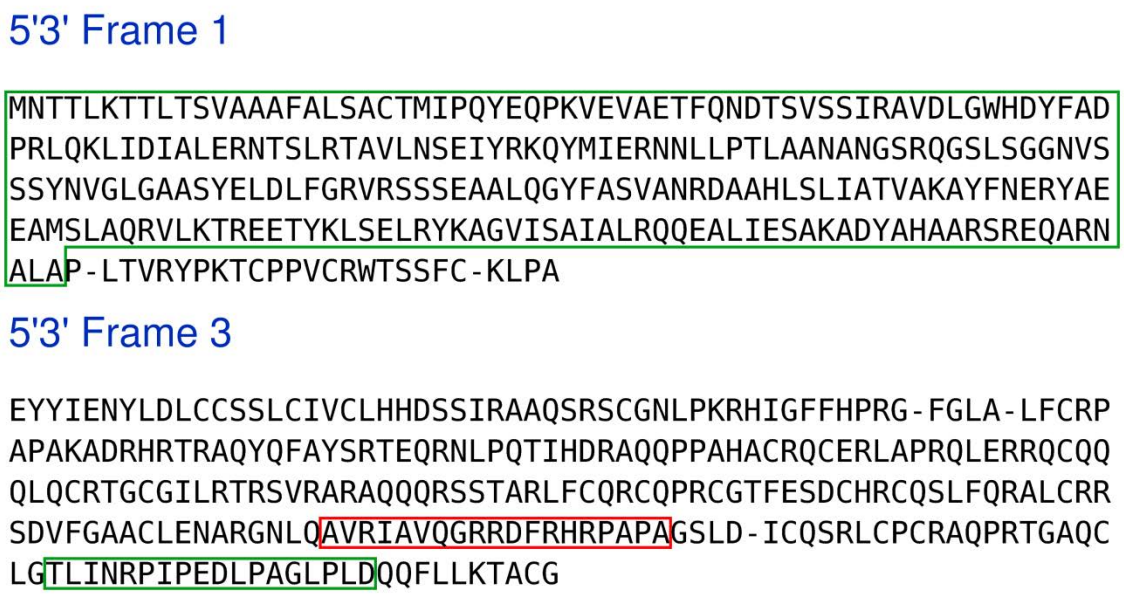

Figure 3:14 - Translation of pET21-mtrE forward sequencing.

Output from the expasy.org “Translate Tool”, using the results from forward sequencing of pET21-mtrE as the input. Green boxes indicate where the sequence matches the *N. gonorrhoeae* FA19 reference sequence; the red box indicates where the sequence matches the *N. gonorrhoeae* FA136 sequence. Reading frame 2 Is omitted as it did not include any of the translated protein sequence.

3'5' Frame 1

CHVAKAISTSVMPKKRCLWRSVS-KRARKPTSCPNCGTRQA-FPPSPCASRKP-LNLPKP
IMPMPRAAANRRAMPWQP-LTVRYPKTCPPVCRWTSSFLLKNCLPV-VPKYCSTVPTSAP
PNTRSNRQTPISVRRAPPFSRPSA-PEASVRALSNWAGCSKAARAFGRSRRLLPCRFLLG
ERTRRTLMWQNCANRHKLLPMNPPSNPPFKTWQTHWRRASSWIKPMTL-ANKAAPLKKRC
AWSDCVTNTAYPARSICSMRNAAAIRQKVRLCRHN-PAPKTLPICTRRSAAD-NGIPKPA
THLRPHSSTTTTT

3'5' Frame 2

ATLPKLFQRALCRRSDVFGAACLENARGNLQAVRIAVQGRRDFRHRPAPAGSLD-ICQSR
LCPCRAQPRTGAQCLGNLD-PSDTRRPARRFAVGQAVFC-KTACRFEFRSIARPSRHPRR
RTRAQTGKRQYRCGARRLFPVHPPDRKRRYGLCRIGRAVQKRHGRLGVRAVYYPADFYLG
NEQGEP-CGKTAPTGTNCCL-IRRPIRLSRRGKRIGGARAAG-SL-RFKQTKPRL-RSVA
LGRTALQTRRIRRARFARCGTQQLFGRRCGFVGTTDPRRKPCRFVQGARRRIETGYPNRQ
PTCGRTRAPPPPP

3'5' Frame 3

PRCQSYFNERYAEEAMSLAQRVLKTREETYKLSELRYKAGVISAIALRQQEALIESAKAD
YAHAARSREQARNALATLINRPIPEDLPAGLPLDKQFFVEKLPAGLSSEVLLDRPDIRAA
EHALKQANANIGAARAAFFPSIRLTGSVGTGSVELGGLFKSGTGVWAFAPSITLPIFTWG
TNKANLDVAKLRQQAQIVAYESAVQSAFQDVANALAAREQLDKAYDALSKQSRASKEALR
LVGLRYKHGVSGALDLLDAERSSYSAEGAALSAQLTRAENLADLYKALGGGLKRDTQTGN
PLAAALEHHHHHH

Figure 3:15 - Translation of pET21-mtrE reverse sequencing.

Output from the expasy.org "Translate Tool", using the results from reverse sequencing of pET21-mtrE as the input. Green boxes indicate where the sequence matches the *N. gonorrhoeae* FA19 reference sequence; the red box indicates where the sequence matches the *N. gonorrhoeae* FA136 sequence.

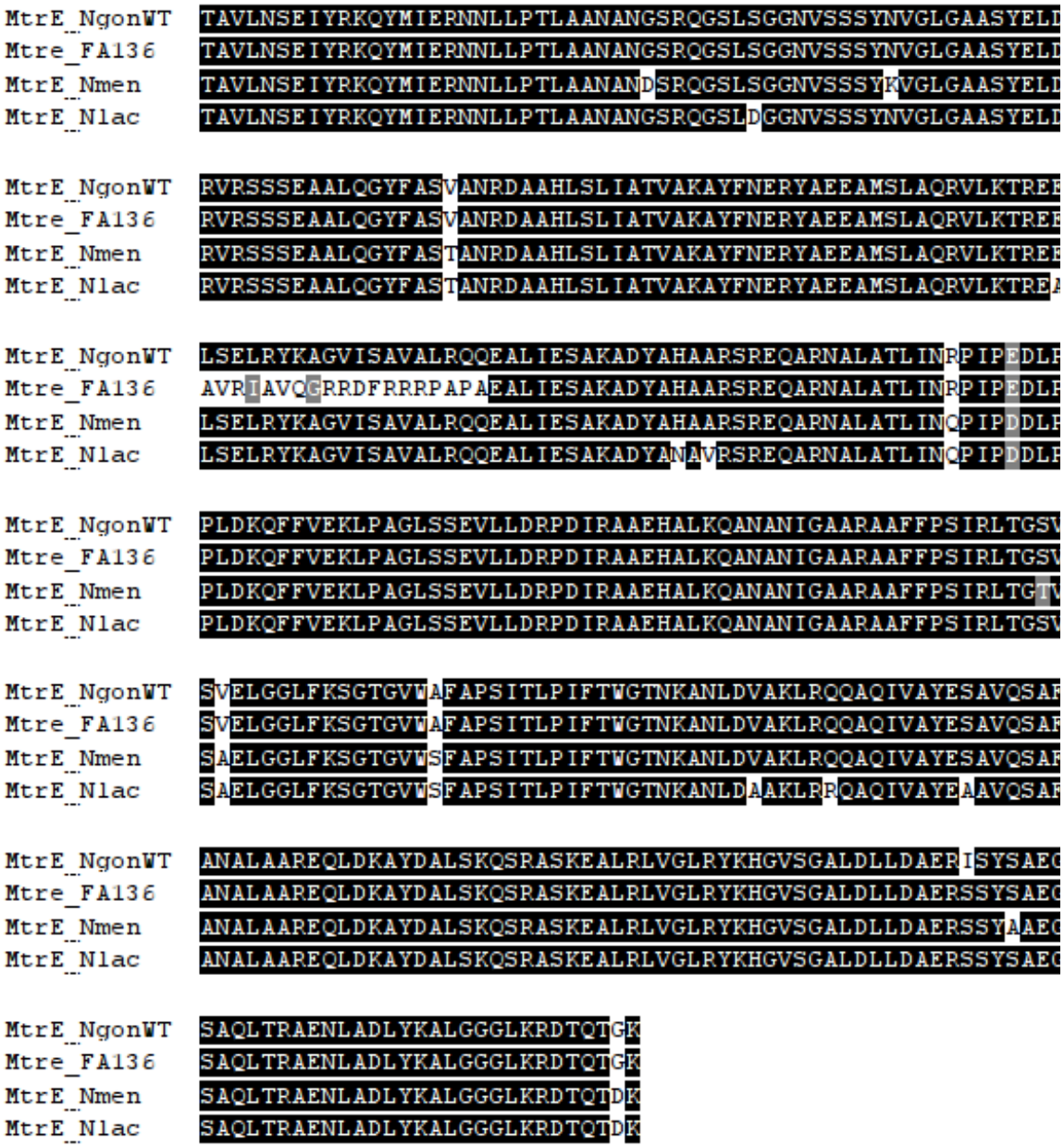

Figure 3:16 - MtrE proteins sequence alignments.

Protein sequence alignments of wild-type *N. gonorrhoeae* (NgonWT), *N. meningitidis* (Nmen) and *N. lactamica* (Nlac) MtrE sequences, with the *N. gonorrhoeae* FA136 MtrE sequence.

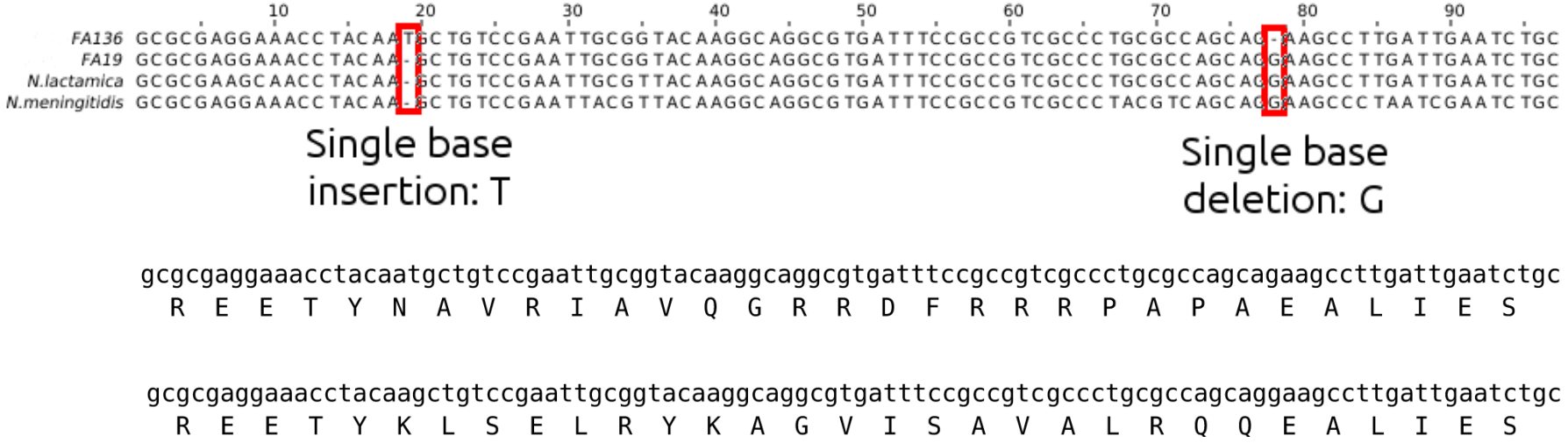

Figure 3:17 - Single nucleotide insertion and deletion in FA136 sequence.

Sequence alignments for *mtrE* genes and the translations of the gene sequences from FA136 and FA19.

CHAPTER 4: RESULTS – PROBING THE INTERACTION FROM THE CHANNEL SIDE

4.1 Minimum inhibitory concentrations

The use of MICs in the study of antibiotic resistance is well-established. When cells are exposed to a sequence of drug concentrations, the lowest concentration at which growth is inhibited by 80% compared to without drug is the MIC of that drug against that strain. As the *tolC* gene is located on a plasmid, and is under the control of the tetracycline repressor, it was necessary to determine a suitable concentration of inducer (anhydrotetracycline, a derivative of tetracycline that de-represses the *tet* promoter, but which does not have any antibacterial activity) to use for all *in vivo* studies. Liquid broth MICs were tested for the wild-type strain with empty vector, *tolC* knockout strain with empty vector, and the complemented strain, at four concentrations of anhydrotetracycline, erythromycin and novobiocin. The results of this are shown in Table 4:1. At the highest concentration of anhydrotetracycline tested (200 $ng.ml^{-1}$), the complemented strain has the same MIC values to both drugs as did the knockout. In the absence of inducer and with 2 $ng.ml^{-1}$ anhydrotetracycline, the complemented strain appeared essentially as wild-type, being not more than one doubling dilution different. The wild-type strain seemed unaffected by the inducer, with the MIC to each drug remaining constant across all inducer concentrations. For future experiments, 20 $ng.ml^{-1}$ anhydrotetracycline was used for induction on agar, and 2 $ng.ml^{-1}$ anhydrotetracycline was used for induction in broth.

Table 4:1 - Minimum inhibitory concentration (in µg.ml^{-1}) of erythromycin and novobiocin in a range of inducer concentrations.

[Inducer] / ng.ml^{-1}	0		2		20		200	
Strain	ERY	NOV	ERY	NOV	ERY	NOV	ERY	NOV
BW25113 pASK-RM	128	512	128	512	128	>512	128	512
BWΔtolC pASK-RM	32	2	32	2	32	2	32	2
BWΔtolC pASK-tolC	64	256	64	256	64	256	32	2

Having made a library of *tolC* point mutants, the MIC for a variety of drugs was tested against the library using the agar dilution method, the results of which are shown in Table 4:2 and Table 4:3. Although it will act as additional inducer, tetracycline was included as a drug against which to assay. All of the drugs tested are reported substrates of AcrAB-TolC except for vancomycin. The BSAC recommended control species ATCC 25922 was included to ensure that the MICs conform to expected values, and therefore that the experiment is valid, although there are no recognised standard MIC values for acriflavine, deoxycholic acid, erythromycin, novobiocin or vancomycin. When tested on chloramphenicol, fusidic acid, nalidixic acid, rifampicin and tetracycline, the MIC for the standard control strain was within a single doubling dilution of each expected value, and therefore accepted as valid values. Ciprofloxacin was also tested, but for all strains the MIC was lower than any tested concentration.

The MICs for all strains were essentially equal on rifampicin. On erythromycin, there was no clear difference between the knockout and complemented strains, although the N145L, D371V and R390E/N392T (RENT) mutations had lower MICs than did the knockout strain. Only the mutants Y344F, Q352A and RENT showed a difference in

MIC to vancomycin greater than a single doubling dilution, although Q129L, N145L, R158D, V198D and K383D had an MIC half that of either the knockout or complemented strain. Despite the possible increase in gene expression from the plasmid, the MIC to tetracycline was within a single doubling dilution of the complemented strain for all mutants except Q129L, N145L, Y344F and RENT; however, the wild-type and knockout strains were different by two doubling dilutions, and therefore classified as different to each other but neither different from the complemented strain. Chloramphenicol, fusidic acid and novobiocin MICs were all decreased by the S350F, Y362F/R367S (YFRS) and D371V mutations, in addition to the knockout, but not by any of the other mutations. These same three mutations, plus K383D decreased the MIC of deoxycholic acid. It was also observed that deoxycholic acid caused an unusual sequence of phenotypes, whereby the size of the colony of all mutants not hyper-susceptible increased with increasing concentrations of the drug, up to the MIC, as shown in Figure 4:1. The extent of this unusual phenotype was such that at 4096 $\mu g.ml^{-1}$, even hyper-susceptible strains – with the exception of the *tolC* knockout – showed a large colony. The same mutations that caused hypersensitivity to deoxycholic acid also caused hypersensitivity to nalidixic acid, as did the N145L mutation. The MIC to acriflavine was also decreased by this subset of mutations, plus the Q352E mutation. Of the mutations tested, D121N, R158D, V198D, N332L, N342A, Q346L, K383E and R390E displayed no significant difference in MIC for any of the drugs tested, compared to the *tolC* complemented strain.

Table 4:2 - Minimum inhibitory concentrations for *tolC* mutants (part 1).

MIC in µg.ml^{-1} of acriflavine (Acf), chloramphenicol (Cam), deoxycholic acid (Doc), erythromycin (Ery), fusidic acid (Fus), nalidixic acid (Nal), rifampicin (Rif), tetracycline (Tet) and vancomycin (Vanc). Highlighted in blue are all values that differ by at least two doubling dilutions compared to the complemented strain. For the reference strain, values in brackets are the accepted standard values.

Strain	Acf	Cam	Doc	Ery	Fus	Nal	Nov	Rif	Tet	Vanc
ATCC 25922	32 (n/a)	4 (2)	4096 (n/a)	32 (n/a)	1024 (>128)	2 (2)	512 (n/a)	8 (16)	1(1)	512 (n/a)
BW25113 pASK-RM	64	4	4096	32	512	8	512	16	1	256
BWΔtolC pASK-RM	4	0.5	128	2	4	1	4	8	0.25	256
BWΔtolC pASK-tolC	32	2	4096	4	64	4	512	8	0.5	256
D121N	16	2	4096	4	128	2	512	8	0.25	256
Q129L	32	2	4096	2	64	2	512	4	0.125	128
N145L	8	1	4096	1	32	0.5	512	8	0.125	128
R158D	32	2	4096	4	64	4	512	4	0.25	128
V198D	32	2	4096	4	64	4	512	4	0.25	128
N332L	32	2	4096	4	128	4	512	8	0.25	256
N342A	16	2	4096	4	64	4	512	8	0.25	256
Y344F	32	2	4096	2	64	2	512	4	0.125	64

Table 4:3 - Minimum inhibitory concentrations for *tolC* mutants (part 2).

Strain	Acf	Cam	Doc	Ery	Fus	Nal	Nov	Rif	Tet	Vanc
BWΔtolC pASK-RM	4	0.5	128	2	4	1	4	8	0.25	256
BWΔtolC pASK-tolC	32	2	4096	4	64	4	512	8	0.5	256
Q346L	32	2	4096	4	64	2	512	8	0.25	256
S350F	2	0.25	128	2	2	0.5	2	8	0.25	256
Q352A	32	2	4096	2	64	4	512	4	0.25	64
Q352E	8	2	4096	4	64	2	256	8	0.25	256
Y362F/R367S	4	0.5	256	2	4	0.5	4	8	0.25	256
D371V	1	0.25	64	0.5	1	0.5	1	4	0.125	256
D374V	8	2	4096	2	64	2	512	8	0.25	256
K383D	8	2	512	2	64	0.5	512	4	0.125	128
K383E	16	2	4096	4	128	4	512	8	0.25	256
R390E	32	2	4096	4	64	4	512	8	0.5	256
R390E/N392T	32	2	4096	1	32	2	512	4	0.125	32

Figure 4:1 - Abnormal growth phenotype on deoxycholic acid.

Values given are deoxycholic acid concentration (μg.ml^{-1}) in the MIC plate . Images are photographs of the colonies; where no colony is visible, the photograph is where on the plate the culture was spotted.

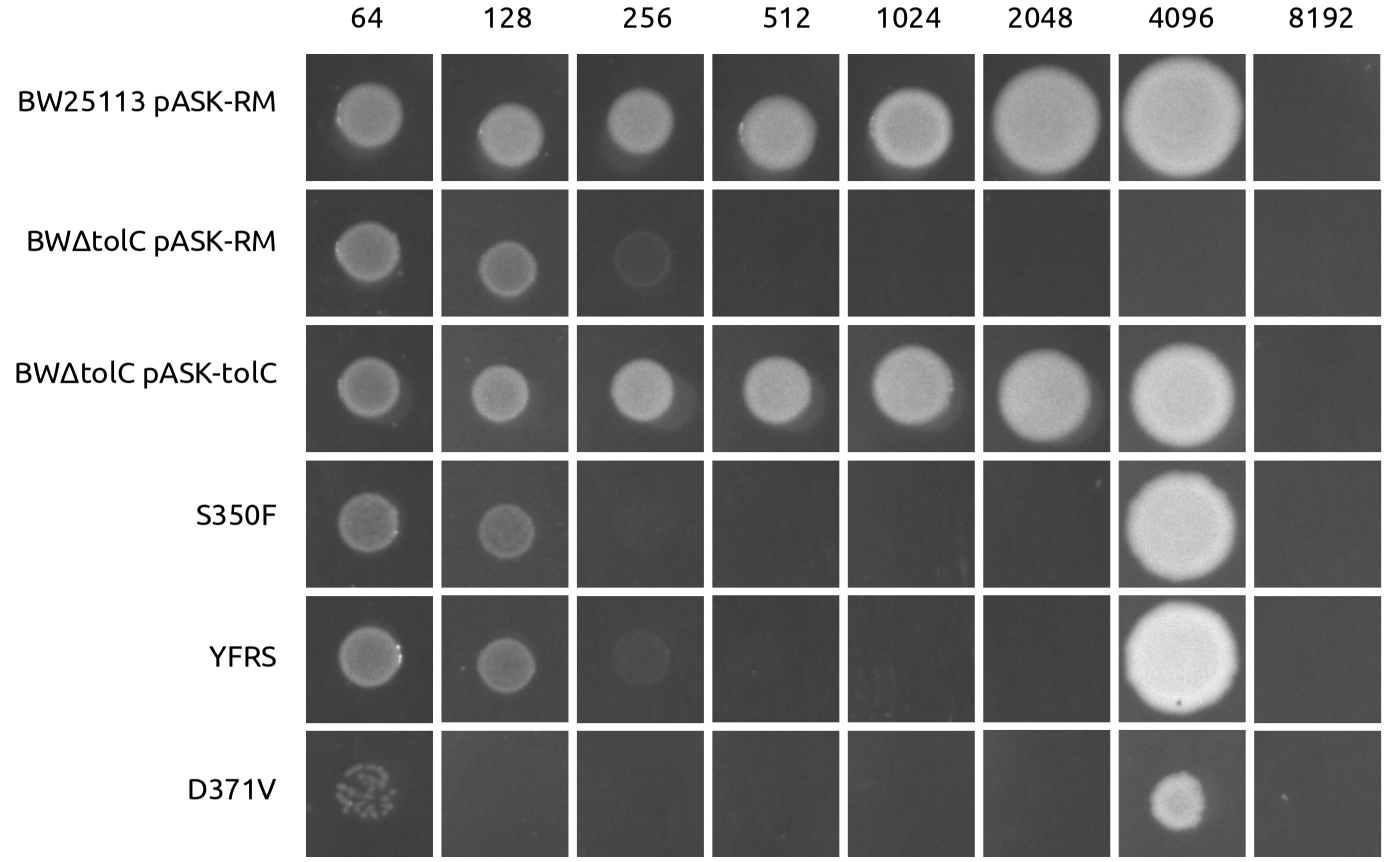

Discussion

In this study, the complemented strain and all of the point mutants have the *tolC* gene under control of the tetracycline promoter. To determine how much inducer should be added to cultures for *in vivo* studies, liquid broth MIC was used to compare the wild-type, knockout and complemented strains. This does not confirm that the promoter activity is similar to that of the chromosomally-encoded *tolC* promoter of the wild-type strain, in the way that quantitative reverse-transcriptase PCR would, nor does it confirm that the amount of TolC protein is comparable between the two strains, as a quantitative Western blot would. It does, however, allow a basic approximation of how much inducer is required for comparable results between the wild-type and *tolC* complemented strains from *in vivo* assays. This small experiment was also vital for confirming that the inducer does not in itself have any effect on the strains used. The MICs of the wild-type strain with the empty vector, and the *tolC* knockout strain with the empty vector, remained constant for each of the inducer concentrations tested, suggesting that in the concentration range used, anhydrotetracycline does not have an antibacterial effect, does not affect *tolC* expression from the chromosome, and does not have a significant inhibitory effect on the AcrAB-TolC efflux pump. Given that the MICs of erythromycin and novobiocin against the complemented strain are decreased to those of the knockout strain at 200 $ng.ml^{-1}$ anhydrotetracycline, this level of induction probably causes OM permeability issues by overproduction of the TolC protein. IBA-Lifesciences, the suppliers of the pASK-IBA13plus vector, state on the plasmid data sheet that 200 $\mu g.l^{-1}$ (200 $ng.ml^{-1}$) should be used for induction, but this is likely the recommendation for protein overproduction for purification purposes. From the results of this small experiment, it was decided that 2 $ng.ml^{-1}$ anhydrotetracycline should be used for *in vivo* assays in broth, while 20 $ng.ml^{-1}$ should be used in agar. As the differences between wild-type and mutant TolC proteins could be very small in any given assay,

overproduction of the protein may mask the differences, therefore a low concentration would be required in liquid broth assays; the increased concentration in agar should account for any differences in diffusion from agar to the cell compared to from solution into the cell.

In one set of MIC agar plates, inducer was aliquoted to universal bottles before addition of the antibiotic stock solutions, rather than into the cooled molten agar. This caused all MIC values for all strains with plasmid-encoded *tolC* to be equal to the knockout, although the values for wild-type strain were normal (results not shown). As anhydrotetracycline is dissolved in methanol and only a very small volume was added to each bottle, it is likely that the solvent evaporated completely, resulting in an anhydrotetracycline residue on the bottom of the bottle. This residue may not have re-dissolved upon addition of either the test antibiotics or the molten agar, leading to an effective concentration of zero anhydrotetracycline in the final agar plates. Alternatively, the anhydrotetracycline may have become less stable, again resulting in an effective zero concentration of inducer in the agar. Such results differ from what was suggested in the liquid broth MICs to determine what concentration of inducer to use, but results from liquid broth MIC can differ when compared to those from agar MIC – this is apparent within these results, particularly when looking at erythromycin, which had a far lower MIC in agar to all three strains than it did in broth.

Several mutations showed no significant (≥2 doubling dilutions) difference from the complemented strain with any of the antibiotics tested. These were D121N, R158D, V198D, N332L, N342A, Q346L, K383E and R390E. All of the other mutations showed a significant difference to at least one of the tested antibiotics. These results indicate that the effect of some of these mutations may be substrate-dependent. Table 4:4 summarises the overall findings from these MIC assays for each mutation,

relative to the complemented strain, while the effects of each mutation are mapped to the structure in Figure 4:2. For mutations made in the lumen of the TolC channel, then the substrate-specific effects could be explained by the substrate-accessible surface of TolC being less conducive to the passing of certain substances than other. This is particularly likely for the D374V mutation, as the three D374 residues form a selective ring low in the TolC lumen. Changing of the lumen surface may also explain why the substrate-specific effect is observed in the R390E/N392T but not the R390E single mutant, as N392 faces into the lumen while R390 faces out; the double mutant was a spontaneous mutation found when screening for R390E site-directed mutants, and was included in this study out of curiosity as to why it had arisen. Although Q129 faces into the lumen, it is predicted to interact with N381 and Q384, and should remain hidden from the substrate by the side chains of these interaction partners, which protrude further into the lumen; disruption of these interactions by mutation could cause a re-alignment of these other side chains, altering the face of the lumen and possibly causing the observed substrate-dependent effect. Being sandwiched between N167 and E385, the side chain of Y344 also faces into the lumen, although as the interactions between these residues is most likely driven by electron delocalisation, the change to phenylalanine should have minimal impact on the physical properties of the lumen surface.

The apparent substrate-specificity was unexpected for N145L, Q352E and K383D, given the hypothesis that these mutations may affect binding of TolC to its partner proteins. If binding is affected, then the effect should logically be apparent for all substrates of the efflux complex, not only a subset of them. Both Q352 and K383 also show mutation-specific effects – Q352A causes susceptibility to vancomycin but not to any efflux substrates, while Q352E causes increased susceptibility to acridine but not any other efflux substrates or vancomycin; K383D causes increased susceptibility to a subset of efflux substrates, but K383E apparently has no effect.

Table 4:4 - Summary of MIC findings for *tolC* mutants.

Mutation	Effect with efflux substrates	Effect shown by vancomycin
Δ*tolC*	Susceptible to most	--
D121N	--	--
Q129L	Susceptible only to Tet	--
N145L	Substrate-specific susceptibility	--
R158D	--	--
V198D	--	--
N332L	--	--
N342A	--	--
Y344F	Susceptible only to Tet	Susceptible to Vanc
Q346L	--	--
S350F	As knockout	--
Q352A	--	Susceptible to Vanc
Q352E	Susceptible only to Acf	--
YFRS	As knockout	--
D371V	As knockout	--
D374V	Susceptible only to Acf	--
K383D	Substrate-specific susceptibility	--
K383E	--	--
R390E	--	--
RENT	Substrate-specific susceptibility	Susceptible to Vanc

-- indicates no difference when compared to the BWΔ*tolC* pASK-*tolC* complemented strain.

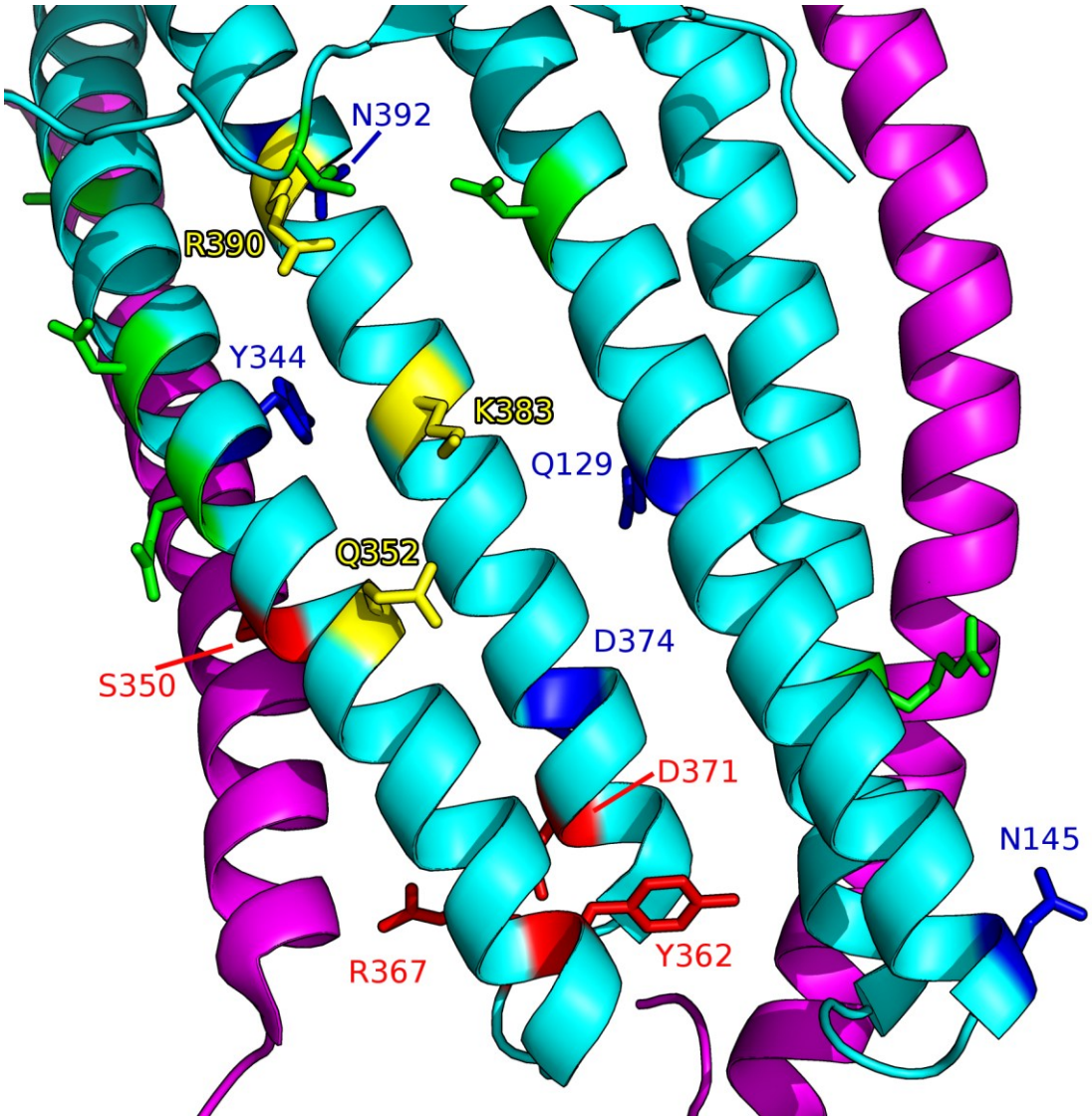

Figure 4:2 - Summary of MIC results on TolC structure.

Onto a single protomer of TolC (1EK9, light blue) are mapped the positions that were mutated, colour coded according to the effect of the mutation as determined by MIC assays. In magenta are the adjacent helices from the other protomers. Green: mutation has no effect (positions not labelled). Yellow: effect observed is dependent on the amino acid mutated to. Blue: mutation has a substrate-specific effect. Red: mutation shows same phenotype as *tolC* knockout.

Vancomycin is not an efflux substrate, but is reported to traverse the OM by utilising open efflux channels such as TolC; the MIC results here therefore suggest that the Y334F and Q352A mutations, plus the R390E/N392T double mutation, cause the TolC channel to allow greater influx of vancomycin due to being more open. While the Y344F mutation was expected to impact inter-helical interactions N167 and E385 at the part of TolC where narrowing of the channel begins, it is not clear whether this effect is caused by this or a change in binding of the MFP. As the channel dilates, Y344 should become more accessible to the MFP, and could therefore become involved in the stabilisation of the open structure, as well as holding the channel closed when MFP is not bound. The Q352A mutation affects the external face of the TolC channel, and should not contribute to inter-helical bonding in the closed state. Therefore, this mutation is unlikely to cause channel dilation on its own – it is more likely that the observed effect is MFP-dependent, as seen in the case of the E434K mutation in MtrE. Both the R390E and YFRS mutations have previously been published as causing pore dilation, tested by vancomycin zones of inhibition for R390E and by conductance assays for YFRS. Neither of these mutations showed increased susceptibility to vancomycin by MIC assay in this study. Conductance assays, though useful in assessing how likely the channel is to dilate when a current is applied, do not give any information as to the opening or closing of a channel protein *in vivo*, particularly when the process is controlled by a partner protein. Perhaps the YFRE mutation, which has been shown *in vivo* to cause vancomycin hyper-susceptibility, would have been a better choice of mutation for this study. Published susceptibility testing of the R390E mutation was done using basal expression from the pTrc99 vector, and therefore different expression levels may account for the difference in results between that study and this. The double mutation R390E/N392T has not previously been reported, but appears from this study to cause far greater susceptibility to vancomycin than does the R390E single mutation. Given that N392

faces into the lumen of TolC, and appears to provide only a very minor contribution to inter-helical interactions, this result cannot be explained from MIC assays alone. Unfortunately, as there are multiple MFPs that could potentially interact with TolC in any *in vivo* assay, determination of the MFP-dependency of the vancomycin susceptible phenotype of these mutations was not possible within the scope of this study. The laboratory of Dr Jessica Blair has made good progress towards creating a *Salmonella* strain in which the genes encoding all TolC-dependent MFPs have been removed from the chromosome, but such a strain has taken several years of step-wise gene deletion and was not available during this study.

Whilst MIC assays are an approved method of determining whether a strain is susceptible or resistant to a particular drug, they have some limitations. Firstly, the results can be interpreted differently by different people – as drug concentration increases, the colony may appear to fade, or may start to appear as many small colonies within the spotted area. The point at which growth is inhibited sufficiently for the MIC to be assigned is therefore not as clear as a simple *"is there any growth or not?"*. Secondly, they are end-point assays, and give no indication as to how colonies have grown to their observed size, nor can any extrapolation be made as to whether or not the drug has completely inhibited growth or merely slowed it such that an observation is made earlier in the growth curve of the colony. This could be particularly relevant to the D371V mutant, which showed a decreased MIC to most of the efflux substrates tested. This strain had already been observed to form visible colonies at a slower rate than any of the other colonies, and therefore it is unclear if the measured MIC is an accurate representation, or if the MIC values would be higher if the plates were allowed a longer incubation.

4.2 Growth kinetics

To determine finer details of the effect the *tolC* mutations have upon antibiotic resistance than can be determined from MIC assays, the growth kinetics of each mutant were analysed. This was done on 96-well plates, with readings automatically taken every two and a half minutes by Fluostar plate readers. The concentrations of inducer and test drug to use were informed by MIC results, such that the test drugs are at sub-lethal concentration for the complemented strain, but sufficiently high concentration to show any increase in sensitivity caused by the mutations. In all cases, anhydrotetracycline was added to a final concentration of 2 $ng.ml^{-1}$ to ensure adequate induction of *tolC* expression.

As each plate was measured at a different time and on one of three different machines, there was considerable variation between replicates. Therefore to normalise the data, each growth curve was analysed to find the generation time and defined as a relative growth rate against the complemented strain in the same conditions on the same plate. From the semi-log plot of the raw data, linear sections of the growth curve were selected (examples shown in Figure 4:3), with the first and last data points of these selected portions used for the calculation of generation time. The calculation was done in Microsoft Excel, by $(60 \times \log_{10}2 \times (\text{end time} - \text{start time})) / (\log_{10} \text{end } OD_{600} - \log_{10} \text{start } OD_{600})$, giving generation time in minutes. To complete the normalisation, the generation time of the complemented strain was divided by the generation time of each mutant, and then multiplied by 100 to express a relative growth rate as a percentage of that of the complemented strain. A p-value was then calculated for each strain against the complemented strain using Welch's T-test, with a P-value of <0.05 deemed significantly different from the complemented strain. Stationary phase OD_{600} was also analysed, to compare with the information from MIC assays and to determine what effects are observable as a result of the incorporated mutations.

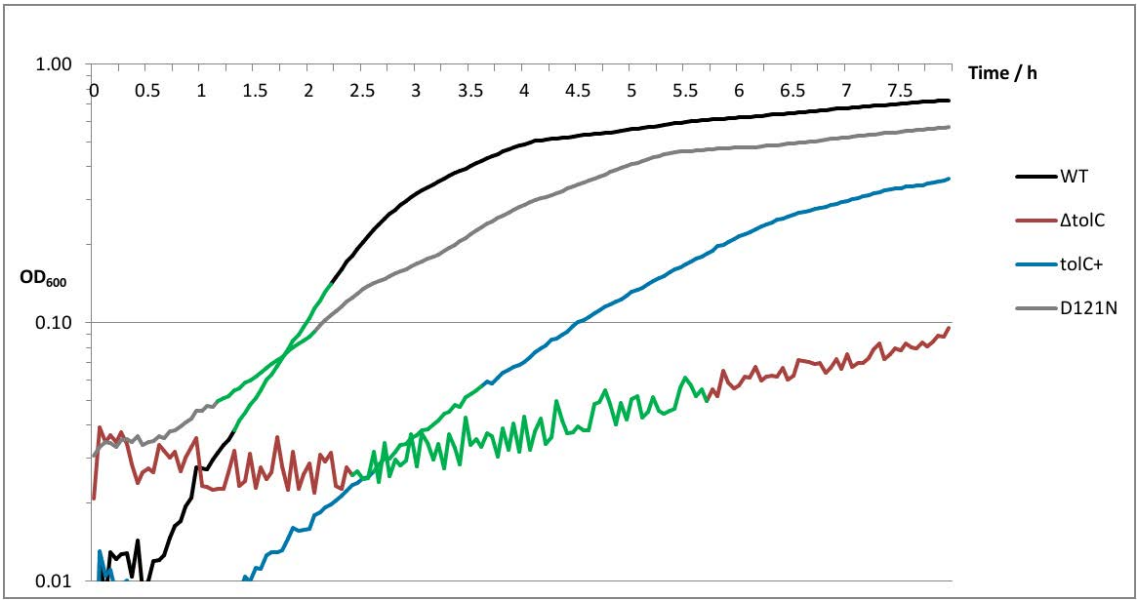

Figure 4:3 - Example growth curve indicating where growth rates are calculated. Growth rates were taken from the linear portion of semi-log plots of OD_{600} against time. Shown in green are the portions of example curves from which growth rates were calculated. For curves with high noise, such as the ΔtolC example, the most linear portion was chosen, with limits set by most stable consecutive readings.

As rifampicin showed the same MIC to both the knockout and complemented strains, it was not used in growth kinetics assays. Erythromycin was not included in growth kinetics assays as the difference in MIC against the knockout and complemented strains was minimal and not deemed significant. Tetracycline showed only a minimal, insignificant difference in MIC against the knockout and complemented strains, and, as this would also likely affect expression of *tolC* from the plasmid, was also omitted from the growth kinetics assays.

Deoxycholic acid was used at a final concentration of 500 μg.ml^{-1}, to avoid the complications of increased growth of all mutants at higher concentrations of this drug, seen in the MIC results. At this concentration, the knockout and three point mutants – S350F, YFRS and D371V, all grew to a lower OD_{600} in their stationary phase than did the wild-type or complemented strains (bold in Table 4:5). These strains also showed a clear decrease in growth rate compared to the complemented strain (Figure 4:4 and Table 4:5). Several point mutations showed a small effect on growth rate, without greatly impacting on the OD_{600} at stationary phase. These mutations were D121N, N332L, Y334F, K383D and R390E, which all had a negative impact on growth rate. Each of these show a p-value of <0.05 when tested against the complemented strain (bold in Table 4:5). The V198D mutation showed generally to increase the growth rate relative to the complemented strain, but Welch's T-test determined this to be not significantly different (p-value = 0.059); however, the lowest value in this data range is below the 95% confidence interval (seen in Figure 4:4).

Assays were done using nalidixic acid as a test substrate, at 1 μg.ml^{-1} final concentration. In these conditions, the mutations S350F, YFRS and D371V all caused the OD_{600} at stationary phase to be significantly lower than reached by the complemented strain (bold in Table 4:6), although the same was not true of the knockout strain. Comparing relative growth rates, the knockout strain again showed no difference compared to the complemented strain, nor to BW25113 pASK-RM, indicating that the knockout is capable of growing as wild-type in these conditions. The YFRS, D371V and K383D mutations all caused growth rate to decrease significantly in these conditions (Figure 4:5), compared to the complemented strain (p-values shown in bold in Table 4:6). Although the p-values did not indicate the mutations S350F or D374V to significantly affect growth rate (p-values italicised in Table 4:6), manually scrutinising the data indicate that these mutations probably do

cause a significant change in growth rate, once outlier values are taken into account. The indicated average relative growth rate for the N145L mutant is higher than four out of five of the contributing data values, the other being above the 95% confidence interval; however, even if this outlying value were omitted, the p-value would still be 0.09, and thus still not classified as significant.

In the presence of 1 $\mu g.ml^{-1}$ chloramphenicol, the *tolC* knockout strain showed a significant difference in both stationary phase OD_{600} and relative growth rate, when compared to the complemented strain (Table 4:7 and Figure 4:6). The generation time of the complemented strain was also longer in these growth conditions than that of BW25113 pASK-RM, and longer than the generation time of the complemented strain in the absence of chloramphenicol. The point mutations S350F, YFRS, D371V and R390E showed the same phenotypes as the knockout strain, with very low OD_{600} at stationary phase and a very low relative growth rate. Although the D121N mutation did not cause the OD_{600} at stationary phase to decrease, it did cause a small but statistically significant decrease in relative growth rate. There are clear outliers for mutations V198D, N332L and D374V, which are outside the 95% confidence intervals; exclusion of these values would result in average relative growth rates of 61%, 76% and 70%, respectively, with p-values of 0.019, 0.048 and 0.016, respectively, when tested against the complemented strain, compared to the p-values of 0.214, 0.551 and 0.449 when tested using the complete set of data (shown italicised in Table 4:7).

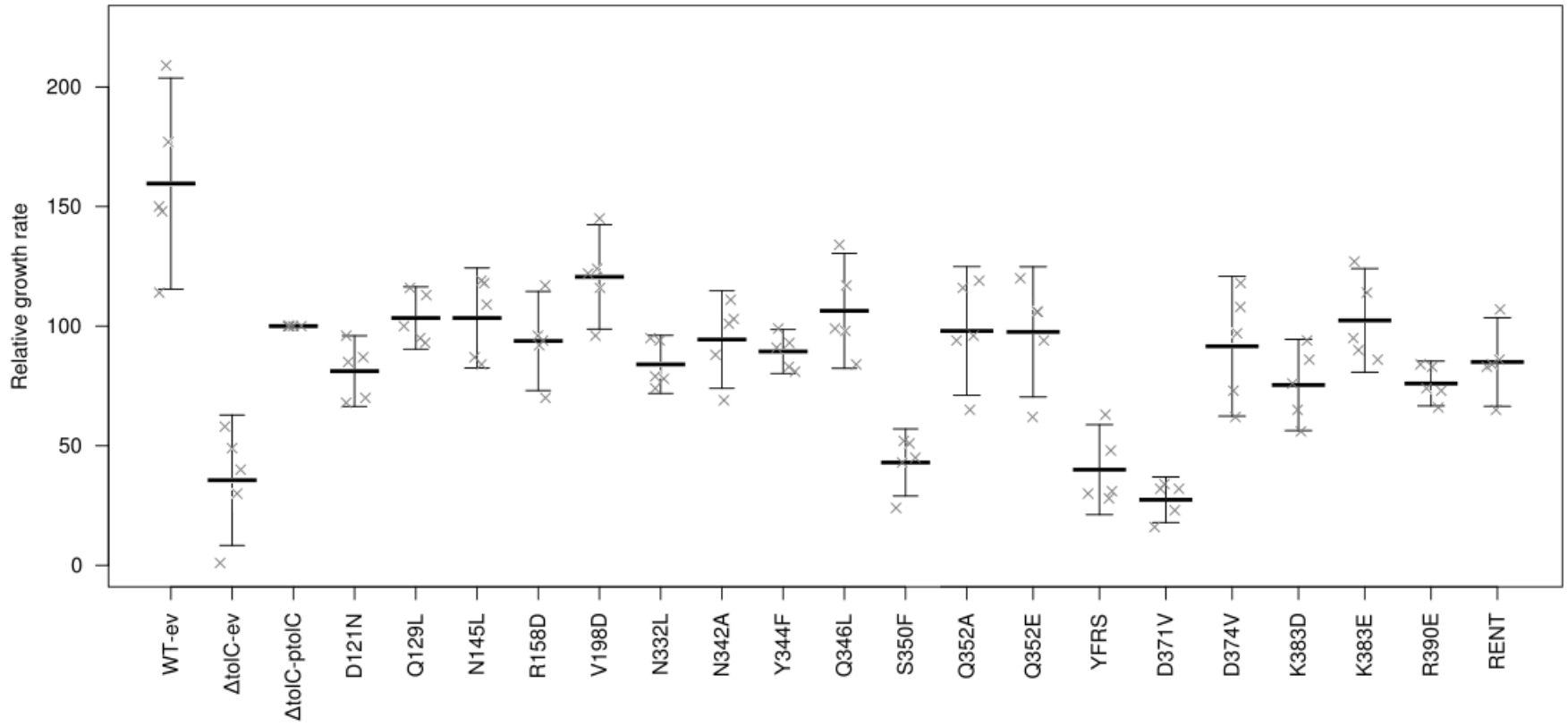

Figure 4:4 - Relative growth rates for *tolC* mutants in the presence of 500 µg.ml^{-1} deoxycholic acid.

Values are given as a percentage of the BWΔ*tolC*pASK-acrAB strain growth rate. Each x represents the value for an individual biological replicate. Lines indicate average ± 95% confidence interval.

Table 4:5 - Growth information of *tolC* mutants in the presence of 500 µg.ml^{-1} deoxycholic acid.

Strain	Average relative growth rate (%) ± SD	P-value against tolC complement	Stationary phase OD_{600} ± SD
BW25113 pASK-RM	160 ± 36	**0.020**	1.00 ± 0.08
BWΔtolC pASK-RM	36 ± 22	**0.003**	**0.04 ± 0.03**
BWΔtolC pASK-tolC	100 ± 0	--	0.99 ± 0.11
D121N	81 ± 12	**0.024**	1.00 ± 0.07
Q129L	104 ± 10	0.509	1.00 ± 0.08
N145L	103 ± 17	0.675	0.97 ± 0.16
R158D	94 ± 17	0.453	1.03 ± 0.09
V198D	121 ± 18	0.059	0.94 ± 0.12
N332L	84 ± 10	**0.022**	1.09 ± 0.09
N342A	95 ± 16	0.488	1.01 ± 0.10
Y344F	89 ± 8	**0.033**	1.06 ± 0.09
Q346L	106 ± 19	0.501	1.04 ± 0.13
S350F	43 ± 11	**3 x 10^{-4}**	**0.11 ± 0.06**
Q352A	98 ± 22	0.846	1.05 ± 0.17
Q352E	98 ± 22	0.819	1.07 ± 0.12
YFRS	40 ± 15	**0.001**	**0.23 ± 0.12**
D371V	27 ± 8	**2 x 10^{-5}**	**0.08 ± 0.02**
D374V	91 ± 24	0.470	1.06 ± 0.09
K383D	76 ± 15	**0.023**	1.06 ± 0.08
K383E	103 ± 18	0.774	0.98 ± 0.10
R390E	76 ± 8	**0.002**	1.01 ± 0.09
RENT	85 ± 15	**0.088**	1.05 ± 0.13

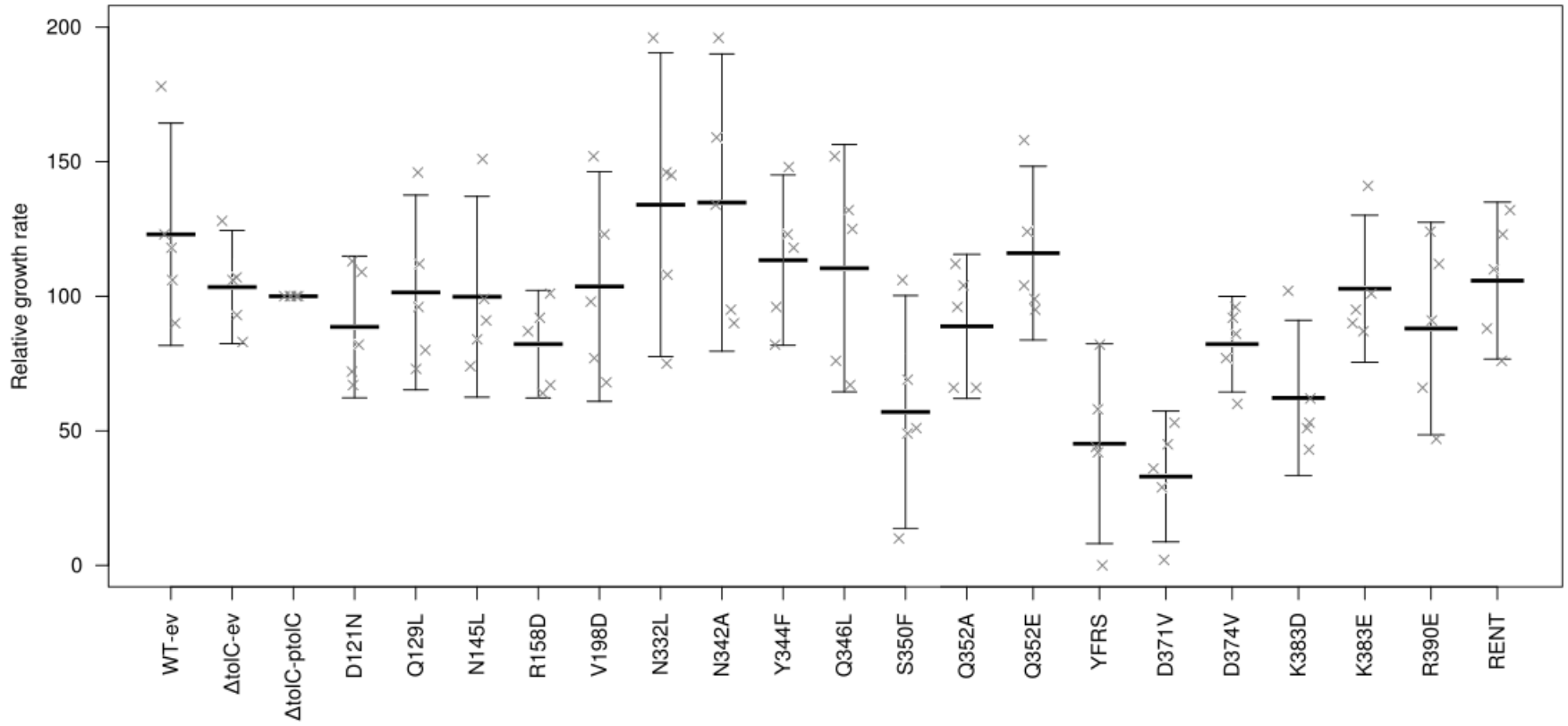

Figure 4:5 - Relative growth rates for *tolC* mutants in the presence of 1 µg.ml^{-1} nalidixic acid.

Values are given as a percentage of the BWΔ*tolC*pASK-acrAB strain growth rate. Each x represents the value for an individual biological replicate. Lines indicate average ± 95% confidence interval.

Table 4:6 - Growth information of *tolC* mutants in the presence of 1 µg.ml^{-1} nalidixic acid.

Strain	Average relative growth rate (%) ± SD	P-value against tolC complement	Stationary phase OD_{600} ± SD
BW25113 pASK-RM	123 ± 33	0.197	0.98 ± 0.18
BWΔtolC pASK-RM	103 ± 17	0.677	0.83 ± 0.01
BWΔtolC pASK-tolC	100 ± 0	--	0.89 ± 0.07
D121N	89 ± 21	0.295	0.83 ± 0.07
Q129L	101 ± 29	0.920	0.89 ± 0.04
N145L	100 ± 30	0.989	0.92 ± 0.07
R158D	82 ± 16	*0.069*	0.89 ± 0.08
V198D	104 ± 34	0.826	0.82 ± 0.08
N332L	134 ± 45	0.170	0.83 ± 0.08
N342A	135 ± 44	0.155	0.85 ± 0.10
Y344F	113 ± 25	0.305	0.85 ± 0.09
Q346L	110 ± 37	0.564	0.87 ± 0.10
S350F	57 ± 35	*0.051*	**0.39 ± 0.28**
Q352A	89 ± 22	0.310	0.90 ± 0.09
Q352E	116 ± 26	0.241	0.90 ± 0.08
YFRS	45 ± 30	**0.015**	**0.31 ± 0.32**
D371V	33 ± 20	**0.002**	**0.08 ± 0.05**
D374V	82 ± 15	*0.050*	0.88 ± 0.08
K383D	62 ± 23	**0.022**	0.94 ± 0.11
K383E	103 ± 22	0.790	0.89 ± 0.14
R390E	88 ± 32	0.446	0.75 ± 0.07
RENT	106 ± 24	0.610	0.83 ± 0.11

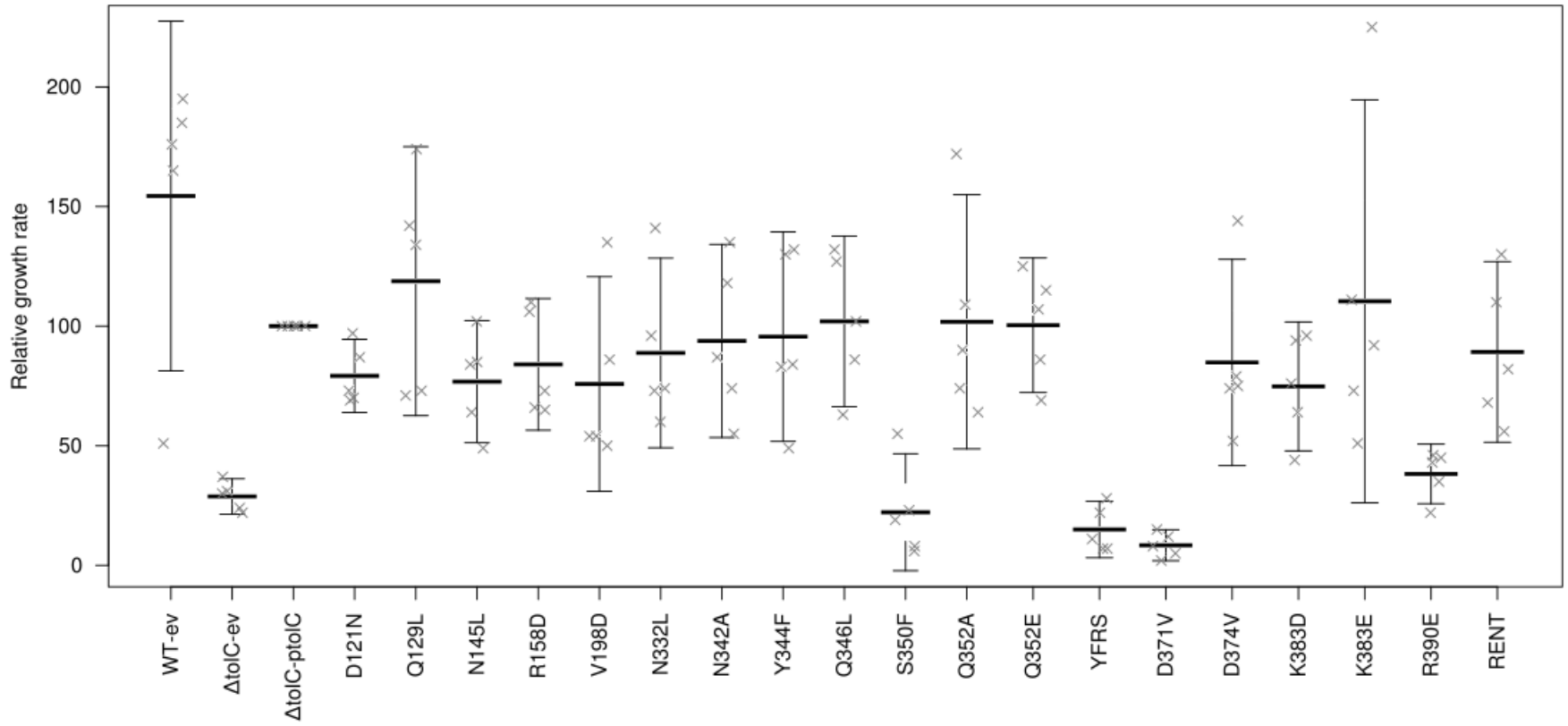

Figure 4:6 - Relative growth rates for tolC mutants in the presence of 1 µg.ml^{-1} chloramphenicol.

Values are given as a percentage of the BWΔ*tolC*pASK-acrAB strain growth rate. Each x represents the value for an individual biological replicate. Lines indicate average ± 95% confidence interval.

Table 4:7 - Growth information of tolC mutants in the presence of 1 µg.ml^{-1} chloramphenicol.

Strain	Average relative growth rate (%) ± SD	P-value against tolC complement	Stationary phase OD_{600} ± SD
BW25113 pASK-RM	154 ± 59	0.105	0.68 ± 0.04
BWΔtolC pASK-RM	29 ± 6	**1 x 10^{-5}**	**0.12 ± 0.04**
BWΔtolC pASK-tolC	100 ± 0	--	0.47 ± 0.13
D121N	79 ± 12	**0.019**	0.48 ± 0.23
Q129L	119 ± 45	0.395	0.57 ± 0.10
N145L	77 ± 21	0.985	0.47 ± 0.17
R158D	84 ± 22	0.217	0.49 ± 0.21
V198D	76 ± 36	*0.214*	0.41 ± 0.21
N332L	89 ± 32	*0.551*	0.54 ± 0.07
N342A	94 ± 32	0.735	0.55 ± 0.09
Y344F	96 ± 35	0.846	0.51 ± 0.17
Q346L	102 ± 29	0.835	0.57 ± 0.07
S350F	22 ± 20	**0.001**	**0.10 ± 0.07**
Q352A	102 ± 43	0.906	0.52 ± 0.09
Q352E	100 ± 23	0.891	0.50 ± 0.20
YFRS	15 ± 9	**4 x 10^{-5}**	**0.06 ± 0.05**
D371V	9± 5	**3 x 10^{-6}**	**0.05 ± 0.05**
D374V	85 ± 35	*0.449*	0.49 ± 0.12
K383D	75 ± 22	0.060	0.36 ± 0.14
K383E	111 ± 68	0.723	0.56 ± 0.16
R390E	38 ± 10	**2 x 10^{-4}**	**0.18 ± 0.22**
RENT	89 ± 31	0.728	0.56 ± 0.03

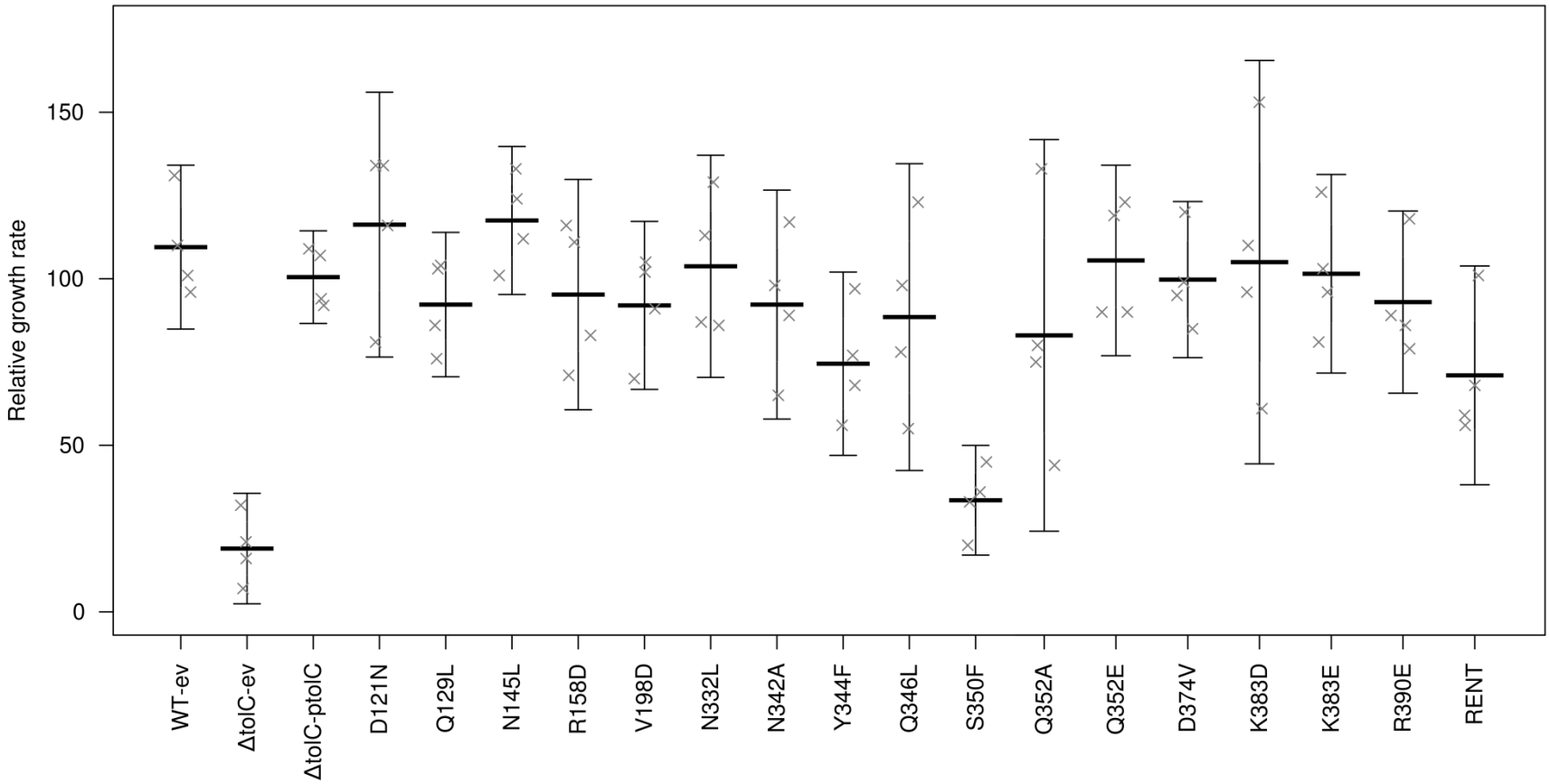

Figure 4:7 - Relative growth rates for *tolC* mutants in the presence of 200 µg.ml^{-1} fusidic acid.

Values are given as a percentage of the BWΔ*tolC*pASK-acrAB strain growth rate. Each x represents the value for an individual biological replicate. Lines indicate average ± 95% confidence interval.

Table 4:8 - Growth information of *tolC* mutants in the presence of 200 µg.ml^{-1} fusidic acid.

Strain	Average relative growth rate (%) ± SD	P-value against *tolC* complement
BW25113 pASK-RM	110 ± 15	0.360
BWΔtolC pASK-RM	19 ± 10	**2 x 10^{-5}**
BWΔtolC pASK-tolC	101 ± 9	--
D121N	116 ± 25	0.304
Q129L	92 ± 13	0.354
N145L	117 ± 14	0.094
R158D	95 ± 21	0.677
V198D	92 ± 16	0.394
N332L	104 ± 21	0.789
N342A	92 ± 22	0.518
Y344F	75 ± 17	**0.049**
Q346L	88 ± 28	0.477
S350F	34 ± 10	**7 x 10^{-5}**
Q352A	83 ± 37	0.418
Q352E	105 ± 18	0.641
D374V	100 ± 15	0.934
K383D	105 ± 38	0.831
K383E	101 ± 19	0.927
R390E	93 ± 17	0.476
RENT	71 ± 20	*0.057*

When grown in the presence of 100 μg.ml^{-1} vancomycin, none of the mutations caused a change in the OD_{600} at stationary phase (Table 4:9). Only the D371V and K383D point mutations showed any statistically significant effect on the relative growth rate in vancomycin, although D374V appears to cause a minor increase in growth rate and R158D appears to cause a decrease in growth rate. Recalculation of the average relative growth rate of D374V with its clear outlier excluded gives a value of 105 ± 2, with a p-value of 0.009 against the complemented strain when recalculated. In the case of R158D, all of the individual relative growth rates from each plate is lower than that of the complemented strain, and the lowest of all of these (furthest from being the same as the complement, seen in Figure 4:8) is the outlier; recalculation of the average relative growth rate for R158D excluding the outlier gives a value of 88 ± 7, and a p-value of 0.037 against the complemented strain.

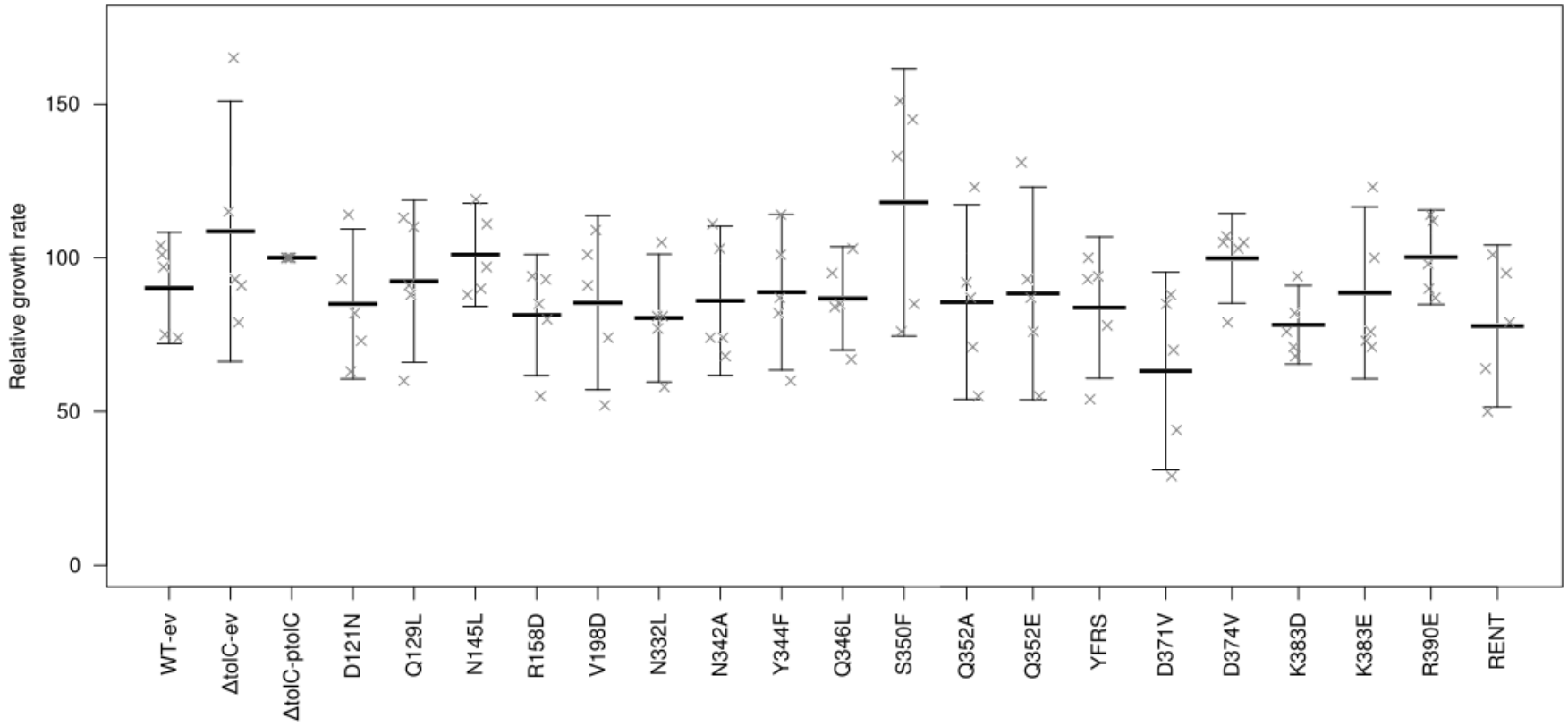

Figure 4:8 - Relative growth rates for tolC mutants in the presence of 100 µg.ml^{-1} vancomycin.

Values are given as a percentage of the BWΔ*tolC*pASK-acrAB strain growth rate. Each x represents the value for an individual biological replicate. Lines indicate average ± 95% confidence interval.

Table 4:9 - Growth information of *tolC* mutants in the presence of 100 µg.ml^{-1} vancomycin.

Strain	Average relative growth rate (%) ± SD	P-value against tolC complement	Stationary phase OD_{600} ± SD
BW25113 pASK-RM	90 ± 14	0.2065	0.73 ± 0.09
BWΔtolC pASK-RM	109 ± 34	0.603	0.72 ± 0.06
BWΔtolC pASK-tolC	100 ± 0	--	0.66 ± 0.06
D121N	85 ± 20	0.163	0.63 ± 0.08
Q129L	92 ± 21	0.469	0.58 ± 0.09
N145L	101 ± 13	0.877	0.62 ± 0.09
R158D	81 ± 16	*0.059*	0.56 ± 0.15
V198D	85 ± 23	0.225	0.60 ± 0.06
N332L	80 ± 17	*0.059*	0.60 ± 0.04
N342A	86 ± 20	0.184	0.61 ± 0.08
Y344F	89 ± 20	0.287	0.61 ± 0.06
Q346L	87 ± 13	0.095	0.61 ± 0.05
S350F	118 ± 35	0.314	0.44 ± 0.29
Q352A	86 ± 25	0.275	0.67 ± 0.06
Q352E	88 ± 28	0.405	0.61 ± 0.08
YFRS	84 ± 19	0.122	0.46 ± 0.28
D371V	63 ± 26	**0.033**	0.57 ± 0.10
D374V	100 ± 12	*0.971*	0.64 ± 0.06
K383D	78 ± 10	**0.009**	0.65 ± 0.08
K383E	89 ± 23	0.321	0.64 ± 0.08
R390E	100 ± 13	0.973	0.70 ± 0.08
RENT	78 ± 21	0.079	0.55 ± 0.19

Discussion

Due to the limited information that can be ascertained from MIC assays, growth kinetics assays were used to find finer differences between mutants. The MIC results can best be related to the stationary phase OD_{600} values from the growth kinetics assays. The MIC for the *tolC* knockout strain showed increased susceptibility to deoxycholic acid, chloramphenicol, fusidic acid, nalidixic acid and novobiocin, while stationary phase OD_{600} values from growth kinetics indicate deficiencies in overall growth in deoxycholic acid, chloramphenicol, fusidic acid and novobiocin but not in nalidixic acid. This is despite the concentration of nalidixic acid used in the growth kinetics assays being higher than the MIC of the knockout strain to nalidixic acid when tested on agar. Similarly, the N145L and K383D mutations appeared susceptible to 1 $\mu g.ml^{-1}$ nalidixic acid on agar, but the OD_{600} at stationary phase indicates that these mutations do not cause susceptibility. Fusidic acid also shows discrepancy between the MIC data and stationary phase OD_{600} values, as both YFRS and D371V showed a decrease in MIC to this substance, but grew to similar OD_{600} as the complemented strain in liquid culture. According to stationary phase OD_{600} values, vancomycin failed to inhibit growth of any of the mutants, although MIC data indicates that Y344F, Q352A and RENT mutants are more susceptible. This can at least in part be attributed to the difference in growth on agar compared to in liquid culture, as was apparent in the differences between erythromycin MIC values on agar compared to those in liquid broth when determining the concentration of anhydrotetracycline to use for induction.

Despite the discrepancies between MIC results and stationary phase OD_{600} values, the main reason for using growth kinetics in this study was to determine if the mutations have any effect on how the bacteria reach any perceived endpoint. A summary of the growth rate relative to the *tolC* complemented strain is shown in

Table 4:10 and indicated on the protein structure in Figure 4:9. From the summary table, the substrate-specific effect seen in the MIC results is again very clear from relative growth rate results. All of the mutations N145L, R158D, V198D, N332L, Y344F, D374V, R390E and RENT show some substrate-specificity to their effect. Such results indicate the importance of testing a variety of efflux substrates in a study such as this, and not relying on a sole reporter, which may not reveal all mutations that have an impact on functionality. Meanwhile, the S350F, D371V and K383D mutations appear to impact growth rate in all of the tested substrates, and K383D additionally caused a decrease in the growth rate in the presence of vancomycin. At this point, it should be made clear that the results for the D371V mutant in growth kinetics are not comparable to any of the other mutants, the wild-type, knockout or complement, as the growth rate in broth lacking any antibiotic was also significantly decreased in this mutant relative to the other strains.

Assessing how open the TolC channel is likely to be by use of vancomycin susceptibility suggests that three of the mutations (excluding D371V) cause the channel to be more open than the wild-type channel, while the D374V mutation probably decreases vancomycin influx through the channel. All three of the mutations which cause a decrease in growth rate in the presence of vancomycin also impact growth rate in the presence of efflux substrates: K383D causes a decrease in the presence of any of the efflux substrates, N332L causes a decrease in the presence of chloramphenicol or deoxycholic acid and R158D causes a decrease in the presence of nalidixic acid or novobiocin. On the 1EK9 structure of TolC, all of these three mutated positions are on the outside of the channel, with side chains facing out away from the protein, rather than facing an adjacent helix. Of these positions, R158 is closest to the periplasmic tip of TolC, on the third helical turn from the tip, and its only apparent binding partner within the TolC trimer is Q346, with which inter-protomeric hydrogen bonds could form. However, mutation of Q346 to leucine,

which cannot participate in hydrogen bonding, did not cause the same apparent vancomycin sensitivity. On the fifth helical turn from the tip, K383 is the next furthest of these mutated positions from the periplasmic tip. The effect at this position seems to be side-chain length-dependent, as mutation to the longer glutamic acid shows no effect in any of the tested substances, despite the same charge reversal being present in both mutations. An equivalent mutation to K383D has previously been reported on MtrE, on which the wild-type equivalent position is E434, mutation of which to lysine causes an MFP-dependent increase in vancomycin susceptibility. Furthest from the periplasmic tip, N332 is on the outside of the helical barrel but at the level of the equatorial domain, and possibly makes inter-protomeric hydrogen bonds with D176 and N177. Mutation to the hydrophobic leucine could therefore cause a reorganisation of side chains around this area, forcing a separation of the helices and therefore increasing the likelihood of channel opening.

Overall, growth kinetics analysis has revealed that some mutations have an effect which could not be seen on MIC testing. Some of the statistically significant differences are a fairly small decrease in relative growth rate, with some mutants still growing at 80% of the rate of the wild-type complemented strain. However, there were some differences seen in the MIC assays that were not present in growth kinetics. Using a higher antibiotic concentration may have provided greater difference between mutations, but a compromise was required in order to permit maximal growth of the complemented strain while still potentially inhibiting growth of efflux-compromised mutants. Results may also have been more comparable had liquid broth MIC assays been used, though these are more suited to a large number of antibiotics being screened against a smaller number of strains.

Table 4:10 - Summary of growth rates relative to *tolC*-complemented strain. Up and down indicate that the growth rate is increased and decreased relative to the *tolC* complemented strain, respectively. A dash indicates no difference from the complemented strain. N/a indicates that the mutation was not tested with that particular antibiotic. Doc: deoxycholic acid. Nal: nalidixic acid. Cam: chloramphenicol. Nov: novobiocin. Fus: fusidic acid. Vanc: vancomycin

Strain	Doc	Nal	Cam	Nov	Fus	Vanc
BW25113 pASK-RM	Up	-	-	Up	-	-
BWΔtolC pASK-RM	Down	-	Down	Down	Down	-
D121N	Down	-	Down	Down	-	-
Q129L	-	-	-	Down	-	-
N145L	-	-	-	Down	-	-
R158D	-	Down	-	Down	-	Down
V198D	-	-	Down	-	-	-
N332L	Down	-	Down	-	-	Down
N342A	-	-	-	-	-	-
Y344F	Down	-	-	Down	Down	-
Q346L	-	-	-	-	-	-
S350F	Down	Down	Down	Down	Down	-
Q352A	-	-	-	-	-	-
Q352E	-	-	-	-	-	-
YFRS	Down	Down	Down	N/a	N/a	-
D371V	Down	Down	Down	Down	N/a	Down
D374V	-	Down	Down	Down	-	Up
K383D	Down	Down	Down	Down	-	Down
K383E	-	-	-	-	-	-
R390E	Down	-	Down	N/a	-	-
RENT	Down	-	-	N/a	-	-

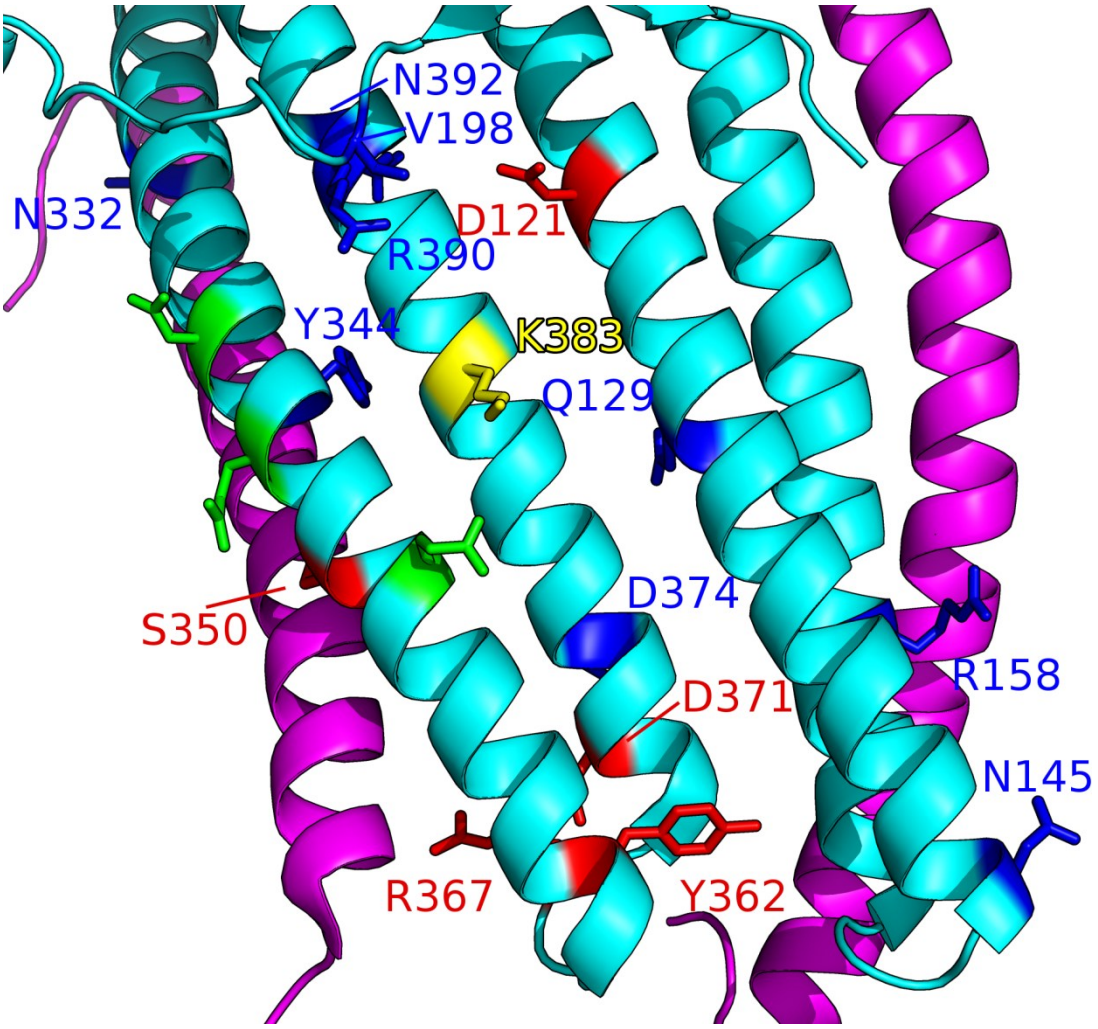

Figure 4:9 - Summary of growth kinetics results on TolC structure.
Onto a single protomer of TolC (1EK9, light blue) are mapped the positions that were mutated, colour coded according to the effect of the mutation as determined by growth kinetics assays. In magenta are the adjacent helices from the other protomers. Green: mutation has no effect (positions not labelled). Yellow: effect observed is dependent on the amino acid mutated to. Blue: mutation has an antibiotic-specific effect. Red: mutation shows same phenotype as *tolC* knockout.

4.3 Dye efflux assays

To give a more direct assessment of pump activity than growth kinetics, cells were assessed for their capability to extrude the fluorescent dye, Nile Red, which fluoresces when in hydrophobic environments such as the membrane. Using the proton decoupling drug CCCP to inhibit RND-efflux activity, cells were pre-loaded with Nile Red, diluted in PBS and loaded to 96-well plates with black-sided wells. The OD_{600} was measured, to calculate units of fluorescence per unit of OD, and the fluorescence measured every 27 s (the minimum plate cycle time). After five readings, glucose was injected to the wells to re-energise the cells, and fluorescence measurements continued. Cells that had been killed by boiling were included as a negative control, which would give maximum fluorescence. All measurements were blank-corrected against a control well containing no cells. Each fluorescence measurement was divided by the OD_{600} measurement for the well, normalising the data to "fluorescence per unit OD_{600}". To account for the amount of variation in raw blank-corrected fluorescence readings between wells, the data were further normalised by dividing each OD-corrected value by the initial OD-corrected value for that well, to give a proportion of initial fluorescence. Example curves after all normalisation steps are shown in Figure 4:10.

Injection of glucose is a slower step than the measurement of fluorescence, therefore there was a larger interval of 84 s between fluorescence readings immediately before and after glucose injection (marked as "Lag" on Figure 4:10). This gap between readings was too large to determine any efflux kinetics, as steady state had already been achieved by the time the first post-injection reading was completed. However, it was still possible to calculate the proportion decrease of fluorescence. As the raw blank-corrected readings were increasing and decrease randomly with noise, the average of five consecutive readings was used for calculation of the proportion loss, to account for this variation and prevent selection

of any particularly high or low values. Therefore, the equation used to calculate the proportion (as a percentage) decrease of fluorescence was *100 x (1 – (average of five normalised readings post-injection / average of five normalised readings pre-injection).* The results from this calculation are shown in Figure 4:11, using *n* = 2 biological replicates. Negative values, indicating that fluorescence rose after injection of glucose, indicate that the dye was not being removed from a hydrophobic environment; the boiled cell negative control showed a small increase in fluorescence, as did the *tolC* knockout strain and the D371V mutant. As this experimental design was unable to provide any detail of efflux kinetics, it was not repeated with extra biological replicates, and therefore statistical analysis is of limited power. Despite this, the *tolC* knockout and both the V198D and D371V mutants had p-values <0.05 when Welch's T-test was used to compare them to the complemented strain. The mutations N145L, R158D, N332L, N342A, S350F, K383D, R390E and RENT all have p-values <0.3 and all had higher retention of fluorescence.

To attempt to measure kinetics of efflux using this technique, the Fluostar programme was modified to read in well-mode rather than plate mode. This change makes the machine complete the entire read and injection process for a single well before moving onto the next, rather than reading each well in turn once per cycle, thus eliminating the slow process of injecting each well in turn on the whole plate. Using this mode, none of the strains, including the wild-type strain, showed any efflux activity (results indicated in Figure 4:12). The absolute fluorescence readings also decreased markedly from the start of the plate to the end of the plate (from tens of thousands to only hundreds of fluorescence units). Dye efflux assays were therefore abandoned with *n* = 2 in plate mode and no information available from well mode, and therefore no kinetic detail was discernable.

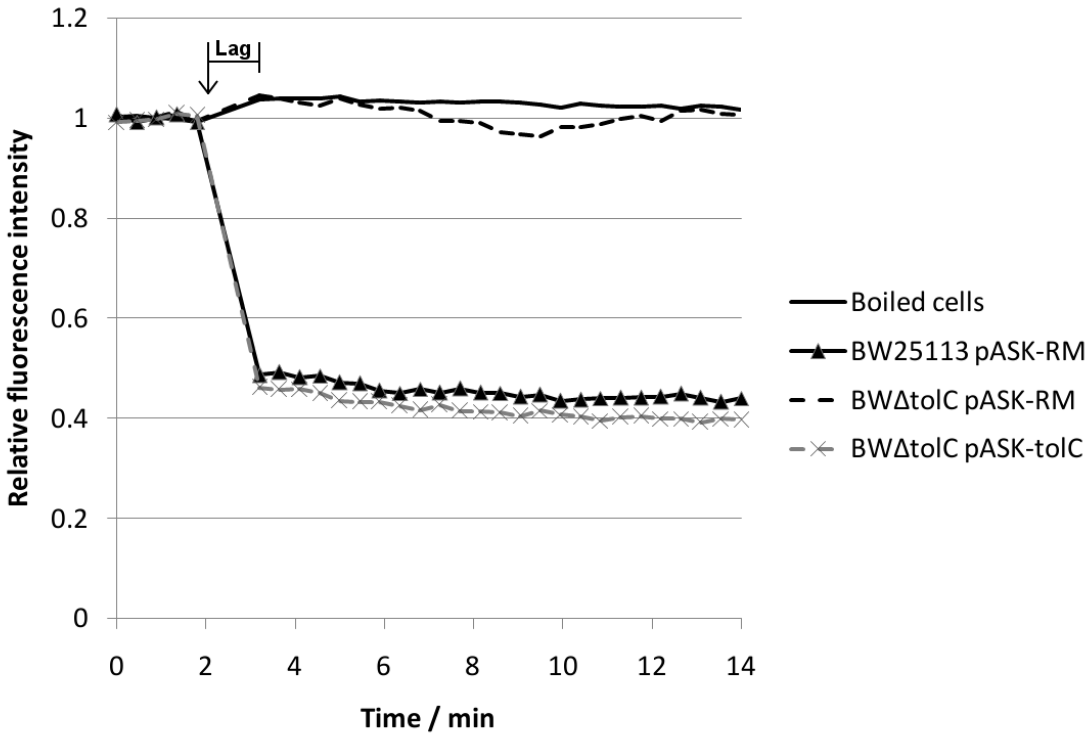

Figure 4:10 - Fluorescence intensity change with time in dye efflux assay. Values have been corrected to account for OD_{600} differences in each well. Data is from a plate-mode assay. The fluorescence intensity has been calculated as a proportion of the starting intensity. Injection of glucose is marked by an arrow, and the section marked as "Lag" indicates the delay between injection and the next reading.

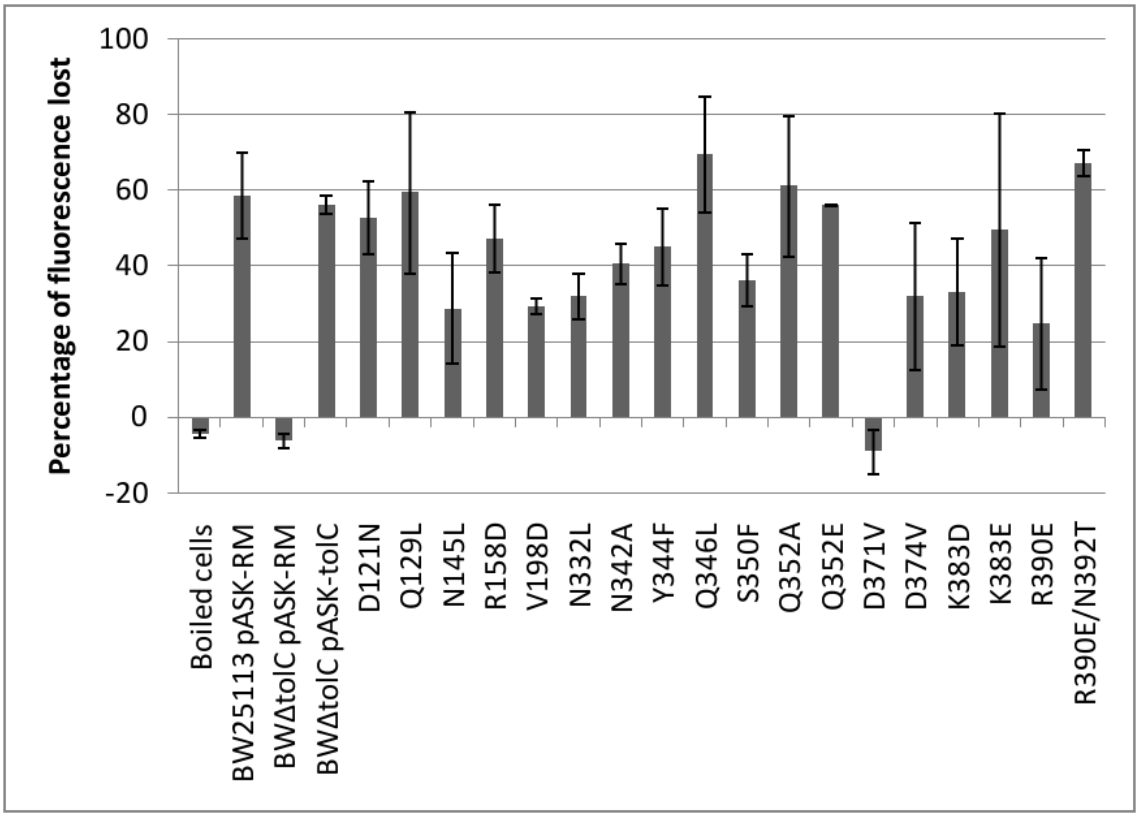

Figure 4:11 - Percentage of fluorescence lost by *tolC* mutants in a plate-mode dye efflux assay.

Values have been corrected to account for OD_{600} differences in each well. The percentage of fluorescence lost refers to the relative fluorescence per unit OD_{600} before and after injection of glucose when the assay was run in plate mode. Negative values indicate that post-injection, the fluorescence reading increased relative to pre-injection; a value of 100 would indicate complete loss of fluorescence. $n = 2$ biological replicates, error bars represent standard deviation.

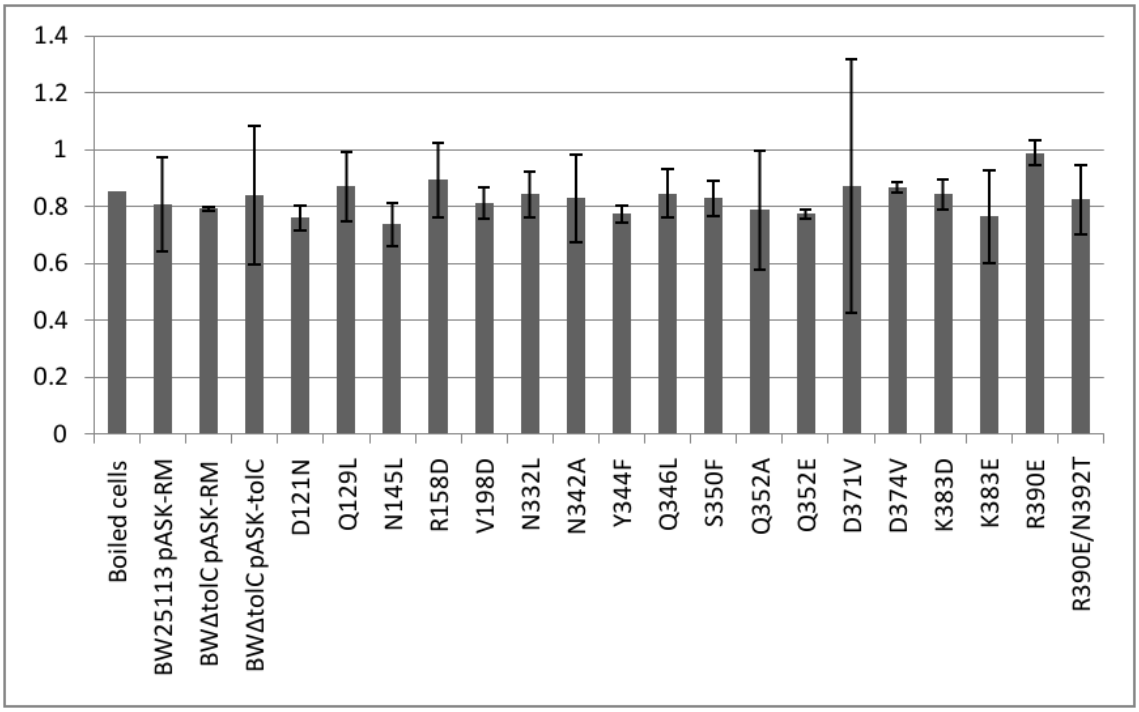

Figure 4:12 - Proportion of fluorescence retained by *tolC* mutants in a well-mode dye efflux assay.

Values have been corrected to account for OD_{600} differences in each well. The proportion of fluorescence retained refers to the relative fluorescence per unit OD_{600} before and after injection of glucose. A value of 1 would indicate that the fluorescence is the same before and after injection; a value of 0 would indicate complete loss of fluorescence. n = 2 biological replicates, error bars represent standard deviation.

Discussion

Growth kinetics and MIC assays utilised cellular growth to report on efflux activity, but do not give a direct measurement of efflux pump function. To provide a more direct measurement of pump function, fluorescent dye efflux assays were used. Nile Red was chosen as the dye because it fluoresces in hydrophobic environments, such as the cell membrane, and has been shown to be a good reporter of efflux activity. Other efflux substrate dyes that could be used include Hoechst H33342 and ethidium bromide, both of which also have excitation and emission wavelengths compatible with the Fluostar plate readers used. However, both H33342 and ethidium bromide

fluoresce when bound to nucleic acids, and therefore the observed loss of fluorescence is a result of dye separating from nucleic acid, rather than the actual efflux activity. Loss of Nile Red fluorescence, meanwhile, indicates removal of the dye from the membrane, which should be a direct result of AcrB activity, as this pump takes its substrates from the cytoplasmic membrane.

This approach was used in an effort to determine some efflux kinetics for the different mutations. However, as efflux occurs rapidly upon re-energisation of the cells, only steady-state parameters (before and after efflux) could be assessed. Attempting to read in well-mode to eliminate the long delay between re-energisation and the next measurement resulted in very little apparent efflux for any strain. In plate mode, the entire assay is completed in 15 minutes, whereas in well-mode, each well is individually focused on for 5 min, which may increase settlement of cells and any precipitates, leading to inaccurate readings. It will also increase the amount of water lost through evaporation in wells read later than those read earlier, as the injector requires the plate to be uncovered for the duration of the assay. The difference in time taken to start readings for each well also means that the cells within each well are de-energised by CCCP for different durations, before addition of glucose to recover the cells. As Nile Red is a lipophilic dye, and fluoresces in hydrophobic environments, it is likely that background fluorescence will increase over time as more dye adheres to the plastic surface of the 96-well plate, as seen by Hoechst H33342 binding to both PTFE and quartz (Verchère *et al.*, 2013). Some precipitation was also observed in the Nile Red stock solution a day after the assays were completed; it is possible that some small granules of precipitated Nile Red also stared to form in the assay wells, which would also increase background fluorescence over time and lead to varying degrees of light scattering from the solution, which may affect readings. As this approach was only able to provide information regarding

the steady state of each mutant, and at the population level, the technique was abandoned in favour of flow cytometry.

Despite the above, some results were obtained from dye efflux assays – as Figure 4:11 indicates, the D371V mutant appears to be as defective in dye efflux as is the *tolC* knockout strain. From the plate-mode data, Welch's T-test comparing each mutation against the complemented strain indicates that the only other mutation which has a statistically significant effect (albeit from only two biological replicates) is V198D (p-value = 0.011), which showed a decrease in fluorescence intensity only about half that of the complemented strain. Meanwhile, more replicates would probably show N332L and N342A to also be statistically significantly different, as Welch's T-test with n = 2 gave values of 0.076 and 0.087, respectively, for these mutations when compared against the complemented strain. In contradiction to the results from MIC and growth kinetics assays, the R390E/R392T double mutant may be capable of removing more Nile Red from the cell (67%) than can the complemented strain (56%), with a p-value of 0.060 when n = 2 and the mutant was compared against the complemented strain by Welch's T-test. Although the MIC and growth kinetics assays suggest that the RENT mutant may be slightly defective in efflux activity, they also show a substrate-specific effect – it is therefore plausible that the slight increase in efflux activity shown by dye efflux assays is also substrate-specific, and that the results with H33342 or ethidium bromide may be quite different.

4.4 Flow cytometry

Experiments in this section were designed by Dr Jessica Blair, who also assisted with initial running and interpretation of these experiments.

All of the results so far have investigated the effect of the mutations at the population level. To assess what impact the mutations are having on individual cells, flow cytometry was used to measure ethidium bromide fluorescence on a cell by cell basis. To allow identification of cells within the mixture, cells were essentially counter-stained with Syto84, a DNA intercalating fluorophore which is not pumped out of *E. coli* cells. The Attune flow cytometer used for these experiments has two lasers, on yellow and blue channels, allowing excitation and measuring of emission at two distinct wavelengths in a single experiment. In this experimental setup, Syto84 fluorescence was measured on the yellow laser channel, and ethidium bromide fluorescence measured on the blue laser channel. As is standard practice in flow cytometry experiments, forward scatter and side scatter were also measured, which report as first approximations on relative particle size and complexity, respectively. Any particle that is measured by the flow cytometer should therefore have relatively high forward scatter, side scatter and yellow laser channel fluorescence intensity.

On the Attune software, graphs were selected to plot side scatter against forward scatter, and Syto84 fluorescence against forward scatter, as well as a histogram showing the frequency of occurrence of each value for Syto84 fluorescence (shown in Figure 4:13). A rough gate was positioned on the graph showing Syto84 fluorescence and forward scatter, such that all particles measured within this gate would likely be cells, and was therefore named “cells”. The flow cytometer was then run, set to record a minimum of 150,000 events within this gate, ensuring sufficient cell count from the experiment. The gate was then altered for each sample in post-processing, to select the data points that are most likely to be cells, and exclude any

that might, for example, show a disproportionately high Syto84 fluorescence given the forward scatter value, which would likely not be cellular. The plot of side scatter against forward scatter was used to aid the positioning of this gate, as it showed de-selection of events as they were excluded from the gate, thus allowing events of low complexity to be excluded.

The “cells” gate was then used as the selection for analysis by other charts. Numerical data in this section were taken from histogram plots showing the number of events with each value of ethidium bromide fluorescence. As seen in Figure 4:14, there were two distinct peaks on the histogram, one showing higher ethidium bromide fluorescence and the other lower. New gates were positioned to separate these peaks, allowing events in subsequent graphs to be coloured according to which of these sub-populations they belonged.

It is feasible that larger cells might be capable of containing more ethidium bromide, as concentration equals amount of substance divided by volume; a cell of greater volume requires a greater amount of substance in order to reach the same internal concentration of that substance. Therefore, ethidium bromide fluorescence was plotted against forward scatter, to ensure that there was no correlation between perceived cell size and the intensity of ethidium bromide fluorescence. If ethidium bromide fluorescence intensity of the cell was a function of cell size, then this graph would show a continuous population with a shift from low fluorescence to high fluorescence with increasing forward scatter. However, as Figure 4:14 indicates, there are two distinct populations with broadly equally forward scatter (the populations have the same x-axis values) but different fluorescence intensities.

Both Syto84 and ethidium bromide fluoresce when bound to nucleic acids. It is therefore not unreasonable that fluorescence resonance energy transfer may cause a shift in emission wavelengths of one or both of these fluorophores, when both are

bound. It may also be possible that binding of one either enhances or inhibits binding of the other. To ensure that there was no correlation between the two fluorescence readings, Syto84 fluorescence was plotted against ethidium bromide fluorescence, shown in Figure 4:14. As was the case when comparing ethidium bromide fluorescence with forward scatter, there were two distinct populations on this graph, both of which showed broadly equal Syto84 fluorescence (the populations have broadly equal y-axis values) but with different ethidium bromide fluorescence intensities.

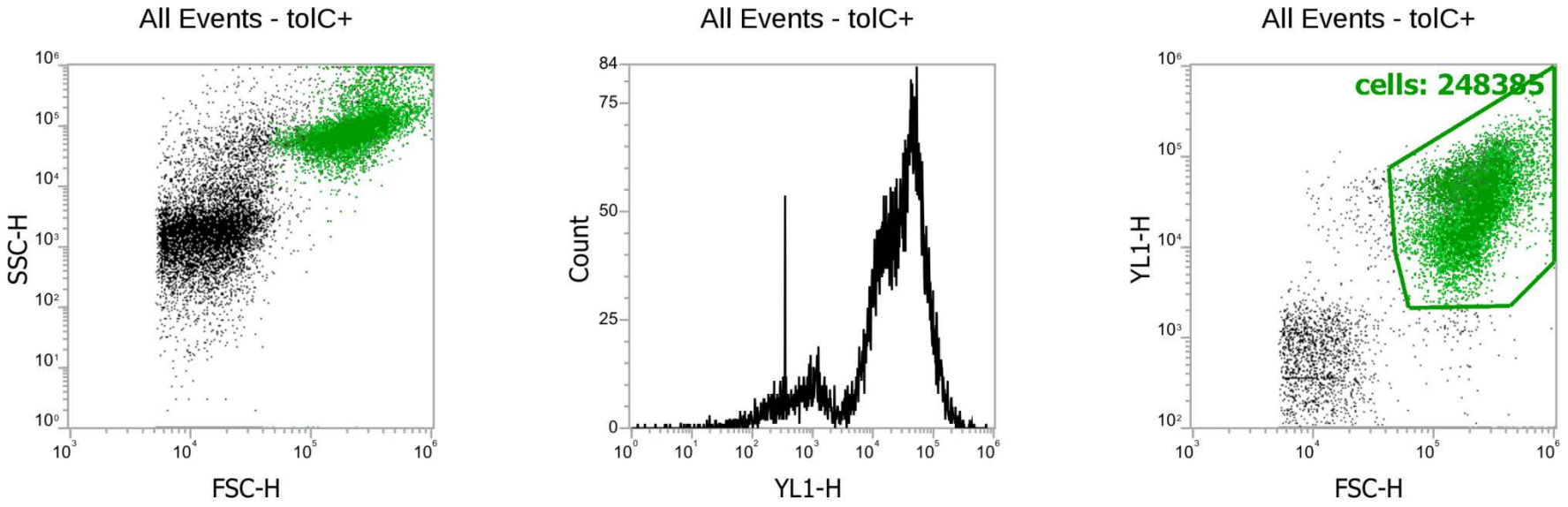

Figure 4:13 - Gating for cells in flow cytometry.

Scatter plots and histogram showing all detected events in an example of a tolC-complemented strain used in flow cytometry. Left: forward (x-axis) and side (y-axis) scatter can be used as a first approximation of particle size and complexity, respectively. The yellow laser channel (YL1-H) measures Syto84 fluorescence. The histogram (middle) indicates the number of measured events by Syto84 fluorescence and therefore gives an indication as to the number of cells compared to other events. Right: a gate (indicated by a green outline) was used to select for events that are likely to be cells based on both forward scatter (particle size) and Syto84 fluorescence; this gate was named “cells”. Once applied, the “cells” gate coloured events on the left chart in the same green.

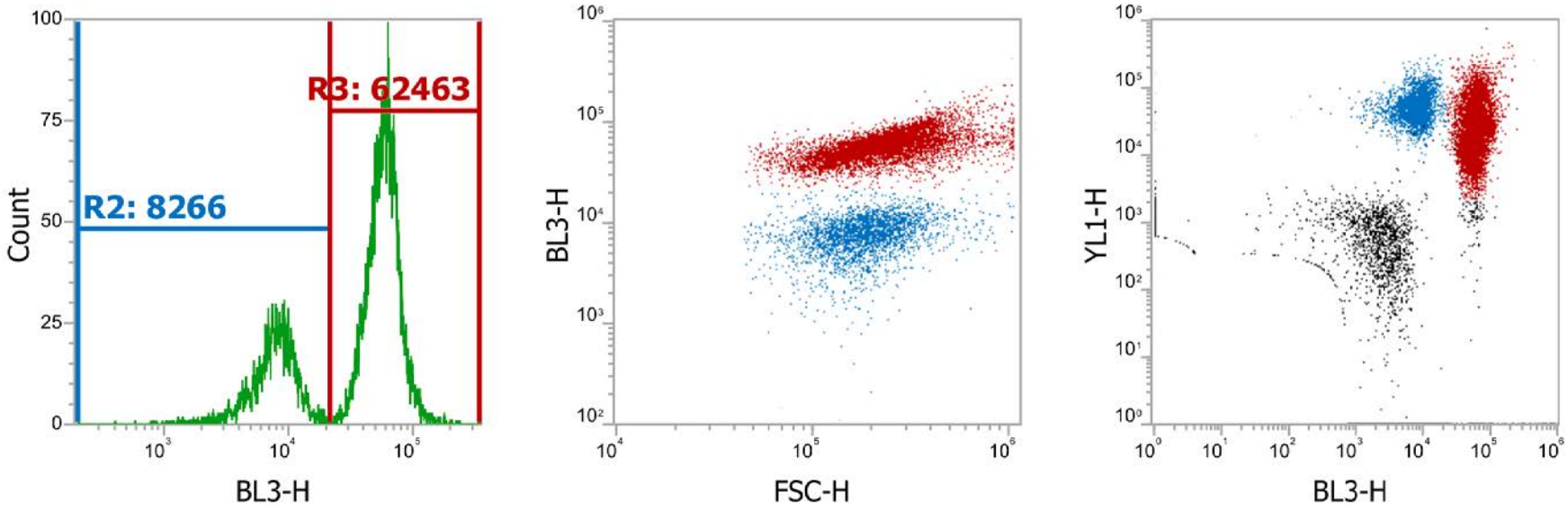

Figure 4:14 – Flow cytometry data indicate two distinct populations within a culture.

The histogram (left) showing the distribution of ethidium bromide fluorescence within the gated cell population shows two distinct peaks, each corresponding to a sub-population. This example is the same tolC-complement example as inFigure 4:13; this particular example is shown as it best illustrates the presence of two distinct peaks - it is not an average representation of this strain. The sub-population showing lower ethidium bromide fluorescence was gated and displayed in blue, while that showing higher fluorescence gated and displayed in red. The average fluorescence intensity for each peak is shown. To check that the difference in fluorescence between events was not due to a difference in particle size, ethidium bromide fluorescence was plotted against forward scatter (middle); this chart should indicate no correlation. Ethidium bromide fluorescence was also plotted against Syto84 fluorescence (right), to ensure that there was no cross-detection or interference between fluorescence channels, and that ethidium bromide fluorescence per cell is not dependent (positively or negatively) upon Syto84 accumulation.

To compare mutations by flow cytometry, all cultures contained 2 $ng.ml^{-1}$ anhydrotetracycline. Three biological replicates were analysed for each mutation. Most cultures showed the same split population as described above, with a sub-population showing high ethidium bromide fluorescence and another sub-population showing low ethidium bromide fluorescence, although some cultures did show only a single peak for ethidium bromide fluorescence, as displayed in Figure 4:15. For cultures showing only one peak, the gate boundary for high and low fluorescence intensity groups was set at the tail of the peak, where the count was less than five. This was also done on the single very broad peak that was present for the YFRS mutant. Given that the YFRS peak extended over the entire high fluorescence peak of the complemented strain, but only over a small portion of the low fluorescence peak, this broad peak was measured as the high fluorescence peak, with the low fluorescence gate set with the same rules as for the other histograms with only a single peak. On any histogram that showed a second peak, no matter how small, the gate boundary was set at the value with the minimum count between the two peaks. The results for each mutant are shown in Table 4:11.

Considering the proportion of cells that appear in each peak (displayed in Figure 4:16), the *tolC* knockout and point mutants S350F and YFRS showed almost 100% of cells to have high ethidium bromide fluorescence. The point mutations D371V and K383D both caused a change in the proportion of cells with high or low ethidium bromide fluorescence such that a higher proportion showed high fluorescence than in the wild-type or complemented strains, but a lesser proportion than in the knockout strain. A Bonferroni pairwise T-test gives p-values of 0.015, $4.7x10^{-6}$, $5.8x10^{-6}$ and $5.4x10^{-6}$ for the complemented strain against D371V, the knockout strain, S350F and YFRS, respectively, while all other pairwise T-tests against the complemented strain gives 1.00 as the p-value. These same mutations showed p-values <0.01 when compared against the complemented strain by Bonferroni

pairwise T-test of the total population x-mean ethidium bromide fluorescence intensity. The other mutations again had p-values against the complemented strain of 1.00 when tested by Bonferroni pairwise T-test. The whole population and each sub-population fluorescence intensities are displayed in Figure 4:17.

In the lower fluorescence intensity sub-population for each strain, most of the strains appear to show similar fluorescence intensities. Only the D371V mutation showed a statistically significant difference when all values were analysed by Bonferroni pairwise T-test. In this case, the average fluorescence intensity of the sub-population increased from approximately 9000 units in the complemented strain to approximately 18000 units in the D371V point mutant. Similarly, Bonferroni pairwise T-test showed no significant difference between any of the mutants, except for D371V against each of the wild-type, knockout and complemented strains, and S350F against only the wild-type strain. The fluorescence intensity of the higher fluorescence sub-population was higher in both the S350F and D371V mutants than for the same sub-population in any of the other strains.

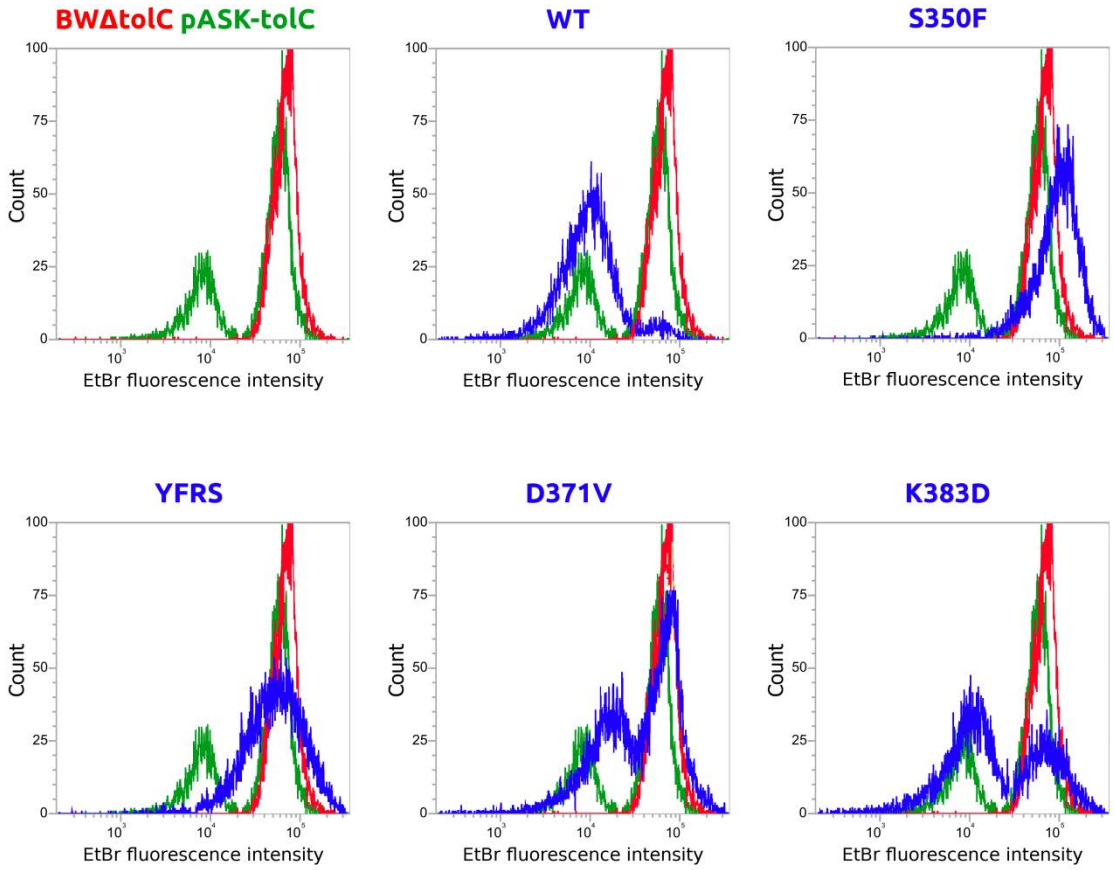

Figure 4:15 - Comparison of flow cytometry histograms for *tolC* mutants. Example histograms showing examples of distribution of ethidium bromide fluorescence in the population, compared to that of the Δ*tolC* and *tolC* complemented strains. Distribution can be predominantly low-intensity (WT), a single high-intensity population (S350F), a single population with wide range of intensities (YFRS) or split population with (D371V) or without (K383D) a clear majority in one sub-population.

Table 4:11 - Data derived for *tolC* mutants from flow cytometry.

Values given are average ± standard deviation.

Strain	Whole population fluorescence intensity ($x10^3$)	Proportion of population with low EtBr fluorescence	Low fluorescence sub-population fluorescence intensity ($x10^3$)	Proportion of population with high EtBr fluorescence	High fluorescence sub-population fluorescence intensity ($x10^3$)
BW25113 pASK-RM	17.4 ± 2.9	89%	12.6 ± 0.6	11%	56.5 ± 3.1
BWΔtolC pASK-RM	75.9 ± 5.6	<1%	10.9 ± 5.8	>99%	76.0 ± 5.6
BWΔtolC pASK-tolC	22.7 ± 17.1	77%	8.8 ± 0.9	23%	66.6 ± 5.6
D121N	22.3 ± 12.8	83%	9.7 ± 0.7	16%	88.4 ± 7.1
N145L	11.3 ± 1.3	96%	8.5 ± 0.7	4%	88.9 ± 8.9
Y344F	13.8 ± 3.5	93%	8.9 ± 1.1	7%	88.3 ± 7.1
S350F	97.0 ± 23.2	1%	9.0 ± 1.4	99%	98.0 ± 23.9
YFRS	65.2 ± 3.6	<1%	5.5 ± 3.3	>99%	65.6 ± 3.9
D371V	73.5 ± 20.7	39%	18.0 ± 5.5	61%	110.6 ± 26.9
K383D	36.7 ± 1.6	62%	11.1 ± 1.1	36%	81.1 ± 4.5

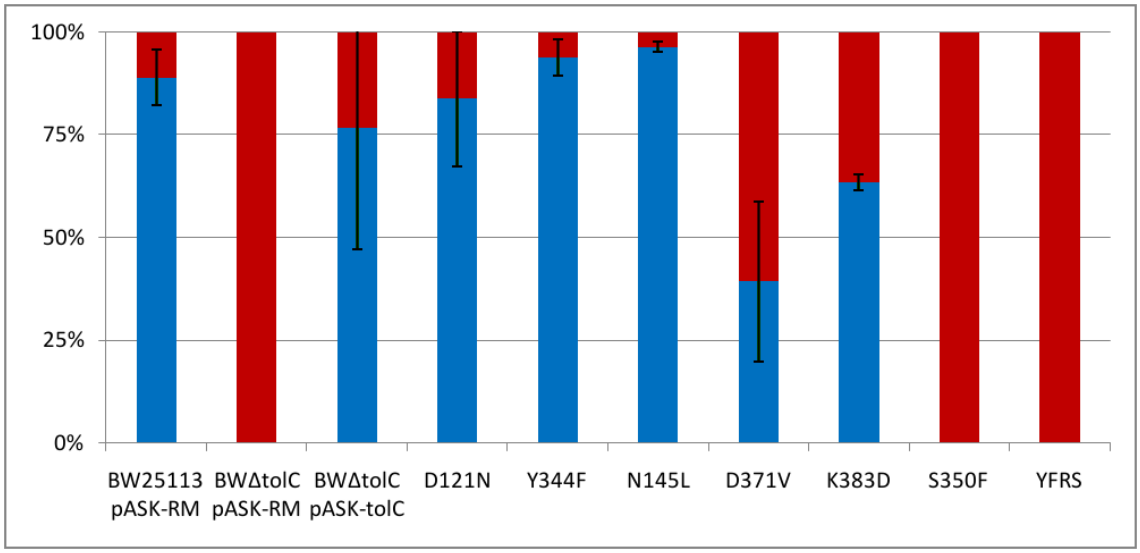

Figure 4:16 - Proportion of cells in each sub-population seen in flow cytometry. The proportion of total cells that form the sub-populations with low (blue) and high (red) ethidium bromide fluorescence intensity. Error bars indicate standard deviation.

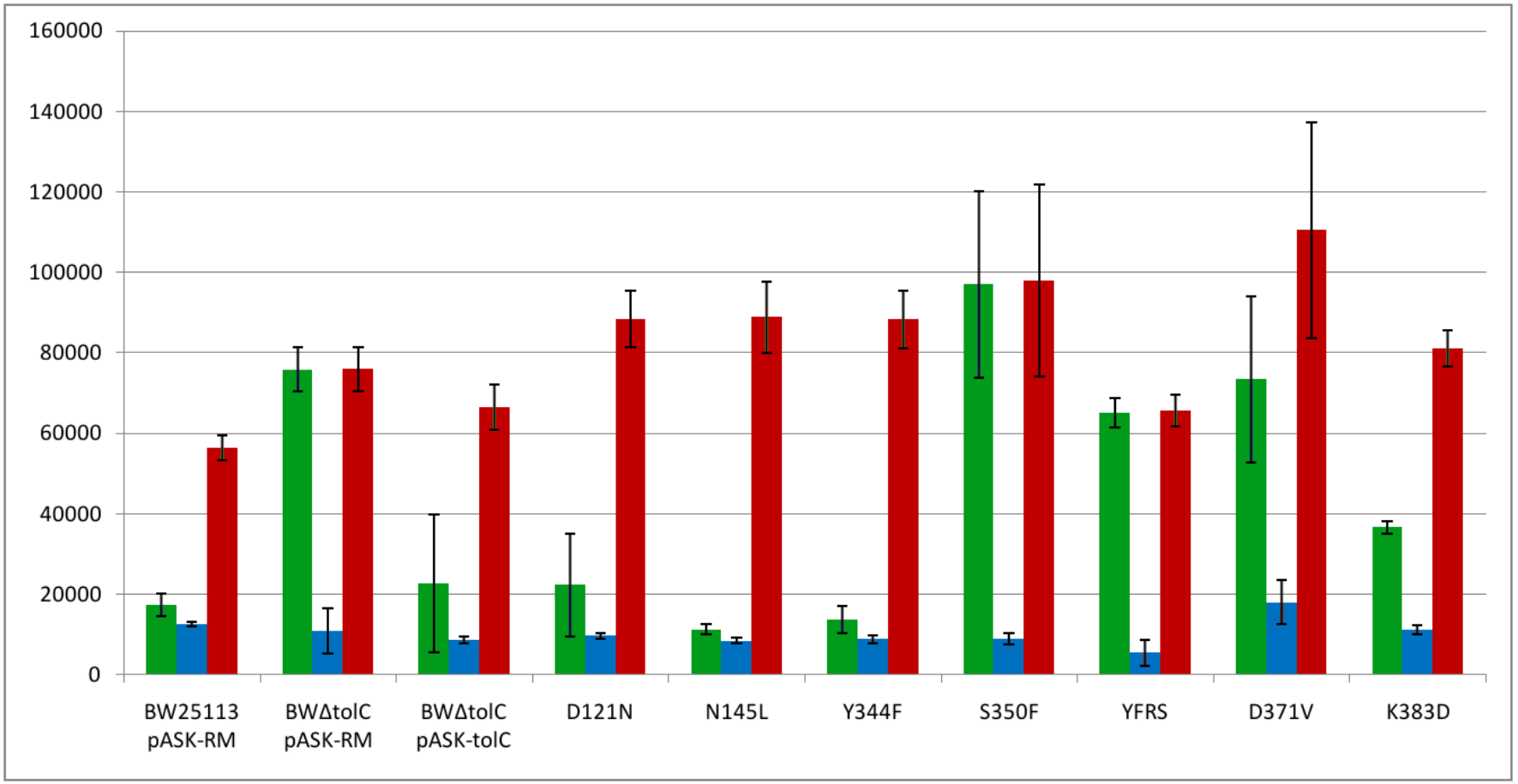

Figure 4:17 - Graphical representation of fluorescence intensities in flow cytometry.

Fluorescence intensity of the total population (green), and the sub-populations with lower (blue) and higher (red) fluorescence intensities. Error bars indicate standard deviation.

Discussion

Flow cytometry is a powerful approach for obtaining single-cell information from a population of cells. Although it is an established method for studying eukaryotic cells, it is less routinely used in the study of bacteria. Despite this the relatively limited application of flow cytometry in bacteriology, there have been some publications indicating the potential use for this technology, particularly in the field of multidrug resistance. Over 20 years ago, addition of metabolic inhibitors, including CCCP, to cells being analysed by flow cytometry showed an increase in ethidium bromide fluorescence, which was attributed to inhibition of AcrAB (Jernaes & Steen, 1994). A little more recently, it has been used to show that exposure to chlorpromazine increases the accumulation of ethidium bromide in *E. coli* (Paixão *et al.*, 2009), presumably by a combination of restricting *acrB* expression and inhibiting multidrug efflux pumps (Bailey *et al.*, 2008). Another study has shown how flow-cytometry (and the associated fluorescence-activated cell sorting) can be used as a step towards finding mutations increasing efflux activity (Whitehead *et al.*, 2011), in the case of this example by de-repression of *acrEF*. However, this thesis appears to be the first example of point mutations within bacterial tripartite efflux assemblies being analysed by flow cytometry, and therefore is the first time that flow cytometry has been used in the investigation of bacterial tripartite efflux pump assembly.

The most striking aspect of the results obtained from flow cytometry is that the population of both the wild-type strain and most of the mutants tested is split into two distinct sub-populations. One sub-population displays low fluorescence intensity on the channel measuring ethidium bromide fluorescence, and the other displays high fluorescence intensity. The results can be interpreted as meaning that the sub-population with low fluorescence displays higher efflux activity than that with high fluorescence. This heterogeneity of the population has previously been observed in a

strain expressing an OmpC:GFP fusion, to report on expression of *ompC* (Sanchez-Romero & Casadesus, 2014); in that study, heterogeneity was observed in both GFP fluorescence intensity and ethidium bromide fluorescence, although one of the sub-populations in that study apparently showed essentially zero ethidium bromide fluorescence, and it is unclear how cells were gated to eliminate non-cellular events from the data.

As was done with MIC assays, the effect of anhydrotetracycline was analysed by using a series of concentrations in the growth medium. Flow cytometry results broadly correlate with those seen in the MIC assay, whereby no or very little inducer cause higher efflux activity than the higher concentrations of inducer. In the case of the *tolC* gene being under control of the tetracycline promoter, this effect could also be explained as an increased inducer concentration leads to greater overexpression of the TolC protein, which means there are more channels available for the dye (or, in MIC assays, antibiotic) to use to gain access to the periplasm. When anhydrotetracycline was added to cultures at a final concentration of 2 $ng.ml^{-1}$, the wild-type and complemented strains appeared to be essentially the same as each other – the decreased fluorescence in the "efflux active" population of the complemented strain, and the decreased fluorescence in the "efflux deficient" population of the wild-type strain, are not statistically significant. Therefore, 2 $ng.ml^{-1}$ is a suitable concentration at which to use anhydrotetracycline for this study. Importantly, anhydrotetracycline does not appear to be an inhibitor of AcrB at this low concentration, as the fluorescence intensity of the "efflux active" peak is the same at 2 $ng.ml^{-1}$ anhydrotetracycline as it is in the absence of it. However, the data suggest that at higher concentrations, anhydrotetracycline may have an inhibitory effect, as ANOVA analysis indicates a significant (though small) difference between the fluorescence intensities of the "efflux active" sub-population, whereby 20 or

200 ng.ml^{-1} anhydrotetracycline causes higher fluorescence than 0 or 2 ng.ml^{-1} anhydrotetracycline.

Given that the difference between mutants used in this study is the point mutation each has in its coding sequence, any defect in functionality was expected to manifest as an increase in fluorescence in the "efflux active" peak (upper part of Figure 4:18). However, this is not what was observed. Instead, the population fluorescence intensity was driven by a change in the proportion of the population that was efflux active or efflux deficient (lower part of Figure 4:18). This split population could possibly be explained in part by the unequal partitioning of AcrAB-TolC upon cell division (Bergmiller *et al.*, 2017), whereby half of all newly-divided cells contain very little AcrAB-TolC, and so will form a temporarily efflux deficient sub-population. Of the mutants tested, S350F appeared as knockout, with the population almost entirely efflux deficient, while D371V and K383D showed an increased proportion of efflux deficient cells compared to the complemented strain. These results are consistent with the other *in vivo* data as shown in Sections 4.1and 4.2, and the split population may help to explain the apparent discrepancy whereby a population is sufficiently impacted by a toxic efflux substrate to grow more slowly, yet still be capable of achieving wild-type levels of overall growth (for example, on MIC plates and the stationary phase OD_{600} readings in growth kinetics). Only the D371V mutant showed an increase in fluorescence intensity of the "efflux active" peak, suggesting that this mutation either decreases efflux efficiency of ethidium bromide by TolC-dependent efflux systems, or that the dye can re-gain entry to cell more quickly in this mutant. Both the D371V and S350F mutants showed increased fluorescence in the "efflux deficient" peaks, compared to any of the wild-type, knockout or complemented strains. This indicates that these mutations either have a pleiotropic effect, or enable dye to gain entry to the cell more easily. In both of these mutants, it was noted that within the higher fluorescence peak, fluorescence intensity showed

some correlation with forward scatter, suggesting that larger cells showed more ethidium bromide fluorescence. Fortunately, the same was not true when considering any populations as a whole – overall, ethidium bromide fluorescence and forward scatter did not correlate.

The only strain to show a single peak shifted towards higher fluorescence intensity, and which was also a broader peak, was the YFRS mutant. The network of hydrogen bonds which hold TolC closed when not bound to an MFP is disrupted in this mutant, causing the channel to be more prone to allowing influx of substances. The broadness of the peak for this mutant may be caused by a difference in *tolC* expression across the population, whereby efflux is occurring poorly in most cells, but those cells expressing more TolC allow more rapid influx of the dye back into the cell. Alternatively, the mutation may be preventing efficient division of cells, as the highest fluorescence readings were in the cells with highest forward scatter readings.

Mutants D121N, N145L and Y344F did not show any differences compared to the complemented strain, despite being included in the flow cytometry assay due to other *in vivo* approaches showing each of them to cause substrate-specific effects. The lack of difference compared to the complemented strain be another example of any effect being susbtrate-specific, and it may therefore be the case that repeating flow cytometry experiments with another fluorescent efflux susbtrate may prove these mutations to impact efflux. A recent study used flow cytometry to show that deletion of *tolC* and addition of the proton decoupling agent CCCP cause an increase in the intracellular accumulation of trimethoprim (Phetsang *et al.*, 2016), which is another fluorescent substrate of AcrAB-TolC. Alternatively, Nile Red could be used, as this was seen in dye efflux assays (Section 4.3) to be an effective reporter of AcrAB-TolC activity. However, when choosing an efflux substrate dye for use in flow

cytometry, the excitation and emission wavelengths of both the efflux substrate and the cellular marker dye (in this case, Syto84) must be considered in the context of the lasers available on the flow cytometer. The lasers available for this study had wavelengths of 488 nm and 561 nm, for excitation of the dyes. According to the product data provided by the supplier for Syto84, this dye has an excitation maximum of 567 nm, and thus must be used on the yellow (561 nm) laser. As Nile Red has an excitation maximum of approximately 550 nm, this would also require detection on the yellow laser channel. Therefore, Nile Red is not compatible with Syto84 for use on the Yellow/Blue Attune flow cytometer, and an alternative cellular marker would be required in order to use Nile Red.

It would be very useful to assess membrane permeability by flow cytometry using a fluorescent conjugant of vancomycin, such as BODIPY-FL-vancomycin. Unfortunately, the BODIPY-FL fluorescent conjugant has an excitation maximum of 505 nm, and, given the narrow peak on the excitation spectrum for this molecule, it may therefore not excite particularly well with the 488 nm laser. It is also unclear what effect the conjugant moiety may have on movement of vancomycin through the TolC channel, as the BODIPY-FL moiety adds to the bulk of an already large vancomycin molecule.

Expected:

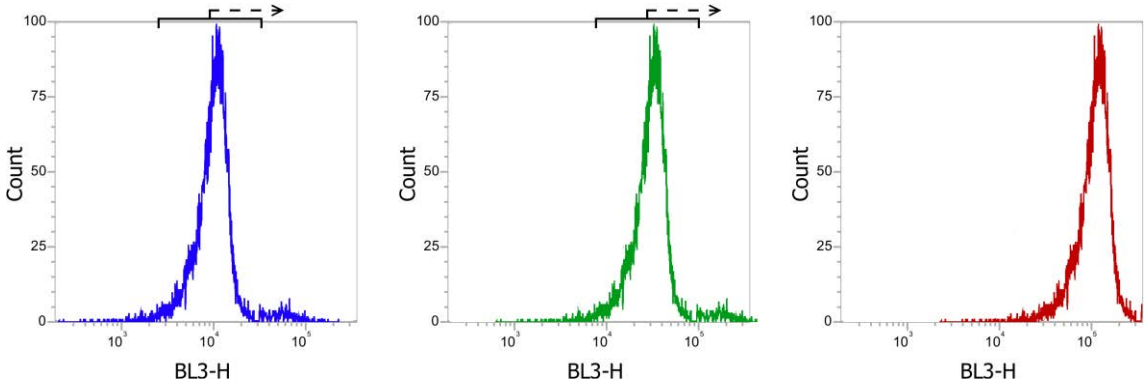

Observed:

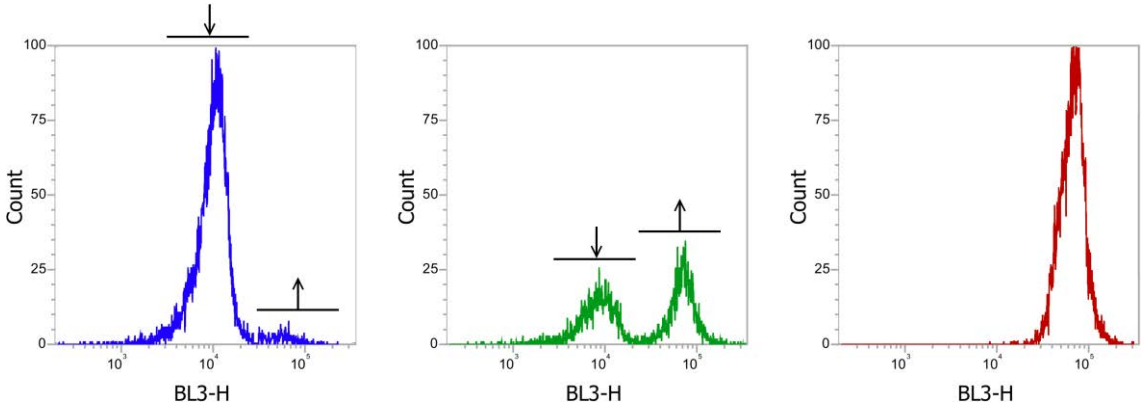

Figure 4:18 - Expected and observed difference in fluorescence intensity with decreasing efflux activity.

From left to right, efflux is depicted as decreasing, from efflux active (blue) through partially efflux active (green) to efflux deficient (red) populations. The top row indicates the expected effect of decreasing efflux efficiency, whereby the single peak was expected to move right as efflux activity decreased, as ethidium bromide fluorescence per cell increased. What actually happens is shown in the bottom row, whereby the “efflux active” peak drops in count and the “efflux deficient” peak gains in count.

4.5 Confirmation of the presence of TolC protein during *in vivo* analyses

Given results from *in vivo* assays, it was necessary to confirm that mutant protein was present in cells grown in the conditions used. To achieve this, cells were grown in the same conditions as for the flow cytometry assays but scaled up to 500 ml to enable isolation of the membranes. Cells were harvested at stationary phase and lysed using an Emulsiflex C3 homogeniser. Membrane fractions were then harvested, solubilised and the relative total membrane protein concentration of each sample measured by Bradford assay. An equal amount of total membrane protein from each sample was then resolved by SDS-PAGE, and the proteins blotted by Western blot, probed using polyclonal α-TolC antibodies. Alkaline phosphatase-conjugated secondary antibody was then added, allowing the use of the chromogenic substrate NBT/BCIP for developing the blot. A photograph of the relevant part of the developed blot is shown in Figure 4:19. The blot indicated that the wild-type strain produced very little TolC protein compared to the *tolC*-complemented strain. Of the mutations that showed the greatest apparent effect on efflux activity, D121N, S350F, and YFRS showed comparable levels of TolC protein as the complemented strain. The K383D and R390E mutations showed slightly lower levels of TolC protein than the complemented strain, but more than the wild-type strain. The amount of D371V mutant TolC protein was substantially lower than amount of TolC in the complemented strain, but was comparable to the amount of TolC protein in the wild-type strain. Multiple bands are visible for each strain, presumably one band corresponding to the full-length unprocessed protein and another to the mature protein.

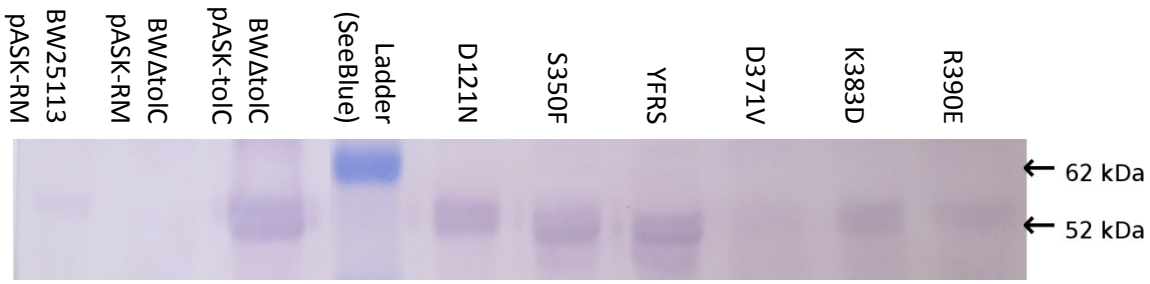

Figure 4:19- Western blot confirming TolC protein is present during assays. Photograph of Western blot showing TolC protein (52 kDa) for mutants of *tolC* grown in the same conditions as in preparation for flow cytometry. Following SDS-PAGE resolution of membrane preparations, proteins were transferred to nitrocellulose and probed with (rabbit-raised) α-TolC polyclonal antibody, followed by α-rabbit AP-conjugated secondary antibody. Chromogenic substrate NBT/BCIP was added to develop the blot. The sample volume loaded for SDS-PAGE was adjusted to load equal amounts of total membrane protein per sample. The 62 kDa marker band is visible.

Discussion

There are several possible reasons why a protein may lose functionality after mutagenesis. Whilst the aim of much of the mutagenesis in this study was to cause loss of function by preventing binding of TolC to its cognate MFPs, the assays used to assess functionality cannot determine why a certain mutation has the effect it does. To check that mutant protein is expressed and present in the membrane, membranes were purified from cultures of the mutation-bearing strains and analysed by Western blot with polyclonal α-TolC antibodies. All of the mutant TolC proteins were present in the membrane with at least as much abundance as in the wild-type strain, and therefore a lack of protein expression or aberrant localisation is the not the cause of loss of functionality. It is not known which part of TolC is recognised by the antibodies used in this study, but for correct recognition of the protein, it is likely that the protein must be folded at least mostly correctly. Protein misfolding is

therefore also unlikely as a cause of the differences in functionality, although it remains a possibility.

Of the mutant proteins, lowest abundance was observed for D371V, which also had the greatest effect on phenotype. However, the relative protein abundance is not the sole cause of all the differences in phenotype, as the knockout strain grows well in normal laboratory conditions. As the band intensity is similar to that of the wild-type strain BW25113 pASK-RM, it is also highly unlikely that the relative decrease in amount of TolC D371V compared to the complemented strain caused the increased susceptibility to antibiotics and decreased efflux of dyes. This mutation was predicted to have one definite effect, in replacing part of the gate that selectively excludes ions from passing through the periplasmic end of TolC, and a second possible effect of preventing binding of the MFP tip – or even possibly the top of the RND transporter – to the tip of TolC. Which of these actually happens cannot be determined from these *in vivo* assays alone, though use of *in vitro* protein-protein interaction analyses, such as the glycerol gradient approach used in Section 6.1 would allow determination of whether or not TolC-D371V can interact, even if it cannot function, with AcrA.

CHAPTER 5: RESULTS – PROBING THE INTERACTION FROM THE MFP SIDE

5.1 Minimum inhibitory concentrations

As with the process of investigating the MFP-OMC interaction from the side of the channel, minimum inhibitory concentration assays were used as an approved method of testing whether or not the mutations cause resistance or susceptibility to the library of tested antibiotics. The results from the *tolC* MIC results with differing concentrations of anhydrotetracycline were used to calibrate the *acrA* MIC experiments; anhydrotetracycline was added to a final concentration of 20 ng.ml^{-1} in the MIC agar. The same library of antibacterial compounds was screened for the *acrA* mutants as for the *tolC* mutants. The MICs of each antibiotic to each mutation is detailed in Table 5:1. None of acriflavine, chloramphenicol, nalidixic acid, rifampicin or tetracycline showed any difference between the knockout, complement or mutants. Deoxycholic acid showed no significant difference between the wild-type, knockout and complemented strains, but the GS-tip, Δhelices and Δhairpin mutations all caused a decrease in the MIC from 4 mg.ml^{-1} to 1 mg.ml^{-1}, a difference of two doubling dilutions. The MIC of fusidic acid was lower against any strain expressing any variant of *acrA* from a plasmid than against the knockout strain, which in turn was lower than against the wild-type strain with empty vector. While the knockout and complemented strains showed no significant difference when challenged with erythromycin, both were significantly less tolerant to erythromycin than was the wild-type strain. The *acrA* mutant in which the AcrA hairpin helices were removed, leaving the tip intact, was less tolerant to erythromycin than the complemented strain, but the other mutants appeared the same as both the knockout and complemented strains. The MIC of novobiocin against the complemented strain was the same as against the wild-type strain; the MIC of novobiocin against the *acrA* knockout strain was significantly lower than against the complemented strain. The GS-tip, Δhelices and Δhairpin mutants were all as susceptible to novobiocin as was the knockout strain.

Table 5:1 - Minimum inhibitory concentration values for *acrA* mutants.

MIC in μg.ml^{-1} of acriflavine (Acf), chloramphenicol (Cam), deoxycholic acid (Doc), erythromycin (Ery), fusidic acid (Fus), nalidixic acid (Nal), rifampicin (Rif), tetracycline (Tet) and vancomycin (Vanc). Highlighted in blue are all values that differ by at least two doubling dilutions compared to the complemented strain. For the reference strain, values in brackets are the accepted standard values.

Strain	Acf	Cam	Doc	Ery	Fus	Nal	Nov	Rif	Tet	Vanc
ATCC 25922	32 (n/a)	4 (2)	4096 (n/a)	32 (n/a)	1024 (>128)	2 (2)	512 (n/a)	8 (16)	1(1)	512 (n/a)
BW25113 pASK-RM	64	4	4096	32	512	8	512	16	1	256
BWΔacrA pASK-RM	8	0.5	2048	4	16	2	64	8	0.25	256
BWΔacrA pASK-acrAB	4	0.5	4096	2	4	1	512	8	0.125	64
S139G	4	0.5	4096	2	4	1	512	8	0.125	128
TVYF	4	0.25	4096	1	2	1	512	4	0.125	128
GS-tip	4	0.25	1024	1	2	1	32	4	0.125	64
Δhelices	4	0.25	1024	0.5	1	1	32	8	0.125	128
Δhairpin	4	0.25	1024	1	2	1	32	4	0.125	64

As before, the antibiotic challenge with vancomycin is different to the challenge with other drugs used in this study, in that it is not an efflux substrate but rather utilises the OMC to gain access to the periplasm through the outer membrane. Vancomycin susceptibility was increased in the complemented strain compared to either the wild-type or knockout strains, with a difference of two doubling dilutions. Both the GS-tip and Δhairpin mutants showed the same increased susceptibility to vancomycin as did the complemented strain. To determine the TolC-dependency of the increased vancomycin susceptibility caused by the GS-tip mutant, the MIC was also determined for the BWΔtolC pASK-acrA(GS-tip)B strain, and found to be 256 $\mu g.ml^{-1}$, the same as the BWΔtolC pASK-RM strain. Each of the S139G, TVYF and Δhelices mutants had an MIC to vancomycin between those of the knockout and complemented strains, of a single doubling dilution difference compared to either, and therefore could not be classified as significantly differently to either.

Of the efflux substrates, only deoxycholic acid and novobiocin showed MIC profiles as expected, based on the low MIC of the complemented strain in comparison to the wild-type and knockout strains. To assess whether this was due to the concentration of anhydrotetracycline used, the wild-type, *acrA* knockout and *acrA* complemented strains were tested in chequerboard assays. Chequerboard assays test for synergy or antagonism between two compounds by assessing growth at different concentrations of either and both substances. In this case, the concentration of anhydrotetracycline varied by row on a 96-well plate, and the concentration of fusidic acid varied by column on the same plate, essentially allowing comparison of the MIC of fusidic acid against the tested strains at a range of inducer concentrations. In the right-most column, fusidic acid was omitted, leaving only a range of anhydrotetracycline concentrations, while in the bottom row, anhydrotetracycline was omitted, testing the MIC of each strain to fusidic acid without inducer. To remove ambiguity regarding growth, or lack thereof, within any wells, the final OD_{600}

was measured. Any OD_{600} less than 20% that of the maximum on the plate was interpreted as a lack of growth. Table 5:2 shows the OD readings and highlights wells which were recorded as having no growth in these assays.

From the chequerboard assays, it is apparent that fusidic acid has the same MIC against the BW25113 pASK-RM strain regardless of the concentration of the inducer, up to 128 $ng.ml^{-1}$ anhydrotetracycline, at which point the MIC appears to increase to a higher concentration than included in the assay. Although the MIC is lower against the knockout strain than the wild-type, the MIC is again unaffected by anhydrotetracycline concentration. The results for the BWΔ*acrA* pASK-*acrAB* complemented strain however, were very different. In the complemented strain, it appears that there is some synergy between the two compounds, as the MIC to fusidic acid decreases as the concentration of anhydrotetracycline increases. The difference is noticeable between 16 and 32 $ng.ml^{-1}$ anhydrotetracycline, at which concentrations the MIC of fusidic acid changes by six doubling dilutions.

Table 5:2 - Chequerboard assay results.

OD_{600} values read from chequerboard assays of fusidic acid against anhydrotetracycline for the wild-type, Δ*acrA* and *acrA*-complemented strains. Highlighted in grey are values <20% of the maximum OD_{600} value.

BW25113 pASK-RM	[Fusidic acid] / µg.ml^{-1}											
[Anhydrotetracycline] / ng.ml^{-1}	**512**	**256**	**128**	**64**	**32**	**16**	**8**	**4**	**2**	**1**	**0.5**	**0**
128	0.83	0.74	0.63	0.80	0.75	0.83	0.88	0.92	0.92	0.96	0.91	1.07
64	0.17	1.13	0.68	0.80	0.90	0.77	0.84	0.88	0.87	0.88	0.80	0.87
32	0.08	1.06	0.71	0.64	0.77	0.81	0.85	0.78	0.80	0.80	0.76	0.78
16	0.13	1.09	0.76	0.65	0.85	1.03	1.10	0.96	1.03	1.02	0.96	0.87
8	0.14	1.02	0.83	0.71	0.76	0.96	0.96	0.99	0.97	1.05	1.05	1.08
4	0.12	1.13	0.93	0.75	0.90	1.08	1.14	1.08	1.23	1.19	0.93	1.05
2	0.15	0.95	0.90	0.77	0.85	1.00	0.93	0.97	1.01	1.05	1.02	1.04
0	0.13	0.96	1.10	0.95	1.09	1.19	1.07	1.25	1.19	1.29	1.07	0.98

BWΔacrA pASK-RM	[Fusidic acid] / µg.ml^{-1}											
[Anhydrotetracycline] / ng.ml^{-1}	**512**	**256**	**128**	**64**	**32**	**16**	**8**	**4**	**2**	**1**	**0.5**	**0**
128	0.05	0.08	0.14	0.17	0.21	0.23	0.36	0.47	0.59	0.83	1.07	1.33
64	0.06	0.07	0.10	0.21	0.25	0.27	0.32	0.41	0.48	0.73	0.99	1.34
32	0.03	0.04	0.09	0.17	0.25	0.34	0.41	0.46	0.53	0.65	1.14	1.35
16	0.05	0.05	0.08	0.16	0.29	0.39	0.49	0.51	0.58	0.75	1.12	1.38
8	0.07	0.04	0.07	0.15	0.29	0.40	0.50	0.49	0.55	0.70	1.17	1.42
4	0.07	0.05	0.09	0.11	0.29	0.40	0.50	0.54	0.64	0.67	1.03	1.42
2	0.05	0.06	0.08	0.12	0.29	0.36	0.44	0.54	0.66	0.60	1.10	1.43
0	0.05	0.06	0.10	0.15	0.21	0.23	0.30	0.51	0.72	0.57	0.96	1.42

BWΔacrA pASK-acrAB	[Fusidic acid] / µg.ml^{-1}											
[Anhydrotetracycline] / ng.ml^{-1}	**512**	**256**	**128**	**64**	**32**	**16**	**8**	**4**	**2**	**1**	**0.5**	**0**
128	0.05	0.08	0.09	0.04	0.07	0.06	0.08	0.08	0.62	0.51	1.01	1.41
64	0.05	0.05	0.05	0.05	0.05	0.05	0.05	0.07	0.09	0.70	0.88	1.32
32	0.06	0.04	0.04	0.04	0.06	0.06	0.07	0.07	0.13	0.58	0.89	1.39
16	0.08	0.07	0.08	0.24	0.38	0.67	0.14	0.07	0.45	0.74	0.89	1.41
8	0.07	0.07	0.24	0.86	1.08	1.13	1.13	1.16	1.11	1.02	1.02	1.45
4	0.07	0.07	0.44	1.10	1.19	1.13	1.14	1.21	1.21	1.17	1.16	1.45
2	0.08	0.12	0.84	1.13	1.17	1.15	1.19	1.17	1.23	1.26	1.23	1.46
0	0.06	0.27	1.07	1.27	1.24	1.24	1.27	1.36	1.38	1.39	1.40	1.47

Discussion

As there was very little difference between the BWΔacrA pASK-RM and BWΔacrA pASK-acrAB strains, but significant difference between both of these strains and the BW25113 pASK-RM strain, it appears that MIC assays do not work particularly well when expressing *acrAB* from the pASK vector. For most of the antibiotics tested, the knockout and complemented strains appeared the same, and so the colonies that grew on the MIC plates were tested by colony PCR for both chromosomal and plasmid-borne copies of *acrA*, to ensure the genotype had been corrected assigned. The results from the colony PCR indicated that the genotype had been correctly assigned, therefore the reason for the complemented strain appearing knockout instead of wild-type for most antibiotics is unclear. One possibility is that the complemented strain overexpresses AcrA in the conditions used in this MIC assay, causing increased permeability of the cell envelope, which manifests as increased susceptibility to vancomycin, as seen in these MIC assays. Increased permeability of the cell envelope will cause increased susceptibility to most of the efflux substrates, as the rate of influx will increase to match, or even exceed, the rate of efflux, even with less pressure from the concentration gradient. Although several of the tested antibiotics (erythromycin, fusidic acid, novobiocin) are lipophilic and expected to cross the OM by diffusion through the bilayer rather than through porins, they appear to behave differently in the *acrA*-complemented strain. This difference may be explained by differences in how efficiently each drug crosses the bilayer, and how much more easily it can gain access through an open TolC channel. Alternatively, it may be that the shape of the OM changes around the TolC protein when AcrA is bound – either model of interaction of the entire complex must cause the inter-membrane distance to change from its average value. The helical bundling model causes a compression while the tip-to-tip model causes an expansion. If we consider the density of the LPS molecule packing, and in particular consider the O-antigen,

then local curvature of the membrane must cause different relative densities of O-antigen: membrane invagination could be expected to locally increase O-antigen density, while the tips of any protrusion could be expected to have lower O-antigen density. As stated in Section 1.1, the O-antigen is not generally considered important in the study of antibiotic resistance, even though permeation of the OM by macrolides is dependent upon the length of the O-antigen. It may therefore be a worthwhile experiment to repeat these experiments with a deep-rough mutant, to determine the effect of *acrA* deletion and (mild) over-expression in both strains. Although 20 $ng.ml^{-1}$ anhydrotetracycline gave reasonable results in the MIC assays for *tolC* variants, it may not be a suitable concentration of inducer to use for *acrA* variants.

The chequerboard assay of anhydrotetracycline concentration against fusidic acid concentration indicate that anhydrotetracycline does not in itself have any toxic effect at the concentrations used, based on results in the BWΔacrA pASK-RM strain. Results from the BW25513 pASK-RM wild-type strain also show that anhydrotetracycline has no inhibitory effect on AcrAB-TolC activity at the tested concentrations. Therefore, the synergy observed between anhydrotetracycline and fusidic acid against the *acrA* complemented strain must be a result of protein overexpression at higher inducer concentrations. However, the logical assumption to make would be that more AcrAB protein leads to an increased rate of efflux, and therefore logically the results would be expected to show antagonism of fusidic acid by anhydrotetracycline in the *acrA* complemented strain, not synergy. The above hypothesis of overproduction of AcrA leading to increased cell envelope permeability can also explain these results – as more AcrA is expressed, the cell envelope allows more rapid entry of fusidic acid, masking the effect of active efflux and therefore decreasing the MIC of fusidic acid at higher concentrations of inducer. This hypothesis could be tested by a chequerboard assay of anhydrotetracycline and

vancomycin, using the same three strains as in the fusidic acid chequerboard. If this hypothesis is correct, then the same pattern of results would be observed in the vancomycin chequerboard, whereby only in the complemented strain does increasing anhydrotetracycline have any effect, and that effect would be synergy.

As the knockout and complemented strains behaved as expected only in the novobiocin MIC assay, it is difficult to determine much information about the mutants except for using the novobiocin and possibly vancomycin MIC data. The S139G and TVYF point mutants appear to behave as wild-type with respect to novobiocin efflux, but do not permeabilise the cell envelope to vancomycin in the same way as the complemented strain does. Each of the more extreme mutations, however, decrease the MIC to novobiocin considerably, to at least as low as the knockout strain. Of these, the GS-tip and Δhairpin mutants also permeabilise the cell envelope to vancomycin to the same extent as the complemented strain, while the Δhelices mutant does not. This effect is TolC-dependent, at least for the GS-tip mutant. Although highly speculative from MIC data alone, this may indicate that the hairpin tip is required to close but not to open TolC, and that the distance from the lipoyl domain of AcrA to the tip of TolC is insignificant in the closing of TolC, as the Δhelices mutant, which retains the hairpin tip but in much closer proximity to the lipoyl domain, does not display hypersusceptibility to vancomycin. The apparent loss of efflux activity against novobiocin for all of these mutants, however, suggests that the tip region is also essential for normal efflux activity, and that the helices are also essential for efflux activity, either for productive interaction with TolC, or for maintaining the required distance between the lipoyl domain and TolC.

5.2 Growth kinetics

To establish the wider effect of mutations and to determine greater detail about how the mutations affect growth, the mutations were tested in growth kinetics in the presence of sub-inhibitory concentrations of a variety of drugs. Gene expression from the tetracycline promoter was induced by addition of anhydrotetracycline to a final concentration of 2 $ng.ml^{-1}$ in the iso-sensitest broth used for the assays.

In the MIC assays, erythromycin and rifampicin showed no difference between the knockout and complemented strains for either *tolC* or *acrA* mutants, and were therefore not included in the library of drugs used in growth kinetics assays. Tetracycline showed too small a difference in MIC against the different strains to be included in the growth kinetics assays. In the presence of 1 $\mu g.ml^{-1}$ acriflavine, none of the strains, including BW25113 pASK-RM, grew during the growth kinetics experiments, and the data were therefore not analysed and are not presented here.

When challenged with 500 $\mu g.ml^{-1}$ deoxycholic acid, the highest concentration at which the GS-tip, Δhelices and Δhairpin mutants grew in MIC assays, all of the *acrA* mutants achieved a similar OD_{600} at stationary phase as did both the knockout and complemented strains (shown in Table 5:3). However, the growth kinetics in achieving this OD_{600} were different between mutants. Both the Δhelices and Δhairpin mutants grew at a slightly decreased rate compared to the complemented strain (Figure 5:1and Table 5:3). Although this was only an approximately 20% decrease in relative growth rate, Welch's T-test comparing these mutants with the complemented strain indicate that these mutants have a statistically significant effect when a 95% confidence limit is applied. None of the S139G, TVYF or GS-tip mutations caused any difference in growth rate or stationary phase OD_{600} in the presence of 500 $\mu g.ml^{-1}$ deoxycholic acid.

Nalidixic acid showed a greater difference between the mutants and the complemented strain in growth kinetics than in MIC assays. Challenge with 1 μg.ml^{-1} nalidixic acid caused each of the S139G, GS-tip, Δhelices and Δhairpin mutants to grow at decreased rate compared to the complemented strain (Figure 5:2 and Table 5:4). Similarly to the case with deoxycholic acid, the difference in relative growth rates was not large, at 15-25%, but was statistically significant. Under this challenge, the wild-type, *acrA* knockout and *acrA* complemented strains all grew with similar kinetics to each other. None of the mutations caused any difference in the OD_{600} at stationary phase. The TVYF mutation also caused no difference in growth kinetics compared to the complemented strain.

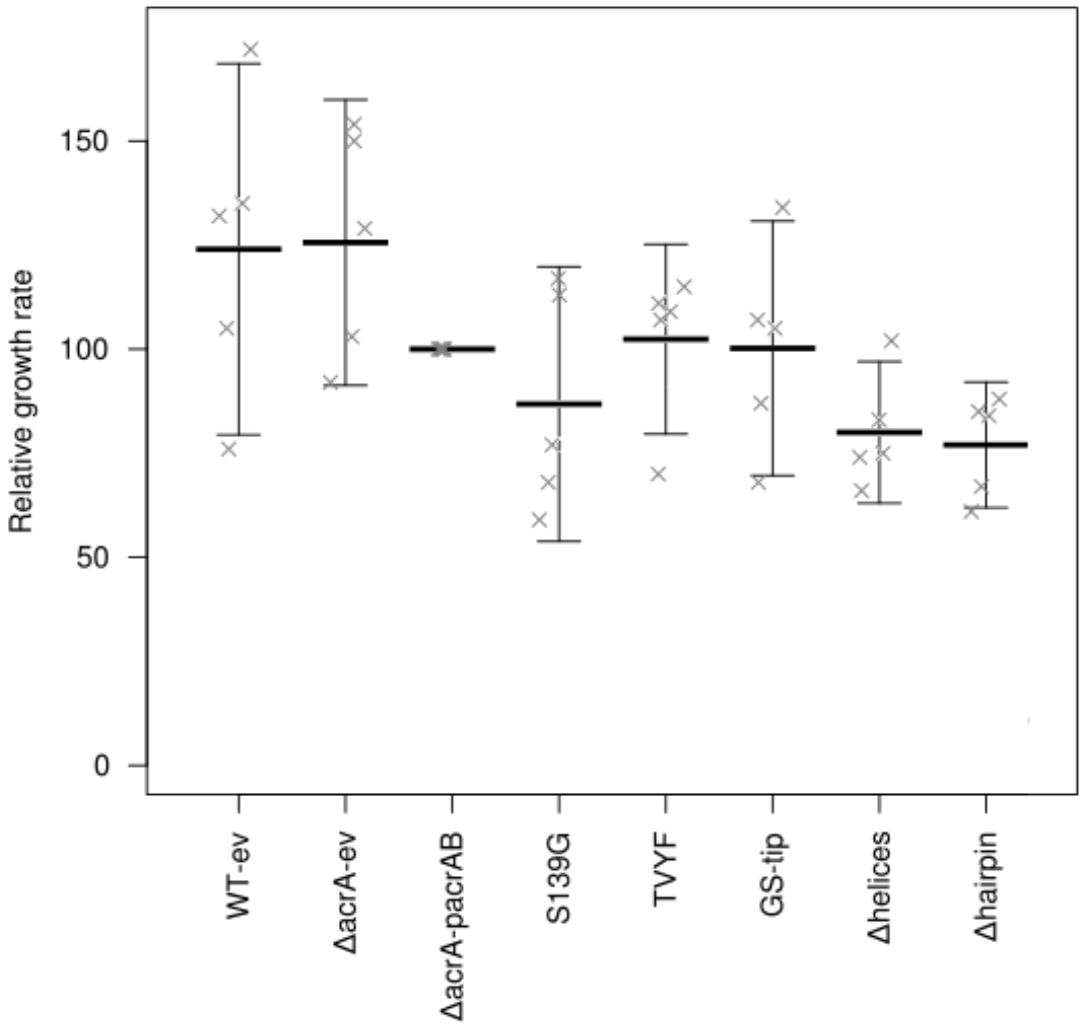

Figure 5:1 - Relative growth rates for *acrA* mutants in the presence of 500µg.ml^{-1} deoxycholic acid.

Values are given as a percentage of the BWΔ*acrA* pASK-acrAB strain growth rate. Each x represents the value for an individual biological replicate. Lines indicate average ± 95% confidence interval.

Table 5:3 - Growth rate information for *acrA* mutants in the presence of 500 µg.ml^{-1} deoxycholic acid.

Strain	Average relative growth rate (%) ± SD	P-value against acrA complement	Stationary phase OD_{600} ± SD
BW25113 pASK-RM	124 ± 36	0.209	0.98 ± 0.10
BWΔacrA pASK-RM	126 ± 28	0.107	0.96 ± 0.09
BWΔacrA pASK-acrAB	100 ± 0	--	0.93 ± 0.12
S139G	87 ± 27	0.329	0.93 ± 0.05
TVYF	103 ± 18	0.785	0.94 ± 0.10
GS-tip	100 ± 25	0.986	0.84 ± 0.15
Δhelices	80 ± 14	**0.031**	0.87 ± 0.10
Δhairpin	77 ± 12	**0.013**	0.72 ± 0.36

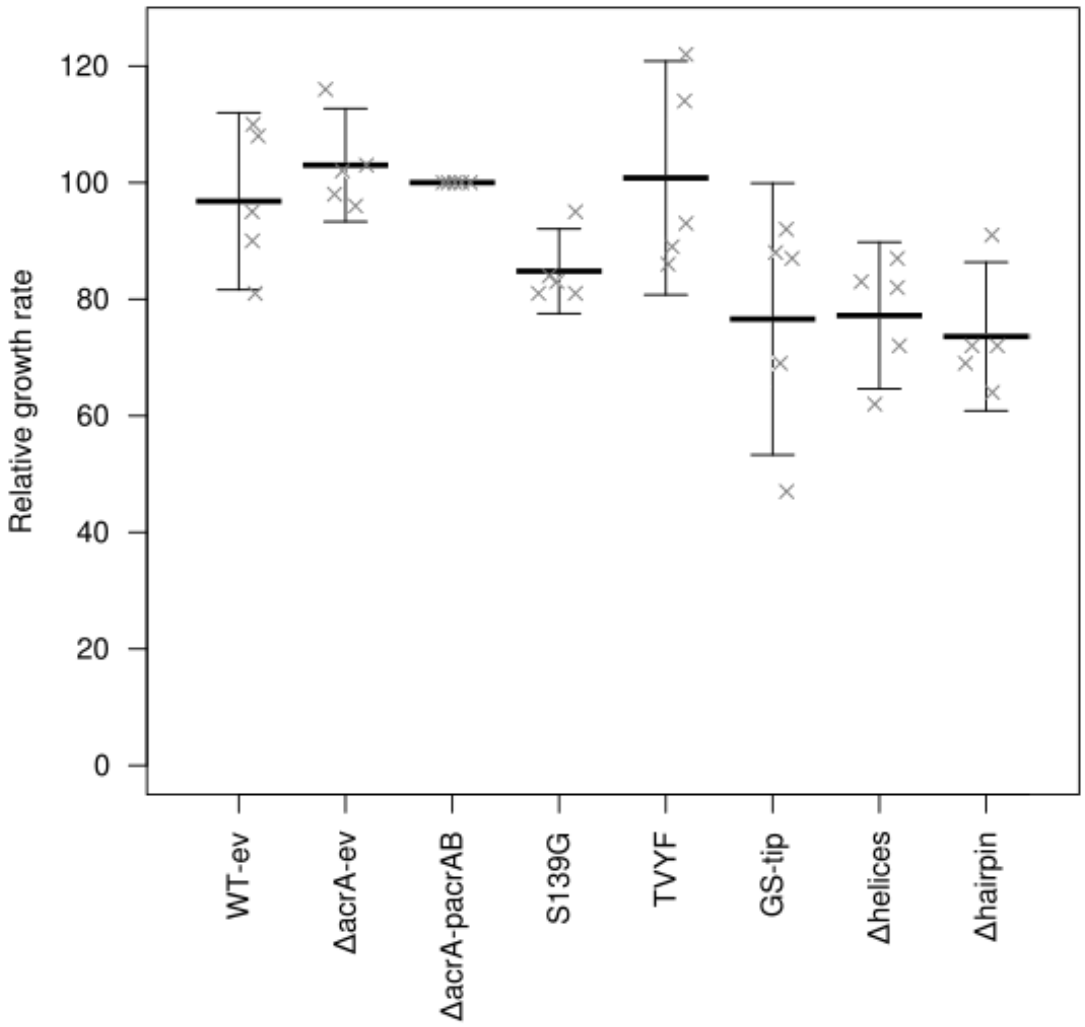

Figure 5:2 - Relative growth rates for *acrA* mutants in the presence of 1 µg.ml^{-1} nalidixic acid.

Values are given as a percentage of the BWΔ*acrA* pASK-acrAB strain growth rate. Each x represents the value for an individual biological replicate. Lines indicate average ± 95% confidence interval.

Table 5:4 - Growth rate information for acrA mutants in the presence of 1µg.ml^{-1} nalidixic acid.

Strain	Average relative growth rate (%) ± SD	P-value against acrA complement	Stationary phase OD_{600} ± SD
BW25113 pASK-RM	97 ± 12	0.590	0.92 ± 0.12
BWΔacrA pASK-RM	103 ± 8	0.439	0.98 ± 0.18
BWΔacrA pASK-acrAB	100 ± 0	--	0.83 ± 0.18
S139G	85 ± 6	**0.004**	0.90 ± 0.15
TVYF	101 ± 16	0.917	0.85 ± 0.14
GS-tip	77 ± 19	**0.049**	0.91 ± 0.05
Δhelices	77 ± 10	**0.007**	0.82 ± 0.09
Δhairpin	74 ± 10	**0.005**	0.87 ± 0.11

Although the MIC assay suggested no difference in chloramphenicol MIC against each of the *acrA* variants, and suggested that the MIC should be 0.5 µg.ml^{-1} to both the *acrA* knockout and the complemented strain, a final concentration of 1 µg.ml^{-1} was used for growth kinetics assays. In these conditions, the stationary phase OD_{600} was lower for the complemented strain than for the wild-type strain with empty vector, while this value was lower still for the *acrA* knockout strain and the GS-tip, Δhelices and Δhairpin mutants (Table 5:5). The S139G and TVYF mutations had no effect on stationary phase OD_{600} and these values were comparable to that of the complemented strain. The relative growth rates show that the S139G and TVYF mutations have no effect compared to the complemented strain, which in turn showed no difference compared to the wild-type strain (Table 5:5 and Figure 5:3). The relative growth rates reflect the stationary phase OD_{600} in so far as the GS-tip, Δhelices and Δhairpin mutations caused a significant decrease in the relative growth rate.

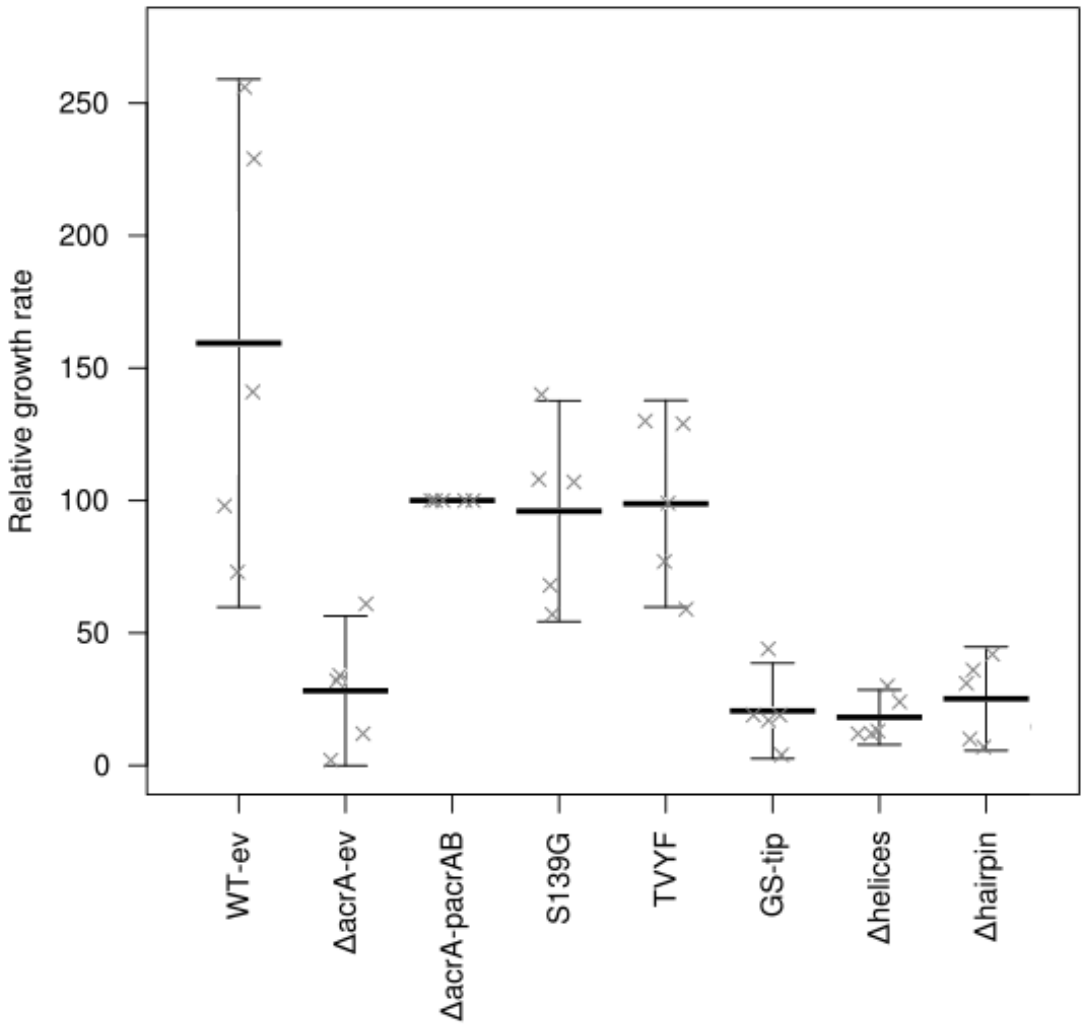

Figure 5:3 - Relative growth rates for *acrA* mutants in the presence of 1 µg.ml^{-1} chloramphenicol.

Values are given as a percentage of the BWΔ*acrA* pASK-acrAB strain growth rate. Each x represents the value for an individual biological replicate. Lines indicate average ± 95% confidence interval.

Table 5:5 - Growth rate information for acrA mutants in the presence of 1µg.ml^{-1} chloramphenicol.

Strain	Average relative growth rate (%) ± SD	P-value against acrA complement	Stationary phase OD_{600} ± SD
BW25113 pASK-RM	160 ± 80	0.173	0.68 ± 0.04
BWΔacrA pASK-RM	28 ± 23	**0.002**	0.10 ± 0.07
BWΔacrA pASK-acrAB	100 ± 0	--	0.38 ± 0.19
S139G	96 ± 33	0.803	0.40 ± 0.19
TVYF	99 ± 31	0.936	0.49 ± 0.11
GS-tip	21 ± 14	**$2.56x10^{-4}$**	0.07 ± 0.04
Δhelices	18 ± 8	**$2.53x10^{-5}$**	0.07 ± 0.05
Δhairpin	25 ± 16	**$4.47x10^{-4}$**	0.06 ± 0.05

To determine the effects of the *acrA* mutants on outer membrane permeability, growth kinetics assays were also done with the addition of vancomycin to 100 μg.ml^{-1} final concentration. In these conditions, the stationary phase OD_{600} was the same for each of the wild-type, *acrA* knockout, *acrA* complement and all of the *acrA* mutants (Table 5:6). However, the kinetics in achieving this OD_{600} were different between the strains (Figure 5:4 and Table 5:6). It appears that the complemented strain grew faster than the wild-type in these conditions, although the difference is not statistically significant. The *acrA* knockout strain grew slower than the wild-type or complemented strains, and this difference was statistically significant. The TVYF mutant grew the same as the wild-type, and like the wild-type strain was not statistically significant compared to the complemented strain. The Δhelices mutant grew relatively slowly compared to the complemented strain, and slower than the wild-type and knockout strains, but these differences were not statistically significant when a 95% confidence limit is applied. Although the relative growth rate of the S139G and Δhairpin mutants appear similar to those of the wild-type and the TVYF mutant, which were not statistically significant, the variance in the data meant that the data for the S139G and Δhairpin mutants are statistically significantly different to the complemented strain when a 95% confidence limit is applied. The GS-tip mutant grew very marginally slower than the S139G and Δhairpin mutants (though not significantly so), and was statistically significant to the complemented strain. Overall, it appears likely that the *acrA* complemented strain grows probably grows faster in the presence of 100 μg.ml^{-1} vancomycin and 2 ng.ml^{-1} anhydrotetracycline than do the wild-type, *acrA* knockout or any of the *acrA* mutants that were tested. A Bonferroni pairwise T-test indicates that the p-value between any pair of strains is 1.00 for all combinations except the complemented strain and: the knockout strain (0.027), GS-tip (0.300), Δhelices (0.139) and Δhairpin (0.813).

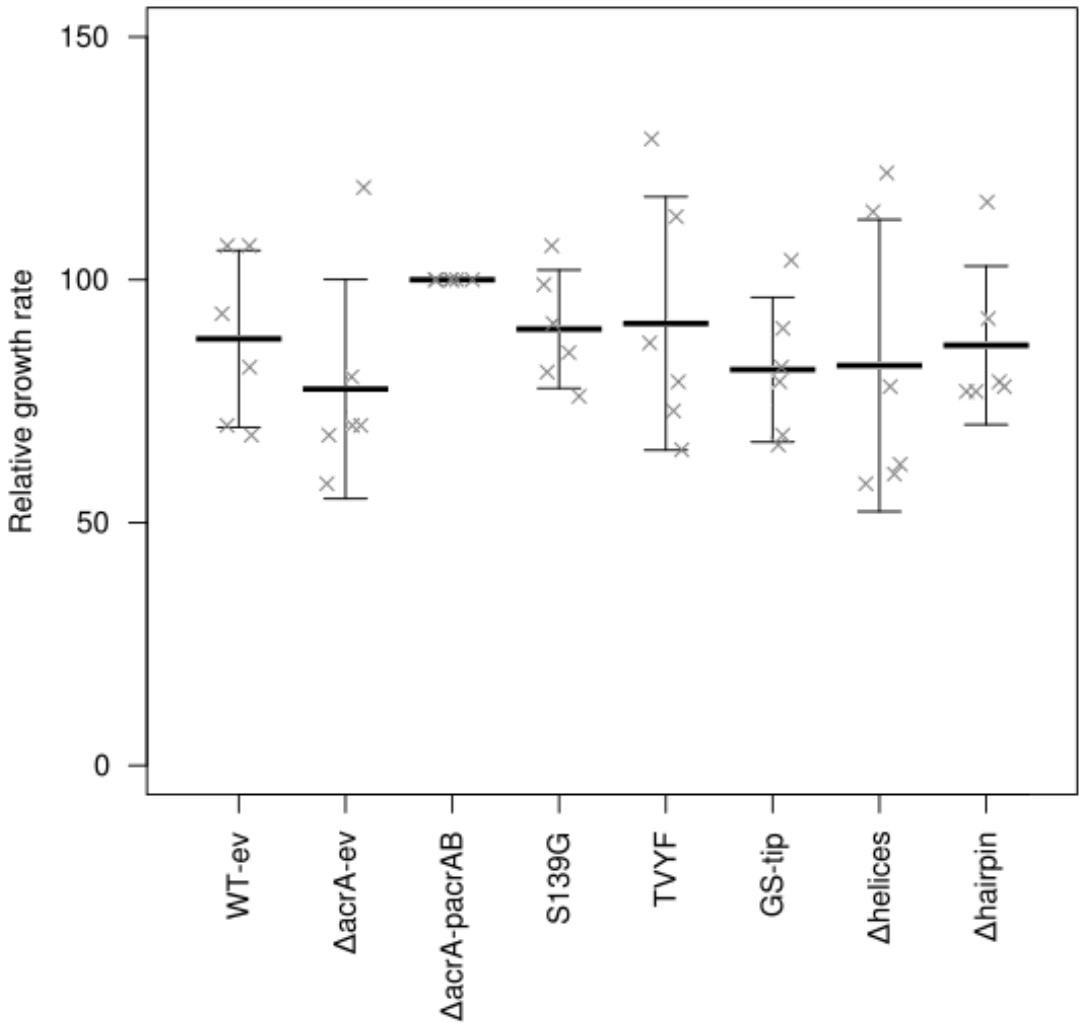

Figure 5:4 - Relative growth rates for *acrA* mutants in the presence of 100 µg.ml^{-1} vancomycin.

Values are given as a percentage of the BWΔ*acrA* pASK-acrAB strain growth rate. Each x represents the value for an individual biological replicate. Lines indicate average ± 95% confidence interval.

Table 5:6 - Growth rate information for acrA mutants in the presence of 100 µg.ml^{-1} vancomycin.

Strain	Average relative growth rate (%) ± SD	P-value against acrA complement	Stationary phase OD_{600} ± SD
BW25113 pASK-RM	84 ± 16	0.094	0.73 ± 0.09
BWΔacrA pASK-RM	69 ± 8	**0.001**	0.70 ± 0.17
BWΔacrA pASK-acrAB	100 ± 0	--	0.70 ± 0.12
S139G	86 ± 9	**0.027**	0.63 ± 0.07
TVYF	84 ± 18	0.114	0.66 ± 0.13
GS-tip	77 ± 10	**0.007**	0.68 ± 0.14
Δhelices	74 ± 23	0.072	0.76 ± 0.06
Δhairpin	81 ± 6	**0.003**	0.71 ± 0.05

The wild-type, Δ*acrA* and *acrA* complemented strains, plus the GS-tip mutant, had been included in early preliminary growth kinetics assays, which were done before the full library of mutants was available. As the GS-tip mutant showed a distinct phenotype in these early preliminary experiments, the plasmid was transformed into the wild-type strain, and used in later preliminary experiments, in which the strains were grown in iso-sensitest broth supplemented with 128 µg.ml^{-1} novobiocin, 2 ng.ml^{-1} anhydrotetracylcine and 100 µg.ml^{-1} ampicillin (relevant results are summarised in Table 5:7). This was done to test whether the GS-tip mutation was dominant or recessive compared to the chromosomally-encoded wild-type AcrA. Ampicillin was added in the preliminary experiments to ensure selection of plasmid-harbouring bacteria, though it was removed from the protocol for the data-collection experiments using other antibiotics as the challenge, described earlier in this section.

Table 5:7 - Relative growth rates of GS-tip mutants in the presence of 128 µg.ml^{-1} novobiocin.

Strain	Average relative growth rate (%) ± SD
BW25113 pASK-RM	117 ± 14
BW25113 pASK-acrA(GS-tip)B	76 ± 19
BWΔacrA pASK-RM	23 ± 16
BWΔacrA pASK-acrAB	100 ± 6
BWΔacrA pASK-acrA(GS-tip)B	19 ± 9

Table 5:8 - Bonferroni pairwise T-test values for GS-tip dominancy experiment.

	BW25113 pASK-RM	BW25113 pASK-acrA(GS-tip)B	BWΔacrA pASK-RM	BWΔacrA pASK-acrAB
BW25113 pASK-acrA(GS-tip)B	0.006	--	6.3×10^{-4}	0.217
BWΔacrA pASK-RM	6.5×10^{-7}	6.3×10^{-4}	--	8.0×10^{-6}
BWΔacrA pASK-acrAB	0.989	0.217	8.0×10^{-6}	--
BWΔacrA pASK-acrA(GS-tip)B	3.6×10^{-7}	2.8×10^{-4}	1.00	4.1×10^{-6}

The results from this experiment show a clear difference between the wild-type, *acrA* knockout and *acrA* complemented strains. The wild-type strain grew faster than the complemented strain, which grew substantially quicker than the knockout strain. The strain encoding only the GS-tip variant of *acrA* grew at the same rate as the knockout strain. The strain with both the chromosomal wild-type copy of the gene and the plasmid-encoded GS-tip variant of the gene grew with approximately half the growth rate of the wild-type strain with empty vector, and approximately 70% the rate of the complemented strain. To determine statistical significance, a Bonferroni pairwise T-test was used, the output of which is shown in Table 5:8. The table indicates that the strain expressing both wild-type and GS-tip mutant AcrA is statistically significantly different to each of the other strains, being able to grow faster than either the knockout strain or the strain expressing only the GS-tip mutant form of AcrA, but slower than the wild-type or complemented strains. It also shows that the wild-type and complemented strains are not significantly different, and that the strains expressing no AcrA or only the GS-tip mutant AcrA are essentially the same as each other.

Discussion

To obtain finer detail about possible minor effects of mutation than can be ascertained from MIC assays alone, growth kinetics experiments were used to compare *acrA* mutations. Results are summarised inTable 5:9, and show a clear difference in the apparent phenotype when looking at relative growth rates or stationary phase OD_{600} values. At 500 $\mu g.ml^{-1}$ in broth, deoxycholic acid does not appear to inhibit growth, based on stationary phase OD_{600} values, although it does cause a decrease in the relative maximum growth rates of the strains in which the AcrA hairpin has been removed, either entirely (Δhairpin) or by removal of only the helices (Δhelices) – this is not surprising, given that the lowest MIC value for any of

the *acrA* variants was double the concentration used in the growth kinetics assay. The same overall results are apparent with 1 μg.ml^{-1} nalidixic acid, additionally both the S139G point mutant and the GS-tip mutant are both also affected in the same way. The effect in nalidixic acid does not correlate quite so well with the MIC data, as nalidixic acid had an MIC value of 1 μg.ml^{-1} against all of these mutants. This discrepancy could be due to differences in growth on agar compared to in liquid broth, or could be an effect of the lower inducer concentration used in the growth kinetics assays.

Stationary phase OD_{600} values and growth rates corresponded well in chloramphenicol and novobiocin, whereby mutants that grew slower achieved a lower OD_{600} at stationary phase. The results obtained in these growth kinetics assays do not match the results in MIC assays, but the difference between the *acrA* knockout and both the wild-type and complemented strains better matches the expected results. Growth kinetics indicate some substrate-specific effect of the S139G mutation, as this mutation caused a decrease in growth rate in the presence of nalidixic acid but not deoxycholic acid or chloramphenicol. All of the mutations which affect the hairpin tip, including S139G and the *acrA* knockout (which by definition also lacks the hairpin tip) were more susceptible to vancomycin. The difference between vancomycin MIC results and the growth kinetics results can be potentially be explained by the difference in expression levels, and fit with the hypothesis set out in the MIC discussion (end of Section 5.1). At lower concentrations of anhydrotetracycline, less AcrA will be produced from the plasmid-encoded gene, and so fewer copies of AcrA are available to interact with TolC, causing fewer inactive AcrA-TolC complexes lacking a transporter protein to form. As energy is required for dissociation of the complex, AcrA-TolC bipartite complexes should theoretically remain bound, and probably – supported by the results here – have a dilated channel. The new hypothesis is therefore that AcrA or AcrB alone are capable of dilating the

TolC channel, and that the AcrA hairpin tip is required to close the channel. Meanwhile, the entire AcrA hairpin is required for active efflux function, hence the decreased growth rate of each of the GS-tip, Δhelices and Δhairpin mutants in (most of) the tested efflux substrates. By explaining how channel dilation is affected by expression of *acrA*, this hypothesis may also explain the difference between MIC assay results and the stationary phase OD_{600} values. As a higher inducer concentration was used in the MIC assays, more non-productive AcrA-TolC bipartite open complexes formed, allowing greater influx of the efflux substrates, as well as vancomycin, hence decreasing the MIC of these efflux substrates against all strains with plasmid-encoded *acrA*, regardless of efflux activity. This also explains why all mutants were capable of growing – even if some of them had decreased growth rate – at the apparent MIC of nalidixic acid against these mutants, when a lower inducer concentration was used.

Table 5:9 – Summary of growth rate change relative to *acrA*-complemented strain.

"Up" or "Down" indicates that the growth rate is increase or decreased relative to the *acrA* complemented strain. A dash indicates no difference from the complemented strain. N/a indicates that the mutation was not tested with that particular antibiotic. Changes in stationary phase OD_{600} are presented in the same way in brackets.

Strain	Doc	Nal	Cam	Nov	Vanc
BW25113 pASK-RM	- (-)	- (-)	- (Up)	- (-)	- (-)
BWΔacrA pASK-RM	- (-)	- (-)	Down	Down (Down)	Down (-)
S139G	- (-)	Down (-)	- (-)	N/a	Down (-)
TVYF	- (-)	- (-)	- (-)	N/a	- (-)
GS-tip	- (-)	Down (-)	Down	Down (Down)	Down (-)
Δhelices	Down (-)	Down (-)	Down	N/a	- (-)
Δhairpin	Down (-)	Down (-)	Down	N/a	Down (-)

5.3 Flow cytometry

Experiments in this section were designed by Dr Jessica Blair, who also assisted with initial running and interpretation of these experiments.

As with investigation of *tolC* mutants, the other *in vivo* approaches investigate the effect of mutations at the population level. Flow cytometry was used to measure ethidium bromide fluorescence on a cell by cell basis. Again, cells were counter-stained with Syto84, and both blue and yellow laser channels were used, to measure ethidium bromide and Syto84 fluorescence, respectively. Forward and side scatter were also used to report on particle size and complexity. The same graphs as were used for gate placement in TolC flow cytometry experiments (Figure 4:13) were generated for each *acrA* mutant and used to position gates to select for cells.

The histograms showing cell counts for each value of ethidium bromide fluorescence showed two distinct peaks, as was seen in Figure 4:14 for the *tolC* mutants. The proportion of cells in each peak was comparable for the wild-type and complemented strains, with a clear majority of cells showing low ethidium bromide fluorescence (proportions of the population which contribute to either sub-population peak are visualised in Figure 5:5). Neither of the Δhairpin or Δhelices mutants showed any cells with low ethidium bromide fluorescence, and both showed a marginal, but not significant, increase in the fluorescence intensity of this peak compared to the complemented strain sub-population showing higher fluorescence intensity (fluorescence intensity for each peak and overall populations are shown in Figure 5:6). Almost all *acrA* knockout cells and GS-tip mutant cells showed high ethidium bromide fluorescence, although there were some events counted with low fluorescence. It was noted that some of the events counted within the GS-tip mutant cells gate showed ethidium bromide fluorescence intensity of zero, which, given the low number of cells in the lower fluorescence sub-population peak for two of the three biological replicates for this mutant, would contribute to the x-mean value of this peak being lower than for other strains.

In the sub-populations showing higher ethidium bromide fluorescence, the wild-type strain showed less fluorescence than the strains expressing either wild-type or mutant AcrA from the pASK plasmid. However, when a 95% confidence interval is applied, the difference in fluorescence intensities of these sub-populations is only significant between the wild-type strain and each of the Δhelices and Δhairpin mutants.

When all parts of the results of this assay are combined, all of the GS-tip, Δhelices and Δhairpin mutants appear essentially as knockout, while the complemented strain appears essentially as wild-type.

Table 5:10 - Summary of information from flow cytometry on *acrA* variants. Values given are average ± standard deviation. * - value significantly increased by an outlier.

Strain	Whole population fluorescence intensity ($x10^3$)	Proportion of population with low EtBr fluorescence	Low fluorescence sub-population fluorescence intensity ($x10^3$)	Proportion of population with high EtBr fluorescence	High fluorescence sub-population fluorescence intensity ($x10^3$)
BW25113 pASK-RM	17.4 ± 2.9	89%	12.6 ± 0.6	11%	56.5 ± 3.1
BWΔacrA pASK-RM	80.2 ± 11.1	0.6%	14.1 ± 1.4	99%	80.6 ± 10.9
BWΔacrA pASK-acrA	26.6 ± 11.0	82%	11.6 ± 1.2	18%	86.6 ± 19.7
GS-tip	69.1 ± 13.3	2%*	7.4 ± 3.3	98%	70.0 ± 12.3
Δhelices	100.6 ± 7.4	0%	-	100%	100.6 ± 7.4
Δhairpin	90.0 ± 5.2	0%	-	100%	90.0 ± 5.2

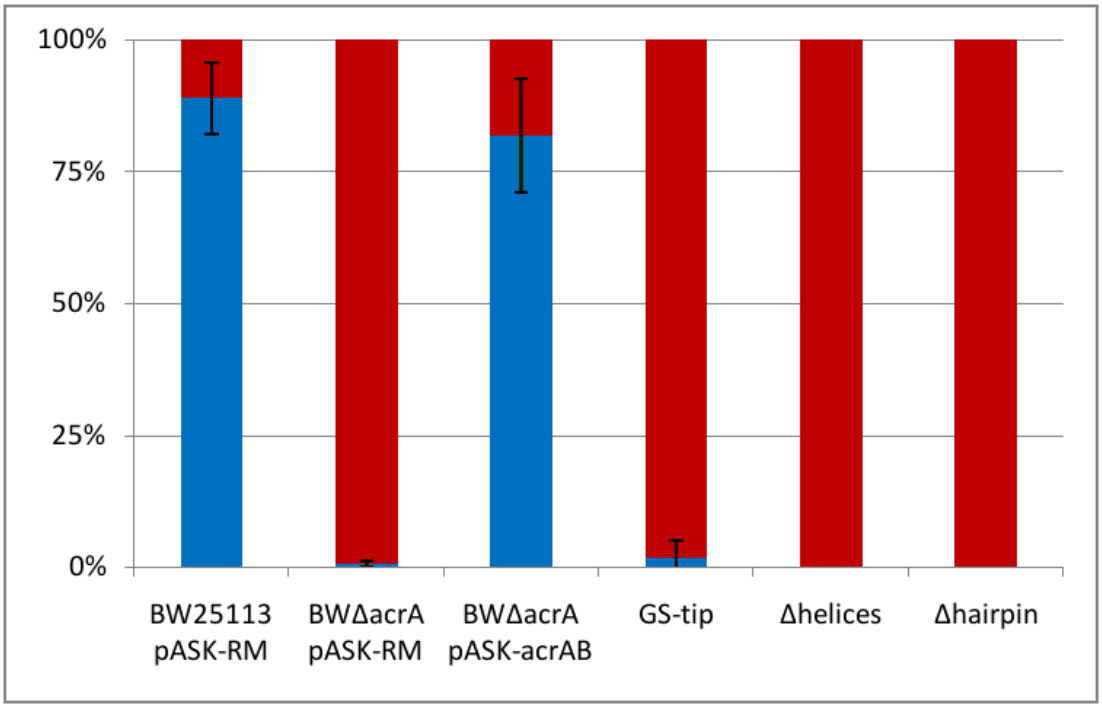

Figure 5:5 - Proportion of cells showing high- or low-level ethidium bromide accumulation.

The proportion of cells shown by flow cytometry to contribute to the lower (blue) or higher (red) ethidium bromide accumulating sub-populations. Error bars indicate standard deviation.

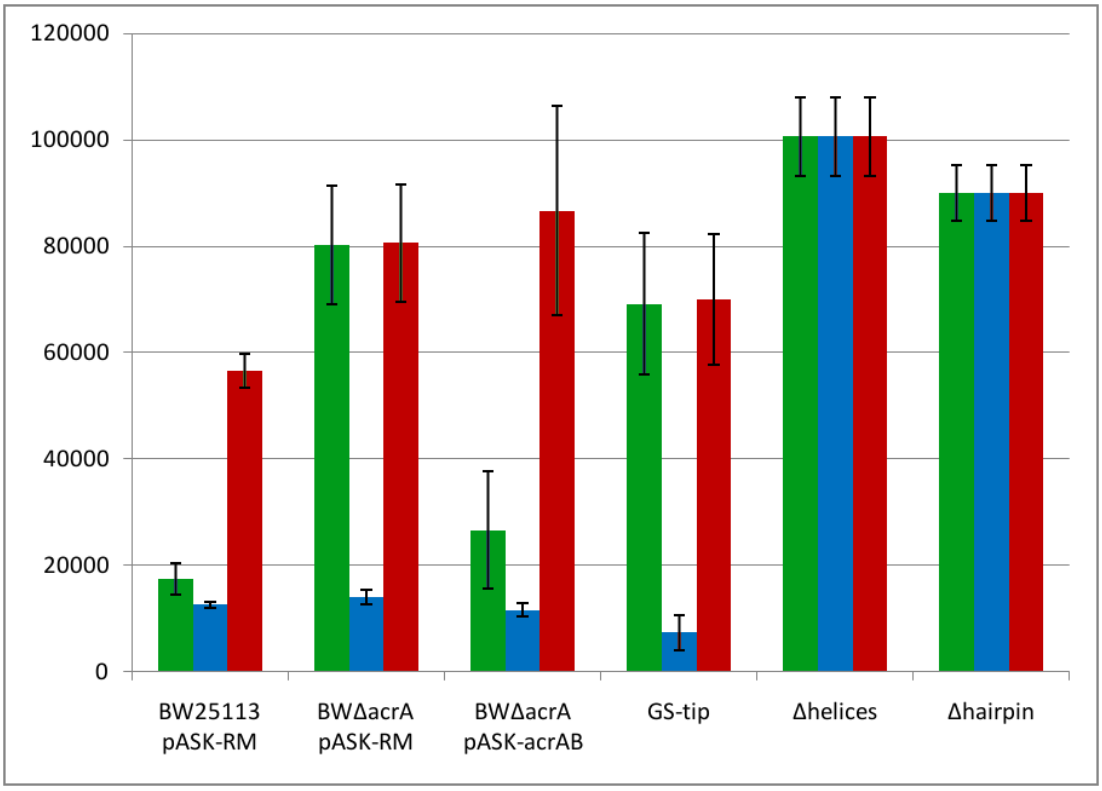

Figure 5:6 - Ethidium bromide fluorescence in *acrA* mutants as determined by flow cytometry.

The average ethidium bromide fluorescence intensity (± standard deviation) for the whole population (green), low fluorescence intensity sub-population (blue) and high fluorescence intensity sub-population (red). Each of the Δhelices and Δhairpin strains showed only a single peak; the value for this peak is here used for each category.

Discussion

Flow cytometry enables greater detail to be ascertained regarding a bacterial culture as a whole. Notably, the wild-type and *acrA* complemented strains show clearly split populations, with 80-90% of cells showing low ethidium bromide fluorescence and the remainder showing high fluorescence. This reflects the results seen in the equivalent experiment using *tolC* variants (Section 4.4), and similar observations have been reported for other proteins when fluorescence protein fusions have been

expressed. As was the case with in the *tolC* experiment, differences in total population fluorescence intensities are driven by the proportion of cells in one sub-population or the other; there does not appear to be any partial decrease in fluorescence intensity for any of the mutants. The two sub-populations can be assigned as "efflux active" for the low fluorescence peak and "efflux deficient" for the high fluorescence peak, as this fits with the expected increase in fluorescence of the *acrA* knockout strain and subsequent recovery in the complemented strain. The knockout strain has a very small sub-population that appears to be efflux active, which could be a result of up-regulation of *acrE* to compensate for loss of *acrA* – deletion of both genes is known to increase susceptibility to ethidium bromide (Smith & Blair, 2014), and therefore should a sub-population respond to the loss of one gene by up-regulation of the other, the phenotype should be at least partially rescued.

Although not deemed significant, the difference in the "efflux deficient" fluorescence intensity for the wild-type strain compared to either the *acrA* knockout or complemented strains could indicate that there is some pleiotropic effect of the chromosomal mutation. As the wild-type strain contains the same empty vector as the knockout strain, the difference cannot be caused by pleiotropic effect of the plasmid backbone. As the differences in fluorescence intensities of the sub-populations of the mutants were not statistically significant from those of the complemented strain, it appears that the only scientifically sound conclusions that can be drawn from this experiment are that firstly, nearly all cells in the knockout, GS-tip, Δhelices and Δhairpin mutants are efflux deficient, and secondly, the relative proportion of cells that are "efflux active" or "efflux deficient" determine the overall fluorescence intensity of the population. The results from this experiment are not incompatible with the hypotheses formed from results in Section 5.1 or Section 5.2, although neither do they directly support those hypotheses. It is unfortunate that

BODIPY-FL-vancomycin, a fluorescent conjugant of the influx-limited vancomycin drug, is not compatible with the specific design of this experiment, as this would help to obtain data that would test the hypotheses formed from Sections 5.1 and 5.2.

As far as the hypothesis that the GS-tip mutation causes a dominant effect over the wild-type AcrA, the data in this experiment suggest that this is probably not the case, although it remains a possibility. The proportion of cells in the lower fluorescence peak is essentially zero in both the GS-tip and knockout strains (values of 0.2%, 0.2% and 7.7% in the GS-tip against 0.2%, 0.5% and 1.1% in the knockout). It is not possible from this experiment to ascertain the reason behind the high ethidium bromide accumulation in the GS-tip mutant – it appears to certainly be efflux deficient, but this could be due to either loss of interaction with TolC or the formation of a non-productive interaction with TolC.

5.4 Confirmation of AcrA presence during *in vivo* analyses

To confirm that differences in *in vivo* assays are not due to differences in protein expression, the presence of AcrA protein from each *acrA* mutant was analysed by Western blot. Each of the strains were grown in 500 ml cultures of the same composition as used when growing cultures for flow cytometry. Membranes were harvested from these cultures, and a Bradford assay used to determine total membrane protein concentration in each sample. The results from the Bradford assays were used to enable volume adjustment when loading samples for SDS-PAGE, ensuring that an equal amount of total membrane protein was loaded for each sample. Following SDS-PAGE resolution of the proteins within the samples, the proteins were transferred to a PVDF membrane and probed with polyclonal α-AcrA antibodies. Alkaline phosphatase-conjugated secondary antibodies were used, and the blots developed with NBT/BCIP chromogenic substrate. A photograph of the developed blot is shown in Figure 5:7. The *acrA* knockout strain showed a band of comparable intensity to the wild-type strain, while the band for the complemented strain was of considerably greater intensity. Of the mutants, only the GS-tip, Δhelices and Δhairpin variants were analysed by this method, given that these showed a significant difference compared to the complemented strain in other methods. The GS-tip mutant showed what appears to be two bands, one for the same size as the wild-type protein and one of a smaller size. These bands were approximately the same intensity as the complemented strain, indicating the same overexpression as seen in the complement. Both the Δhelices and Δhairpin mutants showed lower band intensity, although bands were still clearly visible. Each of these mutants showed two bands, one corresponding in size to the wild-type protein and the other being smaller. For each of these three mutants, the smaller protein corresponds to the mutant protein: the mature wild-type AcrA protein is 39.7 kDa, the GS-tip is 38.9 kDa,

Δhelices is 34.6 kDa and Δhairpin 32.9 kDa. Although the amounts of each protein are not necessarily the same for each mutant, the protein is present.

Given that all of the strains, including the knockout, show a band corresponding to the wild-type AcrA protein, the strains were re-tested by colony PCR to ensure that the chromosomal *acrA* gene was indeed deleted in these mutants, and that there had been no error of strain selection during transformation. During the process of cell disruption and membrane purification, some cells pass through the disruptor intact and are removed by a relatively low-speed centrifugation step. The pellet from this step was used as material for colony PCR. The acrA-upst-F and acrA-dnst-R primer pair were used for amplification, which would generate a PCR product only from chromosomal copy of *acrA*, and of a different size depending upon whether the strain is *acrA*$^{+}$, *acrA::aph* or Δ*acrA*, as the primers anneal up- and down-stream of the recombination sites used for gene deletion. All of the strains generated a PCR product which was shown by agarose gel electrophoresis to be approximately 450 bp in size, corresponding to the Δ*acrA* fragment. This confirmed that the apparently wild-type AcrA band seen on the Western blot in the knockout strain, and in the mutants showing two distinct bands, was not caused by the presence of AcrA which had been produced from a chromosomal copy of the gene.

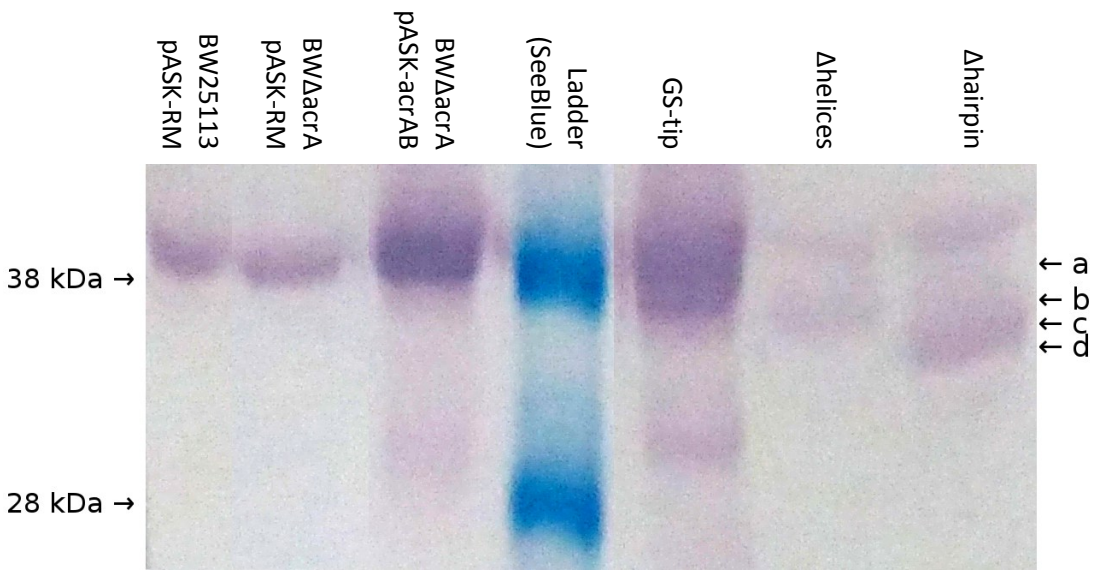

Figure 5:7 - Western blot for AcrA protein in *acrA* mutants.

Mutants of *acrA* were grown in the same conditions as in preparation for flow cytometry and the membranes harvested. The membrane protein sample volume loaded for SDS-PAGE was adjusted to load equal amounts of total membrane protein per sample. The 38 kDa (upper) and 28 kDa (lower) marker bands are visible. Multiple protein bands are visible from the various samples, corresponding to (a) full-length AcrA at 39.7 kDa after removal of the signal sequence; (b) the GS-tip variant of AcrA at 38.9 kDa; (c) AcrA lacking the hairpin helices (Δhelices) at 34.6 kDa and (d) AcrA in which the hairpin structure has been replaced with the BesA loop (Δhairpin) at 32.9 kDa.

Discussion

Having shown that the GS-tip, Δhelices and Δhairpin mutants of *acrA* cause a loss of function phenotype, it was necessary to show that this phenotype is not caused by a loss of protein, protein misfolding or mislocalisation. The results here suggest that AcrA may be present in the knockout strain, although genetic testing subsequently showed that the *acrA* gene was not present in the strain. Given the high similarity between AcrA and AcrE, it is likely that there is some cross-reactivity of the α-AcrA antibody with AcrE, which would explain the presence of the band in the knockout strain. The same band is also present in the GS-tip, Δhelices and Δhairpin mutants, although at lower band intensity. This indicates that although AcrE is likely to be present in these mutants, it is not expressed at the same levels as in the *acrA* knockout strain, presumably because the cells recognise that AcrA protein is present, even if it is not functional.

All of the mutant proteins are expressed, and localise to the membrane. The GS-tip mutant appears to express at around the same level as the wild-type protein from the complemented strain, while both mutants lacking the hairpin structure appear to be expressed at levels closer to the chromosomally-encoded AcrA from the wild-type strain. However, the site on AcrA to which the antibody binds is not known, and, being polyclonal, it is possible that different antibodies within the mixture recognise different parts of the protein. Due to the prominence of hairpin structure, it is likely that at least some of the antibodies recognise this site, which may explain why these two mutants appear to have a lower expression level – they are missing the recognition site of a portion of the antibodies.

Ultimately, the results in this section show that all phenotypic differences between mutants are caused by differences in protein functionality, not by differences in the protein expression or by differences in localisation of the proteins to the membrane.

CHAPTER 6: RESULTS – ANALYSES WITH PURIFIED PROTEINS

Work in all of Chapter 6 was assisted by Dr Martin Picard and Mr Dhenesh Puvanendran, and supported by FEMS Research Grant FEMS-RG-2015-0124.

6.1 Analysis of protein-protein interaction by glycerol gradient fractionation

Each of the AcrAB-TolC component proteins, with 6xHis tag, were expressed from the pET26 vector in the corresponding knockout strain of the C43 (DE3) high expression strain. To optimise protein yield, 1 l cultures were grown in multiple condition sets. In each condition, cultures were grown to an OD_{600} of 0.3 to 0.5, at which point IPTG was added to a final concentration of 0, 10 or 50 μM, and growth continued at 37°C for 16 h, 20°C for 16 h, or 37°C for 3 h, respectively.

Upon cell disruption with a OneShot cell disruptor, it was evident that the majority of the target proteins in cultures with the higher concentration of IPTG had formed inclusion bodies, which was confirmed upon Coomassie staining of soluble, solubilised membrane and insoluble fractions. Cultures grown with induction by 10 μM IPTG grew to a final OD_{600} in a range of 1.8 to 3.5, while uninduced cultures reached final OD_{600} in a range of 3.7 to 6.1; however, when the membrane fractions were analysed by Coomassie staining, the bands corresponding to target protein from uninduced cultures were of similar density to the other membrane proteins. Mutated versions of the proteins were therefore expressed by induction with 10 μM IPTG and growing for 16 h at 20°C post-induction. Each of the wild-type proteins, the GS-tip, Δhairpin and Δhelices variants of AcrA, and the D121N, N145L, R158D, Y344F, S350F, YFRS, K383E and RENT variants of TolC were expressed and subsequently purified by Ni-NTA affinity chromatography. Following concentration of the AcrB protein, it was observed that very little solution remained in the column, and dilution was required in order that the volume was workable. Despite this, the total amount of AcrB protein purified was calculated by nanodrop analysis to be 1.2 mg and analysis by SDS-PAGE indicated that the sample was of high purity. From any single

culture, the protein yield ranged from 0.8 mg (a WT TolC sample) to 2.4 mg (for a sample each of WT AcrA and TolC(D121N)).

Each purified protein was incubated with BAPol to exchange the detergent hydration shell before mixing components in a 120:40:50 µg AcrB:AcrA:TolC ratio, approximately equivalent to a 1:1:1 molar ratio. The mixtures were then subjected to ultracentrifugation on a 10-28% glycerol gradient. As this part of the project was done as part of a research visit, time restraints meant that the only combinations tested were AcrB-AcrA-TolC, AcrB-AcrA-TolC(N145L), AcrB-AcrA(Δhp)-TolC and AcrB-AcrA(Δhelices)-TolC. Fractions were aspirated and resolved by SDS-PAGE. Coomassie staining of the resulting gels (Figure 6:1) showed protein at approximately 120, 100, 90 and 45 kDa for samples from 12-20% glycerol. In the AcrB-AcrA-TolC and AcrB-AcrA-TolC(N145L) samples, these bands were all between 14-20% glycerol, with maximum intensity at 16% glycerol for all the bands; very little protein was seen in these samples from fractions containing less than 14% glycerol, and most of the AcrA could be seen at 90 kDa rather than 45 kDa, indicating dimer formation. All of the same bands were visible for both of the AcrA mutants, although the majority of mutated AcrA was seen at 45 kDa rather than 90 kDa, indicating that it was monomeric. There was also a shift in which fractions yielded the fragments from the AcrA mutants - the higher weight bands were visible from 12-20% glycerol, with the lower weight bands in the 10-16% glycerol range.

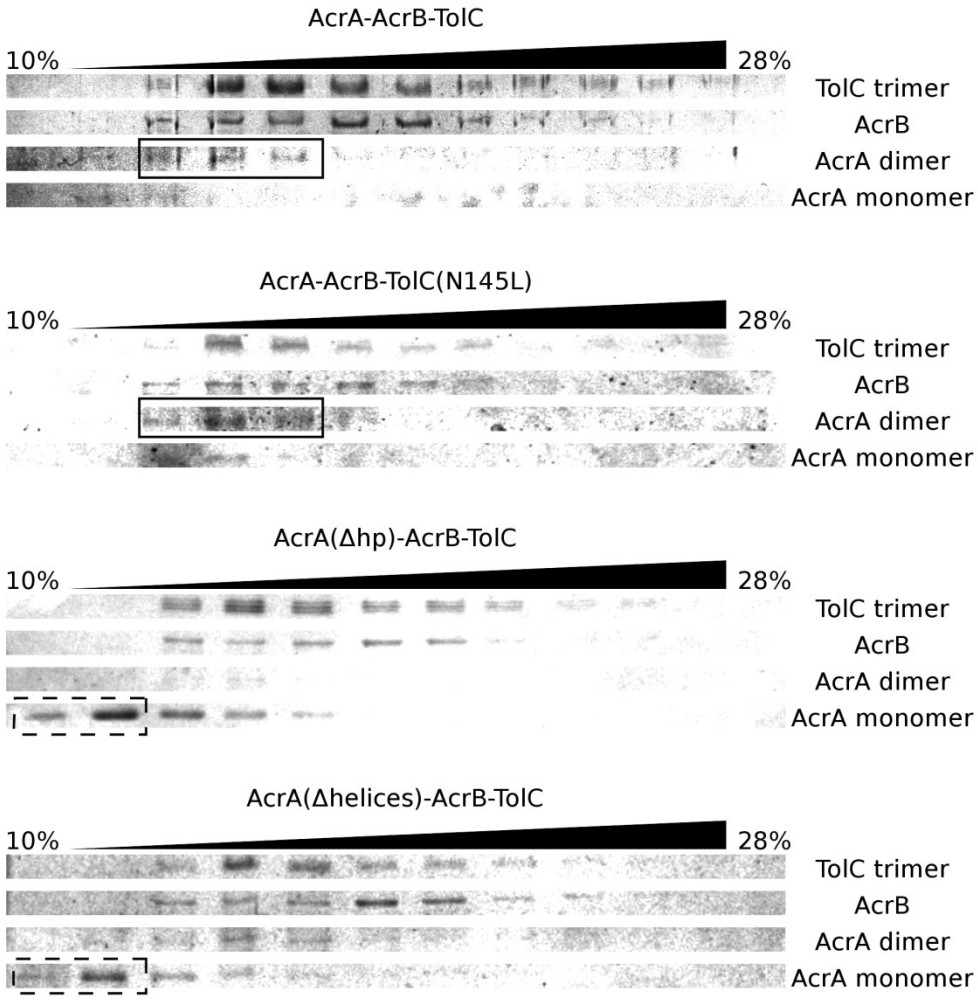

Figure 6:1 - Coomassie staining of glycerol fractions to determine interaction of proteins

After ultracentrifugation on a glycerol gradient, proteins which interact are present in the same glycerol fraction, and therefore appear within the same column on the gel image following SDS-PAGE. Solid boxes indicate where AcrA is found in the same glycerol fraction as AcrB and TolC, while dashed boxes indicate where AcrA has not localised with the other proteins.

Discussion

Glycerol gradients represent a simple yet effective means of testing for protein-protein interactions, provided proteins of interest have different buoyancy. The use of *in vitro* techniques was time-limited in this study, by virtue of being part of a research visit, and therefore have not been utilised to their maximum. The time limitations also meant that vital controls – such as omission of TolC in the analysis of AcrA variants and omission of AcrB when testing TolC variants, were not included. It is also responsible for only having tested very few of the mutant proteins that were expressed. This work needs to be continued and expanded in order to determine whether or not the mutations included in this thesis cause loss of TolC-AcrA interaction, or if there is a different reason for the phenotypes observed using *in vivo* analyses. Alternatively, qualitative approaches such as surface plasmon resonance or thermophoresis could be used to analyse the interactions between each of the components when introducing mutant protein. Either of these approaches would allow binding affinities to be calculated, which would be more persuasive evidence than the binary detail obtained from glycerol gradients.

In both the complete wild-type combination and in the combination with TolC(N145L), AcrA is present in the same fraction as both of the other partner proteins. Without testing potential bipartite combinations (AcrA-TolC, AcrA-AcrB and AcrB-TolC), it is not possible to determine whether or not the TolC(N145L) mutant is deficient or proficient in binding either or both of its partner proteins, although *in vivo* results indicate that this mutation only affects the MIC of nalidixic acid and the growth rate in the presence of novobiocin, and therefore it is likely that the entire complex forms normally in the presence of other substrates. Why any particular substrate would affect binding or functionality of this point mutant is unclear.

From this experiment, it appears that neither of the hairpin mutants can effectively bind to TolC or AcrB. However, it is unclear whether this is due to their decrease propensity to form dimers or because of an otherwise decreased affinity for the partner proteins. The laboratory of Helen Zgurskaya has previously reported that AcrA dimers bind AcrB with greater affinity than do AcrA monomers (Tikhonova *et al.*, 2011). As there is a small amount of dimeric AcrA(Δhelices) protein present in the higher glycerol concentration fraction, with TolC and AcrB, it is unclear whether the interaction that causes this mutant AcrA protein to co-fractionate with its partner proteins. It is possible that either the mutant AcrA shows lesser propensity to form dimers, and therefore has decreased affinity towards AcrB, or if the hairpin is required for TolC interaction, or if both are partially true.

CHAPTER 7: DISCUSSION

The overall aim of this project was to determine the interface between MFPs and OMCs in tripartite multidrug efflux complexes. A series of computational approaches were used in combination with available literature to determine a library of mutations to make in *tolC* and *acrA*. Mutations were designed with the hypothesis that they would affect either TolC channel closure or the TolC-AcrA interaction. The logic and hypotheses for each individual mutation are discussed within the preparatory work section (Sections 3.3 and 3.5). These mutations were subsequently assessed by a variety of *in vivo* techniques, and a research visit to the laboratory of Dr Martin Picard allowed preliminary assessment of the mutations using *in vitro* techniques.

During these studies, the immediate field of multidrug efflux pump assembly progressed rapidly. Whilst some of the publications were reacted to in preparation of experiments for this thesis, important papers were also published too late during this study to take into consideration for experimental design. Despite the advances made in the last four years, the study presented here makes use of a wider range of techniques to assess the importance of individual residues on both the function of the pump as a whole and the inter-component interactions. Each of the experimental approaches used here provide slightly different insight as to the effect of the introduced mutations, and therefore this study represents the most thorough investigation of a set of efflux assembly component point mutations.

7.1 Limitations to general experimental designs in this study

Using a site-directed mutagenic approach in this study, there were two general options for expression of the mutated genes for *in vivo* studies: make site-directed mutations on the chromosome, or utilise a plasmid-borne expression system. Each of these options has its own advantages and limitations. Use of chromosomal

mutagenesis allows expression of the single-copy gene under control of its own native promoter and in its normal genetic context, although in the case of multidrug efflux pump components, this will mean that expression is upregulated as concentration of toxic substances increases, which could affect gene regulation in the case of a mutation decreasing efflux function. However, genome editing requires several processes, each of which can be slow and, in some cases, unreliable. Once the mutagenic process is completed, it is advisable to sequence the whole genome of the newly-created strain, to ensure that no recombination took place at other positions on the chromosome. Chromosomal mutagenesis can therefore be a slow and expensive process. In contrast, mutagenesis on a plasmid requires only PCR, transformation, extraction and sequencing of the plasmid, and the mutated plasmid can then be transformed to any desired strain. For reasons of practicality, the use of a plasmid-based expression system was chosen, despite the biological benefits to mutagenesis of the chromosome.

A variety of expression systems are available on plasmids, each of which is suitable for different purposes. Several studies investigating MFP-OMC function have used the T7 expression system in the pET series of plasmids. However, as the T7 promoter causes very high levels of gene expression with minimal induction of T7 RNA polymerase expression (Hattab *et al.*, 2015), and sufficient protein expression for structural studies (2 mg protein per g of wet cellular weight) even without induction (Walse *et al.*, 2008), this was deemed unsuitable for *in vivo* investigations. Other common inducible gene regulation systems present on vectors include the *lac* and P_{BAD} systems, but both of these are known to be titratable only at the culture level; at the cellular level, these systems are "all-or-nothing", whereby the system is either completely repressed or completely activated (Novick & Weiner, 1957; Morgan-Kiss *et al.*, 2002). Therefore, the tetracycline promoter was chosen for use in this study, as it has not been reported as "all-or-nothing" at the cellular level, and despite showing

basal expression in the absence of induction, expression from this promoter should be titratable and therefore can be controlled to ensure approximately equal levels of expression between mutants (Whetstine *et al.*, 2009). Anhydrotetracycline is a derivative of tetracycline that displays no antibacterial activity but does induce expression from the tetracycline promoter. Although long known to impact metabolism of *E. coli* (Silverman & Atherly, 1978), this is not an issue at the concentrations used in this study (as shown in Section 5.1). It is currently unclear as to whether or not anhydrotetracycline is an efflux substrate of AcrB, as is tetracycline (de Cristobal *et al.*, 2006). If anhydrotetracycline is a substrate of the efflux complex, then it will theoretically be removed from the cell at a lower rate in cells with a mutation that decreases efflux activity, thus allowing higher expression of the inactive or partially-active protein. In such a situation, minor defects in the efflux complex may be hidden by an increased expression level, as the extra complexes compensate for the decreased efficiency of each individual complex.

Having chosen to use the tetracycline promoter for expression of the mutated proteins during *in vivo* assays, it was necessary to determine the concentration of inducer to use for these assays. As detailed in Section 4.1, this was done by means of MIC testing to erythromycin and novobiocin at a variety of 10-fold dilutions of anhydrotetracycline. This showed that anhydrotetracycline should be omitted entirely or used at 2 $ng.ml^{-1}$ to give comparable results between the wild-type strain, expressing *tolC* from the chromosome, and the complemented strain expressing *tolC* from the pASK plasmid. Ideally a quantitative reverse-transcriptase PCR (q-PCR) approach would be used to determine the relative *tolC* transcript levels in each of these strains at a variety of anhydrotetracycline concentrations. This would give direct detail about the effect of anhydrotetracycline on promoter activity, rather than using a phenotype to indirectly derive this information. However, as the *in vivo* experiments used in this study primarily compared the knockout, complement, and

plasmid-encoded mutants, the absolute expression level should not be a major factor in the results, provided that there is sufficient protein expressed in each (except for the knockout) strain.

7.2 A range of assay types is essential in studies of this type

A significant proportion of papers detailing the effects of mutating efflux pump components use only a single susceptibility assay to determine functionality – usually either MIC or zone of inhibition studies. As the results in this thesis show, a mutation can give different results depending on the assay used, and even the parameters analysed within an assay. For example, the TolC N332L mutation appeared to have no effect in MIC assays, but shows a substrate-specific effect in growth kinetics and may show reduced efflux activity in dye efflux assays. Use of only a single assay type would therefore have led to this mutation being dismissed as having no effect which is not true, mainly because the effect is small. In particular, alternatives to MIC assays should be sought for similar projects, as these assays are designed only to attribute a "resistant" or "susceptible" phenotype to a strain – within two consecutive growth incubation periods (a total of 24 h for *E. coli*), they are capable of ascertaining whether or not therapeutic treatment with a particular drug is likely to be effective against a particular strain. Therefore, whilst MIC assays are of undoubted potential within the diagnostic environment, they are insufficiently sensitive for use in determining potentially small differences between mutations.

It appears to be of equal importance to consider viable *in vivo* assays, as these report more accurately upon the natural state of the proteins than do *in vitro* assays which use artificial environments, and *in vitro* assays, which separate efflux activity from other possible contributing effects on the entire cell that are not present in isolated systems. *In vitro* assays therefore have a key advantage in that they are sensitive only

to the changes upon the system under investigation. Any defects that are compensated within the cell will not be compensated *in vitro*, thereby allowing greater focus of interpretation of results. However, it is not known what contribution to efflux pump activity other cellular components may have, such as peptidoglycan, or the exact composition of the periplasmic fluid. Use of artificial buffers may therefore force proteins into unnatural interactions, a possible explanation for the apparent MacA-MacA tip-to-tip interaction which is not in itself discussed as a possible physiologically relevant configuration, although 20% of AcrA is found associated with the outer membrane even in the absence of a cognate OMC (Tikhonova & Zgurskaya, 2004).

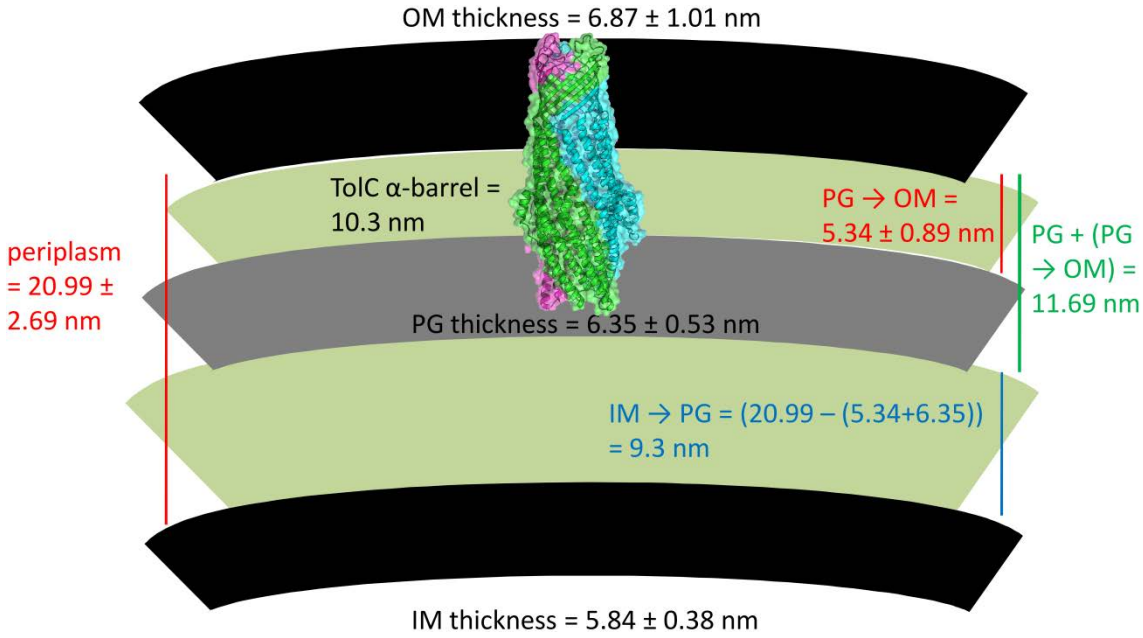

Figure 7:1 - Peptidoglycan surrounds the periplasmic tip of TolC.
Thicknesses and distances between the major components of the cell envelope are shown to scale based on measurements by Matias *et al.* (2003), with TolC shown also to scale. Based upon the distance between the peptidoglycan (PG) and outer membrane (OM), TolC must insert approximately 5 nm into the PG layer.

Peptidoglycan is usually ignored in the study of Gram-negative bacterial multidrug efflux pumps, although drawing of the measured inter-membrane distances, membrane to peptidoglycan distances and thicknesses of each of these structures, and superimposition of TolC in the outer membrane of this drawing, indicates that the coiled-coil domain of TolC (the periplasmic tip and the α-helical barrel up to the equatorial domain) should lie embedded within the peptidoglycan, as shown in Figure 7:1. Only one paper has reported any interaction between peptidoglycan and either TolC or AcrA, indicating that both proteins have an intrinsic affinity for peptidoglycan which is increased by the partner protein (Xu *et al.*, 2012). The role of peptidoglycan in the MFP-OMC interaction is entirely unknown, though it is possible that it assists in maintaining TolC and AcrAB in close proximity or affects the interaction between the components of the assembly. AcrB has been shown to form distinct foci in the presence of TolC but to be mobile within the membrane in the absence of TolC (Yamamoto *et al.*, 2016). It is unclear whether this is entirely due to the lower fluidity of the outer membrane or if the complex is trapped in place by its penetration of the peptidoglycan matrix. If the latter is true, then it is entirely plausible that the local environment of the AcrA-TolC interaction is heavily influenced by the presence of the peptidoglycan, which is omitted from *in vitro* studies.

Whilst structural studies are capable of providing convincing data, and indeed are vital for informing wider studies – this study would have been very different if structures of the components were not available – they are subject to the above limitations of *in vitro* studies. Unfortunately, they are also currently only capable of providing a snapshot view of the assembly, which does not give any indication as to the other stages of a dynamic process. The latest structural studies of multidrug efflux pumps, which show complete complex assembly, provide strong evidence that the tip-to-tip model is accurate, as redefined based upon the data provided by such

structural studies. The caveat, however, is that the accuracy is restricted to a single step within the dynamic process. Given that the complex is de-energised in these structural studies, the step represented by the structural studies is presumably the step at which energy is required for further progression.

7.3 AcrA and TolC mutations can have a substrate-specific effect

Some of the mutations in this study show a substrate-specific effect, particularly the TolC N145L and K383D and AcrA S139G mutations. The most simple explanation for this is that the mutations alter the substrate-exposed surface, which may be the case for N145L (in either model of interaction) and S139G in the tip-to-tip model, but is certainly not the case for K383D, which is on the external face of H8 and faces the periplasm. If the MFP is involved in selection and loading of the substrate to the transporter (Bagai *et al.*, 2008; De Angelis *et al.*, 2010; Mealman *et al.*, 2012), then mutation on the MFP could alter the efflux profile of the complex in a similar fashion to mutation of the transporter binding pockets (Blair *et al.*, 2015). Given the location on the structure of the AcrA S139G mutation, it is unclear how substrate selection could be affected by this mutation, and it is even less clear how TolC mutations would have this effect unless they induce conformational changes in AcrA that indirectly alter substrate specificity.

This is particularly important when comparing data between studies. For example, the AcrA S139D mutation has previously been reported to abolish function, based only on resistance to erythromycin and novobiocin (Kim *et al.*, 2010). Although the mutation made for this thesis essentially removed the side chain from this position, the substrate-specific effect of this mutation indicate that previous studies may make significant conclusions from insufficient evidence. The hydroxyl group of AcrA residue S139 has been proposed to form hydrogen bonds with either the side chain

of TolC T366 or the backbone of TolC G147 (Jeong *et al.*, 2016; Wang *et al.*, 2017). If this position is part of such a limited interface, and causes disruption of that interface, then loss of function should be observed with all substrates, and not only a subset of them. This aspect of the results is therefore incompatible with a purely tip-to-tip interaction between AcrA and TolC.

Naturally substrate-specific MFP-OMC interactions have been observed, notably for MexJ (Chuanchuen *et al.*, 2002). The MexJK MFP and pump utilises either OprM or OpmH in a substrate-specific manner (Chuanchuen *et al.*, 2005). Substrate-specific effects of mutations on either the MFP or OMC should therefore not be completely surprising: had this study been done using MexJK-OprM and MexJK-OpmH rather than AcrAB-TolC, then certain mutations may make one channel more like the other, and alter the channel utilisation in a substrate-specific manner. Whilst it is unclear how the substrate determines which channel protein is used, it now appears that substrate-specific selection of a channel protein by an MFP is altered even by mutation of single residues.

7.4 The choice of mutation at a position affects the change in phenotype

Two positions on TolC were mutated to two different residues: Q352 (to both alanine and glutamate) and K383 (to both aspartate and glutamate). The results for mutations at these positions indicate the importance of the choice of mutation in a study such as this: Q352A showed a decreased MIC to vancomycin, which was not seen in Q352E, while K383D showed increased susceptibility to a variety of substrates, even though K383E appeared wild-type. Combined with the above factor of substrate-specific effects of mutations, this further indicates the robustness required in studies of this type – mutation to a single alternative amino acid may not provide sufficient evidence of the significance of a position; conversely, one mutation

at a position that causes a phenotypic difference may be over-interpreted and make the position seem more important for a certain aspect of the protein's function than what it really is. This is particularly evident with the difference between K838D and K383E, which both involve the same reversal of charge and differ only by a single CH_2 group in the chain length. Such a minor difference in the mutation was not expected to have such a difference on functional impact.

7.5 The helices of the AcrA hairpin are essential for interaction with TolC

Upon deletion of the AcrA hairpin helices, either alone or with replacement of the tip as well, efflux function is completely abolished (Sections 5.1, 5.2 and 5.3). This loss of function appears to be due to loss of interaction with TolC (Section 6.1). This could be expected *in vivo* in either interaction model. In the helical bundling model, these helices are clearly required for the interaction with TolC, while in the tip-to-tip model they are required to bridge the distance between AcrB and TolC. However, even when any spatial requirements of the periplasm (such as the inter-membrane distance) are not present in the experiment due to use of BAPol, the interaction is lost. This suggests that the tip alone (as is present in the Δhelices mutant) is insufficient to recruit TolC, otherwise AcrA(Δhelices) should be able to maintain the TolC interaction but without substantial spatial separation between TolC and AcrB. The logical conclusion from this is that the helices of the MFP hairpin are required for direct interaction with the helices of the OMC, as was believed to be the case before the MacA structure was solved (Akama *et al.*, 2004; Fernandez-Recio *et al.*, 2004; Higgins *et al.*, 2004a). Such a conclusion is supported by evidence in the literature that the entire AcrA hairpin is in close proximity (7 Å) of TolC, and that positions even as high up the α-barrel of TolC as the equatorial domain are with the same close proximity to AcrA (Lobedanz *et al.*, 2007). It is also supported by the periplasmic tip

of TolC seemingly only being required for flexibility – to enable opening and closing of the channel – and not for interaction with any specific part of AcrA, as determined by mutagenesis and analysis of reversion mutants (Weeks *et al.*, 2010).

The results here are therefore incompatible with the electron microscopy data published in the past few years (Du *et al.*, 2014; Daury *et al.*, 2016; Jeong *et al.*, 2016), which suggest that the helices are required only to form a conduit continuous with that of TolC. Although it is possible that the artificial conditions used in structural studies force unnatural configurations of the complex to form, it seems unlikely that data from such approaches are never true *in vivo*, and therefore are probably correct at some stage of complex assembly.

7.6 The AcrA hairpin tip is essential for closing of the TolC channel

Based upon the kinetics of growth in the presence of vancomycin, it appears that any *acrA* mutant lacking a natural hairpin tip sequence grows more slowly than those that have the natural hairpin tip sequence. Furthermore, the hairpin structure itself is not required for the phenotype to match that of the wild-type. This suggests that AcrA is as essential in closing of TolC as it is in efflux of substrates, and that this function is achieved by the hairpin tip. Although this is inconsistent with previously published data regarding the opening and closing of channel proteins by MFPs, it must be remembered that these results are based upon relatively small changes in growth kinetics. This study is therefore more sensitive to differences between mutants than previous studies, which assessed susceptibility by the less sensitive MIC and disc diffusion assays.

This putative function of the hairpin tip could partly explain why the TolC tip mutants YFRS and YFRE were more susceptible to vancomycin in the previous studies. Although these mutations on TolC cause partial channel opening, based on the

crystal structures, the aperture remains too narrow for vancomycin to pass, shown in Figure 7:2. Without further opening, presumably induced by binding of a partner protein, it is therefore unclear how vancomycin uses the channel partially dilated by mutation to gain access to the cell. The vancomycin susceptibility of the partially-opened mutant TolC had been tested in an *acrA* knockout, but it is possible that expression of other MFPs present in the cell, particularly AcrE, caused additional dilation of the channel. In such a scenario, it is reasonable to expect that the mutation of the TolC tips may prevent MFP-induced closing of the channel for the same reason as the AcrA(GS-tip) and AcrA(Δhairpin) mutants were unable to close the wild-type TolC: a tip-to-tip interaction is required for closing of the channel.

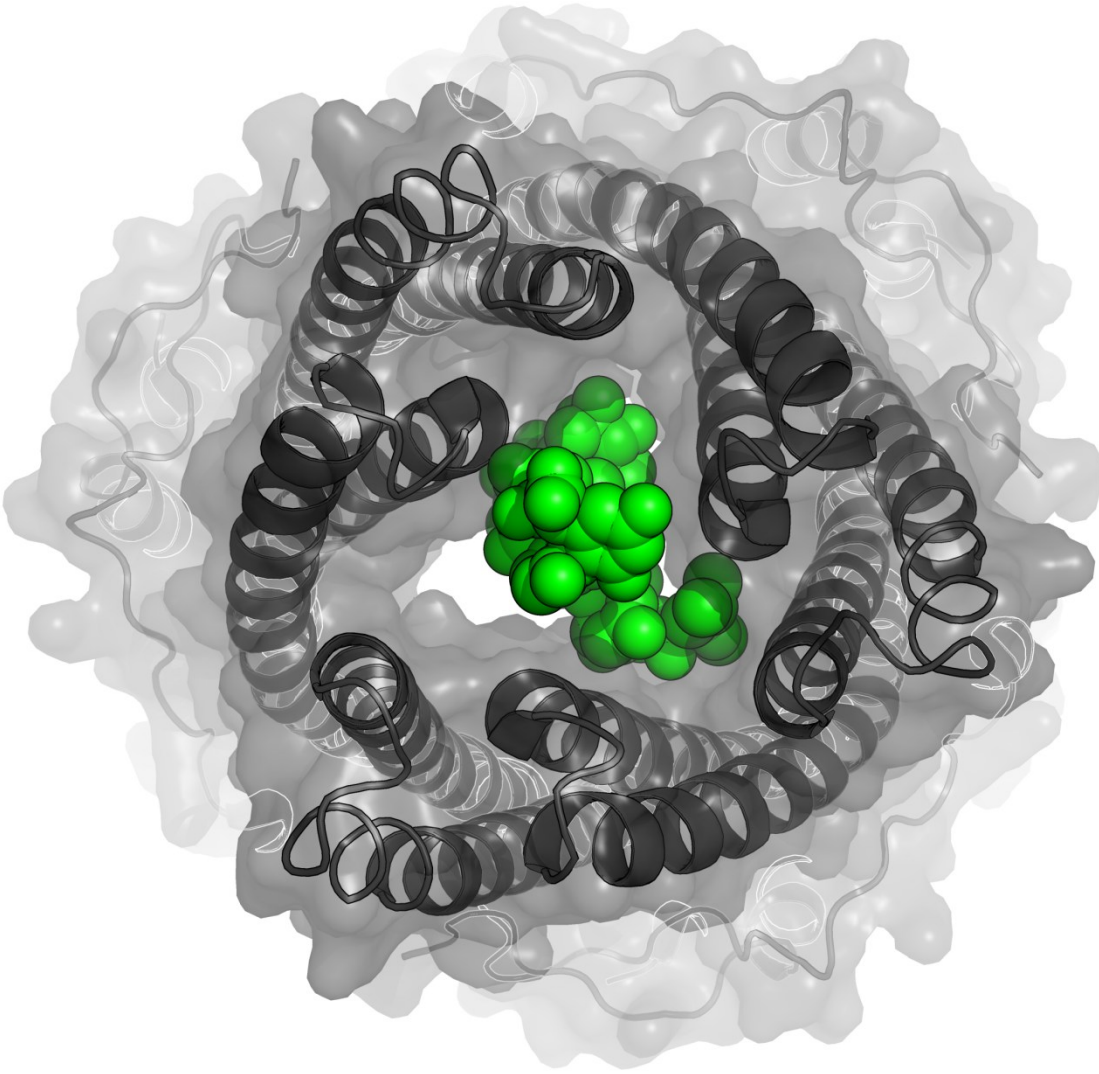

Figure 7:2 - Vancomycin is larger than the mutationally-opened TolC aperture. When docked into the crystal structure of a TolC protein that has been partially dilated by mutation (2XMN; grey), vancomycin (1SHO; green) is larger than the aperture.

In the Δhelices mutant, the hairpin structure is shortened to just 15 Å, with the loop that forms the hairpin tip brought closer to the lipoyl domain by approximately 33 Ångstroms. The dimensions of this mutated hairpin are incompatible with the helical bundling model of interaction, but a tip-to-tip type interaction remains possible, as shown in Figure 7:3. When combined with available structural data of the entire complex, which as discussed in Section 7.2 is de-energised, and also combined with data indicating that energy is required for dissociation of the complex, this leads to the conclusion that the tip-to-tip model represents a stage of the dynamic process at which the channel is closing. The implication of this is that the sequence similarity between hairpin tips of MFPs with unique partners is due to a conserved mechanism of closing the channel aperture and dismantling the complex, but not for the MFP-OMC interaction. This is also compatible with the results from Consurf, which indicate that the OMC tip regions are generally very well conserved between species, while the mid-section of the coiled-coil domain below the equatorial domain is less well conserved, as shown in Figure 7:4. A new hypothesis is therefore presented based on the results here and the available literature: the tip-to-tip model of interaction represents a pre-dissociation state, regardless of whether an efflux event has occurred or not.

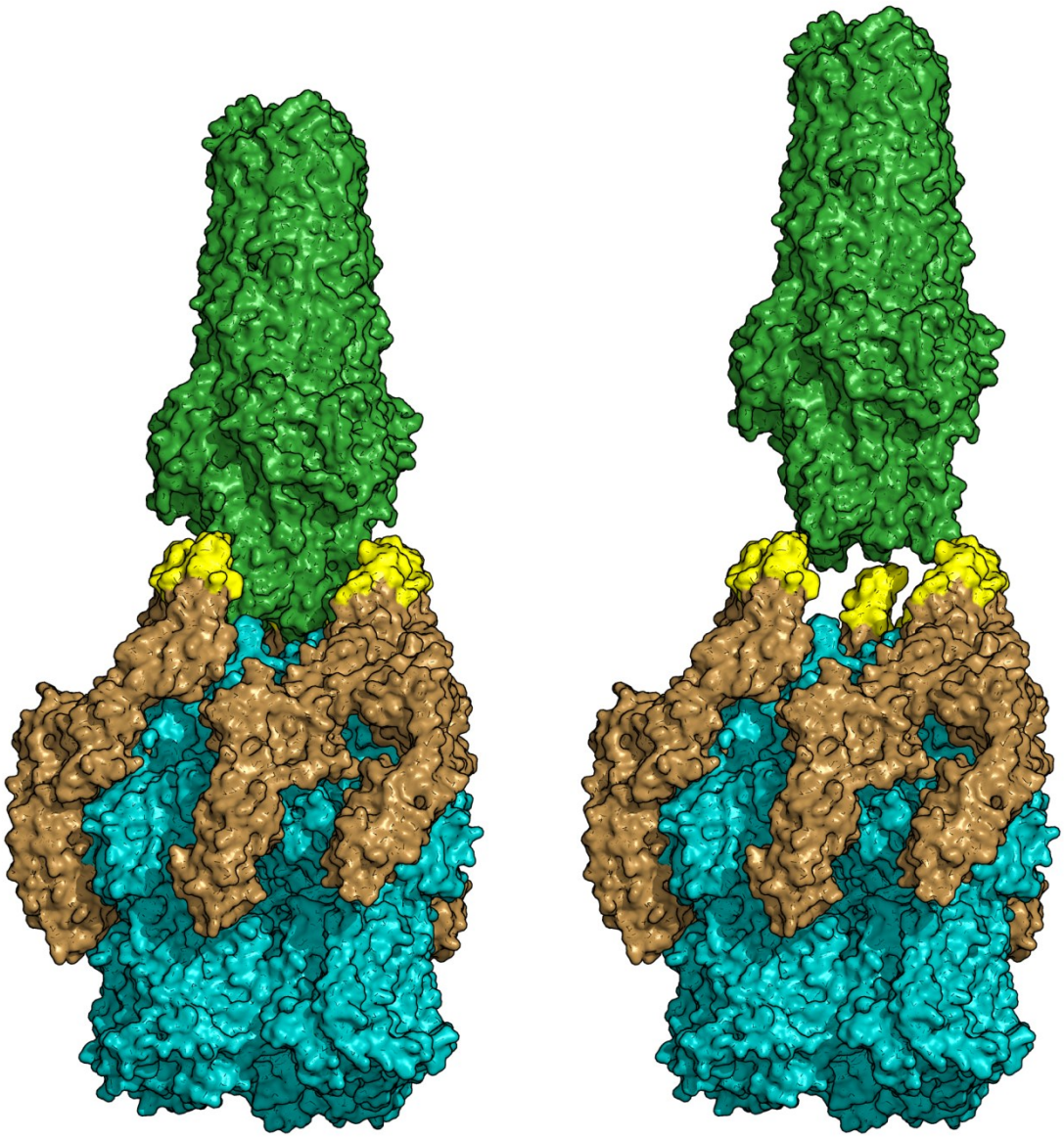

Figure 7:3 - Potential interactions of AcrA(Δhelices) mutant.
The AcrA(Δhelices) mutant, shown in brown with the relocated hairpin tip in yellow, is likely only conducive to a tip-to-tip interaction with TolC (green). In a subtle change, a direct TolC-AcrB (blue) interaction would probably cause incompatibility between the hairpin tip and the lower part of the TolC channel (left), while abolition of the TolC-AcrB interaction would allow a shortened form of the prototypical tip-to-tip interaction (right).

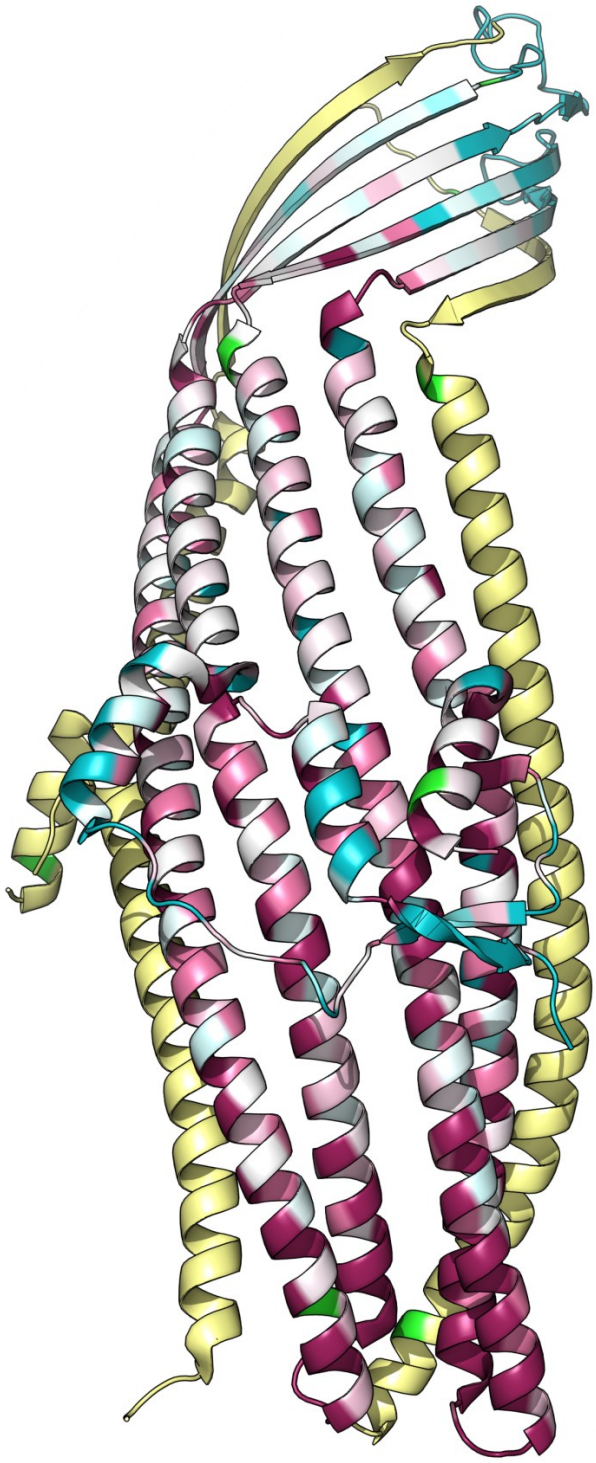

Figure 7:4 - Consurf results for TolC indicating conserved regions.
Using the 1EK9 structure as the query, the Consurf results are mapped directly onto the same structure, to a single protomer. In pale yellow are adjacent helices of the other protomers. Each position is coloured on a scale from blue through white to purple, with blue being hypervariable, white being semi-variable and purple being most conserved. Positions in green are those lacking sufficient data in the alignment to calculate a conservation score.

7.7 An AcrA tip mutant shows a dominant effect over the wild-type protein

Preliminary data (Section 5.1) indicate that when the *acrA*$^{+}$ WT strain is transformed with the pASK-*acrA(GS-tip)B* plasmid, and thus is expected to express both WT and mutant AcrA, the strain becomes more susceptible to novobiocin. This is explained by the dominant phenotype of the GS-tip mutation. There are three likely explanations for the observed effect.

The first explanation involves formation of AcrA-AcrA(GS-tip) heterodimers, in which the mutant protein prevents the WT protein from functioning normally. However, the knockout strain expressing only the GS-tip variant is more like the knockout strain with empty vector, with a more severe phenotype than in the strain expressing both genes. Given that expression from the plasmid was shown to be higher than from the chromosome (if the wild-type and the complemented strains are compared in Section 5.4), it is reasonable to expect that there would be an excess of the GS-tip variant over the wild-type, and that therefore very little, if any, wild-type homodimeric AcrA would be able to form, and therefore that the phenotype of the strain expressing both variants in this way should be more like the knockout than the wild-type, which was not the case. It is therefore unlikely that this explanation alone is capable of explaining the observed results.

The second explanation is that the mutant is capable of binding to TolC, but is non-functional because it is unable to dissociate from or close the TolC channel, thus allowing a greater rate of drug influx. This is consistent with the apparent requirement of the AcrA hairpin tip in closing but not opening of the TolC channel as indicated in this study. It would also remove a proportion of the TolC channel protein from circulation for use by the wild-type AcrA protein. Such effective decrease of the available TolC protein would decrease the likelihood of complete wild-type complexes forming. Given the increased abundance of the mutant compared to wild-

type protein, one might expect that sequestering of the TolC channel would give rise to a severe phenotype, but it has previously been shown that TolC abundance as low as 10% that of the BW25113 strain is sufficient to provide resistance at wild-type levels (Krishnamoorthy *et al.*, 2013). However, the results in that paper were based on MIC testing, which only provide very limited information, as this thesis indicates. It would therefore be interesting to see if the growth kinetics of a strain with TolC levels at only 10% would be impacted, even though the effective MIC is not. This explanation could therefore a possibility, especially if there is also some contribution from the first explanation, which would mean that both TolC and AcrA are sequestered by the AcrA(GS-tip) protein.

The third explanation is that the mutation causes effects in the membrane that are not TolC dependent. This could be due to either AcrA interaction with the outer membrane in a TolC-independent manner (Tikhonova & Zgurskaya, 2004), or differences in wider gene expression caused by differences in transcript levels of RND components (Webber *et al.*, 2009; Buckner *et al.*, 2016; Wang-Kan *et al.*, 2017). From the available data, it is impossible to say whether these are likely effects or not, although a comparative transcriptomics approach could provide some insight as to the likelihood of the latter of these possibilities.

To test each of the first two explanations, surface plasmon resonance or thermophoresis should be performed, to determine relative binding affinities in TolC-AcrA(WT), TolC-AcrA(GS-tip), AcrA(WT)-AcrA(WT) and AcrA(WT)-AcrA(GS-tip). This would indicate whether either of the interactions are impacted by mutation of the MFP tip, as has been reported in the ABC-type efflux pump DevBCA-HgdD from a species of *Anabaena* (Staron *et al.*, 2014).

If either of the first two of the above explanations, or a combination of both of them, are correct, then there may be some potential to use a truncated hairpin peptide

with the GS-tip sequence in a therapeutic approach. It is not at all clear how much of the hairpin is required in interaction with TolC, but the sequence of the mutation, GSGGSG, is 6 amino acids, thus allowing only up to 25 amino acids contributing to helices if the 31 amino acid limit for biotin-facilitated is conformed to (Walker & Altman, 2005). This makes it unlikely, though not impossible, that the dominant peptide could be provided externally.

7.8 Loss of the lower ion-selectivity ring of TolC is detrimental to the cell

The aspartate residues at TolC positions 371 and 374 form two rings of negative charge, which act as a cation trap and form the region of smallest diameter in the TolC lumen (Andersen *et al.*, 2002c). The lower of these, D371, may be involved in stabilising the open state of TolC upon rearrangement of the ionic network at the periplasmic tip of TolC, namely by forming a new interaction with R367. This may partially explain why the R367A mutation causes hypersusceptibility to efflux substrates (Augustus *et al.*, 2004), even though removal of the position charge at this position does not on its own cause constitutive dilation of the TolC channel (Pei *et al.*, 2011).

Previous mutation of these aspartate rings was to alanine, which will not protrude very far into the TolC lumen and therefore contributes little to the overall electrophysical profile of the face of the lumen. Mutation of D371 to alanine was reported not to impact upon either deoxycholic acid resistance nor haemolysin export (Andersen *et al.*, 2002c). Meanwhile, the mutation to valine, as done for this thesis, introduces a new hydrophobic ring at the narrowest part of the channel. This mutation was predicted to cause electrostatic incompatibility of the charge and H-bond network at the periplasmic tip, the new hydrophobic ring, and the existing negatively charged D374 ring one helical turn higher in the TolC lumen. Such

electrostatic incompatibility was expected to cause the tip to force apart, leading to a constitutively open TolC channel. However, from the data presented here, it appears that the introduced hydrophobic ring locks the aperture in the closed conformation, as the valine sidechains have no compatible hydrophobic environments into which to move upon channel opening. Flow cytometry data indicate that this increased energy barrier to TolC is overcome in a proportion of the cells, as the population is split between apparently efflux active and apparently efflux deficient cells. The lower fluorescence of the apparently efflux active population cannot be explained through decreased dye influx alone, as the knockout strain does not show the same split. Unfortunately, this strain grows slower than the wild-type strain even in the absence of antibiotic, and therefore growth kinetic data are not comparable for this strain. The normalised dye efflux results indicate that D371V mutant is entirely deficient in efflux activity of Nile Red, which does not match the likely ethidium bromide efflux profile as suggested by flow cytometry data. As Nile Red adsorbs to hydrophobic surfaces, and is fluorescent in hydrophobic environments, it may be that Nile Red is trapped by the valine ring in the same way as large cations are trapped by the aspartate ring, thereby inhibiting its own efflux. Although the fluorescence assays presented in this thesis suggest that there is a significant decrease in function, the OprN channel from *Pseudomonas aeruginosa* contains valine at this equivalent position (Yonehara *et al.*, 2016), and with MexEF forms a functional efflux pump capable of providing resistance against several substrates, both hydrophilic and hydrophobic(Maseda *et al.*, 2000). It therefore seems unlikely that a hydrophobic valine ring at position 371 introduces a hydrophobic barrier or trap.

The overall effect of the D371V mutant on the cell is very clearly not simply a result of loss of TolC function. Deletion of *tolC* is well tolerated in laboratory conditions, while the D371V mutation is not. Therefore, there is either a difference in

compensatory changes made in response to loss of functional TolC, as are made in a *tolC* knockout (Webber *et al.*, 2009),or the mutation causes the protein to be inherently detrimental to the cell. Given that the same detrimental effect is not seen in other efflux-deficient *tolC* point mutants, such as S350F, the differential gene expression hypothesis is unlikely, although it could be tested by comparative transcriptomics (RNA-seq). It would be interesting to perform a comparative metabolomics analysis of the wild-type, knockout and D371V point mutant, to determine what causes the growth deficiency. It is likely that the protein is incapable of fulfilling its normal role in removal of toxic metabolic products (Ruiz & Levy, 2014), a task presumably fulfilled by other proteins in the knockout (Rosner & Martin, 2009). This mutation also requires further analysis using *in vitro* techniques such as proteoliposome assays, to determine the effect on actual efflux activity.

During mutagenesis, multiple attempts were made to generate a D371V/D374V double mutant. Several candidate plasmid preps were sequenced, and all of them contained secondary mutations within the PCR priming site. Unless the primers used for the double mutation were of very poor quality, these secondary mutations were not encoded within the primers – each sample sequenced contained different mutations. Initially, it was assumed that the sequence for the double mutant contained too much repeat sequence, which can result in errors during amplification, either during PCR or *in vivo* following transformation. However, the phenotype of the D371V single mutant led to consideration that the D371V/D374V double mutation could cause a more severe phenotype, even from background expression in the absence of the inducer, and that the secondary mutations, most of which were frameshift and result in a truncated protein, were required for the survival of the bacterial cells by preventing incorporation of the double mutant into the outer membrane. Testing of this hypothesis would require use of an expression system with lower background expression than from the tetracycline promoter.

7.9 TolC S350F mutant loss-of-function is not caused by low protein levels

The laboratory of Rajeev Misra have previously reported conflicting information about the TolC S350F mutation: the mutant protein is "surprisingly impervious to degradation" (Werner *et al.*, 2003), and yet the same mutation "resulted in somewhat reduced protein levels" (Augustus *et al.*, 2004). The figures associated with the statements did not indicate particularly low protein levels, although the Western blot shown in this thesis (Section 4.5) indicate that in this particular study, the S350F mutant is present in the membrane fraction at approximately the same level as the wild-type protein expressed from the same vector. Not only is a slight decrease in TolC expression unlikely to lead to the apparent loss of function that was reported (Krishnamoorthy *et al.*, 2013), but the phenotype in the presence of vancomycin is also inconsistent with a decrease of TolC protein levels, both in this thesis and in the previous study (Augustus *et al.*, 2004). Although the mutation does not appear to cause a change in MIC to vancomycin, the growth kinetics profile of this mutant in the presence of vancomycin are distinct from those of the knockout and complemented strains. The S350F mutation causes an extended lag phase duration, and the stationary phase OD_{600} is decreased in this mutant in the presence of vancomycin, even though the maximum growth rate does not change, indicating that the mutation has a mild effect on vancomycin susceptibility.

Position 350 of TolC is on the external face of helix 7, with the side chain partially embedded in the space between this helix and H4 of the adjacent protomer. Mutation to phenylalanine was expected to either cause constitutive opening of the channel due to insertion of a bulky side chain between the helices, thus forcing a movement of H7 into the more open conformation, or to force a more closed conformation as one of the side chains of D162 or F350 is moved more towards the

channel lumen. The very mild effect on vancomycin susceptibility suggests that neither of these is likely to be entirely correct. The MFP-dependency of the vancomycin susceptibility of this mutation needs to be determined, probably using a proteoliposome approach to measure transfer of vancomycin through the channel. Based upon the lack of efflux activity and the very mild vancomycin susceptibility, the current hypothesis regarding this mutation is that it prevents normal closure of the channel by the MFP, which also prevents normal cycling of the pump activity.

7.10 Future experiments to consider

There is limited evidence that vancomycin gains entry to the cell through an open TolC channel, based upon vancomycin susceptibility of certain TolC point mutants beings similar to *hlyCABD*$^{+}$ cells (Augustus *et al.*, 2004). However, the TolC-dependence of the vancomycin susceptibility of haemolytic *E. coli* cells was not reported, and it is possible that both HlyCABD and point mutants of TolC independently compromise the structural integrity of the outer membrane. Another research group has used vancomycin as a general indicator of outer membrane disruption in knockout mutants, irrespective of a possible entry route through TolC (Morris, 2014). To determine the extent to which vancomycin gains entry via TolC, TolC-proteoliposomes could be prepared loaded with vancomycin (similar to how OMC-proteoliposomes are prepared loaded with RNA), and the leakage of vancomycin from the proteoliposome to the buffer analysed either by HPLC or by sensitivity screening against a Gram-positive (monodermic) bacterial strain. As there are multiple MFPs in the cell that might induce TolC opening *in vivo*, this proteoliposome approach could also be used to test the MFP-dependence of vancomycin movement through TolC and its mutants.

To determine the exact positions on TolC with which the AcrA hairpin tip interacts, the photoreactive synthetic amino acid benzoyl-phenylalanine could be introduced to the AcrA hairpin tip, ideally replacing each of Y129, Y137 and Y143, independently. Following light-activated cross-linking of the proteins, they would be purified (via a hexahistidine tag on AcrA) and analysed by mass spectrometry. Given that this would generate a fragment unknown within protein databases, the data would require manual analysis, which would be quite time consuming.

Having obtained preliminary data indicating that the AcrA(GS-tip) mutation is partially dominant when co-expressed with the wild-type protein, it would be useful to determine the effect of this mutation on utilisation of TolC by other MFPs. For example, when expressed in a haemolytic strain of *E. coli*, does the AcrA(GS-tip) mutation prevent haemolysin export? This would be tested by a simple haemolytic activity assay on blood agar. Such information could assist in determining what potential there may be for this mutated hairpin structure in therapeutic use.

It is not known from the experiments done so far whether the AcrA loss-of-function mutations are capable of forming dimers or oligomers. To give an indication as to the number of AcrA moieties bound to each other, 2D-PAGE could be used on purified AcrA and its mutants. If sufficiently diluted, it may be possible to determine self-association binding affinities through thermophoresis or surface plasmon resonance.

In light of the substrate-specific effect of some of the TolC mutations, and the available literature indicating that OMC selection by an MFP can be determined in a substrate-specific manner, it would good sense to determine if any of the TolC mutations gain function with non-cognate IMT/MFP pairs. Such an experiment would be similar to that reported by Bokma *et al.* (2006), except that the mutation is directed rather than random. It would also make good sense to test this cross-reactivity with a variety of potential substrates, given the substrate-specific effect of

some of the mutations. This could also be tested by a proteoliposome system, to eliminate possible pleiotropic effects.

CHAPTER 8: SYNTHESIS: A DYNAMIC MODEL OF COMPLEX ASSEMBLY

As alluded to in Sections 7.5 and 7.6, this particular study indicates that both the tip and the helical parts of the MFP hairpin are essential for normal efflux function. The hairpin tip is required for closing of the channel protein, and therefore probably also for dissociation of the complex, while the helices are required for stable interaction with the OMC during the efflux process. Neither part of the hairpin appears to be essential for dilating the aperture of the OMC.

A new dynamic model of interaction is therefore proposed based on the results from this study and consideration of the available literature. This new dynamic model, including some speculation as to the mechanisms, is detailed below; the key steps are:

1. A bipartite assembly of IMT-MFP or IMT-(closed)OMC forms.
2. (a) The third protein joins the complex, forming a tripartite complex conforming to a helical bundling model of interaction and (b) the channel is opened.
3. (a) An efflux event occurs, both passing the substrate directly to the lumen of the OMC and (b) inducing a second conformational change in the MFP.
4. The MFP moves towards a tip-to-tip model of interaction with the OMC.
5. In the tip-to-tip type interaction, the MFP closes the channel, with the substrate in the channel lumen.
6. The MFP dissociates from the OMC and returns to its resting conformation ready to recycle.

The interaction between MFP and IMT is prevented by the pre-formation of MFP-OMC bipartite complexes, but either MFP-IMT or IMT-OMC bipartite complexes can form as the initial step towards tripartite assembly, and the channel is closed during formation of the tripartite complex (Tikhonova *et al.*, 2011). For recycling of the complex, and to minimise unproductive cycling of the transporter upon its

interaction with the MFP (Verchère *et al.*, 2014), it is likely that the IMT-OMC bipartite complex is the most relevant for productive assembly (*STEP 1*). This would also allow monomeric or, more likely, dimeric MFP to wrap around the pre-formed IMT-OMC complex, avoiding the large conformational changes that would be required to allow a claw-like closing of the IMT-bound MFP around the OMC that would slide over the top of the IMT-MFP complex (Figure 8:1). It is unclear how any of the proposed mechanisms take place through the peptidoglycan layer. To avoid opening of the channel in the absence of either of the other components, it may be that opening is only induced upon binding of both partner proteins.

As the only place the IMT can bind the OMC is through interaction of the β-hairpins of the IMT with the periplasmic tip of the OMC, these proteins must interact in this manner, and so the MFP must interact with the OMC as in the helical bundling models, although the exact positions remain debatable (*STEP 2a*). Positions as high up the channel as N332 (a full 9 helical turns from the periplasmic tip) are involved in the interaction with the MFP, and are involved in the MFP-OMC interaction in a substrate-dependent manner. On TolC, D121 (7 helical turns from the periplasmic tip) is also involved in this interaction in a substrate-dependent manner, and mutation of this residue can switch MFP specificity of the channel in a single step. Due to these two positions being on different putative binding grooves – D121 is intra-protomer, while N332 is inter-protomer – it appears that during normal function both grooves are used, indicating a likely 3:6:3 stoichiometry of IMT:MFP:OMC under normal circumstances.

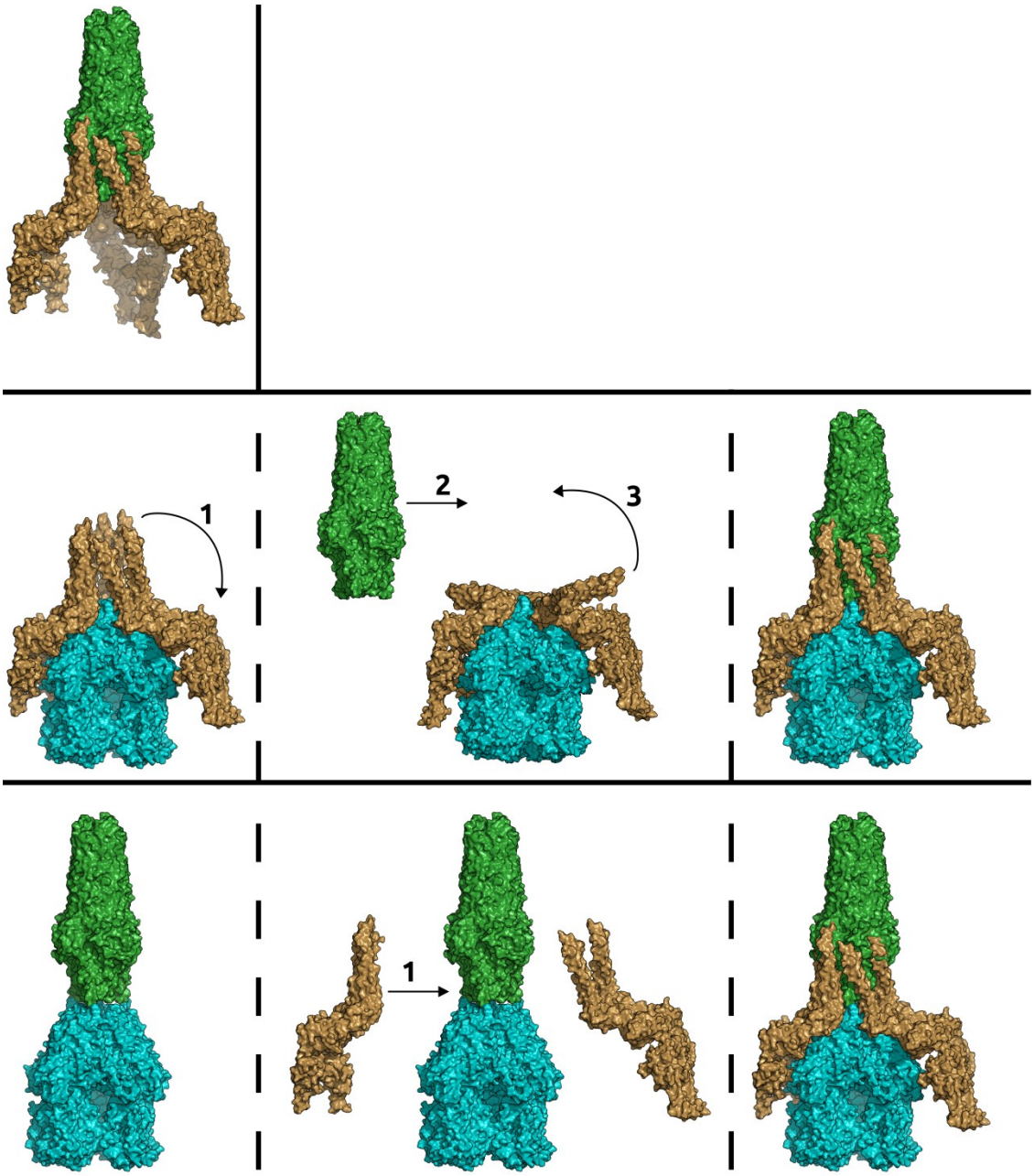

Figure 8:1 - Possible bipartite routes to forming a tripartite RND assembly. Top: If TolC (1EK9, green) and AcrA (2F1M, brown) form a bipartite complex, AcrB cannot be recruited, possibly because of the bipartite complex being membrane-bound at both ends. Middle: When AcrA binds AcrB (1IWG, blue), either the outer membrane must flex outwards to allow TolC to enter from above, or the AcrA hairpin must undergo a claw-like movement to open (1), allowing TolC to move onto the complex (2), and then reverse the initial claw-like opening to close around TolC. More likely (bottom), AcrB transiently recruits TolC, allowing AcrA to enter the complex without allosteric restrictions.

Upon binding of the MFP to the OMC as per the helical bundling model, the MFP and OMC each independently undergo a conformational change. The OMC moves into its open conformation in readiness for the efflux event, assisted also by its interaction with the IMT. Meanwhile, the MFP moves about its hinge regions into a conformation that would, on its own, be unable to bind the IMT, explaining the aforementioned observation that the MFP-OMC bipartite complex cannot bind the IMT (*STEP 2b*). Upon recruitment of the MFP to the complex, one of the transporter protomers transitions from its tight state to its open state, causing release of the substrate. As the substrate must traverse the docking domain of the transporter upon the conformational change of the transporter, the channel should have completed its own conformational change and be fully dilated by the time the substrate is free of the transporter. Therefore, the transporter is able to pass the substrate directly into the lumen of the channel, where there must presumably be a transient interaction between the OMC and the substrate, possibly also destabilising the interaction between the IMT and OMC (*STEP 3a*). The conformational change of the transporter (or, possibly, the destabilisation of the IMT-OMC interaction) induces a second conformational change in the MFP, causing the MFP to re-arrange its interaction with the OMC and transferring potential energy to the MFP (*STEP 3b*). Such re-arrangement essentially causes the OMC to slide away from the IMT and enter the tip-to-tip model of interaction (*STEP 4*). In this configuration, the complex presumably also causes a localised protrusion at the outer membrane, which logically would also lead a localised thinning of O-antigen around the channel exit, possibly facilitating faster exit of the substrate from the channel to the extracellular milieu.

From the tip-to-tip type interaction, the potential energy stored with the MFP is transferred to the OMC, overcoming the energy barriers required to close the channel back into its coiled-coil state (*STEP 5*). As part of the closing mechanism and in order to return to its resting state in which it is capable of binding to both partner

proteins, the MFP must also undergo a further conformational change to dissociate from the complex (*STEP 6*). In order to completely recycle the complex, there may be an intermediate MFP conformation at this step, which causes the MFP to dissociate from both the IMT and OMC – logically it would be once dissociated from both partner proteins that the MFP would return to its resting state.

CHAPTER 9: REFERENCES AND APPENDIX

9.1 References

Abdali, N., *et al.* (2017) Reviving antibiotics: Efflux pump inhibitors that interact with AcrA, a membrane fusion protein of the AcrAB-ToIC multidrug efflux pump. *ACS Infect.Dis.,* **3:** pp.89-98.

Abraham, E. & Chain, E. (1940) An enzyme from bacteria able to destroy penicillin. *Nature,* **146:** pp.837-837.

Abrams, A.J., Trees, D.L. and Nicholas, R.A. (2015) Complete genome sequences of three *Neisseria gonorrhoeae* laboratory reference strains, determined using PacBio single-molecule real-time technology. *Genome Announcements,* **3:**.

Addington, T.A., *et al.* (2013) JANUS: Prediction and ranking of mutations required for functional interconversion of enzymes. *J.Mol.Biol.,* **425:** pp.1378-1389.

Akama, H., *et al.* (2004) Crystal structure of the membrane fusion protein, MexA, of the multidrug transporter in *Pseudomonas aeruginosa. J.Biol.Chem.,* **279:** pp.25939-25942.

Andersen, C., Hughes, C. and Koronakis, V. (2002a) Electrophysiological behavior of the TolC channel-tunnel in planar lipid bilayers. *J.Membr.Biol.,* **185:** pp.83-92.

Andersen, C., *et al.* (2002b) Transition to the open state of the ToIC periplasmic tunnel entrance. *Proc.Natl.Acad.Sci.U.S.A.,* **99:** pp.11103-11108.

Andersen, C., Koronakis, E., Hughes, C. and Koronakis, V. (2002c) An aspartate ring at the TolC tunnel entrance determines ion selectivity and presents a target for blocking by large cations. *Mol.Microbiol.,* **44:** pp.1131-1139.

Andrews, J.M. (2012) **Determination of Minimum Inhibitory Concentrations.** [Online]. Available from: http://bsac.org.uk/wp-content/uploads/2012/02/Chapter-2-Determination-of-MICs-2006updated.pdf.

Ashkenazy, H., Erez, E., Martz, E., Pupko, T. and Ben-Tal, N. (2010) ConSurf 2010: Calculating evolutionary conservation in sequence and structure of proteins and nucleic acids. *Nucleic Acids Res.***, 38**: pp.W529-W533.

Augustus, A.M., Celaya, T., Husain, F., Humbard, M. and Misra, R. (2004) Antibiotic-sensitive TolC mutants and their suppressors. *J.Bacteriol.***, 186**: pp.1851-1860.

Baba, T., *et al.* (2006) Construction of *Escherichia coli* K-12 in-frame, single-gene knockout mutants: The Keio collection. *Molecular Systems Biology***, 2**: pp.2006.0008.

Bagai, I., Rensing, C., Blackburn, N.J. and McEvoy, M.M. (2008) Direct metal transfer between periplasmic proteins identifies a bacterial copper chaperone. *Biochemistry (N.Y.)***, 47**: pp.11408-11414.

Bailey, A.M., Paulsen, I.T. and Piddock, L.J.V. (2008) RamA confers multidrug resistance in *Salmonella enterica* via increased expression of *acrB*, which is inhibited by chlorpromazine. *Antimicrob.Agents Chemother.***, 52**: pp.3604-3611.

Bansal-Mutalik, R. & Nikaido, H. (2014) Mycobacterial outer membrane is a lipid bilayer and the inner membrane is unusually rich in diacyl phosphatidylinositol dimannosides. Proc.Natl.Acad.Sci.U.S.A., 111: pp.4958-4963.

Baugh, S., Ekanayaka, A.S., Piddock, L.J.V. and Webber, M.A. (2012) Loss of or inhibition of all multidrug resistance efflux pumps of *Salmonella enterica* serovar Typhimurium results in impaired ability to form a biofilm. *J.Antimicrob.Chemother.*, **67**: pp.2409-2417.

Baugh, S., Phillips, C.R., Ekanayaka, A.S., Piddock, L.J.V. and Webber, M.A. (2014) Inhibition of multidrug efflux as a strategy to prevent biofilm formation. *J.Antimicrob.Chemother.*, **69**: pp.673-681.

Bavro, V.N., *et al.* (2008) Assembly and channel opening in a bacterial drug efflux machine. *Mol.Cell*, **30**: pp.114-121.

Bay, D.C., Rommens, K.L. and Turner, R.J. (2008) Small multidrug resistance proteins: A multidrug transporter family that continues to grow. *Biochim.Biophys.Acta-Biomembr.*, **1778**: pp.1814-1838.

Bay, D.C., Budiman, R.A., Nieh, M. and Turner, R.J. (2010) Multimeric forms of the small multidrug resistance protein EmrE in anionic detergent. *Biochim.Biophys.Acta-Biomembr.*, **1798**: pp.526-535.

Benz, R., Maier, E. and Gentschev, I. (1993) TolC of *Escherichia coli* functions as an outer-membrane channel. *Zent.Bl.Bakteriol.-Int.J.Med.Microbiol.Virol.Parasitol.Infect.Dis.*, **278**: pp.187-196.

Bergmiller, T., *et al.* (2017) Biased partitioning of the multidrug efflux pump AcrAB-TolC underlies long-lived phenotypic heterogeneity. *Science*, **356**: pp.309-311.

Blair, J.M.A., *et al.* (2015) AcrB drug-binding pocket substitution confers clinically relevant resistance and altered substrate specificity. *Proc.Natl.Acad.Sci.U.S.A.*, **112**: pp.3511-3516.

Blair, J.M.A. & Piddock, L.J.V. (2016) How to measure export via bacterial multidrug resistance efflux pumps. *Mbio*, **7**: pp.e00840-16.

Blanco, P., *et al.* (2016) Bacterial multidrug efflux pumps: Much more than antibiotic resistance determinants. *Microorganisms*, **4**: pp.14.

Bleuel, C., *et al.* (2005) TolC is involved in enterobactin efflux across the outer membrane of *Escherichia coli. J.Bacteriol.*, **187**: pp.6701-6707.

Bohnert, J.A., Karamian, B. and Nikaido, H. (2010) Optimized Nile Red efflux assay of AcrAB-TolC multidrug efflux system shows competition between substrates. *Antimicrob.Agents Chemother.*, **54**: pp.3770-3775.

Bokma, E., Koronakis, E., Lobedanz, S., Hughes, C. and Koronakis, V. (2006) Directed evolution of a bacterial efflux pump: Adaptation of the *E. coli* TolC exit duct to the *Pseudomonas* MexAB translocase. *FEBS Lett.*, **580**: pp.5339-5343.

Buckner, M.M.C., *et al.* (2016) Beyond antimicrobial resistance: Evidence for a distinct role of the AcrD efflux pump in *Salmonella* biology. *Mbio*, **7**: pp.e01916-16.

Bunikis, I., *et al.* (2008) An RND-type efflux system in *Borrelia burgdorferi* is involved in virulence and resistance to antimicrobial compounds. *PLoS Pathog.*, **4**: pp.e1000009.

Caroff, M. & Karibian, D. (2003) Structure of bacterial lipopolysaccharides. *Carbohydr.Res.*, **338**: pp.2431-2447.

Chuanchuen, R., Narasaki, C. and Schweizer, H. (2002) The MexJK efflux pump of *Pseudomonas aeruginosa* requires OprM for antibiotic efflux but not for efflux of triclosan. *J.Bacteriol.*, **184**: pp.5036-5044.

Chuanchuen, R., Murata, T., Gotoh, N. and Schweizer, H. (2005) Substrate-dependent utilization of OprM or OpmH by the *Pseudomonas aeruginosa* MexJK efflux pump. *Antimicrob.Agents Chemother.*, **49**: pp.2133-2136.

Chung, C., Niemela, S. and Miller, R. (1989) One-step preparation of competent *Escherichia coli* - transformation and storage of bacterial cells in the same solution. *Proc.Natl.Acad.Sci.U.S.A.*, **86**: pp.2172-2175.

Clatworthy, A.E., Pierson, E. and Hung, D.T. (2007) Targeting virulence: A new paradigm for antimicrobial therapy. *Nat.Chem.Biol.*, **3**: pp.541-548.

Coates, A.R.M., Halls, G. and Hu, Y. (2011) Novel classes of antibiotics or more of the same? *Br.J.Pharmacol.*, **163**: pp.184-194.

Coldham, N.G., Webber, M., Woodward, M.J. and Piddock, L.J.V. (2010) A 96-well plate fluorescence assay for assessment of cellular permeability and active efflux in *Salmonella enterica* serovar Typhimurium and *Escherichia coli*. *J.Antimicrob.Chemother.*, **65**: pp.1655-1663.

Cowan, S., et al. (1992) Crystal structures explain functional properties of two *Escherichia coli* porins. Nature, **358**: pp.727-733.

Danilchanka, O., Pires, D., Anes, E. and Niederweis, M. (2015) The *Mycobacterium tuberculosis* outer membrane channel protein CpnT confers susceptibility to toxic molecules. *Antimicrob.Agents Chemother.*, **59**: pp.2328-2336.

Darabpour, E., Ardakani, M.R., Motamedi, H., Ghezelbash, G. and Ronagh, M.T. (2010) Isolation of an antibiotic producer *Pseudomonas* sp from the Persian Gulf. *Asian Pac.J.Trop.Med.*, **3**: pp.318-318.

Dastvan, R., Fischer, A.W., Mishra, S., Meiler, J. and Mchaourab, H.S. (2016) Protonation-dependent conformational dynamics of the multidrug transporter EmrE. *Proc.Natl.Acad.Sci.U.S.A.*, **113**: pp.1220-1225.

Datsenko, K.A. & Wanner, B.L. (2000) One-step inactivation of chromosomal genes in *Escherichia coli* K-12 using PCR products. *Proc.Natl.Acad.Sci.U.S.A.*, **97**: pp.6640-6645.

Daury, L., *et al.* (2016) Tripartite assembly of RND multidrug efflux pumps. *Nat.Commun.*, **7**: pp.10731.

De Angelis, F., *et al.* (2010) Metal-induced conformational changes in ZneB suggest an active role of membrane fusion proteins in efflux resistance systems. *Proc.Natl.Acad.Sci.U.S.A.*, **107**: pp.11038-11043.

de Cristobal, R.E., Vincent, P.A. and Salomon, R.A. (2006) Multidrug resistance pump AcrAB-TolC is required for high-level, tet(A)-mediated tetracycline resistance in *Escherichia coli*. *J.Antimicrob.Chemother.*, **58**: pp.31-36.

Deininger, K.N.W., *et al.* (2011) A requirement of TolC and MDR efflux pumps for acid adaptation and GadAB induction in *Escherichia coli*. *PLoS One*, **6**: pp.e18960.

Delcour, A.H. (2009) Outer membrane permeability and antibiotic resistance. *BBA-Proteins Proteomics*, **1794**: pp.808-816.

Demain, A.L. (2009) Antibiotics: Natural products essential to human health. *Med.Res.Rev.*, **29**: pp.821-842.

Du, D., *et al.* (2014) Structure of the AcrAB-TolC multidrug efflux pump. *Nature*, **509**: pp.512-515.

Eicher, T., *et al.* (2012) Transport of drugs by the multidrug transporter AcrB involves an access and a deep binding pocket that are separated by a switch-loop. *Proc.Natl.Acad.Sci.U.S.A.*, **109**: pp.5687-5692.

Eicher, T., *et al.* (2014) Coupling of remote alternating-access transport mechanisms for protons and substrates in the multidrug efflux pump AcrB. *Elife*, **3**:.

Elkins, C. & Nikaido, H. (2003) Chimeric analysis of AcrA function reveals the importance of its C-terminal domain in its interaction with the AcrB multidrug efflux pump. *J.Bacteriol.*, **185**: pp.5349-5356.

Enguéné, V.Y.N., Verchère, A., Phan, G., Broutin, I. and Picard, M. (2015) Catch me if you can: A biotinylated proteoliposome affinity assay for the investigation of assembly of the MexA-MexB-OprM efflux pump from *Pseudomonas aeruginosa*. *Front.Microbiol.*, **6**: pp.541.

Fadli, M., Chevalier, J., Hassani, L., Mezrioui, N.-. and Pages, J.-. (2014) Natural extracts stimulate membrane-associated mechanisms of resistance in Gram-negative bacteria. *Lett.Appl.Microbiol.*, **58**: pp.472-477.

Fares, M.A. & McNally, D. (2006) CAPS: Coevolution analysis using protein sequences. *Bioinformatics*, **22**: pp.2821-2822.

Federici, L., *et al.* (2005) The crystal structure of the outer membrane protein VceC from the bacterial pathogen *Vibrio cholerae* at 1.8 angstrom resolution. *J.Biol.Chem.*, **280**: pp.15307-15314.

Fernandez-Recio, J., *et al.* (2004) A model of a transmembrane drug-efflux pump from Gram-negative bacteria. *FEBS Lett.*, **578**: pp.5-9.

Finkelshtein, A., Roth, D., Ben Jacob, E. and Inghamd, C.J. (2015) Bacterial swarms recruit cargo bacteria to pave the way in toxic environments. *Mbio*, **6**: pp.e00074-15.

Fisher, M.A., *et al.* (2014) Enhancing tolerance to short-chain alcohols by engineering the *Escherichia coli* AcrB efflux pump to secrete the non-native substrate n-butanol. *ACS Synth.Biol.,* **3:** pp.30-40.

Fleming, A. (1929) On the antibacterial action of cultures of a *Penicillium*, with special reference to their use in the isolation of *B. influenzae*. *Br.J.Exp.Pathol.,* **10:** pp.226-236.

Fournier, D., *et al.* (2013) Complexity of resistance mechanisms to imipenem in intensive care unit strains of *Pseudomonas aeruginosa*. *J.Antimicrob.Chemother.,* **68:** pp.1772-1780.

Fox, R. (1996) The post-antibiotic era beckons. *J.R.Soc.Med.,* **89:** pp.602-603.

Fralick, J.A. (1996) Evidence that TolC is required for functioning of the Mar/AcrAB efflux pump of *Escherichia coli*. *J.Bacteriol.,* **178:** pp.5803-5805.

Fuller, A.T.*, et al.* (1971) Pseudomonic acid - antibiotic produced by *Pseudomonas fluorescens*. *Nature,* **234:** pp.416-&.

Gayen, A., Leninger, M. and Traasethl, N.J. (2016) Protonation of a glutamate residue modulates the dynamics of the drug transporter EmrE. *Nat.Chem.Biol.,* **12:** pp.141-145.

Ge, Q., Yamada, Y. and Zgurskaya, H. (2009) The C-terminal domain of AcrA is essential for the assembly and function of the multidrug efflux pump AcrAB-TolC. *J.Bacteriol.,* **191:** pp.4365-4371.

Greene, N.P.*, et al.* (2013) Structure of an atypical periplasmic adaptor from a multidrug efflux pump of the spirochete *Borrelia burgdorferi*. *FEBS Lett.,* **587:** pp.2984-2988.

Gupta, R.S. (2011) Origin of diderm (Gram-negative) bacteria: Antibiotic selection pressure rather than endosymbiosis likely led to the evolution of bacterial cells with two membranes. *Antonie Van Leeuwenhoek International Journal of General and Molecular Microbiology,* **100:** pp.171-182.

Hackett, J., Misra, R. and Reeves, P. (1983) The TolC protein of *Escherichia coli* K-12 is synthesized in a precursor form. *FEBS Lett.,* **156:** pp.307-310.

Hassan, K.A.*, et al.* (2013) Transcriptomic and biochemical analyses identify a family of chlorhexidine efflux proteins. *Proc.Natl.Acad.Sci.U.S.A.,* **110:** pp.20254-20259.

Hassan, K.A., Liu, Q., Henderson, P.J.F. and Paulsen, I.T. (2015a) Homologs of the *Acinetobacter baumannii* AceI transporter represent a new family of bacterial multidrug efflux systems. *Mbio,* **6:**.

Hassan, K.A.*, et al.* (2015b) An ace up their sleeve: A transcriptomic approach exposes the AceI efflux protein of *Acinetobacter baumannii* and reveals the drug efflux potential hidden in many microbial pathogens. *Frontiers in Microbiology,* **6:** pp.333.

Hattab, G., Warschawski, D.E., Moncoq, K. and Miroux, B. (2015) *Escherichia coli* as host for membrane protein structure determination: A global analysis. *Sci Rep,* **5:** pp.12097.

Hayashi, K.*, et al.* (2016) AcrB-AcrA fusion proteins that act as multidrug efflux transporters. *J.Bacteriol.,* **198:** pp.332-342.

He, X.*, et al.* (2010) Structure of a cation-bound multidrug and toxic compound extrusion transporter. *Nature,* **467:** pp.991-U139.

Heine, H., Muller-Loennies, S., Brade, L., Lindner, B. and Brade, H. (2003) Endotoxic activity and chemical structure of lipopolysaccharides from *Chlamydia trachomatis* serotypes E and L-2 and *Chlamydophila psittaci* 6BC. Eur.J.Biochem., 270: pp.440-450.

Higgins, M., Bokma, E., Koronakis, E., Hughes, C. and Koronakis, V. (2004a) Structure of the periplasmic component of a bacterial drug efflux pump. *Proc.Natl.Acad.Sci.U.S.A.,* **101:** pp.9994-9999.

Higgins, M., *et al.* (2004b) Structure of the ligand-blocked periplasmic entrance of the bacterial multidrug efflux protein TolC. *J.Mol.Biol.,* **342:** pp.697-702.

Hinchliffe, P., *et al.* (2014) Structure of the periplasmic adaptor protein from a major facilitator superfamily (MFS) multidrug efflux pump. *FEBS Lett.,* **588:** pp.3147-3153.

Hobbs, E.C., Yin, X., Paul, B.J., Astarita, J.L. and Storz, G. (2012) Conserved small protein associates with the multidrug efflux pump AcrB and differentially affects antibiotic resistance. *Proc.Natl.Acad.Sci.U.S.A.,* **109:** pp.16696-16701.

Horiyama, T., Yamaguchi, A. and Nishino, K. (2010) TolC dependency of multidrug efflux systems in *Salmonella enterica* serovar Typhimurium. *J.Antimicrob.Chemother.,* **65:** pp.1372-1376.

Huber, R., *et al.* (1986) *Thermotoga maritima* sp-nov represents a new genus of unique extremely thermophilic eubacteria growing up to 90-degrees-C. *Arch.Microbiol.,* **144:** pp.324-333.

Iyer, R., Ferrari, A., Rijnbrand, R. and Erwin, A.L. (2015) A fluorescent microplate assay quantifies bacterial efflux and demonstrates two distinct compound binding sites in AcrB. *Antimicrob.Agents Chemother.,* **59:** pp.2388-2397.

Janganan, T.K., *et al.* (2011) Opening of the outer membrane protein channel in tripartite efflux pumps is induced by interaction with the membrane fusion partner. *J.Biol.Chem.,* **286:** pp.5484-5493.

Janganan, T.K., Bavro, V.N., Zhang, L., Borges-Walmsley, M.I. and Walmsley, A.R. (2013) Tripartite efflux pumps: Energy is required for dissociation, but not assembly or opening of the outer membrane channel of the pump. *Mol.Microbiol.,* **88:** pp.590-602.

Jeong, H., *et al.* (2016) Pseudoatomic structure of the tripartite multidrug efflux pump AcrAB-TolC reveals the intermeshing cogwheel-like interaction between AcrA and TolC. *Structure,* **24:** pp.272-276.

Jernaes, M. & Steen, H. (1994) Staining of *Escherichia coli* for flow cytometry: Influx and efflux of ethidium bromide. *Cytometry,* **17:** pp.302-309.

Kamio, Y. & Nikaido, H. (1976) Outer membrane of *Salmonella* Typhimurium - accessibility of phospholipid head groups to phospholipase-C and cyanogen-bromide activated dextran in external medium. *Biochemistry (N.Y.),* **15:** pp.2561-2570.

Kawabe, T., Fujihira, E. and Yamaguchi, A. (2000) Molecular construction of a multidrug exporter system, AcrAB: Molecular interaction between AcrA and AcrB, and cleavage of the N-terminal signal sequence of AcrA. *J.Biochem.,* **128:** pp.195-200.

Kim, H., *et al.* (2010) Functional relationships between the AcrA hairpin tip region and the TolC aperture tip region for the formation of the bacterial tripartite efflux pump AcrAB-TolC. *J.Bacteriol.,* **192:** pp.4498-4503.

Kim, J., *et al.* (2015) Structure of the tripartite multidrug efflux pump AcrAB-TolC suggests an alternative assembly mode. *Mol.Cells,* **38:** pp.180-186.

Kim, J., *et al.* (2016) Crystal structure of a soluble fragment of the membrane fusion protein HlyD in a type I secretion system of gram-negative bacteria. *Structure (London, England : 1993),* **24:** pp.477-485.

Kinana, A.D., Vargiu, A.V. and Nikaido, H. (2016) Effect of site-directed mutations in multidrug efflux pump AcrB examined by quantitative efflux assays. *Biochem.Biophys.Res.Commun.,* **480:** pp.552-557.

Kirby, W. (1944) Extraction of a highly potent penicillin inactivator from penicillin resistant staphylococci. *Science,* **99:** pp.452-453.

Kobayashi, N., Nishino, K. and Yamaguchi, A. (2001) Novel macrolide-specific ABC-type efflux transporter in *Escherichia coli. J.Bacteriol.,* **183:** pp.5639-5644.

Koronakis, V., Sharff, A., Koronakis, E., Luisi, B. and Hughes, C. (2000) Crystal structure of the bacterial membrane protein TolC central to multidrug efflux and protein export. *Nature,* **405:** pp.914-919.

Krishnamoorthy, G., Tikhonova, E.B. and Zgurskaya, H.I. (2008) Fitting periplasmic membrane fusion proteins to inner membrane transporters: Mutations that enable *Escherichia coli* AcrA to function with *Pseudomonas aeruginosa* MexB. *J.Bacteriol.,* **190:** pp.691-698.

Krishnamoorthy, G., Tikhonova, E.B., Dhamdhere, G. and Zgurskaya, H.I. (2013) On the role of TolC in multidrug efflux: The function and assembly of AcrABTolC tolerate significant depletion of intracellular TolC protein. *Mol.Microbiol.,* **87:** pp.982-997.

Krishnamoorthy, G., *et al.* (2016) Breaking the permeability barrier of *Escherichia coli* by controlled hyperporination of the outer membrane. *Antimicrob.Agents Chemother.,* **60:** pp.7372-7381.

Kuroda, T. & Tsuchiya, T. (2009) Multidrug efflux transporters in the MATE family. *BBA-Proteins Proteomics,* **1794:** pp.763-768.

Lacroix, F., *et al.* (1996) *Salmonella* Typhimurium *acrB*-like gene: Identification and role in resistance to biliary salts and detergents and in murine infection. *FEMS Microbiol.Lett.,* **135:** pp.161-167.

Laemmli, U. (1970) Cleavage of structural proteins during assembly of head of bacteriophage-T4. *Nature*, **227:** pp.680-685.

Lamers, R.P., Cavallari, J.F. and Burrows, L.L. (2013) The efflux inhibitor phenylalanine-arginine beta-naphthylamide (PAβN) permeabilizes the outer membrane of Gram-negative bacteria. *PLoS One,* **8:** pp.e60666.

Law, C.J., Maloney, P.C. and Wang, D. (2008) Ins and outs of major facilitator superfamily, antiporters. *Annu.Rev.Microbiol.,* **62:** pp.289-305.

Lee, M., *et al.* (2012) Membrane fusion proteins of type I secretion system and tripartite efflux pumps share a binding motif for TolC in Gram-negative bacteria. *PLoS One,* **7:** pp.e40460.

Lei, H., *et al.* (2014) Crystal structure of the open state of the *Neisseria gonorrhoeae* MtrE outer membrane channel. *PLoS One,* **9:** pp.e97475.

Lin, J., Sahin, O., Michel, L. and Zhang, O. (2003) Critical role of multidrug efflux pump CmeABC in bile resistance and *in vivo* colonization of *Campylobacter jejuni*. *Infect.Immun.,* **71:** pp.4250-4259.

Ling, L.L.*, et al.* (2015) A new antibiotic kills pathogens without detectable resistance. *Nature,* **517:** pp.455-+.

Lobedanz, S.*, et al.* (2007) A periplasmic coiled-coil interface underlying TolC recruitment and the assembly of bacterial drug efflux pumps. *Proc.Natl.Acad.Sci.U.S.A.,* **104:** pp.4612-4617.

Lu, M., Radchenko, M., Symersky, J., Nie, R. and Guo, Y. (2013a) Structural insights into H+-coupled multidrug extrusion by a MATE transporter. *Nat.Struct.Mol.Biol.,* **20:** pp.1310-U242.

Lu, M.*, et al.* (2013b) Structures of a Na^+-coupled, substrate-bound MATE multidrug transporter. *Proc.Natl.Acad.Sci.U.S.A.,* **110:** pp.2099-2104.

Lu, M. (2016) Structures of multidrug and toxic compound extrusion transporters and their mechanistic implications. *Channels,* **10:** pp.88-100.

Lu, S. & Zgurskaya, H.I. (2012) Role of ATP binding and hydrolysis in assembly of MacAB-TolC macrolide transporter. *Mol.Microbiol.,* **86:** pp.1132-1143.

Lu, S. & Zgurskaya, H.I. (2013) MacA, a periplasmic membrane fusion protein of the macrolide transporter MacAB-TolC, binds lipopolysaccharide core specifically and with high affinity. *J.Bacteriol.,* **195:** pp.4865-4872.

Ma, D.*, et al.* (1995) Genes *acrA* and *acrB* encode a stress-induced efflux system of *Escherichia coli*. *Mol.Microbiol.,* **16:** pp.45-55.

Maseda, H., Yoneyama, H. and Nakae, T. (2000) Assignment of the substrate-selective subunits of the MexEF-OprN multidrug efflux pump of *Pseudomonas aeruginosa*. *Antimicrob.Agents Chemother.,* **44:** pp.658-664.

Masi, M., Duret, G., Delcour, A.H. and Misra, R. (2009) Folding and trimerization of signal sequence-less mature TolC in the cytoplasm of *Escherichia coli*. *Microbiology-(UK),* **155:** pp.1847-1857.

Matias, V., Al-Amoudi, A., Dubochet, J. and Beveridge, T. (2003) Cryo-transmission electron microscopy of frozen-hydrated sections of *Escherichia coli* and *Pseudomonas aeruginosa*. *J.Bacteriol.,* **185:** pp.6112-6118.

Mealman, T.D.*, et al.* (2012) N-terminal region of CusB is sufficient for metal binding and metal transfer with the metallochaperone CusF. *Biochemistry (N.Y.),* **51:** pp.6767-6775.

Mikolosko, J., Bobyk, K., Zgurskaya, H.I. and Ghosh, P. (2006) Conformational flexibility in the multidrug efflux system protein AcrA. *Structure,* **14:** pp.577-587.

Minagawa, S.*, et al.* (2012) RND type efflux pump system MexAB-OprM of *Pseudomonas aeruginosa* selects bacterial languages, 3-oxo-acyl-homoserine lactones, for cell-to-cell communication. *BMC Microbiol.,* **12:** pp.70.

Miroux, B. & Walker, J. (1996) Over-production of proteins in *Escherichia coli*: Mutant hosts that allow synthesis of some membrane proteins and globular proteins at high levels. *J.Mol.Biol.,* **260:** pp.289-298.

Monlezun, L.*, et al.* (2015) New OprM structure highlighting the nature of the N-terminal anchor. *Front.Microbiol.,* **6:** pp.667.

Morgan-Kiss, R., Wadler, C. and Cronan, J. (2002) Long-term and homogeneous regulation of the *Escherichia coli araBAD* promoter by use of a lactose transporter of relaxed specificity. *Proc.Natl.Acad.Sci.U.S.A.,* **99:** pp.7373-7377.

Morona, R. & Reeves, P. (1982) The *tolC* locus of *Escherichia coli* affects the expression of 3 major outer-membrane proteins. *J.Bacteriol.,* **150:** pp.1016-1023.

Morris, F.C. (2014) **The Role of Outer Membrane Homeostatis in the Virulence of Gram-Negative Bacteria**., Ph.D Thesis, University of Birmingham.

Murakami, S., Nakashima, R., Yamashita, E. and Yamaguchi, A. (2002) Crystal structure of bacterial multidrug efflux transporter AcrB. *Nature,* **419:** pp.587-593.

Nagel de Zwaig, R. & Luria, S.E. (1967) Genetics and physiology of colicin-tolerant mutants of *Escherichia coli. J.Bacteriol.,* **94:** pp.1112-1123.

Nagel de Zwaig, R. & Luria, S.E. (1969) New class of conditional colicin-tolerant mutants. *J.Bacteriol.,* **99:** pp.78-84.

Nichols, D.*, et al.* (2010) Use of ichip for high-throughput *in situ* cultivation of "uncultivable" microbial species. *Appl.Environ.Microbiol.,* **76:** pp.2445-2450.

Nikaido, H. (1994) Prevention of drug access to bacterial targets - permeability barriers and active efflux. *Science,* **264:** pp.382-388.

Nikaido, H. (2009) Multidrug resistance in bacteria. *Annu.Rev.Biochem.,* **78:** pp.119-146.

Novick, A. & Weiner, M. (1957) Enzyme induction as an all-or-none phenomenon. *Proc.Natl.Acad.Sci.U.S.A.,* **43:** pp.553-566.

O'Daniel, P.I.*, et al.* (2014) Discovery of a new class of non-beta-lactam inhibitors of penicillin-binding proteins with Gram-positive antibacterial activity. *J.Am.Chem.Soc.,* **136:** pp.3664-3672.

Ogawa, W.*, et al.* (2015) Characterization of MATE-type multidrug efflux pumps from *Klebsiella pneumoniae* MGH78578. *PLoS One,* **10:** pp.e0121619.

Ohneck, E.A.*, et al.* (2011) A novel mechanism of high-level, broad-spectrum antibiotic resistance caused by a single base pair change in *Neisseria gonorrhoeae*. *Mbio,* **2:** pp.e00187.

Olabarria, G., Carrascosa, J., dePedro, M. and Berenguer, J. (1996) A conserved motif in S-layer proteins is involved in peptidoglycan binding in *Thermus thermophilus*. *J.Bacteriol.,* **178:** pp.4765-4772.

Oswald, C., Tam, H. and Pos, K.M. (2016) Transport of lipophilic carboxylates is mediated by transmembrane helix 2 in multidrug transporter AcrB. *Nat.Commun.,* **7:** pp.13819.

Paixão, L., *et al.* (2009) Fluorometric determination of ethidium bromide efflux kinetics in *Escherichia coli*. *Journal of Biological Engineering,* **3:** pp.18.

Pei, X., *et al.* (2011) Structures of sequential open states in a symmetrical opening transition of the TolC exit duct. *Proc.Natl.Acad.Sci.U.S.A.,* **108:** pp.2112-2117.

Phan, G., Picard, M. and Broutin, I. (2015) Focus on the outer membrane factor OprM, the forgotten player from efflux pumps assemblies. *Antibiotics-Basel,* **4:** pp.544-566.

Phetsang, W., *et al.* (2016) Fluorescent trimethoprim conjugate probes to assess drug accumulation in wild type and mutant *Escherichia coli*. *ACS Infect.Dis.,* **2:** pp.688-701.

Piddock, L. (2006) Clinically relevant chromosomally encoded multidrug resistance efflux pumps in bacteria. *Clin.Microbiol.Rev.,* **19:** pp.382-402.

Piddock, L.J.V. (2012) The crisis of no new antibiotics-what is the way forward? *Lancet Infect.Dis.,* **12:** pp.249-253.

Poole, K. (2008) Bacterial multidrug efflux pumps serve other functions. *Microbe,* **3:** pp.179-185.

Pos, K.M. (2009) Drug transport mechanism of the AcrB efflux pump. *Biochimica Et Biophysica Acta-Proteins and Proteomics,* **1794:** pp.782-793.

Rosner, J.L. & Martin, R.G. (2009) An excretory function for the *Escherichia coli* outer membrane pore TolC: Upregulation of *marA* and *soxS* transcription and rob activity due to metabolites accumulated in *tolC* mutants. *J.Bacteriol.,* **191:** pp.5283-5292.

Rottem, S. & Leive, L. (1977) Effect of variations in lipopolysaccharide on fluidity of outer membrane of *Escherichia coli*. *J.Biol.Chem.,* **252:** pp.2077-2081.

Ruiz, C. & Levy, S.B. (2014) Regulation of *acrAB* expression by cellular metabolites in *Escherichia coli*. *J.Antimicrob.Chemother.,* **69:** pp.390-399.

Saier, M.H., Jr., Reddy, V.S., Tamang, D.G. and Vaestermark, A. (2014) The transporter classification database. *Nucleic Acids Res.,* **42:** pp.D251-D258.

Sanchez-Romero, M.A. & Casadesus, J. (2014) Contribution of phenotypic heterogeneity to adaptive antibiotic resistance. *Proc.Natl.Acad.Sci.U.S.A.,* **111:** pp.355-360.

Schuster, S., Vavra, M. and Kern, W.V. (2016) Evidence of a substrate-discriminating entrance channel in the lower porter domain of the multidrug resistance efflux pump AcrB. *Antimicrob.Agents Chemother.,* **60:** pp.4315-4323.

Seeger, M.A., *et al.* (2006) Structural asymmetry of AcrB trimer suggests a peristaltic pump mechanism. *Science,* **313:** pp.1295-1298.

Seeger, M.A., *et al.* (2008) The AcrB efflux pump: Conformational cycling and peristalsis lead to multidrug resistance. *Curr.Drug Targets,* **9:** pp.729-749.

Silverman, R. & Atherly, A. (1978) Unusual effects of 5a,6-anhydrotetracycline and other tetracyclines - inhibition of guanosine 5'-diphosphate 3'-diphosphate

metabolism, rna accumulation and other growth-related processes in *Escherichia coli*. *Biochim.Biophys.Acta,* **518:** pp.267-276.

Sjuts, H., *et al.* (2016) Molecular basis for inhibition of AcrB multidrug efflux pump by novel and powerful pyranopyridine derivatives. *Proc.Natl.Acad.Sci.U.S.A.,* **113:** pp.3509-3514.

Smith, H.E. & Blair, J.M.A. (2014) Redundancy in the periplasmic adaptor proteins AcrA and AcrE provides resilience and an ability to export substrates of multidrug efflux. *J.Antimicrob.Chemother.,* **69:** pp.982-987.

Song, S., Hwang, S., Lee, S., Ha, N. and Lee, K. (2014) Interaction mediated by the putative tip regions of MdsA and MdsC in the formation of a salmonella-specific tripartite efflux pump. *PLoS One,* **9:** pp.e100881.

Staron, P., Forchhammer, K. and Maldener, I. (2014) Structure-function analysis of the ATP-driven glycolipid efflux pump DevBCA reveals complex organization with TolC/HgdD. *FEBS Lett.,* **588:** pp.395-400.

Stegmeier, J.F., Polleichtner, G., Brandes, N., Hotz, C. and Andersen, C. (2006) Importance of the adaptor (membrane fusion) protein hairpin domain for the functionality of multidrug efflux pumps. *Biochemistry (N.Y.),* **45:** pp.10303-10312.

Sulavik, M., *et al.* (2001) Antibiotic susceptibility profiles of *Escherichia coli* strains lacking multidrug efflux pump genes. *Antimicrob.Agents Chemother.,* **45:** pp.1126-1136.

Sutcliffe, I.C. (2010) A phylum level perspective on bacterial cell envelope architecture. *Trends Microbiol.,* **18:** pp.464-470.

Symmons, M.F., Bokma, E., Koronakis, E., Hughes, C. and Koronakis, V. (2009) The assembled structure of a complete tripartite bacterial multidrug efflux pump. *Proc.Natl.Acad.Sci.U.S.A.,* **106:** pp.7173-7178.

Symmons, M.F., Marshall, R.L. and Bavro, V.N. (2015) Architecture and roles of periplasmic adaptor proteins in tripartite efflux assemblies. *Front.Microbiol.,* **6:** pp.513.

Tal, N. & Schuldiner, S. (2009) A coordinated network of transporters with overlapping specificities provides a robust survival strategy. *Proc.Natl.Acad.Sci.U.S.A.,* **106:** pp.9051-9056.

Tamura, N., Murakami, S., Oyama, Y., Ishiguro, M. and Yamaguchi, A. (2005) Direct interaction of multidrug efflux transporter AcrB and outer membrane channel TolC detected via site-directed disulfide cross-linking. *Biochemistry (N.Y.),* **44:** pp.11115-11121.

Tatsumi, R. & Wachi, M. (2008) TolC-dependent exclusion of porphyrins in *Escherichia coli*. *J.Bacteriol.,* **190:** pp.6228-6233.

Tavio, M.M., Aquili, V.D., Vila, J. and Poveda, J.B. (2014) Resistance to ceftazidime in *Escherichia coli* associated with AcrR, MarR and PBP3 mutations and overexpression of *sdiA*. *J.Med.Microbiol.,* **63:** pp.56-65.

Thanabalu, T., Koronakis, E., Hughes, C. and Koronakis, V. (1998) Substrate-induced assembly of a contiguous channel for protein export from *E. coli*: Reversible

bridging of an inner-membrane translocase to an outer membrane exit pore. *Embo j.,* **17:** pp.6487-6496.

Thanassi, D., Cheng, L. and Nikaido, H. (1997) Active efflux of bile salts by *Escherichia coli*. *J.Bacteriol.,* **179:** pp.2512-2518.

Tikhonova, E.B. & Zgurskaya, H.I. (2004) AcrA, AcrB, and TolC of *Escherichia coli* form a stable intermembrane multidrug efflux complex. *J.Biol.Chem.,* **279:** pp.32116-32124.

Tikhonova, E.B., Devroy, V.K., Lau, S.Y. and Zgurskaya, H.I. (2007) Reconstitution of the *Escherichia coli* macrolide transporter: The periplasmic membrane fusion protein MacA stimulates the ATPase activity of MacB. *Mol.Microbiol.,* **63:** pp.895-910.

Tikhonova, E.B., Dastidar, V., Rybenkov, V.V. and Zgurskaya, H.I. (2009) Kinetic control of TolC recruitment by multidrug efflux complexes. *Proc.Natl.Acad.Sci.U.S.A.,* **106:** pp.16416-16421.

Tikhonova, E.B., Yamada, Y. and Zgurskaya, H.I. (2011) Sequential mechanism of assembly of multidrug efflux pump AcrAB-ToIC. *Chem.Biol.,* **18:** pp.454-463.

Touzé, T.*, et al.* (2004) Interactions underlying assembly of the *Escherichia coli* AcrAB-TolC multidrug efflux system. *Mol.Microbiol.,* **53:** pp.697-706.

Tsujimoto, H., Gotoh, N. and Nishino, T. (1999) Diffusion of macrolide antibiotics through the outer membrane of *Moraxella catarrhalis*. *J Infect Chemother,* **5:** pp.196-200.

Varela, C., et al. (2012) MmpL genes are associated with mycolic acid metabolism in Mycobacteria and Corynebacteria. Chem.Biol., 19: pp.498-506.

Vargiu, A.V., Ruggerone, P., Opperman, T.J., Nguyen, S.T. and Nikaido, H. (2014) Molecular mechanism of MBX2319 inhibition of *Escherichia coli* AcrB multidrug efflux pump and comparison with other inhibitors. *Antimicrob.Agents Chemother.,* **58:** pp.6224-6234.

Vediyappan, G., Borisova, T. and Fralick, J. (2006) Isolation and characterization of VceC gain-of-function mutants that can function with the AcrAB multiple-drug-resistant efflux pump of *Escherichia coli*. *J.Bacteriol.,* **188:** pp.3757-3762.

Verchère, A., Broutin, I. and Picard, M. (2012) Photo-induced proton gradients for the *in vitro* investigation of bacterial efflux pumps. *Sci Rep,* **2:** pp.306.

Verchère, A., Broutin, I. and Picard, M. (2013) Hoechst likes to play hide and seek ... use it with caution! *Anal.Biochem.,* **440:** pp.117-119.

Verchère, A., Dezi, M., Broutin, I. and Picard, M. (2014) *In vitro* investigation of the MexAB efflux pump from *Pseudomonas aeruginosa*. *J.Vis.Exp.,* pp.e50894.

Verchère, A., Dezi, M., Adrien, V., Broutin, I. and Picard, M. (2015) *In vitro* transport activity of the fully assembled MexAB-OprM efflux pump from *Pseudomonas aeruginosa*. *Nat.Commun.,* **6:** pp.6890.

Walker, J. & Altman, E. (2005) Biotinylation facilitates the uptake of large peptides by *Escherichia coli* and other Gram-negative bacteria. *Appl.Environ.Microbiol.,* **71:** pp.1850-1855.

Walse, B., *et al.* (2008) The structures of human dihydroorotate dehydrogenase with and without inhibitor reveal conformational flexibility in the inhibitor and substrate binding sites. *Biochemistry (N.Y.),* **47:** pp.8929-8936.

Wandersman, C. & Delepelaire, P. (1990) Tolc, an *Escherichia coli* outer-membrane protein required for hemolysin secretion. *Proc.Natl.Acad.Sci.U.S.A.,* **87:** pp.4776-4780.

Wang, Z., *et al.* (2017) An allosteric transport mechanism for the AcrAB-TolC multidrug efflux pump. *Elife,* **10:** pp.24905.

Wang-Kan, X., *et al.* (2017) Lack of AcrB efflux function confers loss of virulence on *Salmonella enterica* serovar Typhimurium. *Mbio,* **8:** pp.e00968-17.

Webber, M., Talukder, A. and Piddock, L. (2005) Contribution of mutation at amino acid 45 of AcrR to *acrB* expression and ciprofloxacin resistance in clinical and veterinary *Escherichia coli* isolates. *Antimicrob.Agents Chemother.,* **49:** pp.4390-4392.

Webber, M.A., *et al.* (2009) The global consequence of disruption of the AcrAB-TolC efflux pump in *Salmonella enterica* includes reduced expression of SPI-1 and other attributes required to infect the host. *J.Bacteriol.,* **191:** pp.4276-4285.

Weeks, J.W., Celaya-Kolb, T., Pecora, S. and Misra, R. (2010) AcrA suppressor alterations reverse the drug hypersensitivity phenotype of a TolC mutant by inducing TolC aperture opening. *Mol.Microbiol.,* **75:** pp.1468-1483.

Weeks, J.W., Bavro, V.N. and Misra, R. (2014) Genetic assessment of the role of AcrB beta hairpins in the assembly of the TolC-AcrAB multidrug efflux pump of *Escherichia coli*. *Mol.Microbiol.,* **91:** pp.965-975.

Weeks, J.W., Nickels, L.M., Ntreh, A.T. and Zgurskaya, H.I. (2015) Non-equivalent roles of two periplasmic subunits in the function and assembly of triclosan pump TriABC from *Pseudomonas aeruginosa*. *Mol.Microbiol.,* **98:** pp.343-356.

Werner, J., Augustus, A. and Misra, R. (2003) Assembly of TolC, a structurally unique and multifunctional outer membrane protein of *Escherichia coli* K-12. *J.Bacteriol.,* **185:** pp.6540-6547.

Whetstine, C.R., Slusser, J.G. and Zueckert, W.R. (2009) Development of a single-plasmid-based regulatable gene expression system for *Borrelia burgdorferi*. *Appl.Environ.Microbiol.,* **75:** pp.6553-6558.

Whitehead, R.N., Overton, T.W., Kemp, C.L. and Webber, M.A. (2011) Exposure of *Salmonella enterica* serovar Typhimurium to high level biocide challenge can select multidrug resistant mutants in a single step. *PLoS One,* **6:** pp.e22833.

Wilkinson, S. (1996) Bacterial lipopolysaccharides - themes and variations. *Prog.Lipid Res.,* **35:** pp.283-343.

World Health Organisation (2014) [Online]. Available from: http://www.who.int/mediacentre/factsheets/fs310/en/ [Accessed 06/10 2014].

Xu, Y., *et al.* (2010) The tip region of the MacA alpha-hairpin is important for the binding to TolC to the *Escherichia col*i MacAB-TolC pump. *Biochem.Biophys.Res.Commun.*, **394**: pp.962-965.

Xu, Y., *et al.* (2011a) Funnel-like hexameric assembly of the periplasmic adapter protein in the tripartite multidrug efflux pump in Gram-negative bacteria. *J.Biol.Chem.*, **286**: pp.17910-17920.

Xu, Y., *et al.* (2011b) Functional implications of an intermeshing cogwheel-like interaction between TolC and MacA in the action of macrolide-specific efflux pump MacAB-TolC. *J.Biol.Chem.*, **286**: pp.13541-13549.

Xu, Y., *et al.* (2012) Assembly and channel opening of outer membrane protein in tripartite drug efflux pumps of Gram-negative bacteria. *J.Biol.Chem.*, **287**: pp.11740-11750.

Yamamoto, K., *et al.* (2016) Substrate-dependent dynamics of the multidrug efflux transporter AcrB of *Escherichia coli*. *Sci Rep*, **6**: pp.21909.

Yamanaka, H., Izawa, H. and Okamoto, K. (2001) Carboxy-terminal region involved in activity of *Escherichia coli* TolC. *J.Bacteriol.*, **183**: pp.6961-6964.

Yamanaka, H., Nomura, T., Morisada, N., Shinoda, S. and Okamoto, K. (2002) Site-directed mutagenesis studies of the amino acid residue at position 412 of *Escherichia coli* TolC which is required for the activity. *Microb.Pathog.*, **33**: pp.81-89.

Yamanaka, H., *et al.* (2004) Amino-acid residues involved in the expression of the activity of *Escherichia coli* TolC. *Microbiol.Immunol.*, **48**: pp.713-722.

Yamanaka, H., *et al.* (2007) Studies on the region involved in the transport activity of *Escherichia coli* TolC by chimeric protein analysis. *Microb.Pathog.*, **42**: pp.184-192.

Yanagisawa, T. & Kawakami, M. (2003) How does *Pseudomonas fluorescens* avoid suicide from its antibiotic pseudomonic acid? Evidence for two evolutionarily distinct isoleucyl-tRNA synthetases conferring self-defense. *J.Biol.Chem.*, **278**: pp.25887-25894.

Yang, J., *et al.* (2015) The I-TASSER suite: Protein structure and function prediction. Nat.Methods, **12**: pp.7-8.

Yang, L., *et al.* (2014) RND transporters protect *Corynebacterium glutamicum* from antibiotics by assembling the outer membrane. *Microbiologyopen*, **3**: pp.484-496.

Yin, Y., He, X., Szewczyk, P., Nguyen, T. and Chang, G. (2006) Structure of the multidrug transporter EmrD from *Escherichia coli*. *Science*, **312**: pp.741-744.

Yonehara, R., Yamashita, E. and Nakagawa, A. (2016) Crystal structures of OprN and OprJ, outer membrane factors of multidrug tripartite efflux pumps of *Pseudomonas aeruginosa*. *Proteins*,.

Yoshihara, E., Maseda, H. and Saito, K. (2002) The outer membrane component of the multidrug efflux pump from *Pseudomonas aeruginosa* may be a gated channel. *Eur.J.Biochem.*, **269**: pp.4738-4745.

Yum, S., *et al.* (2009) Crystal structure of the periplasmic component of a tripartite macrolide-specific efflux pump. *J.Mol.Biol.*, **387**: pp.1286-1297.

Zgurskaya, H. & Nikaido, H. (1999) AcrA is a highly asymmetric protein capable of spanning the periplasm. *J.Mol.Biol.***, 285**: pp.409-420.

Zuo, Z., Wang, B., Weng, J. and Wang, W. (2015) Stepwise substrate translocation mechanism revealed by free energy calculations of doxorubicin in the multidrug transporter AcrB. *Sci Rep***, 5**: pp.13905.

9.3 Appendix 1: PCR primers used in this study

Primer name	Sequence (5'-3')	Annealing temperature (°C)	Supplier
pASK_NdeI-F	TAACTTTAAGAAGGAGATATACATATGAAGAAATTGCTCCCCATTCT	60	Eurogentec
pASK_NdeI-R	AGAATGGGGAGCAATTTCTTCATATGTATATCTCCTTCTTAAAGTTA	60	Eurogentec
pASK_Stop_F	GCCTTCTTATTCGGCCTTGAATTGATCATCTGCGGATTAGAAAAA	60	Eurogentec
pASK_STOP_R	TTTTTCTAATCCGCAGATGATCAATTCAAGGCCGAATAAGAAGGC	60	Eurogentec
TolC_WT_F	CACGAACATATGAAGAAATTGCTCCCCATTCTTATC	63	Eurogentec
TolC_WT_R	GAGTCGCTCGAGGTTACGGAAAGGGTTATGACC	61	Eurogentec
AcrA_WT_F	GGTCAACATATGAACAAAAACAGAGGGTTTACG	61	Eurogentec
AcrA_WT_R	TGGTTGCTCGAGACTTGGACTGTTCAGGCTG	63	Eurogentec
AcrB_WT_F	TAGCTTCATATGCCTAATTTCTTTATCGATCGCCCGATTTTTG	69	Eurogentec
AcrB_WT_R	ATATTCCTCGAGATGATGATCGACAGTATGGCTGTGC	67	Eurogentec
Salm_AcrB_F	TAGCTTCATATGCCTAATTTCTTTATCGATCGCCCGATTTTTG	69	Eurogentec
Salm_AcrB_R	ATATTCCTCGAGGCGATGTTCTGTCGAATGACTATGC	66	Eurogentec
TolC_D121N_F	CCGCTTATTTCAACGTGTTGAATGCTATTAACGTTCTTTCCTATA	60	Eurogentec
TolC_D121N_R	TATAGGAAAGAACGTTAATAGCATTCAACACGTTGAAATAAGCGG	60	Eurogentec
TolC_N332L_F	GACCGTGCGTTCCTCCTTCCTCAACATTAATGCATCTATCA	60	Eurogentec
TolC_N332L_R	TGATAGATGCATTAATGTTGAGGAAGGAGGAACGCACGGTC	60	Eurogentec
TolC_Y344F_F	TCAGTAGCATTAACGCCTTCAAACAAGCCGTAGTTTC	60	Eurogentec
TolC_Y344F_R	GAAACTACGGCTTGTTTGAAGGCGTTAATGCTACTGA	60	Eurogentec
TolC_N145L_F	ATTAGATCAAACCACCCAACGTTTTCTCGTGGGCCTGGTA	60	Eurogentec
TolC_N145L_R	TACCAGGCCCACGAGAAAACGTTGGGTGGTTTGATCTAAT	60	Eurogentec
TolC_R158E_F	GACGTGCAGAACGCCGACGCACAGTACGATAC	60	Eurogentec
TolC_R158E_R	GTATCGTACTGTGCGTCGGCGTTCTGCACGTC	60	Eurogentec
TolC_Q346L_F	AGCATTAACGCCTACAAACTAGCCGTAGTTTCCGC	60	Eurogentec
TolC_Q346L_R	GCGGAAACTACGGCTAGTTTGTAGGCGTTAATGCT	60	Eurogentec
TolC_Q352E_F	AGCCGTAGTTTCCGCTGAAAGCTCATTAGACGC	60	Eurogentec
TolC_Q352E_R	GCGTCTAATGAGCTTTCAGCGGAAACTACGGCT	60	Eurogentec
TolC_Q352A_F	CAAGCCGTAGTTTCCGCTGCAAGCTCATTAGACGCGAT	60	Eurogentec
TolC_Q352A_R	ATCGCGTCTAATGAGCTTGCAGCGGAAACTACGGCTTG	60	Eurogentec

TolC_N342A_F	CAACAACATTAATGCATCTATCAGTAGCATTGCCGCCTACAAACAAGCC	60	Eurogentec
TolC_N342A_R	GGCTTGTTTGTAGGCGGCAATGCTACTGATAGATGCATTAATGTTGTTG	60	Eurogentec
TolC_K383E_F	CGTTGTACAACGCCGAGCAAGAGCTGGCG	60	Eurogentec
TolC_K383E_R	CGCCAGCTCTTGCTCGGCGTTGTACAACG	60	Eurogentec
TolC_K383D_F	CCACGTTGTACAACGCCGATCAAGAGCTGGCGAATGC	60	Eurogentec
TolC_K383D_R	GCATTCGCCAGCTCTTGATCGGCGTTGTACAACGTGG	60	Eurogentec
TolC_D371V/D374V_F	ACGCGTACCATTGTTGTTGTGTTGGTTGCGACCACCAC	60	Eurogentec
TolC_D371V/D374V_R	GTGGTGGTCGCAACCAACACAACAACAATGGTACGCGT	60	Eurogentec
TolC_D371V_F	ACGCGTACCATTGTTGTTGTGTTGGATGCGACC	60	Eurogentec
TolC_D371V_R	GGTCGCATCCAACACAACAACAATGGTACGCGT	60	Eurogentec
TolC_D374V_F	CATTGTTGATGTGTTGGTTGCGAACCACCACGTTGT	60	Eurogentec
TolC_D374V_R	ACAACGTGGTGGTCGCAACCAACACATCAACAATG	60	Eurogentec
TolC_Q129L_F	CTTTCCTATACACAGGCACTGAAAGAAGCGATCTACCGTC	60	Eurogentec
TolC_Q129L_R	GACGGTAGATCGCTTCTTTCAGTGCCTGTGTATAGGAAAG	60	Eurogentec
seq_tolC_upst	CAATCAGCACAACTTCATCACGCAC	67	Alta Bioscience
seq_tolC_dnst	CCTGGTTTTCTGGTGCCATG	65	Alta Bioscience
seq_acrA_upst	GGTGTTAGATTTACATACATTTGTG	58	Alta Bioscience
seq_acrA_dnst	GTCCTGCACTGTTTTCGCATC	65	Alta Bioscience
seq_acrB_upst	GGTGTCCAGGTAAAAGCACAAG	64	Alta Bioscience
seq_acrB_dnst	GACGTAATAACCGAGGAATGAATAAAG	61	Alta Bioscience
tolC_int_F	GCTGAAAGAAGCCGAAAAACGCAACC	70	Alta Bioscience
tolC_int_R	GGTTGCGTTTTTCGGCTTCTTTCAGC	70	Alta Bioscience
acrA_int_R	GACCGTTCTGTACCAATGC	61	Alta Bioscience
acrA_int_F	GCATTGGTACAGAACGGTC	61	Alta Bioscience

acrB_int_F	CCAAGCTCCTTCTTGCCAG	64	Alta Bioscience
acrB_int_R	CTGGCAAGAAGGAGCTTGG	64	Alta Bioscience
pASK_seq_F	GAGTTATTTTACCACTCCCT	56	Alta Bioscience
pASK_seq_R	CGCAGTAGCGGTAAACG	61	Alta Bioscience
pET_seq_F	CGAAATTAATACGACTCACTATAGG	58	Alta Bioscience
pET_seq_R	GCTAGTTATTGCTCAGCG	58	Alta Bioscience
pASK_Stop_F	CGGGGATCCCTCGAGTGAGACCTGCAGGGGGAC	60	Alta Bioscience
pASK_Stop_R	GTCCCCCTGCAGGTCTCACTCGAGGGATCCCCG	60	Alta Bioscience
pASK_NdeI_F	TAACTTTAAGAAGGAGATATACATATGTGGAGCCACCCGCAGTTCGA	60	Alta Bioscience
pASK_NdeI_R	TCGAACTGCGGGTGGCTCCACATATGTATATCTCCTTCTTAAAGTTA	60	Alta Bioscience
I103R;A104R_F	CATTGCCCCATGGCTACATCCGTCGGCAGCAGGACAATAACAGTC	60	Alta Bioscience
I103R;I104R_R	GACTGTTATTGTCCTGCTGCCGACGGATGTAGCCATGGGGCAATG	60	Alta Bioscience
I103D;I104D_F	ACATTGCCCCATGGCTACATCGATGACCAGCAGGACAATAACAGTCAG	60	Alta Bioscience
I103D;I104D_R	CTGACTGTTATTGTCCTGCTGGTCATCGATGTAGCCATGGGGCAATGT	60	Alta Bioscience
P50G_F	GTTCATCAAGGCACAACGATGGGCGACGGTTTTTCAATCTGGCAT	60	Alta Bioscience
P50G_R	ATGCCAGATTGAAAAACCGTCGCCCATCGTTGTGCCTTGATGAAC	60	Alta Bioscience
F53A;W57A_F	GCACAACGATGCCAGACGGTGCTTCAATCGCGCATCACCTTGACGCTC	60	Alta Bioscience
F53A;W57A_R	GAGCGTCAAGGTGATGCGCGATTGAAGCACCGTCTGGCATCGTTGTGC	60	Alta Bioscience
S54P_F	CGATGCCAGACGGTTTTCCAATCTGGCATCACCT	60	Alta Bioscience
S54P_R	AGGTGATGCCAGATTGGAAAACCGTCTGGCATCG	60	Alta Bioscience
H58A;H59A_F	CCAGACGGTTTTTCAATCTGGGCTGCCCTTGACGCTCATGGCATTCC	60	Alta Bioscience
H58A;H59A_R	GGAATGCCATGAGCGTCAAGGGCAGCCCAGATTGAAAAACCGTCTGG	60	Alta Bioscience
H43A_R	ATCGTTGTGCCTTGAGCAACGGCACGAATCGCCAG	60	Alta Bioscience
H43A_F	CTGGCGATTCGTGCCGTTGCTCAAGGCACAACGAT	60	Alta Bioscience

S68A;T70A_F	TGACGCTCATGGCATTCCTTTCAAAGCTATCGCCCCCAAAAACGA	60	Alta Bioscience
S68A;T70A_R	TCGTTTTTGGGGGCGATAGCTTTGAAAGGAATGCCATGAGCGTCA	60	Alta Bioscience
R95A_F	AAAAGCGGTCCTCGACGCAACATTGCCCCATGGC	60	Alta Bioscience
R95A_R	GCCATGGGGCAATGTTGCGTCGAGGACCGCTTTT	60	Alta Bioscience
pBAD_seq_F	ATGCCATAGCATTTTTATCC	55	Alta Bioscience
pBAD_seq_R	GATTTAATCTGTATCAGG	48	Alta Bioscience
kan_seq_F	GCATCAGAGCAGCCGATTGTC	67	Alta Bioscience
kan_seq_R	CATCGCCTTCTATCGCCTTC	64	Alta Bioscience
pKT_seq_t25R	GTTGACCAGGCGGAACATCAATGTG	69	Alta Bioscience
pKT_seq_t25F	CATCTGTCCAACTTCCGCGAC	67	Alta Bioscience
Salm_acrB-	ATATTCCTCGAGGCGATGTTCTGTCGAATGACTATGCTCAATATCTTCGC	72	Alta Bioscience
Salm_acrB+	TAGCTTCATATGCCTAATTTCTTTATCGATCGCCCTATATTTGCGTGGGTG	74	Alta Bioscience
pDOC-TolC-K	AAGTAGAAGCTTAATAATTTTACAGTTTGATCGCGCTAAATCTGCTTCACCACAAGGAATGGACCGGTCAATTGGCTGGAGC		Alta Bioscience
pDOC-TolC-R	ATTGTACATATGCAGACGGGGCCGAAGCCCCGTCGTCGTCATCAGTTACGGAAAGGGTTATGGATATGAATATCCTCCTTAGTTCCTATTCCGAAGTTCC		Alta Bioscience
pDOC-acrA-K	CTTAGAAAGCTTTTAACTTTTGACCATTGACCAATTTGAAATCGGACACTCGAGGTTTACATAGGACCGGTCAATTGGCTGGAGC		Alta Bioscience
pDOC-acrB-R	CTTGCTCATATGTTACGCGGCCTTAGTGATTACACGTTGTATCAATGATGATCGACAGTATGGATATGAATATCCTCCTTAGTTCCTATTCCGAAGTTCC		Alta Bioscience
pDOC-cure-5	GTATGTGAATTCTTAAGTTCTACGTGTTCCGCTTCC		Alta Bioscience
pDOC-cure-3	GTATGTGAATTCATGCTGGAGTTCTTCGCCC		Alta Bioscience
pASK-del-mcs-upst-F	GGGGATCCCTCGAGTGTGACCTGTGAAGTGAA		Alta Bioscience
pASK-del-mcs-upst-R	TTCACTTCACAGGTCACACTCGAGGGATTCCC		Alta Bioscience
pBAD-essential-R	GAAGCATTTATCAGGGTTATTGTCTC	62	Alta Bioscience
acrA_GS-tip_F	TATCAGGGATCCGGTGGTTCAGGGGAGTACGATCAGGCTC		Alta Bioscience

acrA_GS-tip_R	CCCTGAACCACCGGATCCCTGATAACGATTCACCGTC		Alta Bioscience
acrA_Δ106-131/140-164_F	CCTATCAGGCGACATACAAACTGCTCGGTACTCAGTACATCAGTGAAACTGCGCGGATCAAT		Alta Bioscience
acrA_Δ106-131/140-164_R	ATTGATCCGCGCAGTTTCACTGATGTACTGAGTACCGAGCAGTTTGTATGTCGCCTGATAGG		Alta Bioscience
acrA_TY-VF_F	CTGCGACCTATCAGGCGGTATTCGACAGTGCGAAAGGTG	61	Alta Bioscience
acrA_TY-VF_R	CACCTTTCGCACTGTCGAATACCGCCTGATAGGTCGCAG	63	Alta Bioscience
acrA_K-A_F	GATCAATCTGGCTTACACCGCAGTCACCTCTCCGATTAGC		Alta Bioscience
acrA_K-A_R	GCTAATCGGAGAGGTGACTGCGGTGTAAGCCAGATTGATC		Alta Bioscience
HindIII-acrA	ATTAGTAAGCTTGCAACGACGAAAATGTCCAGGAAAAATCCTGG		Alta Bioscience
K-fwd-acrAr	CAGCTCCAGCCAATTGACCGGTCCATGTAAACCTCGAGTGTCCGATTTCAAATTGGTCAATGGTC		Alta Bioscience
p-rev-acrB	CTAGAGAATAGGAACTTCGGAATAGGAACTAAGGAGGATATTCTACAACGTGTAATCACTAAGGCCGCGTAAGCG		Alta Bioscience
SalI-acrBr	ATTATAGTCGACGTTGATCGCCGAGGTTGGGTCGTTTAC	72	Alta Bioscience
HindIII-tolC	ATTAGTAAGCTTGTCAGGTGTGTAACGCTTCATTTATGCCCACTC	72	Alta Bioscience
k-fwd-tolCr	CAGCTCCAGCCAATTGACCGGTCCTTACATTCCTTGTGGTGAAGCAGTATTTAGCGCGATC		Alta Bioscience
p-rev-tolC	CTAGAGAATAGGAACTTCGGAATAGGAACTAAGGAGGATATTCGTATGACGACGACGGGGCTTCG		Alta Bioscience
SalI-tolCr	ATTATAGTCGACGCTCGGTAATACTGACTCTTTCCATCGGTATCAGC	72	Alta Bioscience
K-FWD	GACCGGTCAATTGGCTGGAG	67	Alta Bioscience
P-REV	GGAACTAAGGAGGATATT	51	Alta Bioscience
pDOC-S1	TATGCTTCCGGCTCG	59	Alta Bioscience
pDOC-S2	GGATGTGCTGCAAGG	58	Alta Bioscience
pDOC-CC1F	GCGGAACACGTAGAACTTAAG	61	Alta Bioscience
pDOC-CC2F	CATGCTGGAGTTCTTGCGCCC	70	Alta Bioscience
pDOC-CC1R	CTTAAGTTCTACGTGTTCCGC	61	Alta Bioscience
del-ex.mcs-pask-f	GATCCCTCGAGTGAGACCTTGAAGTGAAAAATGGC		Alta Bioscience

del-ex.mcs-pask-r	GCCATTTTTCACTTCAAGGTCTCACTCGAGGGATC		Alta Bioscience
ClaI-pask-f	CCGCTACTGCGTCATCGATTTCCACGCGCC		Alta Bioscience
ClaI-pask-r	GGCGCGTGGATATCGATGACGCAGTAGCGG		Alta Bioscience
acrAΔhpHup-f	CTATCAGGCGACATACCTGCTCGGTACTCAGT		Alta Bioscience
acrAΔhpHup-r	ACTGAGTACCGAGCAGGTATGTCGCCTGATAG		Alta Bioscience
pASK-ScaI	CTCAGAATGACTTGGTTGAGTACTCACCAGTCACAG		Alta Bioscience
SacII-NmCherry	AATAATCCGCGGGTGAGCAAGGGCGAGGAG	67	Alta Bioscience
strep-SacII-NmCherry	AATAATCCGCGGGGTGAGCAAGGGCGAGGAG	69	Alta Bioscience
SacI-NmCherryR	AATAATGAGCTCGTCCTCGGGGTACATCCGCTC	70	Alta Bioscience
SacI-mzrA	AATAATGAGCTCCAAATACCTCGCATGTCGCTTCGC	69	Alta Bioscience
XhoI-mzrAr	AATAATCTCGAGTCCGAAGCGATGAGAGTTATCCCG	69	Alta Bioscience
NcoI-envZ	AAAATACCATGGCAGGCGATTGCGCTTCTCGC	71	Alta Bioscience
SalI-envZr	AATAATGTCGACCCTTCTTTTGTCGTGCCCTGC	67	Alta Bioscience
SalI-CmCherry	AATAATGTCGACGGCGCCCTGAAGGGCGAG	72	Alta Bioscience
HindIII-CmCherry-hisR	TATTATAAGCTTAGTGATGATGGTGGTGATGCTTGTACAGCTCGTCCATGCGC	69	Alta Bioscience
NcoI-tolC	GATATACCATGGAGAAATTGCTCCCCATTCTTATCGGCCTGAG	72	Alta Bioscience
HindIII-tolCr	TTATTAAAGCTTAGTTACGGAAAGGGTTATGACCGTTACTGGTG	71	Alta Bioscience
SalI-tolCΔc-43r	ATTATTGTCGACTTCCGGATTAGTGGAAACCGGTTTGCTC	71	Alta Bioscience
TolC/DD-VV	CGGTACGCGTACCATTGTTGTCGTGTTGGTCGCGACCACCACGTT		Alta Bioscience
TolC/DD-VV(R)	ATCGTGGTGGTCGCGACCAACACGACAACAATGGTACGCGTACCG		Alta Bioscience
TolC/D371V	GTACGCGTACCATTGTTGTCGTGTTGGATGCGACCACC		Alta Bioscience
TolC/D371V(R)	GGTGGTCGCATCCAACACGACAACAATGGTACGCGTAC		Alta Bioscience
Nco-less-NmCherry	GTAATGCAGAAGAAGACGATGGGCTGGGAGGCCTC		Alta Bioscience

Nco-less-NmCherryR	GAGGCCTCCCAGCCCATCGTCTTCTTCTGCATTAC		Alta Bioscience
AmpR-R	GCCATCCGTAAGATGC	58	Abingdon Health
SalI-GS-6His-GS-NmCherry	AATAATGTCGACGGTAGTGGAGGTCACCACCATCATCACCACGGTAGTGGAGGTGTGAGCAAGGGCGAGGAG		Abingdon Health
NmCherry-HindIIIR	AATAATAAGCTTGTCTCTCGGGGTACATC	59	Abingdon Health
SacIIacrA(N-155)R	AATAATCCGCGGATTCGCCTGTTGCGCATCAGC	70	Abingdon Health
SacI-(C-158)acrA	AATAATGAGCTCGCGGCGAAAGCTGCCGTTG	72	Abingdon Health
SacII-GS-Strep-GS-CmCherry	AATAATCCGCGGGGCAGTGGTGGTTGGAGCCATCCACAGTTTGAAAAAGGCAGTGGTGGTGGCGCCCTGAAGGGCGAG		Abingdon Health
CmCherry-GS-SacIR	AATAATGAGCTCACCTCCACTACCACCTCCACTACCCTTGTACAGCTCGTCCATGC		Abingdon Health
EcoRI-acrAupstF	AAAAAAGAATTCCAACGACGAAAATGTC	52	Abingdon Health
BamHi-acraAupstR	AAATAAGGATCCCCTCGAGTGTCCG	55	Abingdon Health
XhoI-acrBdnstF	AAAAATCTCGAGTACAACGTGTAATCACT	51	Abingdon Health
EcoRI-tolCupstF	AAAAAAGAATTCGTCAGGTGTGTAACG	53	Abingdon Health
BamHI-tolCupstR	TTTTTTGGATCCCCTTGTGGTGAAGC	53	Abingdon Health
XhoI-tolCdnstF	ATAATACTCGAGCTGATGACGACGAC	52	Abingdon Health
tolC-S350F-F	CGCCTACAAACAAGCCGTAGTTTTCGCTCAAAGCTC		Abingdon Health
tolC-S350F-R	GAGCTTTGAGCGAAAACTACGGCTTGTTTGTAGGCG		Abingdon Health
tolC-R390E-F	CAAGCAAGAGCTGGCGAATGCGGAATATAACTACCTGATTAATCAGC		Abingdon Health
tolC-R390E-R	GTTCGTTCTCGACCGCTTACGCCTTATATTGATGGACTAATTAGTCG		Abingdon Health
tolC-D162A-F	CGCCAGCACGGTAGCGTACTGTGCGCG		Abingdon Health
tolC-D162A-R	CGCGCACAGTACGCTACCGTGCTGGCG		Alta Bioscience
tolC-V198D-F	ACTGGCTGCGCTGAATGACGAAAACTTTAAAACCGA		Abingdon Health
tolC-V198D-R	TCGGTTTTAAAGTTTTCGTCATTCAGCGCAGCCAGT		Abingdon Health
tolC-N332D/N335D-F	GACAACATTGATGCATCTATCAGTAGCATTAACGC		Abingdon Health

tolC-N332D/N335D-R	CAATGTTGTCGAAGGAGGAACGCACGG		Abingdon Health
tolC-YF1-F	ATGGAAGCGGGCTTCTCGGTCGGTACG		Abingdon Health
tolC-YF1-R	CGTACCGACCGAGAAGCCCGCTTCCAT		Abingdon Health
tolC-RS2-F	GCTACTCGGTCGGTACGAGTACCATTGTTGATGTG		Abingdon Health
tolC-RS2-R	CACATCAACAATGGTACTCGTACCGACCGAGTAGC		Abingdon Health
SacII-mCherry-f2	AATAATCCGCGGATGGTTTCTAAAGGTGAAGAAGACAACATG	65	Abingdon Health
Strep-SacII-mCherry-f2	AATAATCCGCGGGGTTTCTAAAGGTGAAGAAGACAACATG		Abingdon Health
SacI-N-mCherry-R2	AATAATGAGCTCGTCTTCCGGGTACATACGTTCAG	65	Abingdon Health
SalI-C-mCherry-F2	AATAATGTCGACGGTGCTCTGAAAGGTGAAATCAAAC	65	Abingdon Health
HindIII-mCherry-his-R2	TATTATAAGCTTAGTGATGATGGTGGTGATGTACAGTTCGTCCATACCGTTGG	65	Abingdon Health
ss-mtrE-F	ATGAATACTACATTGAAAACTACCT	57	Abingdon Health
NdeI-mtrE-F	TAATAACATATGAATACTACATTGAAAACTACCTTGACCTCTGTTGCAGCA	72	Abingdon Health
XhoI-mtrE-R	AAATCCCTCGAGTTTGCCGGTTTGGGTATCCCGTTTCAATC	72	Abingdon Health
NdeI-mtrC-F	TCTTTACATATGGCTTTTTATGCTTCTAAGGCGATGCGTGC	72	Abingdon Health
XhoI-mtrC-R	AAAGTGCTCGAGTTTCGCTTCAGAAGCAGGTTTGGCTTCAG	72	Abingdon Health
no-XhoI-mtrE-R	CAATGCGATGTCGATCAGCTTTTGCAGGC	72	Abingdon Health
no-XhoI-mtrE-F	GAGCGCAATACCAGTTTGCGTACAGC	71	Abingdon Health
NcoI-mtrC-F	TTTTTTCCATGGCTTTTTATGCTTCTAAGGCGATGCGTG	67	Abingdon Health
HindIII-mtrC-R	TATCTCAAGCTTATTTCGCTTCAGAAGCAGGTTTGGCTTC	70	Abingdon Health
ss-tolC-F	AAGAAATTGCTCCCCATTC	58	Abingdon Health
pBAD-start-R	CATGGTGAATTCCTCCTG	58	Abingdon Health
pASK-start-R	CATATGTATATCTCCTTCTTAAAGTTAAAC	57	Abingdon Health
mtrC-TA-R	GTTTCGCTTCAGAAGCAGGTTTGGCTTC	71	Invitrogen
mtrE-TA-F	TGAATACTACATTGAAAACTACCTTGACCTCTGTTGCAGC	72	Invitrogen

mtrE-TA-R	GTTTGCCGGTTTGGGTATCCCGTTTCAATC	71	Invitrogen
acrA-dHp-F	ACCAAAGTCACCTCTCCGATTAGCG	69	Invitrogen
tolC-N332DN335D-Q5F	TTGATGCATCTATCAGTAGCATTAACGCCTACAAAC		Invitrogen
acrA-dHp-R	CAATCTGATAGAGAGAGACACCTGCTTCGATG	70	Invitrogen
tolC-N332DN335D-Q5R	TGTTGTCGAAGGAGGAACGCACGGTCTG		Invitrogen
tolC-D371VD374V-Q5F	TTGGTCGCGACCACCACGTTGTACAACG		Invitrogen
mtrC-hp-F	TCCTTCCACTTATGAAGCAGGTCTGG	69	Invitrogen
mtrC-hp-R	CGGTTCAGATTGATGCCGGC	67	Invitrogen
tolC-D371VD374V-Q5R	CACTACAACAATGGTACGCGTACCGAC		Invitrogen
pASK-TA-F	CGAGTGAGACCTGCAGTGAAAAATGGC	70	Invitrogen
tolC-Y362FR367S-Q5F	GGTACGAGTACCATTGTTGATGTGTTGGATGCGA	68	Invitrogen
pBAD-TA-F	CGACCTGCAGGCATGCAAGC	71	Invitrogen
tolC-Y362FR367S-Q5R	GACCGAGAAGCCCGCTTCCATCGCGTC	72	Invitrogen
pBAD-TA-R	GGTGAATTCCTCCTGCTAGCCCA	70	Invitrogen
acrB-D288G-F	GGTCTTGGCATCAAACTGGCTACCG		Invitrogen
acrB-D288G-R	TGACGCTGGCTGACCGT		Invitrogen
acrA-TA-F	TGAACAAAAACAGAGGGTTTACGCCTCTGG	71	Invitrogen
acrA-TA-R	GAGACTTGGACTGTTCAGGCTGAGC	70	Invitrogen
acrB-TA-R	GATGATGATCGACAGTATGGCTGTGCTC	69	Invitrogen
tolC-TA-F	TGAAGAAATTGCTCCCCATTCTTATCGGCCTG	72	Invitrogen
tolC-TA-R	GGTTACGGAAAGGGTTATGACCGTTACTGG	71	Invitrogen
mtrC-TA-F	TGGCTTTTTATGCTTGAAGGCGATGCGTG	72	Invitrogen
acrA-tip-only-S	TCCTGCGACCTATCAGGCGACATACAATCGTTATCAGAAAC TGCTCGGTACTCAGTACATCAGTAAGCAAGAGTACGAT	N/A	Alta Bioscience
acrA-tip-only-A	TCGTACTCTTGCTTACTGATGTACTGAGTACCGAGCAGTTTC TGATAACGATTGTATGTCGCCTGATAGGTCGCAGGAT	N/A	Alta Bioscience
pASK-TA-R	ATGTATATCTCCTTCTTAAAGTTAAACAAAATTATTTCTAGA TTTTTGTCG	66	Alta Bioscience
cftC-F	TGAATATGAACAATCCATTAGAGGTTCTTGGGCATGTATC	70	Alta Bioscience
cftD-R	GACGCTCATGTAAACTTTCTGTTACAGACTCTTCCAG	71	Alta Bioscience
AcrA-Y129TAG-Q5F	GAGAAACTGCTCGGTACTCAG	62	Alta Bioscience
AcrA-Y129TAG-Q5R	TAAACGATTCACCGTCAATTGC	62	Alta Bioscience

AcrA-Y137TAG-Q5F	GATCAGTAAGCAAGAGTACGATCAG	62	Alta Bioscience
AcrA-Y137TAG-Q5R	TACTGAGTACCGAGCAGTTTC	60	Alta Bioscience
EcoRI72-tolCupst-F	AAAAAAGAATTCAGGAAAGTCAGGTGTGTAACGCTTC	67	Invitrogen
LCR-tolCupst-R	TGCATTCCTTGTGGTGAAGCAGTATTTAGC	69	Invitrogen
LCR-pDOC-EcoRI-R	AAGCTTGAATTCATCGATTACCCTGTTATCCCTA	69	Invitrogen
TolC-401C411A-Q5f	TACGTTGAACGAGCAGGCTCTGCTGGCACTGAACAATG	64	Invitrogen
TolC-401C411A-Q5r	CCCAGAGCTGAGCAAATATTCAGCTGATTAATCAGGTAG	58	Invitrogen
LCR-pDOC-NdeI-F	ATGCTAGCGTCGACTAGTAGGGATAACAG	69	Invitrogen
LCR-TolCdnst-F	TGATGACGACGACGGGGCTTCG	72	Invitrogen
P-rev2	CTCGAGATATGAATATCCTCCTTAGTTCCTATTCC	67	Invitrogen
pDOC-C-tolC-upst	ATAACAGGGTAATCGATGAATTCAGGAAAGTCAGGTGT		Invitrogen
tolC-Kan-upst	TCACCACAAGGAATGCAGACCGGTCAATTGGCT		Invitrogen
mtrE-int-F	GACTGGGTGCGGCATC	64	Invitrogen
mtrE-int-R	CAATTCGACAGAACCCGTACC	64	Invitrogen
tolC-Kan-dnst	AGGAGGATATTCATATCTCGAGTGATGACGACGACGG	58	Invitrogen
rlS-rlG-F	GGTAAGCAAGAGTACGATCAGGCTCTGGCT	72	Invitrogen
rlS-rlG-R	GATGTACTGAGTACCGAGCAGTTTCTGATAACGATTCAC	72	Invitrogen
pDOC-C-tolC-dnst	TCAGTATTACCGAGCGTCGACTAGTAGGGATAACAGGG		Invitrogen
EcoRI71-acrAupst-F	AAAAAAGAATTCCGGCGCTTCAGCGACT	71	Invitrogen
LCR-acrAupst-R	ATGTAAACCTCGAGTGTCCGATTTCAAATTGGT	70	Invitrogen
qeyD-qeyA-F	GCTCAGGCTCTGGCTGATGCGC	71	Invitrogen
qeyD-qeyA-R	GTACTCTTGCTTACTGATGTACTGAGTACCGAGCAG	72	Invitrogen
LCR-acrBdnst-F	TACAACGTGTAATCACTAAGGCCGCGTAAG	70	Invitrogen
aaKaa-aaEaa-F	GAAGCTGCCGTTGAAACTGCG	67	Invitrogen
aaKaa-aaMaa-F	ATGGCTGCCGTTGAAACTGCG	66	Invitrogen
aaKaa-aaEaa-R	CGCCGCAGTTACCGCAGCATTC	72	Invitrogen
pDOC-C-acrA-upst	ATAACAGGGTAATCGATGAATTCCGGCGCTTCAG		Invitrogen
acrA-Kan-upst	GACACTCGAGGTTTACATGACCGGTCAATTGGCT	56	Invitrogen

acrB-Kan-dnst	TACAACGTGTAATCACTAAGTGATGACGACGACGG	51	Invitrogen
aavE-aavA-F	CAACTGCGCGGATCAATCTGGCTTACAC	72	Invitrogen
aavE-aavA-R	CAACGGCAGCTTTCGCCGC	72	Invitrogen
pDOC-C-acrB-dnst	GTCAGTATTACCGAGCGTCGACTAGTAGGGATAACAGGG		Invitrogen
TA-mtrE-Nlac-F	TGAATACTACATTGAAAACCACCTTAACTTCTGTTGCGGC	72	Invitrogen
TA-mtrC-Nlac-F	TGGCTTTTTATGCTTCTAAGGCGATGCGT	71	Invitrogen
TA-mtrD-Nlac-F	GGCTAAATTTTTTATCGACCGCCCCATTTTCGC	72	Invitrogen
TA-mtrD-Nlac-R	GATATTGTTTATCGTCCGGACCGGTGATGC	71	Invitrogen
envZ-CmCherry	AGGGCACGACAAAAGAAGGGGGCGCCCTGAAGGGCGAGAT		Invitrogen
CmCherry-pASK	CATGGACGAGCTGTACAAGTTAACTCGAGTGAGACCTG		Invitrogen
pASK-acrA	AAGAAGGAGATATACATATGAACAAAAACAGAGGGTTTAC	50	Invitrogen
acrB-pBAD	GCCATACTGTCGATCATCATTAAGCTTGGCTGTTTTGG	58	Invitrogen
pBAD-tolC	CAGGAGGAATTCACCATGAAGAAATTGCTCCCCATTC	58	Invitrogen
tolC-pASK	GTCATAACCCTTTCCGTAACTAACTCGAGTGAGACCTG	53	Invitrogen
pASK-Start-R	CATATGTATATCTCCTTCTTAAAGTTAAAC	57	Invitrogen
pBAD-HindIII-F	TAAGCTTGGCTGTTTTGG	58	Invitrogen
pBAD-Start-R	CATGGTGAATTCCTCCTG	58	Invitrogen
pASK-XhoI-F	TAACTCGAGTGAGACCTG	58	Invitrogen
mCherry-5-F	GTGAGCAAGGGCGAG		Invitrogen
NmCherry-R	GTCCTCGGGGTACATCC		Invitrogen
CmCherry-F	GGCGCCCTGAAGG		Invitrogen
mCherry-3-R	ACTTGTACAGCTCGTCCA		Invitrogen
pASK-NmCherry	AAGAAGGAGATATACATATGGTGAGCAAGGGCGAG		Invitrogen
NmCherry-mzrA	AGCGGATGTACCCCGAGGACCAAATACCTCGCATGTCGC		Invitrogen
mzrA-F	CAAATACCTCGCATGTCGC	62	Invitrogen
mzrA-R	TCCGAAGCGATGAGAGTTATC	62	Invitrogen
envZ-F	AGGCGATTGCGCTTC	60	Invitrogen
envZ-R	CCCTTCTTTTGTCGTGC	59	Invitrogen
tolC-F	AAGAAATTGCTCCCCATTC		Invitrogen
tolC-R	CGGAAAGGGTTATGACC		Invitrogen
acrA-F	AACAAAAACAGAGGGTTTAC		Invitrogen
acrB-R	ATGATGATCGACAGTATGG		Invitrogen
3-mzrA-pBAD	ATAACTCTCATCGCTTCGGATAAGCTTGGCTGTTTTGG		Invitrogen
pBAD-envZ	AGCAGGAGGAATTCACCATGAGGCGATTGCGCTTCTCGC	63	Invitrogen
ASK-tolC-XhoI-F	AAAAAACTCGAGTAAGAAGGAGATATACATATGAAGA		Invitrogen
tolC-HindIII-R	TTTTTTAAGCTTTTAGTTACGGAAAGGGTTATG		Invitrogen

pET-mCh-F	GTTTCTAAAGGTGAAGAAGACAACATG	62	Invitrogen
pET-CmCh-F	GGTGCTCTGAAAGGTGAAATC	62	Invitrogen
pET-NmCh-R	GTCTTCCGGGTACATACGT	61	Invitrogen
pET-mCh-R	TACAGTTCGTCCATACCGTTG	62	Invitrogen
pASK-NmCherry	AGAAGGAGATATACATATGGTTTCTAAAGGTGAAGAAGAC		Invitrogen
NmCherry-mzrA	ACGTATGTACCCGGAAGACGTGAGCAAGGGCGAG		Invitrogen
pBAD-CmCherry	GCAGGAGGAATTCACCATGGGTGCTCTGAAAGGTGAAATC	59	Invitrogen
CmCherry-mzrA	CAACGGTATGGACGAACTGTAGTGAGCAAGGGCGAG		Invitrogen
LCR-pKD13-F	GACCGGTCAATTGGCTTGTAGGCTGGAGCTGCTTC		Invitrogen
LCR-pKD13-R	CTCGAGATATGAATATCCTCCTTTCCGGGGATCCGTCG		Invitrogen
Kan-acrB-dnst-F	GAGGATATTCATATCTCGAGTACAACGTGTAATCACTAAG		Invitrogen
pASK-mCherry	AAGAAGGAGATATACATATGGTTTCTAAAGGTGAAGA	49	Invitrogen
NmCherry-mzrA	ACGTATGTACCCGGAAGACCAAATACCTCGCATGTCGC	61	Invitrogen
mCherry-mzrA	CAACGGTATGGACGAACTGTACAAATACCTCGCATGTCGC	62	Invitrogen
envZ-CmCherry	GGCACGACAAAAGAAGGGGGTGCTCTGAAAGGTGAAATC	62	Invitrogen
mzrA-pASK	ATAACTCTCATCGCTTCGGATAACTCGAGTGAGACCTG	58	Invitrogen
mCherry-pBAD	CAACGGTATGGACGAACTGTATAAGCTTGGCTGTTTTGG	58	Invitrogen
pUC18-seq-f	CCAGTCACGACGTTGTAAAACG	64	Invitrogen
pUC18-seq-R	AGCGGATAACAATTTCACACAGG	63	Invitrogen
XhoI-MF(pT2SC)	CAACCTCGAGTAATCTCAAGAGTGGCAGC	62	Alta Bioscience
NdeI-MR(pT2SC)	CATTCATATGTTACGCCCCGCCCTGC	73	Alta Bioscience
pASK_NdeI-F	TAACTTTAAGAAGGAGATATACATATGAAGAAATTGCTCCCCATTCT	60	Eurogentec